Intravital Imaging of Metastasis in Zebrafish

by

David Colin Benjamin

B.S., Microbiology, Immunology, and Molecular Genetics
UCLA, 2011

SUBMITTED TO THE DEPARTMENT OF BIOLOGY IN PARTIAL FULFILLMENT OF THE REQUIREMENTS FOR THE DEGREE OF

DOCTOR OF PHILOSOPHY

AT THE

MASSACHUSETTS INSTITUTE OF TECHNOLOGY

JUNE 2018

Signature of Author: Signature redacted
Department of Biology
May 25th, 2018

Certified By: Signature redacted
Richard O. Hynes
Daniel K. Ludwig Professor for Cancer Research
Thesis Supervisor

Accepted By: Signature redacted
Amy Keating
Professor of Biology
Graduate Committee Chair

Intravital Imaging of Metastasis in Zebrafish

By

David Colin Benjamin

Submitted to the department on May 25th, 2018 in partial fulfillment of the requirements for the degree of doctor of philosophy in biology

Abstract

Metastasis is the cause of the overwhelming majority of cancer deaths. However, it remains a poorly understood process. The events at the metastatic site are especially poorly comprehended. These events are dynamic and so require intravital imaging to investigate. However, the intravital imaging of these events in mice is challenging. Sites of metastasis are often in vital organs that are inaccessible to microscopy without surgical intervention. Furthermore, circulating tumor cells are rare and are involved in many transient interactions adding to the challenge. The development of a line of zebrafish, Casper, that is transparent throughout its life suggested that zebrafish might be a powerful system for intravital imaging. I first developed novel injection and imaging techniques to study metastasis through intravital imaging in adult zebrafish. I then followed individual ZMEL1 zebrafish melanoma cells at the metastatic site over the course of two weeks as they grew from single disseminated tumor cells into macroscopic metastases. From these studies, I characterized the steps of metastasis at the metastatic site for this cell line. I also utilized transparent zebrafish embryos to uncover a new role for the oncogene YAP during metastasis. I observed that the over-expression of a Hippo-insensitive mutant of YAP (YAP-AA) promoted brain metastasis following intravenous in zebrafish embryos. I determined that YAP-AA was promoting tumor cell dispersal throughout the embryo by allowing tumor cells to escape the first capillary bed they encounter. Following intravenous injection, control cells lodge in blood vessels in the tail and cease their travel through circulation. However, YAP-AA cells are able to move through these vessels, re-enter circulation and travel to other organs, such as the brain. These observations represent a new mechanism by which tumor cells can increase their dissemination throughout an animal.

Thesis Supervisor: Richard O. Hynes

Title: Daniel K. Ludwig Professor for Cancer Research, Professor Biology

Acknowledgements

The work described in this thesis is the culmination of many years of work and would not have been possible without the guidance, assistance, and cheerleading of many people. I would first like to thank my thesis advisor Richard Hynes. First and foremost, he gave me the independence to bring new experimental systems to the lab and to take my project in new directions. His patience and encouragement were instrumental in getting me through the early years where nothing worked and it seemed like I would be in graduate school forever. He also made sure the lab was a supportive and fun place to work. I would also like to thank my committee members Frank Gertler and Jackie Lees. Their encouragement and helpful suggestions over the years are greatly appreciated. I also thank Dave Langenau for being on my defense committee.

I would like to thank Adam Amsterdam for teaching me everything I know about zebrafish as well as accommodating my many odd requests in the fish facility. I would also like to thank him for his valuable scientific advice and for reviewing my manuscripts. I would also like to thank Tim and Karen in the fish facility for all their years taking of care of my fish and their friendship. I also thank Eliza Vasile in the microscopy facility for teaching me confocal microscopy and her kindness over the years. I have felt that the microscopy facility has been a second home for me during my PhD. I also thank Jeff Wyckoff for his advice and eagerness to help perform experiments. It has always been a pleasure to work with him.

In the Hynes lab, many people have helped me over the years. I would first like to thank John Lamar. He pioneered YAP research in the lab and his generous donation of reagents and data to my project expedited it considerably. I would also like to thank him for spending an innumerable number of hours discussing my science, teaching me techniques, and reviewing my data (I am still waiting on a final bill). His guidance over the years has greatly contributed to my development as a scientist. I would also like to thank Alexandra Naba. Her constant encouragement and scientific advice were instrumental in allowing me to complete my thesis work.

I would also like to thank Jess Hebert for his helpful discussions (scientific or otherwise), for listening to me celebrate and/or complain about my results (mostly complain), as well as editing almost everything I have ever written in the lab. I thank Chenxi Tian for her willingness to help with experiments and her valuable scientific input. Bigyan Bista had the misfortune of being my baymate for most of graduate school. I will always fondly remember our time together (baymates for life!). I also thank Jeff Schindler, Thao Nguyen, and Noor Jailkhani for our fun conversations that made graduate school pass slightly faster. I thank Amy McMahon for the inspiration to use zebrafish as a model system. I thank all the members of the Hynes lab (past and present) whom I have had the privilege of working with.

Outside of the lab, I would like to thank my wife, Selena Huang, for her constant love and support. I am always inspired by her drive, intelligence, and caring. I would also like to thank my former roommates: Dave and Xinchen for making the middle years of graduate school a time I will always fondly remember. I would finally like to thank my parents for their love and for encouraging me to pursue my passions (even when that was to become a classics major). I thank Selena's entire family for warmly welcoming me into their family. I especially thank Lily and Sherman for their love and for taking such good care of me when I visit. Finally, I thank Auri Benjamin for his unlimited love, willingness to wear reindeer ears, and for countless hours spent snuggling on the couch (even if I end up covered in fur).

Table of Contents

Chapter 1.

Introduction

The contents of this chapter were written by David Benjamin with editing by Jess Hebert and Richard Hynes.

An Overview of Metastasis

Metastasis is the cause of the overwhelming majority of cancer mortality (Lambert et al., 2017). While primary tumors can frequently be treated, metastatic disease is usually incurable for several reasons (Steeg, 2006). First, metastases often occur in vital organs limiting surgical options (Budczies et al., 2015). Second, the sheer number of metastases present in patients with end-stage disease can also make surgical intervention impossible (Riggi et al., 2018). Third, micrometastatic lesions may also be present that are too small to be detected and removed surgically (Pantel et al., 1999). Finally, resistance to chemotherapy and radiation often go hand in hand with metastasis (Longley and Johnston, 2005). As many patients do not present with metastatic disease, there is a pressing need for therapeutic options to prevent metastasis (Steeg, 2006). However, development of such therapies is challenging as metastasis is a complex process involving many steps spread out over space and time (Steeg, 2016; Valastyan and Weinberg, 2011; Wan et al., 2013).

Despite the apparent randomness of metastasis in individual patients, metastasis is somewhat predictable when patients are viewed in aggregate. It has long been noted that tumor types have propensities to metastasize to specific organs, termed organotropism (Paget, 1889). For example, melanoma metastasizes to the liver, lungs, brain, and bone at roughly the same frequency (Budczies et al., 2015). However, colon cancer primarily metastasizes to the liver, somewhat to the lungs, and very rarely to the bones (Budczies et al., 2015). It was originally assumed that these patterns of metastatic tropism were wholly determined by the layout of the circulatory system (Virchow, 1859). For example, the liver is the next organ

downstream from the colon in the mammalian circulatory system and so metastatic tumor cells would land in the colon first, following entry into circulation.

This idea was challenged when, in the late 19th century, the English surgeon Stephen Paget analyzed the autopsy records of 735 women who succumbed to breast cancer and noticed that there was a discrepancy between the amount of blood an organ received and the frequency with which breast cancer metastases developed. These observations suggested that the determinants of metastasis were more complex than just the distribution of metastatic tumor cells throughout the body by blood flow (Paget, 1889). To explain his observations, he put forth the "seed and soil" hypothesis. This hypothesis stated that, in order to metastasize, there had to be a cancer cell competent to metastasize (the seed), and it had to land in an environment hospitable to its growth (the soil) (Fidler, 2003).

This hypothesis remained debatable until Fidler and Hart provided conclusive evidence that metastatic tumor cell outgrowth differed between organs. They grafted kidney, lung, or ovarian tissue subcutaneously into mice. Following intravenous injection of B16 mouse melanoma cells, they observed that metastases formed in the lung and ovarian grafts but not the kidney grafts. Using radio-labeled cells, they confirmed that tumor cells arrived at the grafts in equal numbers. These observations combined indicated that the B16 cells arrived at the kidney grafts, yet were unable to form metastases, indicating that something about the microenvironment of the kidney graft was inhospitable to their growth (Hart and Fidler, 1980).

In other experiments, it was shown that a cell's propensity for metastasis can be enriched through *in vivo* selection (Fidler, 1973; Kripke and Fidler). In these experiments, a parental cell line is injected intravenously into a mouse. Once metastases in an organ emerge,

these metastases are removed and cell lines derived. These new cell lines can be injected into a new animal and the process repeated multiple times. Through such experiments, it was shown that cells can undergo relatively stable changes that enhance their metastatic ability (Clark et al., 2000).

With the dawn of the "omics" age, the molecular changes underlying these observations began to be elucidated (Bos et al., 2009; van 't Veer et al., 2002). The comparison of *in vivo*-selected cell lines to their parental population led to the discovery of specific genes which can promote metastasis such as RhoC (Clark et al., 2000). Analysis of lines that had been *in vivo*-selected also led to the identification of genes which mediate metastasis to specific organs including the lung, bone, and brain (Bos et al., 2009; Clark et al., 2000; Kang et al., 2003; Minn et al., 2005). Analysis of primary tumors that had metastasized showed that pro-metastatic gene signatures could be detected in primary tumors as well (Ramaswamy et al., 2003; van 't Veer et al., 2002). This observation led to questions as to whether the ability to metastasize was shared by most cells in the primary tumor or was restricted to a small sub-population (Bernards and Weinberg, 2002; Hynes, 2003; Sherley, 2002).

Data from human patients seems to suggest that the ability to metastasize is an ability restricted to rare variants within primary tumors (Vanharanta and Massagué, 2013). First, genomic studies of patient primary tumors have shown them to be heterogeneous, comprised of many sub-clones each containing unique collections of mutations (Gerlinger et al., 2012; Yachida et al., 2010). In addition to mutational heterogeneity, tumors have also been shown to contain epigenetic heterogeneity and epigenetic changes have been shown to be able to promote metastasis (Mazor et al., 2016; McDonald et al., 2017). Second, when metastases

were compared to primary tumors, individual metastases were shown to be derived from a single sub-clone from the primary tumor (Campbell et al., 2010; Yachida et al., 2010). Finally, data from experiments in mice have shown that primary tumors contain rare variants with enhanced metastatic potential and that metastases can indeed originate from a single tumor cell (Fidler and Talmadge, 1986; Kang et al., 2003; Kripke and Fidler). Furthermore, a more recent study has identified pre-existing mutations that are selected for during the metastatic process in mice (Jacob et al., 2015).

A key question in the field of metastasis is how these rare variants gain the ability to metastasize. As will be described in detail below, tumor cells need to acquire many separate abilities in order to be successful at metastasis. An efficient mechanism for gaining many disparate abilities is to activate broad transcriptional programs. One such transcriptional program that can play a key role in metastasis is the epithelial-mesenchymal transition or EMT. By activating an EMT program, tumor cells are able to simultaneously acquire many of the capacities necessary for metastasis (Lambert:2017eh; Thiery, 2002). EMT programs are controlled by a core set of transcription factors: Twist, Snail, Zeb1, and Zeb2 (De Craene and Berx, 2013; Lamouille et al., 2014). Upstream, these transcription factors are activated by a many signaling pathways including, TGF-β, Wnt, various receptor tyrosine kinases, Hedgehog, and Notch (Lamouille et al., 2014; Xu et al., 2009; Zhan et al., 2017). Microenvironmental cues such as hypoxia (Yang et al., 2008) and inflammatory cytokines (Sullivan et al., 2009; Fernando et al., 2011) can also induce an EMT. EMT in cancer cells can be induced by signals from stromal cells in the primary tumor. For example, macrophages can induce an EMT by secreting Wnt1 in breast cancer (Linde et al., 2018). Neutrophils in the primary tumor can produce TGF-β, a

potent inducer of EMT (Hu et al., 2015). Platelets have been shown to induce an EMT in tumor cells in circulation and so may also be involved in EMT induction in the primary tumor (Labelle et al., 2011).

It has long been known from studies of developmental biology that EMT is not an all-or-nothing process (Nieto, 2013; Thiery, 2002). Rather, cells can co-express epithelial and mesenchymal markers and exist on a spectrum from a partial to a full EMT (Nieto, 2013; Thiery, 2002). More recently, partial EMTs have been appreciated to occur during metastasis and CTCs with intermediate phenotypes have been observed suggesting that partial EMT can promote dissemination (Kalluri and Weinberg, 2009; Khoo et al., 2015; Thiery, 2002; Yu et al., 2013). EMT is also reversible. Cells can regain an epithelial phenotype through the mesenchymal-epithelial transition (MET) and this reversal may be required for metastatic outgrowth (Ocaña et al., 2012; Tsai et al., 2012).

Whether EMT is actually required for metastasis remains controversial (Fischer et al., 2015; Ye et al., 2017). Intravital imaging in mice has shown that tumor cells can undergo an EMT in the primary tumor, metastasize to a distant organ, and revert to an epithelial phenotype during metastatic outgrowth (Beerling et al., 2016). However, determining the necessity of EMT for metastasis is not straightforward. The multitude of transcription factors that can orchestrate an EMT make interpreting inhibition of single transcription factors or combinations of a few difficult (Li and Kang, 2016). In addition, cells may need only achieve a partial EMT to gain the abilities necessary for metastasis (Liao and Yang, 2017). Stable perturbations of the levels of EMT-promoting transcription factors have been shown to enhance metastasis but may not accurately reflect the transient nature of EMT during the natural progression of metastasis

(Yang et al., 2004). It is clear that EMT can be intricately linked to cancer and metastasis, but further work is needed to determine whether or not EMT is truly required for metastasis.

The Metastatic Cascade

The preceding section has covered some of the general principles of metastasis. This section will now turn to a mechanistic description of how metastasis actually occurs at the cellular level. Guiding this discussion will be the intellectual framework that is currently used to understand metastasis: the metastatic cascade (sometimes referred to as the invasion metastasis cascade) (Valastyan and Weinberg, 2011). This cascade describes the series of steps that a tumor cell must successfully complete in order to metastasize (Fig. 1) (Chambers et al., 2002; Fidler, 2003). As has been hinted above, the interactions between tumor cells and the microenvironment play a key role during metastasis (Joyce and Pollard, 2008). Many of the steps of the metastatic cascade have been shown to depend on interactions with stromal (non-tumor cells). For example, platelets, neutrophils, and macrophages have been shown to be key players during metastasis (Labelle and Hynes, 2012). While many other cell types also play a role, this thesis will only describe the role of these three during metastasis.

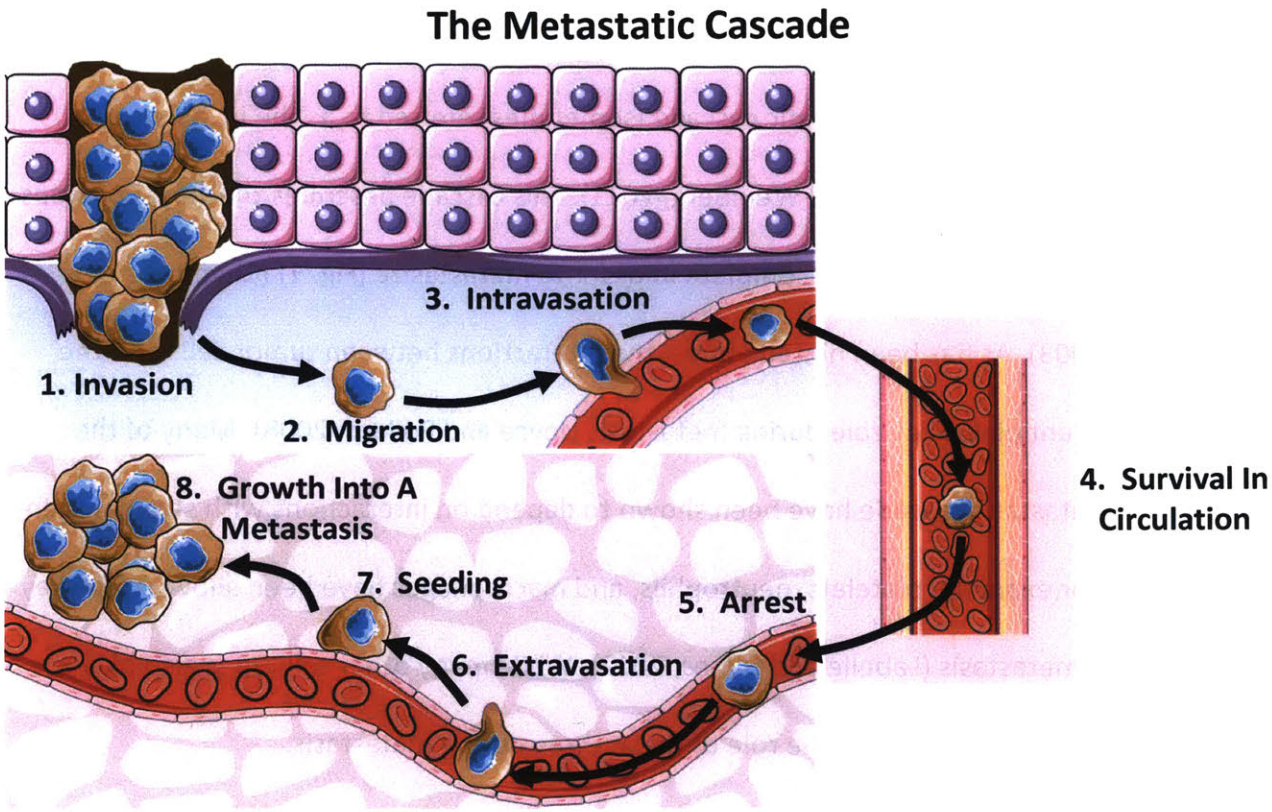

Figure 1. Overview of the metastatic cascade. The metastatic cascade describes the steps a tumor cell needs to successfully complete in order to metastasize. These steps are 1) invasion 2) migration 3) intravasation 4) survival in circulation 5) arrest at the metastatic site 6) extravasation 7) seeding 8) growth into a metastasis. Figure 1 was generated from modified Servier Medical Art under a Creative Commons 3.0 Unported License (https://smart.servier.com).

The first step in the metastatic cascade is invasion through the basement membrane and into adjacent normal tissue (Fig. 1). The basement membrane is a specialized extracelluar matrix (ECM) primarily composed of laminin, collagen IV, nidogen, and perlecan arranged in a thin sheet (Jayadev and Sherwood, 2017; Yurchenco, 2011). Many human malignancies arise from epithelial tissues that are arranged in sheets and surrounded by a basement membrane (Valastyan and Weinberg, 2011). These malignancies are known as carcinomas and represent the vast majority of human cancers (Leber and Efferth, 2009; Siegel et al., 2017; Valastyan and Weinberg, 2011). Other tumor types, such as sarcomas, arise from different cell types and may not need to cross a basement membrane during invasion into adjacent tissue (Helman and Meltzer, 2003).

Invasion through the basement membrane defines the difference between benign and malignant tumors and may be required for dissemination to distant sites (Wan et al., 2013). Mechanistically this is believed to be accomplished, at least in part, through the expression of proteases such as matrix metalloproteinases (MMPs), which degrade the basement membrane (Kessenbrock et al., 2010). Specialized membrane protrusions called invadopodia, which contain MT1-MMP on their surface, have also been shown to promote tissue invasion (Eddy et al., 2017; Gligorijevic et al., 2012; Li et al., 2013). Proteases can also be provided by macrophages and neutrophils to promote invasion. Recruited neutrophils express MMP9, which enhances angiogenesis and invasion (Bekes et al., 2011). Macrophages can produce cathepsin proteases to degrade the ECM as well as promote cancer cells to form invadopodia through EGFR signaling to enhance invasion (Gocheva et al., 2010; Zhou et al., 2014).

Once free of the basement membrane, cancer cells can engage in the next step of the cascade: migration (Fig. 1). Studies of tumor cell migration *in vivo* have identified three main modes of cell migration: mesenchymal, amoeboid, and collective (Friedl and Wolf, 2003; Sahai, 2007). Cells which have undergone an EMT migrate via mesenchymal motility (Clark and Vignjevic, 2015). In this mode of migration, the cell polymerizes actin into a branching network at the front of the cell (Abercrombie et al., 1971; Campellone and Welch, 2010; Svitkina and Borisy, 1999). The protrusions formed at the front of the cell by this rapidly polymerizing actin network are called lamellipodia (Abercrombie et al., 1970; Friedl and Wolf, 2003). Actin polymerization in lamellipodia is regulated by Rac1, a member of the Rho family of small GTPases (Machacek et al., 2009; Ridley et al., 1992; Ridley, 2015; Wu et al., 2009).

At the very front of lamellipodia, small finger-like protrusions rich in actin known as filopodia are formed under the control of the small GTPase cdc42 (Ahmed et al., 2010; Nobes and Hall, 1995). Filopodia serve a number of key roles during migration (Gupton and Gertler, 2007). First, they serve as locations to generate new attachments to the ECM (Jacquemet et al., 2015). These attachments, known as focal adhesions, allow the cell to generate the forces required for migration. Second, filopodia serve as platforms for sensing the environment (Heckman and Plummer, 2013).

Focal adhesions form a direct connection between the ECM and the actin cytoskeleton, allowing a cell to pull directly on its substrate during migration (Gardel et al., 2010; Huttenlocher and Horwitz, 2011; Mayor and Etienne-Manneville, 2016). These structures are large, multi-protein complexes (Case and Waterman, 2015). At their core are integrins, which are heterodimeric receptors for ECM components (Campbell and Humphries, 2011; Hynes,

2002). Integrins are not able to bind the actin cytoskeleton on their own and so are linked to the actin cytoskeleton through a number of scaffolding proteins, including, talin and vinculin (Case and Waterman, 2015; Klapholz and Brown, 2017; Ziegler et al., 2006).

Focal adhesions also contain a many signaling molecules, including FAK, Src, and PI3K which can regulate cell behavior (Mitra et al., 2005; Geiger et al., 2009; Wozniak et al., 2004). Focal adhesions can also serve as the termini for bundles of linear actin called stress fibers (Tojkander et al., 2012). Stress fibers can be used for force generation through the action of the motor protein myosin II on these structures (Burridge and Wittchen, 2013). Myosin II-mediated contraction of these fibers is controlled by RhoA and its downstream effector ROCK (Ridley, 2015)

At the rear of the cell, RhoA regulates actin contraction to pull the rear of the cell forward (Petrie and Yamada, 2015; Reig et al., 2014). RhoA is negatively regulated by Rac1 and CDC42 and vice versa through a number of mechanisms (Ohta et al., 2006; Tsuji et al., 2002; Worthylake and Burridge, 2003; Xu et al., 2003). This regulation maintains actin polymerization at the leading edge and contraction only in the rear of the cell, thereby promoting forward movement (Reig et al., 2014). As the cell moves forwards, focal adhesions towards the rear of the cell disassemble (Parsons et al., 2010). Focal adhesion turn-over is required for migration to progress forwards (Mañes et al., 2000; Parsons et al., 2010). Mesenchymal motility is also associated with the expression of MMPs (Friedl and Alexander, 2011). The cell uses these enzymes to clear a path through the ECM (Even-Ram and Yamada, 2005; Friedl and Alexander, 2011; Friedl and Wolf, 2003).

Tumor cells can also migrate using amoeboid motility, which is named for its similarity to the movement of amoeba (Yumura et al., 1984). In contrast to mesenchymal motility, cells using amoeboid motility lack strong adhesions to the ECM and MMP activity (Friedl and Wolf, 2010; Sahai and Marshall, 2003). Instead, they squeeze through gaps in the ECM by using membrane blebs to extend their cytoplasm (Farina et al., 1998; Pinner and Sahai, 2008a; Tozluoğlu et al., 2013). In contrast to F-actin-rich lamellipodia, these protrusions have little F-actin (Paluch and Raz, 2013). Blebs are formed when the plasma membrane becomes disconnected from the cortical actin cortex (Cunningham, 1995; Keller and Eggli, 1998). Hydrostatic pressure then forces this free section of membrane outwards generating a bleb (Charras and Paluch, 2008). As the bleb expands, membrane flows through the neck of the bleb to support bleb expansion (Charras, 2008).

While the precise mechanism controlling bleb initiation remains unknown, migrating cells have enhanced bleb generation in the direction of migration (Paluch and Raz, 2013). This polarity in initiation may be due to the asymmetric distribution of membrane-cytoskeleton linker proteins of the ERM (Ezrin-Radixin-Moesin) family (Rossy et al., 2007). For example, in migrating A375 cells Ezrin is concentrated towards the rear of the cell (Lorentzen et al., 2011). Amoeboid motility requires high levels of contractility of the cortical actin network in order to generate the hydrostatic forces for bleb formation. As in mesenchymal motility, actin contractility is regulated by RhoA (Sahai and Marshall, 2003) and its downstream effector ROCK (Pinner and Sahai, 2008). Contractility is also regulated by MLCK (Mills et al., 1998). The last step in amoeboid motility is bleb retraction. This occurs when the actin cortex reforms under a bleb's plasma membrane (Charras et al., 2006). In migrating cells, new blebs can form shortly

after the reformation of the cortex to repeat the process in a progressive manner (Blaser et al., 2006).

Cells are capable of switching between mesenchymal and amoeboid motility and have been observed to switch rapidly between the two modes depending on the adhesiveness of their substrate and their confinement (Liu et al., 2015). Other microenvironmental conditions, such as hypoxia, have been shown to regulate the mode of motility (Lehmann et al., 2017). These observations demonstrate the key role that the microenvironment plays in determining which mode of motility cancer cells use during metastasis (Friedl and Wolf, 2010). Cell-intrinsic factors such as actin contractility and protease activity have also been demonstrated to regulate this choice (Paňková et al., 2010; Sahai and Marshall, 2003; Wolf et al., 2003).

In contrast to the migration of individual cells described above, tumor cells, as well as cells during development or wound healing, can also migrate as a group in a process called collective migration (Friedl and Gilmour, 2009; Mayor and Etienne-Manneville, 2016). Collective migration has long been observed in invasive carcinomas by pathologists (Sahai, 2005). During collective migration, cells maintain cell-cell contacts such as adherens junctions and migrate as a cohesive group (Mayor and Etienne-Manneville, 2016). The cells at the front of the migrating group take on the role of "leader cells". These cells serve to guide the "follower cells" which stream behind them (Poujade et al., 2007). These identities are not fixed, and cells can switch between leader and follower roles as the group of cells migrates (Jakobsson et al., 2010).

The molecular machinery involved in collective migration has considerable overlap with that of mesenchymal migration. In leader cells, Rac1 and Cdc42 activity is localized to the leading edge and regulates the formation of lamellipodia and filopodia, respectively (Mayor and

Etienne-Manneville, 2016). Leader cells also use MMPs to clear a path through the ECM for the migrating collection of cells (Friedl and Wolf, 2008; Nabeshima et al., 2000; Wolf et al., 2007). In some cases the MMPs can be provided by other cell types, such as fibroblasts, which can serve as leader cells (Gaggioli et al., 2007). At the rear of the leader cell, RhoA promotes acto-myosin contraction (Zegers and Friedl, 2014). In collective migration, the force generated by the leader cells is transmitted through adherens junctions to follower cells and can drag the entire group forwards (Caussinus et al., 2008; Reffay et al., 2014).

Invasion and migration can be regulated by the microenvironment. The ECM is one such cue that can influence the migration of tumor cells and is also well known to do so in development and wound healing (Clark and Vignjevic, 2015; Friedl and Alexander, 2011; Friedl and Gilmour, 2009; Gritsenko et al., 2012). The ECM can regulate migration through the orientation of matrix fibers, stiffness of ECM components, and through the presentation of growth factors (Clark and Vignjevic, 2015; Friedl and Alexander, 2011; Gritsenko et al., 2012; Provenzano et al., 2006).

Macrophages can also influence tumor cell migration. Macrophages can be recruited to tumor cells by tumor cell-derived CSF-1. These macrophages can then guide tumor cells towards blood vessels by secreting EGF (Goswami et al., 2005; Wyckoff et al., 2004). Neutrophils are another cell type in the primary tumor can promote migration towards blood vessels (Bald et al., 2014).

Once tumor cells encounter a blood vessel, they can undergo the next step of the metastatic cascade: intravasation (Fig. 1). During intravasation tumor cells enter capillaries and are carried off into circulation. There are a number of barriers that tumor cells need to

overcome in order to intravasate. First, capillaries are surrounded by a basement membrane, which tumor cells may need to degrade in order to intravasate (Kalluri, 2003). Consequently, MMPs and invadopodia have been shown to be required for intravasation (Gligorijevic et al., 2012; Kessenbrock et al., 2010; Kim et al., 1998a). Second, capillaries are supported by cells called pericytes that are embedded within the basement membrane. Pericytes serve to maintain vessel stability and their normal functioning may prevent metastasis (Gerhardt and Semb, 2008; Xian et al., 2006). Finally, endothelial cells form strong connections to their neighbors, which, in some cases, may need be penetrated in order for tumor cells to pass through (Anderberg et al., 2013; Zervantonakis et al., 2012).

Some or all of these barriers may be lacking in vessels within primary tumors. It has been observed that blood vessels within tumors can lack the integrity of normal capillaries and frequently lack pericyte coverage (Jain, 2005). Such leaky vessels may provide little barrier to tumor cell entry. Consistent with this idea, one study has found that the majority of tumor cell intravasation occurs within the core of a tumor rather than at the invasive front (Deryugina and Kiosses, 2017). Blood flow in intratumoral vessels may be quite low due to their poor construction or constriction from the growing tumor (Padera et al., 2004; Tong et al., 2004). Therefore, tumor cells may need to migrate to regions of better flow in order to enter systemic circulation.

Tumor cells have also been claimed to perform vascular mimicry, where tumor cells (rather than endothelial cells) form perfused channels within the tumor (Maniotis et al., 1999). Vascular mimicry has been associated with enhanced metastasis, so it seems possible that

tumor cells could shed from these channels, thereby bypassing some of the barriers presented by conventional blood vessels (Wagenblast et al., 2015).

Macrophages have been shown to promote tumor cell intravasation. The association between a macrophage, a tumor cell expressing the pro-invasive gene MENA, and an endothelial cell has been termed the tumor microenvironment of metastasis (TMEM) (Robinson et al., 2009; Roussos et al., 2011a; 2011b). Increased numbers of such associations have been associated with an increased risk of distant metastasis (Rohan et al., 2014). Intravital imaging of individual TMEMs has shown that macrophages can induce transient vascular permeability and allow intravasation (Harney et al., 2015). These macrophages also induce tumor cells to produce invadopodia through Notch signaling (Pignatelli et al., 2016). Platelets can also induce transient vascular permeability to allow tumor cell entry (Schumacher et al., 2013). Endothelial cells themselves, along with other cell types, can promote intravasation by signaling to tumor cells also via the Notch pathway (Sonoshita et al., 2011). Both macrophages and neutrophils in the tumor can produce angiogenic factors that can lead to leaky vasculature that may be more amenable to tumor cell entry (Lin and Pollard, 2007; Nozawa et al., 2006).

Once in circulation, tumor cells face a number of stresses (Fig. 1). One such stress is attack from NK cells. Interactions with platelets and neutrophils have been shown to protect tumor cells from NK cell surveillance (Kopp et al., 2009; Nieswandt et al., 1999; Spiegel et al., 2016). It has been suggested that the physical forces to which a cell is subjected while flowing through circulation may also lead to cell death (Wirtz et al., 2011). It has been proposed that platelets may provide protection from these forces by coating tumor cells (Labelle and Hynes, 2012).

At the metastatic site, tumor cells can cease transit through circulation after becoming lodged in narrow capillaries that are too small for tumor cells to transit (Massagué and Obenauf, 2016). While the dispersion of tumor cells throughout an organism is due in significant part to the pattern of circulation and random chance, the location of tumor cell arrest may not be an entirely random process. It has been observed that peptides can be generated through *in vivo* phage display that home to the vasculature of specific organs (Pasqualini and Ruoslahti, 1996). This had led to the idea that there are vascular "zip codes" that proteins or cells could use to home to a specific organ's vasculature.

The vasculature of specific organs has been shown to express adhesion molecules that can be used by metastasizing tumor cells to target their arrest. For example, prostate cancer frequently metastasizes to the bone. The bone endothelium is known to constitutively express the adhesion molecule E-Selectin (Schweitzer et al., 1996). It has been shown that prostate cancer expression of the carbohydrate Sialyl-Lewis X (which is recognized by E-selectin) enhances adhesion to the bone endothelium (Barthel et al., 2009; Lehr and Pienta, 1998), suggesting that this adhesion may enhance prostate cancer bone metastasis. In another example, expression of the protein metadherin can promote the homing of breast cancer cells to the lung (Brown and Ruoslahti, 2004; Hu et al., 2009). Furthermore, metastatic colon cancer cells have been shown to be able to adhere to the walls of vessels larger than their diameter suggesting that adhesion molecules rather than physical entrapment can mediate arrest in some cases (Schlüter et al., 2006). Conditioned media experiments have shown that tumor cells can secrete factors to induce adhesion molecules on the endothelium of distant organs

(Hiratsuka et al., 2011). This observation suggests that tumor cells could pre-condition a target organ to become more hospitable in preparation for their arrival (Kaplan et al., 2005).

Stromal cells can also play a role in arrest at the metastatic site. Activated platelets express many adhesion molecules on their surface. It has been hypothesized that a tumor cell coated with activated platelets could use these molecules to aid in adhesion to the endothelium at the metastatic site (Labelle et al., 2014). This adhesion to platelets can be mediated by Sialyl-Lewis X on tumor cells being recognized by platelet P-selectin (Fuster et al., 2003; Kim et al., 1998b). Neutrophils have also been observed to aid in the arrest of tumor cells in the liver and lung (Huh et al., 2010; Spicer et al., 2012a). Inflamed neutrophils can express integrin $\alpha_m\beta_2$ (also known as Mac-1) which binds tumor cell ICAM-1 to promote tumor cell arrest in the liver (Spicer et al., 2012b). Inflamed neutrophils can also release neutrophil extracellular traps (NETS), which are primary composed of DNA and histones (Papayannopoulos, 2018). These NETs have been observed to entrap tumor cells thereby aiding their arrest and metastasis (Park et al., 2016; Cools-Lartigue et al., 2013; Demers et al., 2012).

Once arrested in the vasculature at the metastatic site, tumor cells face mechanical stress from blood flow in narrow capillaries. Tumor cells are frequently observed to be stretched and have even been observed to be ripped apart in vessels with high flow rates (Kienast et al., 2009). Tumor cells can actively defend themselves from these forces. For example, expression of PANX1 in arrested tumor cells protects them from stretch-induced apoptosis (Furlow et al., 2015).

An interesting observation, with implications for the ability of tumor cells to arrest in vessels larger than the diameter of an individual tumor cell, is that tumor cells have been

observed to travel in clusters through circulation in human patients (Aceto et al., 2014; Hong et al., 2016). These clusters can potentially grow to be quite large and contain tens of tumor cells (Long et al., 2016). Furthermore, in addition to tumor cells, clusters have also been observed to contain immune cells, platelets, and stromal cells from the primary tumor such as fibroblasts (Aceto et al., 2014; Duda et al., 2010; Sarioglu et al., 2015). At first glance, it seems obvious that these larger aggregates would be better able to arrest in capillaries than individual circulating tumor cells (CTCs). However, clusters of CTCs have been shown to be able to transit small capillaries in a single file line and reform a spherical aggregate once back in a larger vessel making their role in arrest unclear (Au et al., 2016).

The role of clusters in metastasis in general is also an area of active research. Studies from human patients have shown that higher levels of CTC clusters are a poor prognostic indicator in multiple tumor types (Cohen et al., 2008; Cristofanilli et al., 2004; de Bono et al., 2008). Additionally, in mice, clusters have been shown to be better at seeding metastases than individual tumor cells (Aceto et al., 2014). Further evidence of a role for clusters in metastasis formation comes from experiments analyzing the clonality of metastases. It would be expected that metastases derived from single CTCs would be monoclonal while metastases derived from clusters would be polyclonal. When the clonality of metastases was analyzed in a murine model of metastasis, polyclonal metastases were detected indicating that some metastases may have arisen from CTC clusters (Maddipati and Stanger, 2015).

Patient data seem to suggest that most human metastases are derived from a single progenitor cell (ie. are monoclonal) (Campbell et al., 2010; Liu et al., 2009). A factor complicating these analyses is that tumor cells have been observed to be able to travel from a

metastasis back to a primary tumor or from one metastasis to another, a process referred to as re-seeding (Kim et al., 2009). Cells arriving at a metastasis after establishment by a single progenitor clone could result in a metastasis being polyclonal at the time of biopsy but monoclonal early in its evolution. There is some evidence that this process may occur in human patients (Hong et al., 2015). The clonality (and origin, whether from clusters or single cells) of metastases requires further study.

The next step in the metastatic cascade following arrest is exit from blood vessels, which is called extravasation (Fig. 1). While there have been reports that tumor cells can grow intravascularly, in most cases, tumor cells need to exit circulation in order to grow into a new tumor as the intravascular environment is generally hostile to tumor cells due to the physical stresses caused by blood flow, induction of anoikis due the lack of ECM attachment, as well as attack by NK cells (Wong et al., 2002; Zhang et al., 2010b; Al-Mehdi, AB et al., 2000; Gupta et al., 2007; Strilic and Offermanns, 2017).

The difficulty of extravasation varies depending on the organ. In the liver, for example, the endothelial layer is discontinuous and contains many openings (termed fenestrae), which may make extravasation relatively easy. In the brain on the other hand, the endothelial cells are tightly linked and their barrier function is further supported by astrocytes (Abbott et al., 2006; Aird, 2007). In the lung, another common site of metastasis, the endothelium forms a strong barrier as well (Aird, 2007). Consistent with the concept of organs varying in their extravasation difficulty, genes have been found that promote extravasation in an organ-specific manner. For example, ST6GALNAC5 enhances breast cancer extravasation in the brain (Bos et al., 2009)

while COX2, in combination with MMP1,2, and EREG, can mediate breast cancer extravasation in the lungs and brain (Gupta et al., 2007).

Much of our understanding of extravasation has come from studies of how leukocytes extravasate at sites of inflammation (Vestweber, 2015). These data have provided the framework for understanding tumor cell extravasation. However, there are some fundamental differences between the two. Firstly, tumor cells extravasate much more slowly than leukocytes *in vivo* (Reymond et al., 2013). Secondly, leukoytes have two routes through the endothelium: transcellular and paracellular. In the transcellular route, leukocytes travel through the endothelial cells themselves in a channel that forms between the endothelial apical and basal sides. In the paracellular route, leukocytes squeeze between endothelial cells through junctions (Vestweber, 2015). The majority of data from tumor cells suggest that they extravasate via the paracellular route *in vivo* (Leong et al., 2014; Schumacher et al., 2013).

Tumor cells can activate signaling pathways in endothelial cells to allow their passage. For example, tumor cells can secrete Angiopoietin-like 4 (Angptl4), CCL2 and CXCL12, to promote extravasation by a variety of tumor types. Integrin $\alpha_v\beta_3$ has also been shown to promote trans-endothelial migration (Felding-Habermann et al., 2001; Weber et al., 2016). Another mechanism tumor cells use to cross the endothelium is to simply induce endothelial cell death through necroptosis (Strilic et al., 2016). Tumor cells, through Rac and Cdc42 signaling, generate protrusions at the sites of junctions, and these protrusions are required for efficient trans-endothelial migration (Reymond et al., 2013). As in cell migration, Rho/ROCK signaling also plays a role in extravasation (Reymond et al., 2013).

Leukocytes recruited to arrested tumor cells have also been shown to aid in extravasation. Activated platelets can secrete TGF-β, which can induce a partial EMT to enhance extravasation (Labelle et al., 2011). Platelets can also release ATP to activate P2Y2 on endothelial cells to allow tumor cell passage through the endothelial barrier (Schumacher et al., 2013). Neutrophils and macrophages are also recruited to arrested tumor cells and can contribute to extravasation as well (Gil-Bernabé et al., 2012; Labelle et al., 2014). Neutrophils can enhance extravasation through the secretion of MMPs and inflammatory cytokines (Spiegel et al., 2016). Macrophages can produce VEGF-A to induce vascular permeability which enhances tumor cell extravasation (Qian et al., 2011; 2009).

Once past the endothelial cells, the endothelial basement membrane is the final barrier that tumor cells must cross. Experiments have shown that disrupting ITGB1 can prevent tumor cells from degrading the basement membrane leaving them trapped between the endothelium and the basement membrane (Chen et al., 2016b).

Once tumor cells have extravasated, they may enter a state of dormancy, which can last years or even decades (Fig. 1). Dormancy may be a formidable barrier to the development of overt metastases (Kienast et al., 2009; Luzzi et al., 1998b). Dormant cells are often negative for proliferation markers (such as Ki67), are positive for the cell cycle inhibitor p27, and show high levels of p38 signaling (Sosa et al., 2014). The microenvironment at the metastatic site has been shown to be a key regulator of dormancy. Dormant cells are often found in specific niches *in vivo* (Ghajar et al., 2013). Stromal cells can produce dormancy-inducing molecules such as thrombospondin, TGF-β, BMP4/7, and Gas6 (Bragado et al., 2013; Gao et al., 2012; Ghajar et al., 2013; Kobayashi et al., 2011; Taichman et al., 2013). Some factors, such as SPARC, can be

secreted by the tumor cells themselves to maintain dormancy (Sharma et al., 2016). General features of the microenvironment, such as hypoxia, are also able to induce a dormant state (Endo et al., 2017; Fluegen et al., 2017; Hoppe-Seyler et al., 2017). Downstream of many of these signals, the transcription factor NR2F1 has been shown to be a key regulator of dormancy (Sosa, 2016; Sosa et al., 2015).

A question related to dormancy is when does metastasis occur during tumor progression. The discussion so far has used the implicit assumption that metastasis is an event that occurs late during tumor progression. However, this may not always be the case. On one hand, sequencing of pancreatic cancer patient primary tumors and metastases suggests that metastasis is a late event (Yachida et al., 2010). On the other hand, disseminated tumor cells have been detected in patients diagnosed with DCIS, a benign lesion that is believed to be the precursor to breast cancer (Banys et al., 2012). Furthermore, circulating epithelial cells have been detected in patients with benign inflammatory conditions, suggesting that dissemination can occur in the absence of transformation (Pantel et al., 2012). Experiments in mice have also demonstrated that metastasis can occur early during tumor development (Harper et al., 2016; Hosseini et al., 2016; Hüsemann et al., 2008). Determining when metastasis occurs during tumor progression is a key question for cancer researchers as it has implications for treatment. If metastasis occurs early during tumor development, these early disseminated tumor cells could lie dormant for years and be the origin of relapses well after a primary tumor has been removed.

The outgrowth of metastases (and escape from dormancy) is dependent on a cell adapting to the local microenvironment, which can be quite different from that of the primary

tumor. In order to proliferate at the metastatic site, cells must develop adhesions to the ECM (Aguirre Ghiso et al., 1999; Barkan et al., 2010; Shibue et al., 2013; 2012). Cells can also influence changes at the metastatic site to enable their outgrowth. The ECM protein Tenascin C has been shown to be required for breast cancer cell metastatic outgrowth in the lung. In small tumors, Tenascin C is made exclusively by tumor cells. However, tumor cells eventually induce the lung stroma to produce Tenascin C, thereby conditioning the lung microenvironment to suit their needs (Oskarsson et al., 2011). Many additional ECM proteins have also been shown to be important for metastatic colonization (Malanchi et al., 2011; Naba et al., 2014) indicating that remodeling the ECM at the metastatic site is an important part of metastasis. In the bone, metastatic tumor cells engage with osteoclasts or osteoblasts to grow as osteolytic or osteoblastic metastases respectively (Weilbaecher et al., 2011). In the brain, astrocytes secrete plasminogen activator, which leads to the cleavage of FasL to an activated form that can kill metastatic tumor cells. In order to survive in the brain, tumor cells produce serpins, which inhibit plasminogen activator (Valiente et al., 2014). As with primary tumors, the induction of angiogenesis is also a key step in the outgrowth of metastases in some cases (Chambers et al., 2002; Folkman, 1995; 2002; Holmgren et al., 1995; Joyce and Pollard, 2008; Kienast et al., 2009; O'Reilly et al., 1994; Sosa et al., 2014).

Cells may also need to adapt to the metabolic environment at the metastatic site, as the target organ may have very different levels of oxygen and nutrients compared to the primary tumor (Schild et al., 2018). In the brain, a wide variety of metastatic tumor cells have been shown to develop the ability to use acetate as an energy source, which is reminiscent of the metabolism of endogenous brain cells and a metabolic pathway not used in the organ of origin

for these metastases (Mashimo et al., 2014). The lungs have relatively high levels of oxygen and glucose compared to most organs and especially compared to primary tumors, which may be hypoxic. Unsurprisingly, oxidative stress is a barrier to lung metastasis and metastatic tumor cells have been seen to adopt multiple mechanisms to defend against it (LeBleu et al., 2014; Piskounova et al., 2015; Stresing et al., 2013). The liver, on the other hand, has low levels of oxygen and glucose. In order to adapt to this microenvironment, tumor cells switch to glycolytic metabolism through HIF-1α/PDK1 signaling (Dupuy et al., 2015). Metastatic cells in the liver can also adapt to take advantage of the abundant creatine that is produced by hepatocytes to aid in their growth (Loo et al., 2015).

Interactions with macrophages and neutrophils are also important for the outgrowth of metastases at the metastatic site. Macrophages can directly aid the growth of tumor cells by binding to VCAM1 on tumor cells (Chen et al., 2011). Neutrophils can enhance the growth of metastases by expanding the pool of metastasis-initiating cells (Wculek and Malanchi, 2015). Neutrophils can also inhibit metastasis. Tumor-bearing mice have been found to contain a set of neutrophils with tumoricidal activity that can inhibit metastasis (Granot et al., 2011). On the other hand, the majority of studies report that neutrophils enhance metastasis (Coffelt et al., 2016). Reconciling these conflicting data will be an important step in improving our understanding on how the microenvironment influences growth at the metastatic site.

The metastatic cascade as discussed above has proven to be a useful framework for understanding metastasis (Fig. 1). However, it is not a complete description of the metastatic process. One aspect of metastasis that is not well integrated into the metastatic cascade is the relation of lymphatic metastases to distant metastases (Wong and Hynes, 2006). A key question

in the field is whether lymph nodes are layover destinations for tumor cells on their way to distant organs or merely signs that a tumor has become able to metastasize. What is clear, is that metastasis to draining lymph nodes is a frequent clinical observation that is negatively correlated with long-term survival (Pereira et al., 2015; Kawada and Taketo, 2011). Compared with capillaries, lymphatic vessels lack many barriers to entry by tumor cells such as continuous basement membrane or strong endothelial cell-cell junctions (Stacker et al., 2014). Furthermore, tumors have been shown to induce increased flow through draining lymphatics, which may enhance their movement through these vessels (Ruddell et al., 2008). In mouse models, tumor cells can also induce lymphangiogenesis (the growth of new lymphatic vessels) within a tumor through the production of VEGF-C (Karpanen et al., 2001; Mandriota et al., 2001; Skobe et al., 2001) and VEGF-D (Stacker et al., 2001) to promote distant metastasis. Expression of these genes is associated with lymph node metastasis in human cancer (Schietroma et al., 2003).

Once tumor cells are in a draining lymph node, where they go remains an open question. One genomic study of mouse primary tumors, lymphatic metastases, and distant metastases has identified a liver metastasis that appears to be derived from a lymph node metastasis (McFadden et al., 2014). However, this study also found many distant metastases that did not have lymphatic origins. More recent studies have shown that tumor cells can traffic from lymph nodes to seed distant metastases and have observed intravasation from lymph nodes *in vivo* (Brown et al., 2018; Pereira et al., 2018). However, in human patients, the majority of distant metastases seem to derive from the primary tumor as opposed to from lymph node metastases (Naxerova et al., 2017).

Lymph node metastases may merely be a sign that a tumor has acquired aggressive metastatic properties and is actively spreading. One of these aggressive metastatic properties might be evasion from the immune system (Vesely et al., 2011). It even appears that lymph nodes may play an active role in aiding tumor cell evasion from the immune system. In support of this model, it has been observed that direct injection of tumor cells into naive lymph nodes results in their rapid destruction. However, when tumor cells are injected into a draining lymph node of an established primary tumor, they survive and can grow into a metastasis (Preynat-Seauve et al., 2007). Furthermore, tumor cell VEGF-C expression has been shown to induce tumor cell tolerance in mice (Lund et al., 2012).

In order to metastasize to distant organs, transit through hematogenous circulation seems to be the primary route. Lymphatic circulation re-connects with hematogenous circulation at the subclavian veins, which are quite distant from most primary tumors. Unsurprisingly, this connection point does not seem to be used by metastasizing tumor cells leaving lymph nodes (Brown et al., 2018). It appears that tumor cells residing in lymph nodes enter hematogenous circulation through capillaries in lymph nodes in a manner analogous to cells at a primary tumor (Pereira et al., 2018). Following entry into circulation, the steps of metastasis for tumor cells from a primary tumor or lymph node tumor are identical. Once a tumor cell intravasates from a lymph node, the steps of the metastatic cascade are identical to a tumor cell coming from a primary tumor.

Intravital Imaging of Metastasis

Metastasis is a complex and dynamic process. The many steps occur in multiple locations and on time scales ranging from seconds to weeks in model organisms. In order to truly understand metastasis, it is important to be able to image the metastatic process as it occurs *in vivo* with single-cell resolution. Most of the results described above used end-point assays or fixed organs harvested at single time points during metastasis. While these studies have revealed much about metastasis, they are missing many of the details of that can only be obtained from intravital imaging studies. In the next section, I will review the current state of the art of intravital imaging in rodents and how these techniques have been used to increase our understanding of metastasis.

Intravital Imaging of Metastasis in Rodents

As reviewed above, the *in vivo* microenvironment has profound effects on metastasizing tumor cells. While *in vitro* models of steps of the metastatic cascade continue to improve, they are still unable to completely replicate the *in vivo* setting. Intravital microscopy allows the study of the steps of metastasis in the tumor cells' natural environment. These studies, some of which have been alluded to earlier, have greatly improved our knowledge of metastasis. Mice are currently the most commonly used organism to model cancer. As such, this section will focus first on intravital imaging studies in mice.

Intravital imaging is routinely used at the whole-organism scale in cancer research to visualize the growth and spread of tumors. Tumor cells that express luciferase or recently developed far-red and infrared fluorescent proteins allow tumors to be visualized through the skin and tissue of a mouse without any surgical manipulation (Filonov et al., 2011; Zinn et al.,

2008). These reagents allow mice to be imaged repeatedly over time to follow the effects of treatment on tumor growth and metastasis. However, at its root, metastasis is the interaction of single (or small groups of) tumor cells with their environment. Therefore, intravital imaging with single-cell resolution is required (Sahai, 2007).

Intravital imaging at the microscopic scale is called intravital microscopy and has been aided by rapid advances in confocal microscopy. A key problem in imaging thick samples (such as live organisms) is that light from above and below the focal plane can interfere with the image, making interpretation difficult or impossible. Confocal microscopy places a pin hole in focus with (confocal to) the focal plane just before the detector. This pinhole blocks all out-of-focus light allowing a thin optical section to be imaged (Paddock, 2014). An added benefit of this approach is that multiple optical sections taken at different depths can be recombined to produce a 3-dimensional image (Paddock, 2014). Given that the pinhole blocks out the majority of light emitted from the sample, the strong excitation provided by a laser is critical to getting enough signal from a sample. Today, laser scanning confocal microscopy is the dominant technique. In this approach, the laser is scanned across the sample in the XY plane to induce fluorescence at one point at a time. This allows the detector to be a highly sensitive photo-multiplier tube. The final image is constructed from the photomultiplier tube signal at each point as the laser scanned across the sample (Shotton, 1989).

The development of two-photon microscopy has greatly increased the depth of imaging that can be achieved in intravital microscopy. Human and mouse tissues are most transparent in the near-infrared range and become progressively more opaque towards the UV or deeper in the IR range (Smith et al., 2009). Standard confocal microscopy requires an excitation

wavelength that is less than the emission wavelength. This fact often places the excitation wavelength in regions of the spectrum that are not good at penetrating tissue and makes imaging more than 100um into tissue difficult (Ustione and Piston, 2011). Two-photon microscopy takes advantage of a physical phenomenon where two photons of twice the excitation wavelength that simultaneously hit a fluorescent molecule can combine to excite the fluorophore (Ustione and Piston, 2011). This allows the excitation wavelength to be in the near-infrared window and can be used to image up to 700μm into tumors (Jain et al., 2002). The brain has proven to be the most amenable organ for two-photon microscopy with imaging depths of up to 1600μm reported (Kobat et al., 2011). This great depth allows imaging of metastases deep within the organ. The key technological breakthrough that led to two-photon microscopy was the development of a pulsed laser that can generate the photon flux sufficient for the two-photon process to occur (So et al., 2000). Two-photon microscopy can also detect second harmonic signals which allow ECM fibers to be imaged without any exogenous labeling (Campagnola and Dong, 2011).

Metastasis generally occurs in organs that are beyond the reach of intravital microscopy (and even two-photon microscopy) without surgical intervention. The bone marrow in the skull, the mammary fat pad, and the liver can only be imaged following the creation of a skin flap that can be pulled back to access the organ (Ewald et al., 2011; Mazo et al., 1998; Yang et al., 2002). Early intravital imaging studies used this approach to study migration in primary tumors as well as arrest and extravasation at the metastatic site (Farina et al., 1998; Luzzi et al., 1998a; Morris et al., 1993; Sipkins et al., 2005).

While these techniques are simple, they generally do not allow repeated imaging over extended time periods. Longer-term imaging has been enabled by the development of surgically implanted imaging windows (Alieva et al., 2014; Kitamura et al., 2017). Imaging windows consist of a coverslip that is surrounded by a mounting apparatus that can be surgically attached to an animal. Imaging windows have been designed for imaging the brain, mammary fat pad, and abdominal organs such as the liver and intestine (Kedrin et al., 2008; Kienast et al., 2009; Ritsma et al., 2013). Once successfully implanted, these windows can be used to image repeatedly over the course of weeks. Long-term imaging through these windows has allowed the careful study of the behavior of metastatic tumor cells in the brain and liver (Kienast et al., 2009; Ritsma et al., 2012). These detailed studies have revealed dynamic steps in the metastatic process that had previously been inaccessible to study.

Another important organ for the study of metastasis has been the lung, which has been especially useful for the study of the temporal dynamics of metastasis. In these studies, tumor cells are injected intravenously into the tail vein of a mouse. As the lungs are the first capillary bed downstream, most tumor cells become trapped there. By removing the lungs at various time points post-injection, the timing of extravasation and the interactions between tumor cells and stromal cells have been elucidated (Labelle and Hynes, 2012). The study of cells at fixed time points has its limitations, and imaging windows to perform intravital imaging in the lung have been developed in response (Looney et al., 2010).

The lung poses special challenges for intravital imaging as the lung is constantly in motion in a live animal. One solution has been to utilize vacuum pressure to adhere the lung to the window and minimize lung movement. More recently, a permanent window that does not

require a vacuum has been developed (Entenberg et al., 2017). Through these systems, the early responses of the immune system to tumor cells as well as the growth of tumor cells into micrometastases have been imaged (Headley et al., 2016).

The development of new fluorescent reagents has increased the power of intravital imaging to unravel the processes that occur during metastasis. New fluorescent proteins which are brighter or have emissions shifted towards the near-IR continue to be developed (Matela et al., 2017; Rodriguez et al., 2016). Recently, photoactivatible, photoswitchable, and photoconvertible proteins have been developed. These proteins can be induced, usually through violet illumination, to change their fluorescent properties. Photoactivatable proteins are induced to become fluorescent following illumination. Photoswitchable proteins can be repeatedly switched between two different fluorescent states, for example, between red fluorescence and green fluorescence. Finally, photoconvertible proteins can be converted between two fluorescent states but this conversion is irreversible (i.e from green to red but not back again). These proteins allow specific cells to be tagged and followed at later time points and have been used to study metastasis by tracking migration in primary tumors as well as to track the path that metastasizing tumor cells take through an animal (Gligorijevic et al., 2012; Pereira et al., 2018).

Fluorescent protein techniques with long histories in *in vitro* systems can also be used to gain new insights with intravital imaging. For example, classical fluorescent fusion proteins allow the behavior of individual proteins or protein complexes to be studied in vivo. In one such example, a fluorescent N-WASP fusion protein has been used to monitor the role of invadopodia during intravasation in primary tumors (Gligorijevic et al., 2012). Another group of

fluorescent reagents commonly used *in vitro* are FRET-based reporters. FRET reporters have been used extensively to monitor signaling pathways *in vitro* (Rowland et al., 2015) and have been used *in vivo* to determine signaling dynamics during metastasis (Timpson et al., 2011).

In the experiments described above, fluorescent proteins were placed under ubiquitous promoters and were subsequently expressed constitutively. However, fluorescent proteins can be placed under conditional reporters to label specific cell types, respond to signaling pathways, or indicate cell state changes. For example, mice have been generated with various labeled stromal cell types (including endothelial cells and various myeloid cells), which has allowed imaging *in vivo* of the interactions between stromal cells and tumor cells (Harney et al., 2015; Headley et al., 2016; Kienast et al., 2009; Lohela et al., 2014). When the conditional promoter is in the tumor cells themselves, fluorescent proteins can be used to monitor cell-state changes such as EMT or the activity of signaling pathways such as the TGF-β pathway (Fischer et al., 2015; Giampieri et al., 2009). The induction of expression of a fluorescent protein can also be achieved with Cre-responsive systems. In one elegant study using Cre recombinase, extracellular vesicles were demonstrated to be able to transmit mRNAs from primary tumor to metastases in mice (Zomer et al., 2015). Tumor cells can be engineered to have multiple fluorescent proteins that are randomly activated, such the confetti system (Livet et al., 2007; Schepers et al., 2012; Snippert et al., 2010). These systems give individual cells unique fluorescent colors and have been used to track the clonal dynamics of metastases (Maddipati and Stanger, 2015).

Intravital imaging in mice has considerably advanced our knowledge of metastasis. However, the techniques involved, including the surgical implantation of imaging windows,

remain quite complicated and can be subject to a high failure rate (Jeff Wyckoff, personal communication). These difficulties have restricted the routine use of intravital microscopy to a few labs. When this thesis work began, zebrafish embryos had been recently demonstrated to be a powerful system for imaging aspects of metastasis (Stoletov et al., 2010). Furthermore, a number of developments suggested that intravital imaging in adult zebrafish could be feasible and significantly less complicated than imaging in mice (Stoletov et al., 2007; White et al., 2008). In the next section, I will review the use of zebrafish as a model to study metastasis.

The Use of Zebrafish To Study Metastasis:

When this work began, there were rapid advances being made in the use of zebrafish to study metastasis. There had recently been a proliferation of new genetic models that promised to expand the types of cancer that could be studied using zebrafish. In addition, a new line of zebrafish that is transparent throughout its life promised to provide a unique tool for intravital imaging in adults (White et al., 2008). The field was also undergoing an exciting transition. Despite more than 50 years of use as a model organism, zebrafish had only recently been developed as a model system to study metastasis (Grunwald and Eisen, 2002; White et al., 2013). The new potential avenues of zebrafish research opening up combined with the strengths of the zebrafish model system led to their addition to our research program.

Zebrafish possess a number of traits that make them an attractive model system for the study of metastasis. First, the physiology of zebrafish is generally conserved with humans. Zebrafish contain most of the same organs as mammals with a few notable exceptions such as mammary glands, lungs, and the prostate (White et al., 2013). Another difference is that, in

adult zebrafish, the head kidney is the site of hematopoiesis rather than the bone marrow (Davidson and Zon, 2004). Despite the difference in the location of adult hematopoiesis, zebrafish have a robust immune system which contains the same major cell types as the mammalian immune system (Renshaw and Trede, 2012; Trede et al., 2004a). Consistent with their conserved physiology, tumors in zebrafish are histologically similar to their human counterparts (Berghmans et al., 2005a).

At the genetic level, there is also considerable conservation. While zebrafish and mammals diverged 450 million years ago, both contain the same basic complement of genes. Approximately 70% of human genes have a known ortholog in zebrafish (Howe et al., 2013). A complication in identifying orthologs in zebrafish is that the teleost lineage underwent a whole genome duplication event 350 million years ago (Meyer and Schartl, 1999). It seems likely that as our understanding of the zebrafish genome improves, more orthologs will be identified (Postlethwait, 2007). Of the orthologs that have been identified, many are functionally conserved. For example, function of key oncogenes and tumor suppressor genes are conserved between mammals and zebrafish. Inactivating mutations in the key tumor suppressors P53, PTEN, or APC lead to the development of tumors in mutant zebrafish (Berghmans et al., 2005b; Faucherre et al., 2008; Haramis et al., 2006). Conversely, over-expression or expression of oncogenes with activating mutations such as Myc, $BRAF^{V600E}$ or $KRAS^{G12D}$ also leads to the development of tumors in zebrafish (Langenau et al., 2007; 2003; Patton et al., 2005). When these tumors are analyzed at the genetic level, there is considerable similarity between zebrafish and human tumors both in the structural features of the genome, such as aneuploidy,

as well as in patterns of gene expression (Lam et al., 2006; Rudner et al., 2011; Zhang et al., 2010a).

In addition to their conservation with mammals, zebrafish have many other benefits as a model system. Zebrafish are small and much cheaper to house than mice. Zebrafish also have unmatched fecundity for a vertebrate model. A single mating pair can produce up to 200 embryos every week (Lieschke and Currie, 2007). These characteristics allow large genetic screens to be conducted that would be unmanageable in mice. The development of the Tol2 transposon system allows the high efficiency generation of transgenic animals through technically simple injections of embryos at the one-cell stage (Kawakami et al., 2000). The Tol2 system has recently been engineered to deliver CRISPR reagents, allowing the rapid generation of knockout animals (Ablain et al., 2015; Chang et al., 2013; Hwang et al., 2013a; 2013b; Jao et al., 2013).

One of the key reasons why zebrafish appeared to be a promising system for studying metastasis was the development of a line of zebrafish that is transparent throughout its entire life cycle. This line, called Casper for its ghost-like appearance, is the result of a cross between the *nacre* and *roy* mutant lines (White et al., 2008). Zebrafish have three types of pigment cells: dark black melanophores, highly reflective iridophores, and yellow xanthophores (Rawls et al., 2001). *Nacre* mutants lack melanophores while *roy* mutant fish lack iridophores (D'Agati et al., 2017; Lister et al., 1999; Ren et al., 2002). Zebrafish tissue is naturally fairly transparent so when the opaque melanophores and reflective iridophores in the skin are removed, this renders the animal amenable to intravital imaging without the need for the surgical implantation of imaging windows. Casper fish have been used to image metastasis using whole

body fluorescence imaging (Heilmann et al., 2015). Furthermore, individual metastases can be imaged with single-cell resolution (Tang et al., 2016).

Zebrafish have become a popular system in which to model cancer, however, their use to model metastasis is a relatively recent development. One reason for this lag has been the lack of reliable cell culture techniques in zebrafish. The development of cell culture technology was a major advance in the field of cancer research (Fogh et al., 1977). The ability to derive cell lines for in vitro study or manipulation has consequently been fundamental for the study of metastasis (Khanna and Hunter, 2005). The recent development of a protocol to derive cell lines from zebrafish tumors promises to transform zebrafish cancer research. The first line generated in our laboratory by Amy McMahon using this technique was called ZMEL1 (Heilmann et al., 2015). The ZMEL1 cell line can form tumors following orthotopic implantation and can metastasize (Heilmann et al., 2015). ZMEL1 cells can be infected with a lentiviral transduction system *in vitro*, which will allow genetic manipulation prior to transplantation (Fazio et al., 2017). Historically, RNAi has failed to work in zebrafish, however, the genetic basis for this failure, two substitution mutations in Ago2, has been recently identified (Chen et al., 2017; Kelly and Hurlstone, 2011). This development may potentially bring this technology, which is commonly used in mammalian cell lines, to zebrafish to complement CRISPR knockouts.

Due to the absence of clonal zebrafish lines, the ZMEL1 cell line is (and most transplantable zebrafish tumors are) not syngeneic with any individual fish (Moore and Langenau, 2016). Therefore, various methods of immunosuppression are required for successful engraftment. Originally, fish were irradiated prior to transplantation (Heilmann et al.,

2015). However, the recent development of immunocompromised lines of zebrafish has allowed transplantation without irradiation. Zebrafish have been developed with a frame-shift mutation in the *rag2* gene. These fish lack T-cells and are able to accept other zebrafish tumor transplants (Tang et al., 2014). Tumors can be repeatedly transplanted into these fish in classical *in vivo* selection experiments to generate tumors with high and low metastatic potential (Tang et al., 2016). More recently, fish with mutations in *prkdc*, the gene which is responsible for the SCID phenotype in mice and humans, have been developed which lack both B and T cells (Moore et al., 2016). These immunocompromised fish are valuable tools which allow transplantation without further manipulation such as irradiation.

While the transplantation of zebrafish tumors has become routine, xenotransplantation of human and mouse cells into adult zebrafish remains challenging. Although there have been some anecdotal reports of successful xenotransplantation, there is currently no standard approach (Eden et al., 2015; Stoletov et al., 2007; Zhang et al., 2014). My work in the course of this thesis has highlighted the difficulty in reproducing of some of these approaches (see Chapter 2) (Benjamin and Hynes, 2017). This may be due to the generation of similar lines by different groups. For example, two lines of *prkdc* mutant zebrafish were generated by different groups around the same time. One line was shown to allow engraftment of tumor cells, albeit with low efficiency, while the other was unable to accept xenotransplanted human tumor cells (Benjamin and Hynes, 2017; Jung et al., 2016). One approach that seems promising is tolerizing zebrafish to human cells. In this approach, small numbers of lethally irradiated human tumor cells are injected into 2-day-old embryos. Following injection, the embryos develop normally into adults. When these adults are challenged with the originally injected tumor cell line,

engraftment is successful, indicating that tolerance has been achieved (Zhang et al., 2016). However, this approach is labor-intensive as each fish for an experiment must be generated through these injections. A simple, reliable method for xenotransplantation into adult zebrafish currently remains elusive.

One response to the challenges of xenotransplantation into adults has been to use embryos instead. Zebrafish embryos do not have an adaptive immune system until one month post-fertilization, so they will accept human and mouse xenografts (Trede et al., 2004b). This ease of xenotransplantation has made zebrafish embryos a more popular system for studying metastasis than zebrafish adults to date. Some of the advantages of zebrafish embryos are that even wild-type embryos are transparent and develop outside the mother, which allows experimental manipulation and imaging. Furthermore, by 2 days post-fertilization (dpf), the time point used in most studies, embryos have a fully functional closed circulatory system, a key requirement for studies of metastasis (Isogai et al., 2001). Moreover, embryos fit in 96 well plates and can absorb drugs from the water, which can allow high-throughput screens in a living vertebrate (MacRae and Peterson, 2015).

Zebrafish embryos can also be used to model tumor cell interactions with the microenvironment. Despite lacking an adaptive immune system, embryos have functional innate immune cells such as macrophages and neutrophils by 2dpf (Davidson and Zon, 2004). Furthermore, zebrafish lines have been generated with a wide number of fluorescently-labeled cell types, including macrophages, neutrophils, endothelial cells, and thrombocytes (Ellett et al., 2011; Lawson and Weinstein, 2002; Lin et al., 2005; Renshaw et al., 2006). Due to the ease of imaging in the embryo, these lines have proven to be valuable tools for studying tumor cell

interactions with the stroma during metastasis (Chen et al., 2016a; He et al., 2012; Nicoli and Presta, 2007; Nicoli et al., 2007; Roh-Johnson et al., 2017; Stoletov et al., 2010).

Human immune cells can also be injected into embryos to study tumor-immune cell interactions (Wang et al., 2015). The ability to transplant functional human immune cells is especially important as many cytokine-receptor interactions are not conserved between humans and zebrafish (Svoboda et al., 2016). Other microenvironmental factors, such as hypoxia, can also be modeled by changing the environment in which embryos are housed to study their role in metastasis (Lee et al., 2009; Rouhi et al., 2010).

Finally, morpholino technology can be used to rapidly generate knockdown embryos (Nasevicius and Ekker, 2000). These embryos can then be used to study the effects of knocking down microenvironmental genes on metastasis (He et al., 2012). Given the months to years it takes to generate a knockout mouse, the ability to rapidly assay the effects of gene depletion in the microenvironment is a major advantage of zebrafish embryos.

In the metastasis field, metastasis experiments can broadly be divided into spontaneous and experimental metastasis assays. In spontaneous metastasis assays, there is a primary tumor and the entire metastatic cascade is modeled as tumor cells metastasize from this primary tumor. In experimental metastasis assays, tumor cells are injected directly into circulation, bypassing the early steps of the metastatic cascade (Gómez-Cuadrado et al., 2017). Through these assays, the steps in metastasis in which a gene may be functioning can be identified.

Spontaneous and experimental metastasis can both be performed using zebrafish embryos (Fig. 2A). Spontaneous metastasis assays can be performed by injecting tumor cells into the perivitelline space above the yolk sac . Cells will metastasize from these "primary" tumors to the tail of the fish. A cell line's metastatic propensity in such assays was well correlated to its behavior in mice, suggesting that many aspects of metastasis are conserved in the embryo system (Teng et al., 2013). Cells injected into this location have also been used to study the interaction of tumor cells with the innate immune system during the early steps of metastasis. Cells can also be injected into the pericardial space to form a primary tumor. This method has been used to study the invasion of heterogeneous mixtures of cells (Chapman et al., 2014).

Experimental metastasis assays are also possible in zebrafish embryos (Fig. 2B). Generally, these are performed by injecting tumor cells into the Duct of Cuvier, which is a large vessel in the embryo that drains directly into the heart. Following injection, embryos can be imaged for hours at a time, providing a powerful platform to study the events in circulation and at the metastatic site. For example, zebrafish embryos have been used to study the behavior of CTCs in circulation and show that they can deform to transit narrow capillaries (Au et al., 2016). Zebrafish have also been used to study arrest, extravasation, and migration at the metastatic site (He et al., 2012; Stoletov et al., 2010).

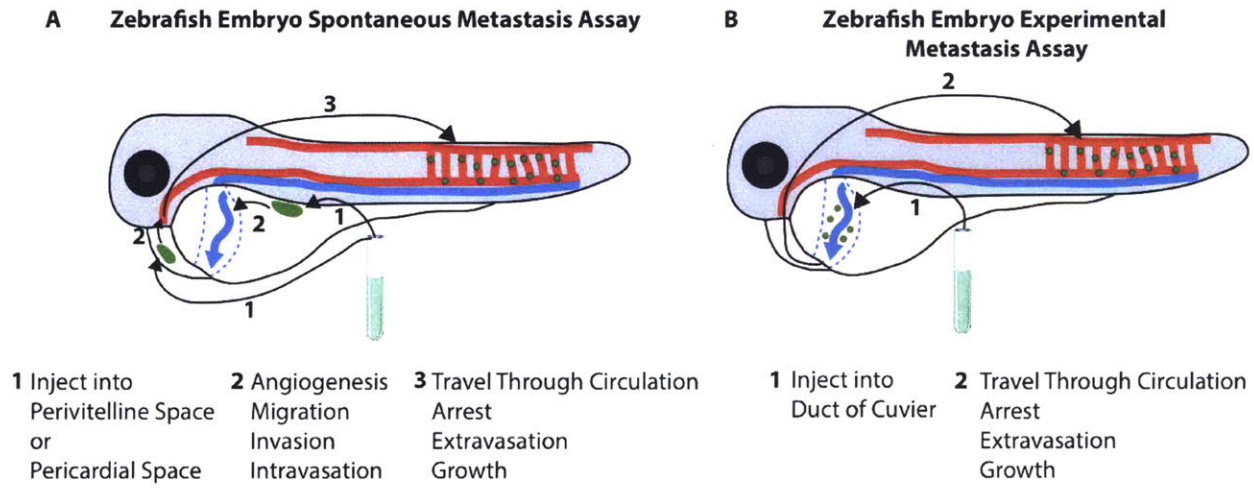

Figure 2. Zebrafish embryo metastasis assays. (A) Spontaneous metastasis assays may be performed by (1) generating a "primary" tumor through injections into the perivitelline space or the pericardial space. (2) A number of aspects of metastasis can be assayed at these "primary tumors". (3) Cells can metastasize from the "primary tumor" allowing the study of latter steps of the metastatic cascade as well. (**B**) Experimental metastasis assays may be performed by (1) injecting cells into circulation via the Duct of Cuvier. (2) These cells then travel through circulation to other locations in the embryo allowing the study of the latter steps of the metastatic cascade. Figure 2 was generated from modified Servier Medical Art under a Creative Commons 3.0 Unported License (https://smart.servier.com).

In summary, zebrafish adults and embryos can both be used as systems to model metastasis. Given that cancer is primarily a disease of adults, the ability to model cancer in an adult microenvironment is a major strength of adult zebrafish (U.S Cancer Statistics Working Group). However, the inability to transplant human cell lines, which have well characterized metastatic phenotypes and are easy to manipulate genetically, is a major limitation. The ability to xenotransplant human cells makes embryos a powerful system for studying metastasis. However, it remains unclear how well the embryonic microenvironment replicates the situation in adult patients during metastasis. Given the complementary strengths of adults and embryos, both were used in the work described in this thesis.

Intravital Imaging of Metastasis in Zebrafish:

This thesis set out to use zebrafish (adults and embryos) as an intravital imaging system to better understand the events at the metastatic site. It has been estimated that less than 0.01% of tumor cells that are shed from a primary tumor grow into metastases (Fidler, 1970). This statistic indicates that the barriers found in circulation and at the metastatic site are rate-limiting for metastasis. Therefore, a better understanding of the events at the metastatic site may provide insights that could be used in the clinic to prevent metastasis.

In **Chapter 2**, I will review the state of intravital imaging of metastasis when this work began and how zebrafish had previously been used to image metastasis. I will then discuss the development of new methods to use adult Casper zebrafish for the live imaging of metastasis. Finally, I will show the utility of these methods by following individual cancer cells at the metastatic site for two weeks as they grow from single cells to macroscopic metastases.

In **Appendix A**, I will first describe our attempts at imaging the interactions between tumor cells, thrombocytes, neutrophils, and macrophages in adult fish and the challenges we encountered. I will then describe how we instead imaged the interactions between tumor cells and neutrophils in embryos.

In **Chapter 3**, I will review the biology of the oncogene YAP and its role in metastasis. I will then describe experiments where we show that YAP promotes brain metastasis in zebrafish embryos. Finally, I will describe our use of zebrafish embryos to gain new insights into how YAP promotes metastasis.

In **Chapter 4**, I will summarize the results described in this thesis. I will describe the new questions that arose from this work as well as questions that remain unanswered. Finally, I will propose new avenues of potential study based on these areas.

References

Abbott, N.J., Rönnbäck, L., and Hansson, E. (2006). Astrocyte-endothelial interactions at the blood-brain barrier. Nat. Rev. Neurosci. *7*, 41–53.

Abercrombie, M., Heaysman, J.E., and Pegrum, S.M. (1970). The locomotion of fibroblasts in culture. II. "RRuffling". Exp Cell Res. *60*, 437–444.

Abercrombie, M., Heaysman, J.E., and Pegrum, S.M. (1971). The locomotion of fibroblasts in culture. IV. Electron microscopy of the leading lamella. Exp Cell Res. *67*, 359–367.

Aceto, N., Bardia, A., Miyamoto, D.T., Donaldson, M.C., Wittner, B.S., Spencer, J.A., Yu, M., Pely, A., Engstrom, A., Zhu, H., et al. (2014). Circulating tumor cell clusters are oligoclonal precursors of breast cancer metastasis. Cell *158*, 1110–1122.

Aguirre Ghiso, J.A., Kovalski, K., and Ossowski, L. (1999). Tumor dormancy induced by downregulation of urokinase receptor in human carcinoma involves integrin and MAPK signaling. The Journal of Cell Biology *147*, 89–104.

Ahmed, S., Goh, W.I., and Bu, W. (2010). I-BAR domains, IRSp53 and filopodium formation. Semin. Cell Dev. Biol. *21*, 350–356.

Aird, W.C. (2007). Phenotypic heterogeneity of the endothelium: II. Representative vascular beds. Circulation Research *100*, 174–190.

Alieva, M., Ritsma, L., Giedt, R.J., and Weissleder, R. (2014). Imaging windows for long-term intravital imaging: General overview and technical insights. Intravital.

Anderberg, C., Cunha, S.I., Zhai, Z., Cortez, E., Pardali, E., Johnson, J.R., Franco, M., Páez-Ribes, M., Cordiner, R., Fuxe, J., et al. (2013). Deficiency for endoglin in tumor vasculature weakens the endothelial barrier to metastatic dissemination. J. Exp. Med. *210*, 563–579.

Au, S.H., Storey, B.D., Moore, J.C., Tang, Q., Chen, Y.-L., Javaid, S., Sarioglu, A.F., Sullivan, R., Madden, M.W., O'Keefe, R., et al. (2016). Clusters of circulating tumor cells traverse capillary-sized vessels. Proc. Natl. Acad. Sci. U.S.a. *113*, 4947–4952.

Bald, T., Quast, T., Landsberg, J., Rogava, M., Glodde, N., Lopez-Ramos, D., Kohlmeyer, J., Riesenberg, S., van den Boorn-Konijnenberg, D., Hömig-Hölzel, C., et al. (2014). Ultraviolet-radiation-induced inflammation promotes angiotropism and metastasis in melanoma. Nature *507*, 109–113.

Banys, M., Gruber, I., Krawczyk, N., Becker, S., Kurth, R., Wallwiener, D., Jakubowska, J., Hoffmann, J., Rothmund, R., Staebler, A., et al. (2012). Hematogenous and lymphatic tumor cell dissemination may be detected in patients diagnosed with ductal carcinoma in situ of the breast. Breast Cancer Res. Treat. *131*, 801–808.

Barkan, D., Touny, El, L.H., Michalowski, A.M., Smith, J.A., Chu, I., Davis, A.S., Webster, J.D., Hoover, S., Simpson, R.M., Gauldie, J., et al. (2010). Metastatic growth from dormant cells induced by a col-I-enriched fibrotic environment. Cancer Research *70*, 5706–5716.

Barthel, S.R., Wiese, G.K., Cho, J., Opperman, M.J., Hays, D.L., Siddiqui, J., Pienta, K.J., Furie, B., and Dimitroff, C.J. (2009). Alpha 1,3 fucosyltransferases are master regulators of prostate cancer cell trafficking. Proc. Natl. Acad. Sci. U.S.a. *106*, 19491–19496.

Beerling, E., Seinstra, D., de Wit, E., Kester, L., van der Velden, D., Maynard, C., Schäfer, R., van Diest, P., Voest, E., van Oudenaarden, A., et al. (2016). Plasticity between Epithelial and Mesenchymal States Unlinks EMT from Metastasis-Enhancing Stem Cell Capacity. CellReports *14*, 2281–2288.

Bekes, E.M., Schweighofer, B., Kupriyanova, T.A., Zajac, E., Ardi, V.C., Quigley, J.P., and Deryugina, E.I. (2011). Tumor-recruited neutrophils and neutrophil TIMP-free MMP-9 regulate coordinately the levels of tumor angiogenesis and efficiency of malignant cell intravasation. The American Journal of Pathology *179*, 1455–1470.

Benjamin, D.C., and Hynes, R.O. (2017). Intravital imaging of metastasis in adult Zebrafish. 1–12.

Berghmans, S., Jette, C., Langenau, D., Hsu, K., Stewart, R., Look, T., and Kanki, J.P. (2005a). Making waves in cancer research: new models in the zebrafish. BioTechniques *39*, 227–237.

Berghmans, S., Murphey, R.D., Wienholds, E., Neuberg, D., Kutok, J.L., Fletcher, C.D.M., Morris, J.P., Liu, T.X., Schulte-Merker, S., Kanki, J.P., et al. (2005b). tp53 mutant zebrafish develop malignant peripheral nerve sheath tumors. Proc. Natl. Acad. Sci. U.S.a. *102*, 407–412.

Bernards, R., and Weinberg, R.A. (2002). A progression puzzle. Nature *418*, 823–823.

Blaser, H., Reichman-Fried, M., Castanon, I., Dumstrei, K., Marlow, F.L., Kawakami, K., Solnica-Krezel, L., Heisenberg, C.-P., and Raz, E. (2006). Migration of zebrafish primordial germ cells: a role for myosin contraction and cytoplasmic flow. Developmental Cell *11*, 613–627.

Bos, P.D., Zhang, X.H.F., Nadal, C., Shu, W., Gomis, R.R., Nguyen, D.X., Minn, A.J., van de Vijver, M.J., Gerald, W.L., Foekens, J.A., et al. (2009). Genes that mediate breast cancer metastasis to the brain. Nature *459*, 1005–1009.

Bragado, P., Estrada, Y., Parikh, F., Krause, S., Capobianco, C., Farina, H.G., Schewe, D.M., and Aguirre-Ghiso, J.A. (2013). TGF-β2 dictates disseminated tumour cell fate in target organs through TGF-β-RIII and p38α/β signalling. Nature Reviews Drug Discovery *15*, 1351–1361.

Brown, D.M., and Ruoslahti, E. (2004). Metadherin, a cell surface protein in breast tumors that mediates lung metastasis. Ccell *5*, 365–374.

Brown, M., Assen, F.P., Leithner, A., Abe, J., Schachner, H., Asfour, G., Bago-Horvath, Z., Stein, J.V., Uhrin, P., Sixt, M., et al. (2018). Lymph node blood vessels provide exit routes for metastatic tumor cell dissemination in mice. Science *359*, 1408–1411.

Budczies, J., Winterfeld, von, M., Klauschen, F., Bockmayr, M., Lennerz, J.K., Denkert, C., Wolf, T., Warth, A., Dietel, M., Anagnostopoulos, I., et al. (2015). The landscape of metastatic progression patterns across major human cancers. Oncotarget *6*, 570–583.

Burridge, K., and Wittchen, E.S. (2013). The tension mounts: stress fibers as force-generating mechanotransducers. The Journal of Cell Biology *200*, 9–19.

Campagnola, P.J., and Dong, C.Y. (2011). Second harmonic generation microscopy: principles and applications to disease diagnosis. Laser and Photonics Reviews *5*, 13–26.

Campbell, I.D., and Humphries, M.J. (2011). Integrin structure, activation, and interactions. Cold Spring Harbor Perspectives in Biology *3*.

Campbell, P.J., Yachida, S., Mudie, L.J., Stephens, P.J., Pleasance, E.D., Stebbings, L.A., Morsberger, L.A., Latimer, C., McLaren, S., Lin, M.-L., et al. (2010). The patterns and dynamics of genomic instability in metastatic pancreatic cancer. Nature *467*, 1109–1113.

Campellone, K.G., and Welch, M.D. (2010). A nucleator arms race: cellular control of actin assembly. Nat Rev Mol Cell Biol *11*, 237–251.

Case, L.B., and Waterman, C.M. (2015). Integration of actin dynamics and cell adhesion by a three-dimensional, mechanosensitive molecular clutch. Nat Cell Biol *17*, 955–963.

Caussinus, E., Colombelli, J., and Affolter, M. (2008). Tip-cell migration controls stalk-cell intercalation during Drosophila tracheal tube elongation. Curr. Biol. *18*, 1727–1734.

Chambers, A.F., Groom, A.C., and MacDonald, I.C. (2002). Metastasis: Dissemination and growth of cancer cells in metastatic sites. Nat Rev Cancer *2*, 563–572.

Chapman, A., Fernandez del Ama, L., Ferguson, J., Kamarashev, J., Wellbrock, C., and Hurlstone, A. (2014). Heterogeneous tumor subpopulations cooperate to drive invasion. CellReports *8*, 688–695.

Charras, G.T. (2008). A short history of blebbing. J Microsc *231*, 466–478.

Charras, G., and Paluch, E. (2008). Blebs lead the way: how to migrate without lamellipodia. Nat Rev Mol Cell Biol *9*, 730–736.

Charras, G.T., Hu, C.-K., Coughlin, M., and Mitchison, T.J. (2006). Reassembly of contractile actin cortex in cell blebs. The Journal of Cell Biology *175*, 477–490.

Chen, G.R., Sive, H., and Bartel, D.P. (2017). A Seed Mismatch Enhances Argonaute2-Catalyzed Cleavage and Partially Rescues Severely Impaired Cleavage Found in Fish. Molecular Cell *68*, 1095–1107.e1095.

Chen, J., Zhou, W., Jia, Q., Chen, J., Zhang, S., Yao, W., Wei, F., Zhang, Y., Yang, F., Huang, W., et al. (2016a). Efficient extravasation of tumor-repopulating cells depends on cell deformability. Nature Reviews Drug Discovery *6*, 19304.

Chen, M.B., Lamar, J.M., Li, R., Hynes, R.O., and Kamm, R.D. (2016b). Elucidation of the Roles of Tumor Integrin β1 in the Extravasation Stage of the Metastasis Cascade. Cancer Research *76*, 2513–2524.

Chen, Q., Zhang, X.H.F., and Massagué, J. (2011). Macrophage binding to receptor VCAM-1 transmits survival signals in breast cancer cells that invade the lungs. Cancer Cell *20*, 538–549.

Clark, A.G., and Vignjevic, D.M. (2015). Modes of cancer cell invasion and the role of the microenvironment. Current Opinion in Cell Biology *36*, 13–22.

Clark, E.A., Golub, T.R., Lander, E.S., and Hynes, R.O. (2000). Genomic analysis of metastasis reveals an essential role for RhoC. Nature *406*, 532–535.

Coffelt, S.B., Wellenstein, M.D., and de Visser, K.E. (2016). Neutrophils in cancer: neutral no more. Nat Rev Cancer *16*, 431–446.

Cohen, S.J., Punt, C.J.A., Iannotti, N., Saidman, B.H., Sabbath, K.D., Gabrail, N.Y., Picus, J., Morse, M., Mitchell, E., Miller, M.C., et al. (2008). Relationship of circulating tumor cells to tumor response, progression-free survival, and overall survival in patients with metastatic colorectal cancer. J. Clin. Oncol. *26*, 3213–3221.

Cools-Lartigue, J., Spicer, J., McDonald, B., Gowing, S., Chow, S., Giannias, B., Bourdeau, F., Kubes, P., and Ferri, L. (2013). Neutrophil extracellular traps sequester circulating tumor cells and promote metastasis. J. Clin. Invest. *123*, 3446–3458.

Cristofanilli, M., Budd, G.T., Ellis, M.J., Stopeck, A., Matera, J., Miller, M.C., Reuben, J.M., Doyle, G.V., Allard, W.J., Terstappen, L.W.M.M., et al. (2004). Circulating tumor cells, disease progression, and survival in metastatic breast cancer. N. Engl. J. Med. *351*, 781–791.

Cunningham, C.C. (1995). Actin polymerization and intracellular solvent flow in cell surface blebbing. The Journal of Cell Biology *129*, 1589–1599.

Davidson, A.J., and Zon, L.I. (2004). The 'definitive' (and 'primitive') guide to zebrafish hematopoiesis. Oncogene *23*, 7233–7246.

de Bono, J.S., Scher, H.I., Montgomery, R.B., Parker, C., Miller, M.C., Tissing, H., Doyle, G.V., Terstappen, L.W.W.M., Pienta, K.J., and Raghavan, D. (2008). Circulating tumor cells predict

survival benefit from treatment in metastatic castration-resistant prostate cancer. Clinical Cancer Research *14*, 6302–6309.

De Craene, B., and Berx, G. (2013). Regulatory networks defining EMT during cancer initiation and progression. Nature Reviews Drug Discovery *13*, 97–110.

Demers, M., Krause, D.S., Schatzberg, D., Martinod, K., Voorhees, J.R., Fuchs, T.A., Scadden, D.T., and Wagner, D.D. (2012). Cancers predispose neutrophils to release extracellular DNA traps that contribute to cancer-associated thrombosis. Proc. Natl. Acad. Sci. U.S.a. *109*, 13076–13081.

Deryugina, E.I., and Kiosses, W.B. (2017). Intratumoral Cancer Cell Intravasation Can Occur Independent of Invasion into the Adjacent Stroma. CellReports *19*, 601–616.

Duda, D.G., Duyverman, A.M.M.J., Kohno, M., Snuderl, M., Steller, E.J.A., Fukumura, D., and Jain, R.K. (2010). Malignant cells facilitate lung metastasis by bringing their own soil. Proc. Natl. Acad. Sci. U.S.a. *107*, 21677–21682.

Dupuy, F., Tabariès, S., Andrzejewski, S., Dong, Z., Blagih, J., Annis, M.G., Omeroglu, A., Gao, D., Leung, S., Amir, E., et al. (2015). PDK1-Dependent Metabolic Reprogramming Dictates Metastatic Potential in Breast Cancer. Cell Metabolism *22*, 577–589.

D'Agati, G., Beltre, R., Sessa, A., Burger, A., Zhou, Y., Mosimann, C., and White, R.M. (2017). A defect in the mitochondrial protein Mpv17 underlies the transparent casper zebrafish. Developmental Biology *430*, 11–17.

Eddy, R.J., Weidmann, M.D., Sharma, V.P., and Condeelis, J.S. (2017). Tumor Cell Invadopodia: Invasive Protrusions that Orchestrate Metastasis. Trends Cell Biol. *27*, 595–607.

Eden, C.J., Ju, B., Murugesan, M., Phoenix, T.N., Nimmervoll, B., Tong, Y., Ellison, D.W., Finkelstein, D., Wright, K., Boulos, N., et al. (2015). Orthotopic models of pediatric brain tumors in zebrafish. Oncogene *34*, 1736–1742.

Ellett, F., Pase, L., Hayman, J.W., Andrianopoulos, A., and Lieschke, G.J. (2011). mpeg1 promoter transgenes direct macrophage-lineage expression in zebrafish. Blood *117*, e49–e56.

Endo, H., Okami, J., Okuyama, H., Nishizawa, Y., Imamura, F., and Inoue, M. (2017). The induction of MIG6 under hypoxic conditions is critical for dormancy in primary cultured lung cancer cells with activating EGFR mutations. Oncogene *36*, 2824–2834.

Entenberg, D., Voiculescu, S., Guo, P., Borriello, L., Wang, Y., Karagiannis, G.S., Jones, J., Baccay, F., Oktay, M., and Condeelis, J. (2017). A permanent window for the murine lung enables high-resolution imaging of cancer metastasis. Nat Meth *15*, 73–80.

Even-Ram, S., and Yamada, K.M. (2005). Cell migration in 3D matrix. Current Opinion in Cell Biology *17*, 524–532.

Ewald, A.J., Werb, Z., and Egeblad, M. (2011). Dynamic, long-term in vivo imaging of tumor-stroma interactions in mouse models of breast cancer using spinning-disk confocal microscopy. Cold Spring Harb Protoc *2011*, pdb.top97.

Farina, K.L., Wyckoff, J.B., Rivera, J., Lee, H., Segall, J.E., Condeelis, J.S., and Jones, J.G. (1998). Cell motility of tumor cells visualized in living intact primary tumors using green fluorescent protein. Cancer Res. *58*, 2528–2532.

Faucherre, A., Taylor, G.S., Overvoorde, J., Dixon, J.E., and Hertog, J.D. (2008). Zebrafish pten genes have overlapping and non-redundant functions in tumorigenesis and embryonic development. Oncogene *27*, 1079–1086.

Fazio, M., Avagyan, S., van Rooijen, E., Mannherz, W., Kaufman, C.K., Lobbardi, R., Langenau, D.M., and Zon, L.I. (2017). Efficient Transduction of Zebrafish Melanoma Cell Lines and Embryos Using Lentiviral Vectors. Zebrafish *14*, 379–382.

Felding-Habermann, B., O'Toole, T.E., Smith, J.W., Fransvea, E., Ruggeri, Z.M., Ginsberg, M.H., Hughes, P.E., Pampori, N., Shattil, S.J., Saven, A., et al. (2001). Integrin activation controls metastasis in human breast cancer. Proc. Natl. Acad. Sci. U.S.a. *98*, 1853–1858.

Fernando, R.I., Castillo, M.D., Litzinger, M., Hamilton, D.H., and Palena, C. (2011). IL-8 signaling plays a critical role in the epithelial-mesenchymal transition of human carcinoma cells. Cancer Research *71*, 5296–5306.

Fidler, I.J. (1970). Metastasis: quantitative analysis of distribution and fate of tumor emboli labeled with 125 I-5-iodo-2'-deoxyuridine. J. Natl. Cancer Inst. *45*, 773–782.

Fidler, I.J., and Talmadge, J.E. (1986). Evidence that intravenously derived murine pulmonary melanoma metastases can originate from the expansion of a single tumor cell. Cancer Res. *46*, 5167–5171.

Fidler, I.J. (2003). The pathogenesis of cancer metastasis: the "seed and soil" hypothesis revisited.

Filonov, G.S., Piatkevich, K.D., Ting, L.-M., Zhang, J., Kim, K., and Verkhusha, V.V. (2011). Bright and stable near-infrared fluorescent protein for in vivo imaging. Nat. Biotechnol. *29*, 757–761.

Fischer, K.R., Durrans, A., Lee, S., Sheng, J., Li, F., Wong, S.T.C., Choi, H., Rayes, El, T., Ryu, S., Troeger, J., et al. (2015). Epithelial-to-mesenchymal transition is not required for lung metastasis but contributes to chemoresistance. Nature *527*, 472–476.

Fluegen, G., Avivar-Valderas, A., Wang, Y., Padgen, M.R., Williams, J.K., Nobre, A.R., Calvo, V., Cheung, J.F., Bravo-Cordero, J.J., Entenberg, D., et al. (2017). Phenotypic heterogeneity of disseminated tumour cells is preset by primary tumour hypoxic microenvironments. Nature Reviews Drug Discovery *19*, 120–132.

Fogh, J., Fogh, J.M., and Orfeo, T. (1977). One hundred and twenty-seven cultured human tumor cell lines producing tumors in nude mice. Journal of the National Cancer Institute *59*, 221–226.

Folkman, J. (1995). Angiogenesis in cancer, vascular, rheumatoid and other disease. Nature Medicine *1*, 27–31.

Folkman, J. (2002). Role of angiogenesis in tumor growth and metastasis. Semin. Oncol. *29*, 15–18.

Friedl, P., and Alexander, S. (2011). Cancer invasion and the microenvironment: plasticity and reciprocity. Cell *147*, 992–1009.

Friedl, P., and Gilmour, D. (2009). Collective cell migration in morphogenesis, regeneration and cancer. Nat Rev Mol Cell Biol *10*, 445–457.

Friedl, P., and Wolf, K. (2003). Tumour-cell invasion and migration: diversity and escape mechanisms. Nat Rev Cancer *3*, 362–374.

Friedl, P., and Wolf, K. (2008). Tube travel: the role of proteases in individual and collective cancer cell invasion. Cancer Research *68*, 7247–7249.

Friedl, P., and Wolf, K. (2010). Plasticity of cell migration: a multiscale tuning model. The Journal of Cell Biology *188*, 11–19.

Furlow, P.W., Zhang, S., Soong, T.D., Halberg, N., Goodarzi, H., Mangrum, C., Wu, Y.G., Elemento, O., and Tavazoie, S.F. (2015). Mechanosensitive pannexin-1 channels mediate microvascular metastatic cell survival. Nat Cell Biol *17*, 943–952.

Fuster, M.M., Brown, J.R., Wang, L., and Esko, J.D. (2003). A disaccharide precursor of sialyl Lewis X inhibits metastatic potential of tumor cells. Cancer Res. *63*, 2775–2781.

Gaggioli, C., Hooper, S., Hidalgo-Carcedo, C., Grosse, R., Marshall, J.F., Harrington, K., and Sahai, E. (2007). Fibroblast-led collective invasion of carcinoma cells with differing roles for RhoGTPases in leading and following cells. Nat Cell Biol *9*, 1392–1400.

Gao, H., Chakraborty, G., Lee-Lim, A.P., Mo, Q., Decker, M., Vonica, A., Shen, R., Brogi, E., Brivanlou, A.H., and Giancotti, F.G. (2012). The BMP inhibitor Coco reactivates breast cancer cells at lung metastatic sites. Cell *150*, 764–779.

Gardel, M.L., Schneider, I.C., Aratyn-Schaus, Y., and Waterman, C.M. (2010). Mechanical integration of actin and adhesion dynamics in cell migration. Annu. Rev. Cell Dev. Biol. *26*, 315–333.

Gerhardt, H., and Semb, H. (2008). Pericytes: gatekeepers in tumour cell metastasis? J. Mol. Med. *86*, 135–144.

Gerlinger, M., Rowan, A.J., Horswell, S., Math, M., Larkin, J., Endesfelder, D., Gronroos, E., Martinez, P., Matthews, N., Stewart, A., et al. (2012). Intratumor heterogeneity and branched evolution revealed by multiregion sequencing. N. Engl. J. Med. *366*, 883–892.

Ghajar, C.M., Peinado, H., Mori, H., Matei, I.R., Evason, K.J., Brazier, H., Almeida, D., Koller, A., Hajjar, K.A., Stainier, D.Y.R., et al. (2013). The perivascular niche regulates breast tumour dormancy. Nat Cell Biol *15*, 807–817.

Giampieri, S., Manning, C., Hooper, S., Jones, L., Hill, C.S., and Sahai, E. (2009). Localized and reversible TGFbeta signalling switches breast cancer cells from cohesive to single cell motility. Nature Reviews Drug Discovery *11*, 1287–1296.

Gil-Bernabé, A.M., Ferjancic, S., Tlalka, M., Zhao, L., Allen, P.D., Im, J.H., Watson, K., Hill, S.A., Amirkhosravi, A., Francis, J.L., et al. (2012). Recruitment of monocytes/macrophages by tissue factor-mediated coagulation is essential for metastatic cell survival and premetastatic niche establishment in mice. Blood *119*, 3164–3175.

Gligorijevic, B., Wyckoff, J., Yamaguchi, H., Wang, Y., Roussos, E.T., and Condeelis, J. (2012). N-WASP-mediated invadopodium formation is involved in intravasation and lung metastasis of mammary tumors. Journal of Cell Science *125*, 724–734.

Gocheva, V., Wang, H.-W., Gadea, B.B., Shree, T., Hunter, K.E., Garfall, A.L., Berman, T., and Joyce, J.A. (2010). IL-4 induces cathepsin protease activity in tumor-associated macrophages to promote cancer growth and invasion. Genes & Development *24*, 241–255.

Goswami, S., Sahai, E., Wyckoff, J.B., Cammer, M., Cox, D., Pixley, F.J., Stanley, E.R., Segall, J.E., and Condeelis, J.S. (2005). Macrophages promote the invasion of breast carcinoma cells via a colony-stimulating factor-1/epidermal growth factor paracrine loop. Cancer Res. *65*, 5278–5283.

Gómez-Cuadrado, L., Tracey, N., Ma, R., Qian, B., and Brunton, V.G. (2017). Mouse models of metastasis: progress and prospects. Disease Models & Mechanisms *10*, 1061–1074.

Granot, Z., Henke, E., Comen, E.A., King, T.A., Norton, L., and Benezra, R. (2011). Tumor entrained neutrophils inhibit seeding in the premetastatic lung. Cancer Cell *20*, 300–314.

Gritsenko, P.G., Ilina, O., and Friedl, P. (2012). Interstitial guidance of cancer invasion. J. Pathol. *226*, 185–199.

Grunwald, D.J., and Eisen, J.S. (2002). Headwaters of the zebrafish -- emergence of a new model vertebrate. Nat Rev Genet *3*, 717–724.

Gupta, G.P., Nguyen, D.X., Chiang, A.C., Bos, P.D., Kim, J.Y., Nadal, C., Gomis, R.R., Manova-Todorova, K., and Massagué, J. (2007). Mediators of vascular remodelling co-opted for sequential steps in lung metastasis. Nature *446*, 765–770.

Gupton, S.L., and Gertler, F.B. (2007). Filopodia: the fingers that do the walking. Sci. STKE *2007*, re5–re5.

Haramis, A.-P.G., Hurlstone, A., van der Velden, Y., Begthel, H., van den Born, M., Offerhaus, G.J.A., and Clevers, H.C. (2006). Adenomatous polyposis coli-deficient zebrafish are susceptible to digestive tract neoplasia. EMBO Rep *7*, 444–449.

Harney, A.S., Arwert, E.N., Entenberg, D., Wang, Y., Guo, P., Qian, B.-Z., Oktay, M.H., Pollard, J.W., Jones, J.G., and Condeelis, J.S. (2015). Real-Time Imaging Reveals Local, Transient Vascular Permeability, and Tumor Cell Intravasation Stimulated by TIE2hi Macrophage-Derived VEGFA. Cancer Discovery *5*, 932–943.

Harper, K.L., Sosa, M.S., Entenberg, D., Hosseini, H., Cheung, J.F., Nobre, R., Avivar-Valderas, A., Nagi, C., Girnius, N., Davis, R.J., et al. (2016). Mechanism of early dissemination and metastasis in Her2⁺ mammary cancer. Nature *540*, 588–592.

Hart, I.R., and Fidler, I.J. (1980). Role of Organ Selectivity in the Determination of Metastatic Patterns of B16 Melanoma. Cancer Res. *40*, 2281–2287.

He, S., Lamers, G.E., Beenakker, J.-W.M., Cui, C., Ghotra, V.P., Danen, E.H., Meijer, A.H., Spaink, H.P., and Snaar-Jagalska, B.E. (2012). Neutrophil-mediated experimental metastasis is enhanced by VEGFR inhibition in a zebrafish xenograft model. J. Pathol. *227*, 431–445.

Headley, M.B., Bins, A., Nip, A., Roberts, E.W., Looney, M.R., Gerard, A., and Krummel, M.F. (2016). Visualization of immediate immune responses to pioneer metastatic cells in the lung. Nature *531*, 513–517.

Heckman, C.A., and Plummer, H.K. (2013). Filopodia as sensors. Cell. Signal. *25*, 2298–2311.

Heilmann, S., Ratnakumar, K., Langdon, E.M., Kansler, E.R., Kim, I.S., Campbell, N.R., Perry, E.B., McMahon, A.J., Kaufman, C.K., van Rooijen, E., et al. (2015). A Quantitative System for Studying Metastasis Using Transparent Zebrafish. Cancer Res. *75*, 4272–4282.

Helman, L.J., and Meltzer, P. (2003). Mechanisms of sarcoma development. Nat Rev Cancer *3*, 685–694.

Hiratsuka, S., Goel, S., Kamoun, W.S., Maru, Y., Fukumura, D., Duda, D.G., and Jain, R.K. (2011). Endothelial focal adhesion kinase mediates cancer cell homing to discrete regions of the lungs via E-selectin up-regulation. Proc. Natl. Acad. Sci. U.S.a. *108*, 3725–3730.

Holmgren, L., O'Reilly, M.S., and Folkman, J. (1995). Dormancy of micrometastases: balanced proliferation and apoptosis in the presence of angiogenesis suppression. Nature Medicine *1*, 149–153.

Hong, M.K.H., Macintyre, G., Wedge, D.C., Van Loo, P., Patel, K., Lunke, S., Alexandrov, L.B., Sloggett, C., Cmero, M., Marass, F., et al. (2015). Tracking the origins and drivers of subclonal metastatic expansion in prostate cancer. Nature Communications *6*, 6605.

Hong, Y., Fang, F., and Zhang, Q. (2016). Circulating tumor cell clusters: What we know and what we expect (Review). Int. J. Oncol. *49*, 2206–2216.

Hoppe-Seyler, K., Bossler, F., Lohrey, C., Bulkescher, J., Rösl, F., Jansen, L., Mayer, A., Vaupel, P., Dürst, M., and Hoppe-Seyler, F. (2017). Induction of dormancy in hypoxic human papillomavirus-positive cancer cells. Proc. Natl. Acad. Sci. U.S.a. *114*, E990–E998.

Hosseini, H., Obradović, M.M.S., Hoffmann, M., Harper, K.L., Sosa, M.S., Werner-Klein, M., Nanduri, L.K., Werno, C., Ehrl, C., Maneck, M., et al. (2016). Early dissemination seeds metastasis in breast cancer. Nature *540*, 552–558.

Howe, K., Clark, M.D., Torroja, C.F., Torrance, J., Berthelot, C., Muffato, M., Collins, J.E., Humphray, S., McLaren, K., Matthews, L., et al. (2013). The zebrafish reference genome sequence and its relationship to the human genome. Nature *496*, 498–503.

Hu, G., Chong, R.A., Yang, Q., Wei, Y., Blanco, M.A., Li, F., Reiss, M., Au, J.L.S., Haffty, B.G., and Kang, Y. (2009). MTDH activation by 8q22 genomic gain promotes chemoresistance and metastasis of poor-prognosis breast cancer. Cancer Cell *15*, 9–20.

Hu, P., Shen, M., Zhang, P., Zheng, C., Pang, Z., Zhu, L., and Du, J. (2015). Intratumoral neutrophil granulocytes contribute to epithelial-mesenchymal transition in lung adenocarcinoma cells. Tumour Biol. *36*, 7789–7796.

Huh, S.J., Liang, S., Sharma, A., Dong, C., and Robertson, G.P. (2010). Transiently entrapped circulating tumor cells interact with neutrophils to facilitate lung metastasis development. Cancer Research *70*, 6071–6082.

Huttenlocher, A., and Horwitz, A.R. (2011). Integrins in cell migration. Cold Spring Harbor Perspectives in Biology *3*, a005074.

Hüsemann, Y., Geigl, J.B., Schubert, F., Musiani, P., Meyer, M., Burghart, E., Forni, G., Eils, R., Fehm, T., Riethmüller, G., et al. (2008). Systemic spread is an early step in breast cancer. Ccell *13*, 58–68.

Hynes, R.O. (2002). Integrins: bidirectional, allosteric signaling machines. Cell *110*, 673–687.

Hynes, R.O. (2003). Metastatic potential: generic predisposition of the primary tumor or rare, metastatic variants-or both? Cell *113*, 821–823.

Isogai, S., Horiguchi, M., and Weinstein, B.M. (2001). The vascular anatomy of the developing zebrafish: an atlas of embryonic and early larval development. Developmental Biology *230*, 278–301.

Jacob, L.S., Vanharanta, S., Obenauf, A.C., Pirun, M., Viale, A., Socci, N.D., and Massagué, J. (2015). Metastatic Competence Can Emerge with Selection of Preexisting Oncogenic Alleles without a Need of New Mutations. Cancer Research *75*, 3713–3719.

Jacquemet, G., Hamidi, H., and Ivaska, J. (2015). Filopodia in cell adhesion, 3D migration and cancer cell invasion. Current Opinion in Cell Biology *36*, 23–31.

Jain, R.K. (2005). Normalization of tumor vasculature: an emerging concept in antiangiogenic therapy. Science *307*, 58–62.

Jain, R.K., Munn, L.L., and Fukumura, D. (2002). Dissecting tumour pathophysiology using intravital microscopy. Nat Rev Cancer *2*, 266–276.

Jakobsson, L., Franco, C.A., Bentley, K., Collins, R.T., Ponsioen, B., Aspalter, I.M., Rosewell, I., Busse, M., Thurston, G., Medvinsky, A., et al. (2010). Endothelial cells dynamically compete for the tip cell position during angiogenic sprouting. Nature Reviews Drug Discovery *12*, 943–953.

Jayadev, R., and Sherwood, D.R. (2017). Basement membranes. Curr. Biol. *27*, R207–R211.

Joyce, J.A., and Pollard, J.W. (2008). Microenvironmental regulation of metastasis. Nat Rev Cancer *9*, 239–252.

Jung, I.H., Chung, Y.-Y., Jung, D.E., Kim, Y.J., Kim, D.H., Kim, K.-S., and Park, S.W. (2016). Impaired Lymphocytes Development and Xenotransplantation of Gastrointestinal Tumor Cells in Prkdc-Null SCID Zebrafish Model. Neo *18*, 468–479.

Kalluri, R. (2003). Basement membranes: structure, assembly and role in tumour angiogenesis. Nat Rev Cancer *3*, 422–433.

Kalluri, R., and Weinberg, R.A. (2009). The basics of epithelial-mesenchymal transition. J. Clin. Invest. *119*, 1420–1428.

Kang, Y., Siegel, P.M., Shu, W., Drobnjak, M., Kakonen, S.M., Cordon-Cardo, C., Guise, T.A., and Massagué, J. (2003). A multigenic program mediating breast cancer metastasis to bone. Ccell *3*, 537–549.

Kaplan, R.N., Riba, R.D., Zacharoulis, S., Bramley, A.H., Vincent, L., Costa, C., MacDonald, D.D., Jin, D.K., Shido, K., Kerns, S.A., et al. (2005). VEGFR1-positive haematopoietic bone marrow progenitors initiate the pre-metastatic niche. Nature *438*, 820–827.

Karpanen, T., Egeblad, M., Karkkainen, M.J., Kubo, H., Ylä-Herttuala, S., Jäättelä, M., and Alitalo, K. (2001). Vascular endothelial growth factor C promotes tumor lymphangiogenesis and intralymphatic tumor growth. Cancer Res. *61*, 1786–1790.

Kawada, K., and Taketo, M.M. (2011). Significance and mechanism of lymph node metastasis in cancer progression. Cancer Research *71*, 1214–1218.

Kawakami, K., Shima, A., and Kawakami, N. (2000). Identification of a functional transposase of the Tol2 element, an Ac-like element from the Japanese medaka fish, and its transposition in the zebrafish germ lineage. Proc. Natl. Acad. Sci. U.S.a. *97*, 11403–11408.

Kedrin, D., Gligorijevic, B., Wyckoff, J., Verkhusha, V.V., Condeelis, J., Segall, J.E., and van Rheenen, J. (2008). Intravital imaging of metastatic behavior through a mammary imaging window. Nat Meth *5*, 1019–1021.

Keller, H., and Eggli, P. (1998). Protrusive activity, cytoplasmic compartmentalization, and restriction rings in locomoting blebbing Walker carcinosarcoma cells are related to detachment of cortical actin from the plasma membrane. Cell Motil. Cytoskeleton *41*, 181–193.

Kelly, A., and Hurlstone, A.F. (2011). The use of RNAi technologies for gene knockdown in zebrafish. Brief Funct Genomics *10*, 189–196.

Kessenbrock, K., Plaks, V., and Werb, Z. (2010). Matrix metalloproteinases: regulators of the tumor microenvironment. Cell *141*, 52–67.

Khanna, C., and Hunter, K. (2005). Modeling metastasis in vivo. Carcinogenesis *26*, 513–523.

Khoo, B.L., Lee, S.C., Kumar, P., Tan, T.Z., Warkiani, M.E., Ow, S.G.W., Nandi, S., Lim, C.T., and Thiery, J.P. (2015). Short-term expansion of breast circulating cancer cells predicts response to anti-cancer therapy. Oncotarget *6*, 15578–15593.

Kienast, Y., Baumgarten, von, L., Fuhrmann, M., Klinkert, W.E.F., Goldbrunner, R., Herms, J., and Winkler, F. (2009). Real-time imaging reveals the single steps of brain metastasis formation. Nature Medicine *16*, 116–122.

Kim, J., Yu, W., Kovalski, K., and Ossowski, L. (1998a). Requirement for specific proteases in cancer cell intravasation as revealed by a novel semiquantitative PCR-based assay. Cell *94*, 353–362.

Kim, M.-Y., Oskarsson, T., Acharyya, S., Nguyen, D.X., Zhang, X.H.F., Norton, L., and Massagué, J. (2009). Tumor self-seeding by circulating cancer cells. Cell *139*, 1315–1326.

Kim, Y.J., Borsig, L., Varki, N.M., and Varki, A. (1998b). P-selectin deficiency attenuates tumor growth and metastasis. Proc. Natl. Acad. Sci. U.S.a. *95*, 9325–9330.

Kitamura, T., Pollard, J.W., and Vendrell, M. (2017). Optical Windows for Imaging the Metastatic Tumour Microenvironment in vivo. Trends in Biotechnology *35*, 5–8.

Klapholz, B., and Brown, N.H. (2017). Talin - the master of integrin adhesions. Journal of Cell Science *130*, 2435–2446.

Kobat, D., Horton, N.G., and Xu, C. (2011). In vivo two-photon microscopy to 1.6-mm depth in mouse cortex. J Biomed Opt *16*, 106014.

Kobayashi, A., Okuda, H., Xing, F., Pandey, P.R., Watabe, M., Hirota, S., Pai, S.K., Liu, W., Fukuda, K., Chambers, C., et al. (2011). Bone morphogenetic protein 7 in dormancy and metastasis of prostate cancer stem-like cells in bone. J. Exp. Med. *208*, 2641–2655.

Kopp, H.-G., Placke, T., and Salih, H.R. (2009). Platelet-derived transforming growth factor-beta down-regulates NKG2D thereby inhibiting natural killer cell antitumor reactivity. Cancer Research *69*, 7775–7783.

Kripke, M.L., and Fidler, I. Metastasis Results from Preexisting Variant Cells Within a Malignant Tumor. Cancer Res. *48*, 4007–4010.

Labelle, M., and Hynes, R.O. (2012). The Initial Hours of Metastasis: The Importance of Cooperative Host-Tumor Cell Interactions during Hematogenous Dissemination. Cancer Discovery *2*, 1091–1099.

Labelle, M., Begum, S., and Hynes, R.O. (2011). Direct Signaling between Platelets and Cancer Cells Induces an Epithelial-Mesenchymal-Like Transition and Promotes Metastasis. Cancer Cell *20*, 576–590.

Labelle, M., Begum, S., and Hynes, R.O. (2014). Platelets guide the formation of early metastatic niches. Proc. Natl. Acad. Sci. U.S.a. *111*, E3053–E3061.

Lam, S.H., Wu, Y.L., Vega, V.B., Miller, L.D., Spitsbergen, J., Tong, Y., Zhan, H., Govindarajan, K.R., Lee, S., Mathavan, S., et al. (2006). Conservation of gene expression signatures between zebrafish and human liver tumors and tumor progression. Nat. Biotechnol. *24*, 73–75.

Lambert, A.W., Pattabiraman, D.R., and Weinberg, R.A. (2017). Emerging Biological Principles of Metastasis. Cell *168*, 670–691.

Lamouille, S., Xu, J., and Derynck, R. (2014). Molecular mechanisms of epithelial-mesenchymal transition. Nat Rev Mol Cell Biol *15*, 178–196.

Langenau, D.M., Keefe, M.D., Storer, N.Y., Guyon, J.R., Kutok, J.L., Le, X., Goessling, W., Neuberg, D.S., Kunkel, L.M., and Zon, L.I. (2007). Effects of RAS on the genesis of embryonal rhabdomyosarcoma. Genes & Development *21*, 1382–1395.

Langenau, D.M., Traver, D., Ferrando, A.A., Kutok, J.L., Aster, J.C., Kanki, J.P., Lin, S., Prochownik, E., Trede, N.S., Zon, L.I., et al. (2003). Myc-induced T cell leukemia in transgenic zebrafish. Science *299*, 887–890.

Lawson, N.D., and Weinstein, B.M. (2002). In Vivo Imaging of Embryonic Vascular Development Using Transgenic Zebrafish. Developmental Biology *248*, 307–318.

Leber, M.F., and Efferth, T. (2009). Molecular principles of cancer invasion and metastasis (review). Int. J. Oncol. *34*, 881–895.

LeBleu, V.S., O'Connell, J.T., Gonzalez Herrera, K.N., Wikman, H., Pantel, K., Haigis, M.C., de Carvalho, F.M., Damascena, A., Domingos Chinen, L.T., Rocha, R.M., et al. (2014). PGC-1α mediates mitochondrial biogenesis and oxidative phosphorylation in cancer cells to promote metastasis. Nature Reviews Drug Discovery *16*, 992–1003–1–15.

Lee, S.L.C., Rouhi, P., Dahl Jensen, L., Zhang, D., Ji, H., Hauptmann, G., Ingham, P., and Cao, Y. (2009). Hypoxia-induced pathological angiogenesis mediates tumor cell dissemination, invasion, and metastasis in a zebrafish tumor model. Proc. Natl. Acad. Sci. U.S.a. *106*, 19485–19490.

Lehmann, S., Boekhorst, te, V., Odenthal, J., Bianchi, R., van Helvert, S., Ikenberg, K., Ilina, O., Stoma, S., Xandry, J., Jiang, L., et al. (2017). Hypoxia Induces a HIF-1-Dependent Transition from Collective-to-Amoeboid Dissemination in Epithelial Cancer Cells. Curr. Biol. *27*, 392–400.

Lehr, J.E., and Pienta, K.J. (1998). Preferential adhesion of prostate cancer cells to a human bone marrow endothelial cell line. J. Natl. Cancer Inst. *90*, 118–123.

Leong, H.S., Robertson, A.E., Stoletov, K., Leith, S.J., Chin, C.A., Chien, A.E., Hague, M.N., Ablack, A., Carmine-Simmen, K., McPherson, V.A., et al. (2014). Invadopodia Are Required for Cancer Cell Extravasation and Are a Therapeutic Target for Metastasis. CellReports *8*, 1558–1570.

Li, W., and Kang, Y. (2016). Probing the Fifty Shades of EMT in Metastasis. Trends in Cancer *2*, 65–67.

Liao, T.-T., and Yang, M.-H. (2017). Revisiting epithelial-mesenchymal transition in cancer metastasis: the connection between epithelial plasticity and stemness. Mol Oncol *11*, 792–804.

Lieschke, G.J., and Currie, P.D. (2007). Animal models of human disease: zebrafish swim into view. Nat Rev Genet *8*, 353–367.

Lin, E.Y., and Pollard, J.W. (2007). Tumor-associated macrophages press the angiogenic switch in breast cancer. Cancer Res. *67*, 5064–5066.

Lin, H.-F., Traver, D., Zhu, H., Dooley, K., Paw, B.H., Zon, L.I., and Handin, R.I. (2005). Analysis of thrombocyte development in CD41-GFP transgenic zebrafish. Blood *106*, 3803–3810.

Linde, N., Casanova-Acebes, M., Sosa, M.S., Mortha, A., Rahman, A., Farias, E., Harper, K., Tardio, E., Reyes Torres, I., Jones, J., et al. (2018). Macrophages orchestrate breast cancer early dissemination and metastasis. Nature Communications *9*, 21.

Lister, J.A., Robertson, C.P., Lepage, T., Johnson, S.L., and Raible, D.W. (1999). nacre encodes a zebrafish microphthalmia-related protein that regulates neural-crest-derived pigment cell fate. Development *126*, 3757–3767.

Liu, W., Laitinen, S., Khan, S., Vihinen, M., Kowalski, J., Yu, G., Chen, L., Ewing, C.M., Eisenberger, M.A., Carducci, M.A., et al. (2009). Copy number analysis indicates monoclonal origin of lethal metastatic prostate cancer. Nature Medicine *15*, 559–565.

Liu, Y.-J., Le Berre, M., Lautenschlaeger, F., Maiuri, P., Callan-Jones, A., Heuzé, M., Takaki, T., Voituriez, R., and Piel, M. (2015). Confinement and low adhesion induce fast amoeboid migration of slow mesenchymal cells. Cell *160*, 659–672.

Livet, J., Weissman, T.A., Kang, H., Draft, R.W., Lu, J., Bennis, R.A., Sanes, J.R., and Lichtman, J.W. (2007). Transgenic strategies for combinatorial expression of fluorescent proteins in the nervous system. Nature *450*, 56–62.

Lohela, M., Casbon, A.-J., Olow, A., Bonham, L., Branstetter, D., Weng, N., Smith, J., and Werb, Z. (2014). Intravital imaging reveals distinct responses of depleting dynamic tumor-associated macrophage and dendritic cell subpopulations. Proc. Natl. Acad. Sci. U.S.a. *111*, E5086–E5095.

Long, E., Ilie, M., Bence, C., Butori, C., Selva, E., Lalvée, S., Bonnetaud, C., Poissonnet, G., Lacour, J.-P., Bahadoran, P., et al. (2016). High expression of TRF2, SOX10, and CD10 in circulating tumor microemboli detected in metastatic melanoma patients. A potential impact for the assessment of disease aggressiveness. Cancer Med *5*, 1022–1030.

Longley, D.B., and Johnston, P.G. (2005). Molecular mechanisms of drug resistance. J. Pathol. *205*, 275–292.

Loo, J.M., Scherl, A., Nguyen, A., Man, F.Y., Weinberg, E., Zeng, Z., Saltz, L., Paty, P.B., and Tavazoie, S.F. (2015). Extracellular metabolic energetics can promote cancer progression. Cell *160*, 393–406.

Looney, M.R., Thornton, E.E., Sen, D., Lamm, W.J., Glenny, R.W., and Krummel, M.F. (2010). Stabilized imaging of immune surveillance in the mouse lung. Nat Meth *8*, 91–96.

Lorentzen, A., Bamber, J., Sadok, A., Elson-Schwab, I., and Marshall, C.J. (2011). An ezrin-rich, rigid uropod-like structure directs movement of amoeboid blebbing cells. Journal of Cell Science *124*, 1256–1267.

Lund, A.W., Duraes, F.V., Hirosue, S., Raghavan, V.R., Nembrini, C., Thomas, S.N., Issa, A., Hugues, S., and Swartz, M.A. (2012). VEGF-C promotes immune tolerance in B16 melanomas and cross-presentation of tumor antigen by lymph node lymphatics. CellReports *1*, 191–199.

Luzzi, K.J., MacDonald, I.C., Schmidt, E.E., Kerkvliet, N., Morris, V.L., Chambers, A.F., and Groom, A.C. (1998a). Multistep nature of metastatic inefficiency: dormancy of solitary cells after successful extravasation and limited survival of early micrometastases. The American Journal of Pathology *153*, 865–873.

Luzzi, K.J., MacDonald, I.C., Schmidt, E.E., Kerkvliet, N., Morris, V.L., Chambers, A.F., and Groom, A.C. (1998b). Multistep Nature of Metastatic Inefficiency. The American Journal of Pathology *153*, 865–873.

MacRae, C.A., and Peterson, R.T. (2015). Zebrafish as tools for drug discovery. Nature Reviews Drug Discovery *14*, 721–731.

Maddipati, R., and Stanger, B.Z. (2015). Pancreatic Cancer Metastases Harbor Evidence of Polyclonality. Cancer Discovery *5*, 1086–1097.

Malanchi, I., Santamaria-Martínez, A., Susanto, E., Peng, H., Lehr, H.-A., Delaloye, J.-F., and Huelsken, J. (2011). Interactions between cancer stem cells and their niche govern metastatic colonization. Nature *481*, 85–89.

Mandriota, S.J., Jussila, L., Jeltsch, M., Compagni, A., Baetens, D., Prevo, R., Banerji, S., Huarte, J., Montesano, R., Jackson, D.G., et al. (2001). Vascular endothelial growth factor-C-mediated lymphangiogenesis promotes tumour metastasis. Embo J. *20*, 672–682.

Maniotis, A.J., Folberg, R., Hess, A., Seftor, E.A., Gardner, L.M., Pe'er, J., Trent, J.M., Meltzer, P.S., and Hendrix, M.J. (1999). Vascular channel formation by human melanoma cells in vivo and in vitro: vasculogenic mimicry. The American Journal of Pathology *155*, 739–752.

Mañes, S., Mira, E., Gómez-Moutón, C., Lacalle, R.A., and Martínez, C. (2000). Cells on the move: a dialogue between polarization and motility. IUBMB Life *49*, 89–96.

Mashimo, T., Pichumani, K., Vemireddy, V., Hatanpaa, K.J., Singh, D.K., Sirasanagandla, S., Nannepaga, S., Piccirillo, S.G., Kovacs, Z., Foong, C., et al. (2014). Acetate is a bioenergetic substrate for human glioblastoma and brain metastases. Cell *159*, 1603–1614.

Massagué, J., and Obenauf, A.C. (2016). Metastatic colonization by circulating tumour cells. Nature *529*, 298–306.

Matela, G., Gao, P., Guigas, G., Eckert, A.F., Nienhaus, K., and Nienhaus, G.U. (2017). A far-red emitting fluorescent marker protein, mGarnet2, for microscopy and STED nanoscopy. Chem. Commun. (Camb.) *53*, 979–982.

Mayor, R., and Etienne-Manneville, S. (2016). The front and rear of collective cell migration. Nat Rev Mol Cell Biol *17*, 97–109.

Mazo, I.B., Gutierrez-Ramos, J.-C., Frenette, P.S., Hynes, R.O., Wagner, D.D., and Andrian, von, U.H. (1998). Hematopoietic Progenitor Cell Rolling in Bone Marrow Microvessels: Parallel Contributions by Endothelial Selectins and Vascular Cell Adhesion Molecule 1. Journal of Experimental Medicine *188*, 465–474.

Mazor, T., Pankov, A., Song, J.S., and Costello, J.F. (2016). Intratumoral Heterogeneity of the Epigenome. Cancer Cell *29*, 440–451.

McDonald, O.G., Li, X., Saunders, T., Tryggvadottir, R., Mentch, S.J., Warmoes, M.O., Word, A.E., Carrer, A., Salz, T.H., Natsume, S., et al. (2017). Epigenomic reprogramming during pancreatic cancer progression links anabolic glucose metabolism to distant metastasis. Nature Reviews Drug Discovery *49*, 367–376.

McFadden, D.G., Papagiannakopoulos, T., Taylor-Weiner, A., Stewart, C., Carter, S.L., Cibulskis, K., Bhutkar, A., McKenna, A., Dooley, A., Vernon, A., et al. (2014). Genetic and clonal dissection of murine small cell lung carcinoma progression by genome sequencing. Cell *156*, 1298–1311.

Meyer, A., and Schartl, M. (1999). Gene and genome duplications in vertebrates: the one-to-four (-to-eight in fish) rule and the evolution of novel gene functions. Current Opinion in Cell Biology *11*, 699–704.

Mills, J.C., Stone, N.L., Erhardt, J., and Pittman, R.N. (1998). Apoptotic membrane blebbing is regulated by myosin light chain phosphorylation. The Journal of Cell Biology *140*, 627–636.

Mitra, S.K., Hanson, D.A., and Schlaepfer, D.D. (2005). Focal adhesion kinase: in command and control of cell motility. Nat Rev Mol Cell Biol *6*, 56–68.

Moore, J.C., and Langenau, D.M. (2016). Allograft Cancer Cell Transplantation in Zebrafish. Adv. Exp. Med. Biol. *916*, 265–287.

Moore, J.C., Tang, Q., Yordán, N.T., Moore, F.E., Garcia, E.G., Lobbardi, R., Ramakrishnan, A., Marvin, D.L., Anselmo, A., Sadreyev, R.I., et al. (2016). Single-cell imaging of normal and malignant cell engraftment into optically clear prkdc-null SCID zebrafish. J. Exp. Med. *213*, 2575–2589.

Morris, V.L., MacDonald, I.C., Koop, S., Schmidt, E.E., Chambers, A.F., and Groom, A.C. (1993). Early interactions of cancer cells with the microvasculature in mouse liver and muscle during hematogenous metastasis: videomicroscopic analysis. Clin. Exp. Metastasis *11*, 377–390.

Naba, A., Clauser, K.R., Lamar, J.M., Carr, S.A., and Hynes, R.O. (2014). Extracellular matrix signatures of human mammary carcinoma identify novel metastasis promoters. Elife *3*, e01308.

Nabeshima, K., Inoue, T., Shimao, Y., Okada, Y., Itoh, Y., Seiki, M., and Koono, M. (2000). Front-cell-specific expression of membrane-type 1 matrix metalloproteinase and gelatinase A during cohort migration of colon carcinoma cells induced by hepatocyte growth factor/scatter factor. Cancer Res. *60*, 3364–3369.

Nasevicius, A., and Ekker, S.C. (2000). Effective targeted gene "knockdown" in zebrafish. Nat Genet *26*, 216–220.

Naxerova, K., Reiter, J.G., Brachtel, E., Lennerz, J.K., van de Wetering, M., Rowan, A., Cai, T., Clevers, H., Swanton, C., Nowak, M.A., et al. (2017). Origins of lymphatic and distant metastases in human colorectal cancer. Science *357*, 55–60.

Nicoli, S., and Presta, M. (2007). The zebrafish/tumor xenograft angiogenesis assay. Nat Protoc *2*, 2918–2923.

Nicoli, S., Ribatti, D., Cotelli, F., and Presta, M. (2007). Mammalian tumor xenografts induce neovascularization in zebrafish embryos. Cancer Res. *67*, 2927–2931.

Nieswandt, B., Hafner, M., Echtenacher, B., and Männel, D.N. (1999). Lysis of tumor cells by natural killer cells in mice is impeded by platelets. Cancer Res. *59*, 1295–1300.

Nieto, M.A. (2013). Epithelial plasticity: a common theme in embryonic and cancer cells. Science *342*, 1234850.

Nobes, C.D., and Hall, A. (1995). Rho, rac, and cdc42 GTPases regulate the assembly of multimolecular focal complexes associated with actin stress fibers, lamellipodia, and filopodia. Cell *81*, 53–62.

Nozawa, H., Chiu, C., and Hanahan, D. (2006). Infiltrating neutrophils mediate the initial angiogenic switch in a mouse model of multistage carcinogenesis. Proc. Natl. Acad. Sci. U.S.a. *103*, 12493–12498.

O'Reilly, M.S., Holmgren, L., Shing, Y., Chen, C., Rosenthal, R.A., Moses, M., Lane, W.S., Cao, Y., Sage, E.H., and Folkman, J. (1994). Angiostatin: a novel angiogenesis inhibitor that mediates the suppression of metastases by a Lewis lung carcinoma. Cell *79*, 315–328.

Ohta, Y., Hartwig, J.H., and Stossel, T.P. (2006). FilGAP, a Rho- and ROCK-regulated GAP for Rac binds filamin A to control actin remodelling. Nat Cell Biol *8*, 803–814.

Oskarsson, T., Acharyya, S., Zhang, X.H.F., Vanharanta, S., Tavazoie, S.F., Morris, P.G., Downey, R.J., Manova-Todorova, K., Brogi, E., and Massagué, J. (2011). Breast cancer cells produce tenascin C as a metastatic niche component to colonize the lungs. Nature Medicine *17*, 867–874.

Paddock, S.W. (2014). Confocal microscopy: methods and protocols (New York, NY: Springer New York).

Padera, T.P., Stoll, B.R., Tooredman, J.B., Capen, D., di Tomaso, E., and Jain, R.K. (2004). Pathology: cancer cells compress intratumour vessels. Nature *427*, 695–695.

Paget, S. (1889). The distribution of secondary growths in cancer of the breast. The Lancet *133*, 571–573.

Paluch, E.K., and Raz, E. (2013). The role and regulation of blebs in cell migration. Current Opinion in Cell Biology *25*, 582–590.

Pantel, K., Cote, R.J., and Fodstad, O. (1999). Detection and clinical importance of micrometastatic disease. J. Natl. Cancer Inst. *91*, 1113–1124.

Pantel, K., Denève, E., Nocca, D., Coffy, A., Vendrell, J.-P., Maudelonde, T., Riethdorf, S., and Alix-Panabières, C. (2012). Circulating epithelial cells in patients with benign colon diseases. Clin. Chem. *58*, 936–940.

Papayannopoulos, V. (2018). Neutrophil extracellular traps in immunity and disease. Nature Reviews Immunology *18*, 134–147.

Park, J., Wysocki, R.W., Amoozgar, Z., Maiorino, L., Fein, M.R., Jorns, J., Schott, A.F., Kinugasa-Katayama, Y., Lee, Y., Won, N.H., et al. (2016). Cancer cells induce metastasis-supporting neutrophil extracellular DNA traps. Sci Transl Med *8*, 361ra138–361ra138.

Parsons, J.T., Horwitz, A.R., and Schwartz, M.A. (2010). Cell adhesion: integrating cytoskeletal dynamics and cellular tension. Nat Rev Mol Cell Biol *11*, 633–643.

Pasqualini, R., and Ruoslahti, E. (1996). Organ targeting in vivo using phage display peptide libraries. Nature *380*, 364–366.

Patton, E.E., Widlund, H.R., Kutok, J.L., Kopani, K.R., Amatruda, J.F., Murphey, R.D., Berghmans, S., Mayhall, E.A., Traver, D., Fletcher, C.D.M., et al. (2005). BRAF Mutations Are Sufficient to Promote Nevi Formation and Cooperate with p53 in the Genesis of Melanoma. Current Biology *15*, 249–254.

Pereira, E.R., Jones, D., Jung, K., and Padera, T.P. (2015). The lymph node microenvironment and its role in the progression of metastatic cancer. Semin. Cell Dev. Biol. *38*, 98–105.

Pereira, E.R., Kedrin, D., Seano, G., Gautier, O., Meijer, E.F.J., Jones, D., Chin, S.-M., Kitahara, S., Bouta, E.M., Chang, J., et al. (2018). Lymph node metastases can invade local blood vessels, exit the node, and colonize distant organs in mice. Science *359*, 1403–1407.

Petrie, R.J., and Yamada, K.M. (2015). Fibroblasts Lead the Way: A Unified View of 3D Cell Motility. Trends Cell Biol. *25*, 666–674.

Pignatelli, J., Bravo-Cordero, J.J., Roh-Johnson, M., Gandhi, S.J., Wang, Y., Chen, X., Eddy, R.J., Xue, A., Singer, R.H., Hodgson, L., et al. (2016). Macrophage-dependent tumor cell transendothelial migration is mediated by Notch1/MenaINV-initiated invadopodium formation. Nature Reviews Drug Discovery *6*, 37874.

Pinner, S., and Sahai, E. (2008). PDK1 regulates cancer cell motility by antagonising inhibition of ROCK1 by RhoE. Nat Cell Biol *10*, 127–137.

Piskounova, E., Agathocleous, M., Murphy, M.M., Hu, Z., Huddlestun, S.E., Zhao, Z., Leitch, A.M., Johnson, T.M., DeBerardinis, R.J., and Morrison, S.J. (2015). Oxidative stress inhibits distant metastasis by human melanoma cells. Nature *527*, 186–191.

Postlethwait, J.H. (2007). The zebrafish genome in context: ohnologs gone missing. J. Exp. Zool. *308B*, 563–577.

Poujade, M., Grasland-Mongrain, E., Hertzog, A., Jouanneau, J., Chavrier, P., Ladoux, B., Buguin, A., and Silberzan, P. (2007). Collective migration of an epithelial monolayer in response to a model wound. Proc. Natl. Acad. Sci. U.S.a. *104*, 15988–15993.

Preynat-Seauve, O., Contassot, E., Schuler, P., Piguet, V., French, L.E., and Huard, B. (2007). Extralymphatic tumors prepare draining lymph nodes to invasion via a T-cell cross-tolerance process. Cancer Res. *67*, 5009–5016.

Provenzano, P.P., Eliceiri, K.W., Campbell, J.M., Inman, D.R., White, J.G., and Keely, P.J. (2006). Collagen reorganization at the tumor-stromal interface facilitates local invasion. BMC Med *4*, 38.

Qian, B.-Z., Li, J., Zhang, H., Kitamura, T., Zhang, J., Campion, L.R., Kaiser, E.A., Snyder, L.A., and Pollard, J.W. (2011). CCL2 recruits inflammatory monocytes to facilitate breast-tumour metastasis. Nature *475*, 222–225.

Qian, B., Deng, Y., Im, J.H., Muschel, R.J., Zou, Y., Li, J., Lang, R.A., and Pollard, J.W. (2009). A Distinct Macrophage Population Mediates Metastatic Breast Cancer Cell Extravasation, Establishment and Growth. PLoS ONE *4*, e6562.

Ramaswamy, S., Ross, K.N., Lander, E.S., and Golub, T.R. (2003). A molecular signature of metastasis in primary solid tumors. Nat Genet *33*, 49–54.

Rawls, J.F., Mellgren, E.M., and Johnson, S.L. (2001). How the zebrafish gets its stripes. Developmental Biology *240*, 301–314.

Reffay, M., Parrini, M.C., Cochet-Escartin, O., Ladoux, B., Buguin, A., Coscoy, S., Amblard, F., Camonis, J., and Silberzan, P. (2014). Interplay of RhoA and mechanical forces in collective cell migration driven by leader cells. Nature Reviews Drug Discovery *16*, 217–223.

Reig, G., Pulgar, E., and Concha, M.L. (2014). Cell migration: from tissue culture to embryos. Development *141*, 1999–2013.

Ren, J.Q., McCarthy, W.R., Zhang, H., Adolph, A.R., and Li, L. (2002). Behavioral visual responses of wild-type and hypopigmented zebrafish. Vision Res. *42*, 293–299.

Renshaw, S.A., and Trede, N.S. (2012). A model 450 million years in the making: zebrafish and vertebrate immunity. Disease Models & Mechanisms *5*, 38–47.

Renshaw, S.A., Loynes, C.A., Trushell, D.M.I., Elworthy, S., Ingham, P.W., and Whyte, M.K.B. (2006). A transgenic zebrafish model of neutrophilic inflammation. Blood *108*, 3976–3978.

Reymond, N., d'Água, B.B., and Ridley, A.J. (2013). Crossing the endothelial barrier during metastasis. Nat Rev Cancer *13*, 858–870.

Ridley, A.J. (2015). Rho GTPase signalling in cell migration. Current Opinion in Cell Biology *36*, 103–112.

Riggi, N., Aguet, M., and Stamenkovic, I. (2018). Cancer Metastasis: A Reappraisal of Its Underlying Mechanisms and Their Relevance to Treatment. Annu Rev Pathol *13*, 117–140.

Ritsma, L., Steller, E.J.A., Beerling, E., Loomans, C.J.M., Zomer, A., Gerlach, C., Vrisekoop, N., Seinstra, D., van Gurp, L., Schäfer, R., et al. (2012). Intravital microscopy through an abdominal imaging window reveals a pre-micrometastasis stage during liver metastasis. Sci Transl Med *4*, 158ra145–158ra145.

Ritsma, L., Steller, E.J.A., Ellenbroek, S.I.J., Kranenburg, O., Rinkes, I.H.M.B., and van Rheenen, J. (2013). Surgical implantation of an abdominal imaging window for intravital microscopy. Nat Protoc *8*, 583–594.

Robinson, B.D., Sica, G.L., Liu, Y.-F., Rohan, T.E., Gertler, F.B., Condeelis, J.S., and Jones, J.G. (2009). Tumor microenvironment of metastasis in human breast carcinoma: a potential prognostic marker linked to hematogenous dissemination. Clinical Cancer Research *15*, 2433–2441.

Rodriguez, E.A., Tran, G.N., Gross, L.A., Crisp, J.L., Shu, X., Lin, J.Y., and Tsien, R.Y. (2016). A far-red fluorescent protein evolved from a cyanobacterial phycobiliprotein. Nat Meth *13*, 763–769.

Roh-Johnson, M., Shah, A.N., Stonick, J.A., Poudel, K.R., Kargl, J., Yang, G.H., di Martino, J., Hernandez, R.E., Gast, C.E., Zarour, L.R., et al. (2017). Macrophage-Dependent Cytoplasmic Transfer during Melanoma Invasion In Vivo. Developmental Cell *43*, 549–562.e6.

Rohan, T.E., Xue, X., Lin, H.-M., D'Alfonso, T.M., Ginter, P.S., Oktay, M.H., Robinson, B.D., Ginsberg, M., Gertler, F.B., Glass, A.G., et al. (2014). Tumor microenvironment of metastasis and risk of distant metastasis of breast cancer. J. Natl. Cancer Inst. *106*.

Rossy, J., Gutjahr, M.C., Blaser, N., Schlicht, D., and Niggli, V. (2007). Ezrin/moesin in motile Walker 256 carcinosarcoma cells: signal-dependent relocalization and role in migration. Exp Cell Res. *313*, 1106–1120.

Rouhi, P., Jensen, L.D., Cao, Z., Hosaka, K., Länne, T., Wahlberg, E., Steffensen, J.F., and Cao, Y. (2010). Hypoxia-induced metastasis model in embryonic zebrafish. Nat Protoc *5*, 1911–1918.

Roussos, E.T., Balsamo, M., Alford, S.K., Wyckoff, J.B., Gligorijevic, B., Wang, Y., Pozzuto, M., Stobezki, R., Goswami, S., Segall, J.E., et al. (2011a). Mena invasive (MenaINV) promotes multicellular streaming motility and transendothelial migration in a mouse model of breast cancer. Journal of Cell Science *124*, 2120–2131.

Roussos, E.T., Goswami, S., Balsamo, M., Wang, Y., Stobezki, R., Adler, E., Robinson, B.D., Jones, J.G., Gertler, F.B., Condeelis, J.S., et al. (2011b). Mena invasive (Mena(INV)) and Mena11a isoforms play distinct roles in breast cancer cell cohesion and association with TMEM. Clin. Exp. Metastasis *28*, 515–527.

Rowland, C.E., Brown, C.W., Medintz, I.L., and Delehanty, J.B. (2015). Intracellular FRET-based probes: a review. Methods Appl Fluoresc *3*, 042006.

Ruddell, A., Harrell, M.I., Minoshima, S., Maravilla, K.R., Iritani, B.M., White, S.W., and Partridge, S.C. (2008). Dynamic contrast-enhanced magnetic resonance imaging of tumor-induced lymph flow. Neo *10*, 706–13–1pfollowing713.

Rudner, L.A., Brown, K.H., Dobrinski, K.P., Bradley, D.F., Garcia, M.I., Smith, A.C.H., Downie, J.M., Meeker, N.D., Look, A.T., Downing, J.R., et al. (2011). Shared acquired genomic changes in zebrafish and human T-ALL. Oncogene *30*, 4289–4296.

Sahai, E. (2005). Mechanisms of cancer cell invasion. Curr. Opin. Genet. Dev. *15*, 87–96.

Sahai, E. (2007). Illuminating the metastatic process. Nat Rev Cancer *7*, 737–749.

Sahai, E., and Marshall, C.J. (2003). Differing modes of tumour cell invasion have distinct requirements for Rho/ROCK signalling and extracellular proteolysis. Nat Cell Biol *5*, 711–719.

Sarioglu, A.F., Aceto, N., Kojic, N., Donaldson, M.C., Zeinali, M., Hamza, B., Engstrom, A., Zhu, H., Sundaresan, T.K., Miyamoto, D.T., et al. (2015). A microfluidic device for label-free, physical capture of circulating tumor cell clusters. Nat Meth *12*, 685–691.

Schepers, A.G., Snippert, H.J., Stange, D.E., van den Born, M., van Es, J.H., van de Wetering, M., and Clevers, H. (2012). Lineage tracing reveals Lgr5+ stem cell activity in mouse intestinal adenomas. Science *337*, 730–735.

Schietroma, C., Cianfarani, F., Lacal, P.M., Odorisio, T., Orecchia, A., Kanitakis, J., D'Atri, S., Failla, C.M., and Zambruno, G. (2003). Vascular endothelial growth factor-C expression correlates with lymph node localization of human melanoma metastases. Cancer *98*, 789–797.

Schild, T., Low, V., Blenis, J., and Gomes, A.P. (2018). Unique Metabolic Adaptations Dictate Distal Organ-Specific Metastatic Colonization. Cancer Cell *33*, 347–354.

Schlüter, K., Gassmann, P., Enns, A., Korb, T., Hemping-Bovenkerk, A., Hölzen, J., and Haier, J. (2006). Organ-specific metastatic tumor cell adhesion and extravasation of colon carcinoma cells with different metastatic potential. The American Journal of Pathology *169*, 1064–1073.

Schumacher, D., Strilic, B., Sivaraj, K.K., Wettschureck, N., and Offermanns, S. (2013). Platelet-Derived Nucleotides Promote Tumor-Cell Transendothelial Migration and Metastasis via P2Y. Ccell 1–8.

Schweitzer, K.M., Dräger, A.M., van der Valk, P., Thijsen, S.F., Zevenbergen, A., Theijsmeijer, A.P., van der Schoot, C.E., and Langenhuijsen, M.M. (1996). Constitutive expression of E-selectin and vascular cell adhesion molecule-1 on endothelial cells of hematopoietic tissues. The American Journal of Pathology *148*, 165–175.

Sharma, S., Xing, F., Liu, Y., Wu, K., Said, N., Pochampally, R., Shiozawa, Y., Lin, H.-K., Balaji, K.C., and Watabe, K. (2016). Secreted Protein Acidic and Rich in Cysteine (SPARC) Mediates Metastatic Dormancy of Prostate Cancer in Bone. J. Biol. Chem. *291*, 19351–19363.

Sherley, J.L. (2002). Metastasis: objections to the same-gene model. Nature *419*, 560–authorreply560.

Shibue, T., Brooks, M.W., and Weinberg, R.A. (2013). An integrin-linked machinery of cytoskeletal regulation that enables experimental tumor initiation and metastatic colonization. Cancer Cell *24*, 481–498.

Shibue, T., Brooks, M.W., Inan, M.F., Reinhardt, F., and Weinberg, R.A. (2012). The outgrowth of micrometastases is enabled by the formation of filopodium-like protrusions. Cancer Discovery *2*, 706–721.

Shotton, D.M. (1989). Confocal scanning optical microscopy and its applications for biological specimens. Journal of Cell Science *94*, 175–206.

Siegel, R.L., Miller, K.D., and Jemal, A. (2017). Cancer Statistics, 2017. CA Cancer J Clin *67*, 7–30.

Sipkins, D.A., Wei, X., Wu, J.W., Runnels, J.M., Côté, D., Means, T.K., Luster, A.D., Scadden, D.T., and Lin, C.P. (2005). In vivo imaging of specialized bone marrow endothelial microdomains for tumour engraftment. Nature *435*, 969–973.

Skobe, M., Hawighorst, T., Jackson, D.G., Prevo, R., Janes, L., Velasco, P., Riccardi, L., Alitalo, K., Claffey, K., and Detmar, M. (2001). Induction of tumor lymphangiogenesis by VEGF-C promotes breast cancer metastasis. Nature Medicine *7*, 192–198.

Smith, A.M., Mancini, M.C., and Nie, S. (2009). Bioimaging: second window for in vivo imaging. Nat Nanotechnol *4*, 710–711.

Snippert, H.J., van der Flier, L.G., Sato, T., van Es, J.H., van den Born, M., Kroon-Veenboer, C., Barker, N., Klein, A.M., van Rheenen, J., Simons, B.D., et al. (2010). Intestinal crypt homeostasis results from neutral competition between symmetrically dividing Lgr5 stem cells. Cell *143*, 134–144.

So, P., Dong, C.Y., Masters, B.R., and Berland, K.M. (2000). Two-photon excitation fluorescence microscopy. Annual Reviews Biomedical Engineering *2*, 399–429.

Sonoshita, M., Aoki, M., Fuwa, H., Aoki, K., Hosogi, H., Sakai, Y., Hashida, H., Takabayashi, A., Sasaki, M., Robine, S., et al. (2011). Suppression of colon cancer metastasis by Aes through inhibition of Notch signaling. Cancer Cell *19*, 125–137.

Sosa, M.S. (2016). Dormancy programs as emerging antimetastasis therapeutic alternatives. Mol Cell Oncol *3*, e1029062.

Sosa, M.S., Bragado, P., and Aguirre-Ghiso, J.A. (2014). Mechanisms of disseminated cancer cell dormancy: an awakening field. Nat Rev Cancer *14*, 611–622.

Sosa, M.S., Parikh, F., Maia, A.G., Estrada, Y., Bosch, A., Bragado, P., Ekpin, E., George, A., Zheng, Y., Lam, H.-M., et al. (2015). NR2F1 controls tumour cell dormancy via SOX9- and RARβ-driven quiescence programmes. Nature Communications *6*, 6170.

Spicer, J.D., McDonald, B., Cools-Lartigue, J.J., Chow, S.C., Giannias, B., Kubes, P., and Ferri, L.E. (2012a). Neutrophils Promote Liver Metastasis via Mac-1-Mediated Interactions with Circulating Tumor Cells. Cancer Research *72*, 3919–3927.

Spicer, J.D., McDonald, B., Cools-Lartigue, J.J., Chow, S.C., Giannias, B., Kubes, P., and Ferri, L.E. (2012b). Neutrophils promote liver metastasis via Mac-1-mediated interactions with circulating tumor cells. Cancer Research *72*, 3919–3927.

Spiegel, A., Brooks, M.W., Houshyar, S., Reinhardt, F., Ardolino, M., Fessler, E., Chen, M.B., Krall, J.A., DeCock, J., Zervantonakis, I.K., et al. (2016). Neutrophils Suppress Intraluminal NK Cell-Mediated Tumor Cell Clearance and Enhance Extravasation of Disseminated Carcinoma Cells. Cancer Discovery *6*, 630–649.

Stacker, S.A., Caesar, C., Baldwin, M.E., Thornton, G.E., Williams, R.A., Prevo, R., Jackson, D.G., Nishikawa, S., Kubo, H., and Achen, M.G. (2001). VEGF-D promotes the metastatic spread of tumor cells via the lymphatics. Nature Medicine *7*, 186–191.

Stacker, S.A., Williams, S.P., Karnezis, T., Shayan, R., Fox, S.B., and Achen, M.G. (2014). Lymphangiogenesis and lymphatic vessel remodelling in cancer. Nature Reviews Drug Discovery *14*, 159–172.

Steeg, P.S. (2006). Tumor metastasis: mechanistic insights and clinical challenges. Nature Medicine *12*, 895–904.

Steeg, P.S. (2016). Targeting metastasis. Nature Reviews Drug Discovery *16*, 201–218.

Stoletov, K., Kato, H., Zardouzian, E., Kelber, J., Yang, J., Shattil, S., and Klemke, R. (2010). Visualizing extravasation dynamics of metastatic tumor cells. Journal of Cell Science *123*, 2332–2341.

Stoletov, K., Montel, V., Lester, R.D., Gonias, S.L., and Klemke, R. (2007). High-resolution imaging of the dynamic tumor cell–vascular interface in transparent zebrafish. Proc. Natl. Acad. Sci. U.S.a. *104*, 17406–17411.

Stresing, V., Baltziskueta, E., Rubio, N., Blanco, J., Arriba, M.C., Valls, J., Janier, M., Clézardin, P., Sanz-Pamplona, R., Nieva, C., et al. (2013). Peroxiredoxin 2 specifically regulates the oxidative and metabolic stress response of human metastatic breast cancer cells in lungs. Oncogene *32*, 724–735.

Strilic, B., Yang, L., Albarrán-Juárez, J., Wachsmuth, L., Han, K., Müller, U.C., Pasparakis, M., and Offermanns, S. (2016). Tumour-cell-induced endothelial cell necroptosis via death receptor 6 promotes metastasis. Nature Reviews Drug Discovery *536*, 215–218.

Sullivan, N.J., Sasser, A.K., Axel, A.E., Vesuna, F., Raman, V., Ramirez, N., Oberyszyn, T.M., and Hall, B.M. (2009). Interleukin-6 induces an epithelial-mesenchymal transition phenotype in human breast cancer cells. Oncogene *28*, 2940–2947.

Svitkina, T.M., and Borisy, G.G. (1999). Arp2/3 complex and actin depolymerizing factor/cofilin in dendritic organization and treadmilling of actin filament array in lamellipodia. The Journal of Cell Biology *145*, 1009–1026.

Svoboda, O., Stachura, D.L., Machonova, O., Zon, L.I., Traver, D., and Bartunek, P. (2016). Ex vivo tools for the clonal analysis of zebrafish hematopoiesis. Nat Protoc *11*, 1007–1020.

Taichman, R.S., Patel, L.R., Bedenis, R., Wang, J., Weidner, S., Schumann, T., Yumoto, K., Berry, J.E., Shiozawa, Y., and Pienta, K.J. (2013). GAS6 receptor status is associated with dormancy and bone metastatic tumor formation. PLoS ONE *8*, e61873.

Tang, Q., Abdelfattah, N.S., Blackburn, J.S., Moore, J.C., Martinez, S.A., Moore, F.E., Lobbardi, R., Tenente, I.M., Ignatius, M.S., Berman, J.N., et al. (2014). Optimized cell transplantation using adult rag2 mutant zebrafish. Nat Meth *11*, 821–824.

Tang, Q., Moore, J.C., Ignatius, M.S., Tenente, I.E.S.M., Hayes, M.N., Garcia, E.G., n, N.T.Y.A., Bourque, C., He, S., Blackburn, J.S., et al. (2016). Imaging tumour cell heterogeneity following cell transplantation into optically clear immune- deficient zebrafish. Nature Communications *7*, 1–10.

Teng, Y., Xie, X., Walker, S., White, D.T., Mumm, J.S., and Cowell, J.K. (2013). Evaluating human cancer cell metastasis in zebrafish. BMC Cancer *13*, 453.

Thiery, J.P. (2002). Epithelial-mesenchymal transitions in tumour progression. Nat Rev Cancer *2*, 442–454.

Timpson, P., McGhee, E.J., Morton, J.P., Kriegsheim, von, A., Schwarz, J.P., Karim, S.A., Doyle, B., Quinn, J.A., Carragher, N.O., Edward, M., et al. (2011). Spatial regulation of RhoA activity during pancreatic cancer cell invasion driven by mutant p53. Cancer Research *71*, 747–757.

Tojkander, S., Gateva, G., and Lappalainen, P. (2012). Actin stress fibers--assembly, dynamics and biological roles. Journal of Cell Science *125*, 1855–1864.

Tong, R.T., Boucher, Y., Kozin, S.V., Winkler, F., Hicklin, D.J., and Jain, R.K. (2004). Vascular normalization by vascular endothelial growth factor receptor 2 blockade induces a pressure gradient across the vasculature and improves drug penetration in tumors. Cancer Res. *64*, 3731–3736.

Trede, N.S., Langenau, D.M., Traver, D., Look, A.T., and Zon, L.I. (2004a). The use of zebrafish to understand immunity. Immunity *20*, 367–379.

Trede, N.S., Langenau, D.M., Traver, D., Look, A.T., and Zon, L.I. (2004b). The use of zebrafish to understand immunity. Immunity *20*, 367–379.

Tsuji, T., Ishizaki, T., Okamoto, M., Higashida, C., Kimura, K., Furuyashiki, T., Arakawa, Y., Birge, R.B., Nakamoto, T., Hirai, H., et al. (2002). ROCK and mDia1 antagonize in Rho-dependent Rac activation in Swiss 3T3 fibroblasts. The Journal of Cell Biology *157*, 819–830.

Ustione, A., and Piston, D.W. (2011). A simple introduction to multiphoton microscopy. J Microsc *243*, 221–226.

Valastyan, S., and Weinberg, R.A. (2011). Tumor Metastasis: Molecular Insights and Evolving Paradigms. Cell *147*, 275–292.

Valiente, M., Obenauf, A.C., Jin, X., Chen, Q., Zhang, X.H.F., Lee, D.J., Chaft, J.E., Kris, M.G., Huse, J.T., Brogi, E., et al. (2014). Serpins promote cancer cell survival and vascular co-option in brain metastasis. Cell *156*, 1002–1016.

van 't Veer, L.J., Dai, H., van de Vijver, M.J., He, Y.D., Hart, A.A.M., Mao, M., Peterse, H.L., van der Kooy, K., Marton, M.J., Witteveen, A.T., et al. (2002). Gene expression profiling predicts clinical outcome of breast cancer. Nature *415*, 530–536.

Vanharanta, S., and Massagué, J. (2013). Origins of metastatic traits. Cancer Cell *24*, 410–421.

Vesely, M.D., Kershaw, M.H., Schreiber, R.D., and Smyth, M.J. (2011). Natural innate and adaptive immunity to cancer. Annu. Rev. Immunol. *29*, 235–271.

Vestweber, D. (2015). How leukocytes cross the vascular endothelium. Nature Reviews Immunology *15*, 692–704.

Virchow, R. (1859). Die Cellularpathologie in ihrer Begründung auf physiologische und pathologische Gewebelehre: zwanzig Vorlesungen, gehalten während der Monate ....

Wagenblast, E., Soto, M., Gutiérrez-Ángel, S., Hartl, C.A., Gable, A.L., Maceli, A.R., Erard, N., Williams, A.M., Kim, S.Y., Dickopf, S., et al. (2015). A model of breast cancer heterogeneity reveals vascular mimicry as a driver of metastasis. Nature *520*, 358–362.

Wan, L., Pantel, K., and Kang, Y. (2013). Tumor metastasis: moving new biological insights into the clinic. Nature Medicine *19*, 1450–1464.

Wang, J., Cao, Z., Zhang, X.-M., Nakamura, M., Sun, M., Hartman, J., Harris, R.A., Sun, Y., and Cao, Y. (2015). Novel mechanism of macrophage-mediated metastasis revealed in a zebrafish model of tumor development. Cancer Research *75*, 306–315.

Wculek, S.K., and Malanchi, I. (2015). Neutrophils support lung colonization of metastasis-initiating breast cancer cells. Nature *528*, 413–417.

Weber, M.R., Zuka, M., Lorger, M., Tschan, M., Torbett, B.E., Zijlstra, A., Quigley, J.P., Staflin, K., Eliceiri, B.P., Krueger, J.S., et al. (2016). Activated tumor cell integrin αvβ3 cooperates with platelets to promote extravasation and metastasis from the blood stream. Thromb. Res. *140 Suppl 1*, S27–S36.

Weilbaecher, K.N., Guise, T.A., and McCauley, L.K. (2011). Cancer to bone: a fatal attraction. Nat Rev Cancer *11*, 411–425.

White, R.M., Sessa, A., Burke, C., Bowman, T., LeBlanc, J., Ceol, C., Bourque, C., Dovey, M., Goessling, W., Burns, C.E., et al. (2008). Transparent Adult Zebrafish as a Tool for In Vivo Transplantation Analysis. Cell Stem Cell *2*, 183–189.

White, R., Rose, K., and Zon, L. (2013). Zebrafish cancer: the state of the art and the path forward. Nature Reviews Drug Discovery *13*, 624–636.

Wirtz, D., Konstantopoulos, K., and Searson, P.C. (2011). The physics of cancer: the role of physical interactions and mechanical forces in metastasis. Nat Rev Cancer *11*, 512–522.

Wolf, K., Wu, Y.I., Liu, Y., Geiger, J., Tam, E., Overall, C., Stack, M.S., and Friedl, P. (2007). Multi-step pericellular proteolysis controls the transition from individual to collective cancer cell invasion. Nat Cell Biol *9*, 893–904.

Wong, C.W., Song, C., Grimes, M.M., Fu, W., Dewhirst, M.W., Muschel, R.J., and Al-Mehdi, A.-B. (2002). Intravascular location of breast cancer cells after spontaneous metastasis to the lung. The American Journal of Pathology *161*, 749–753.

Wong, S.Y., and Hynes, R.O. (2006). Lymphatic or hematogenous dissemination: how does a metastatic tumor cell decide? Cell Cycle *5*, 812–817.

Worthylake, R.A., and Burridge, K. (2003). RhoA and ROCK promote migration by limiting membrane protrusions. Journal of Biological Chemistry *278*, 13578–13584.

Wyckoff, J., Wang, W., Lin, E.Y., Wang, Y., Pixley, F., Stanley, E.R., Graf, T., Pollard, J.W., Segall, J., and Condeelis, J. (2004). A paracrine loop between tumor cells and macrophages is required for tumor cell migration in mammary tumors. Cancer Res. *64*, 7022–7029.

Xian, X., Håkansson, J., Ståhlberg, A., Lindblom, P., Betsholtz, C., Gerhardt, H., and Semb, H. (2006). Pericytes limit tumor cell metastasis. J. Clin. Invest. *116*, 642–651.

Xu, J., Lamouille, S., and Derynck, R. (2009). TGF-beta-induced epithelial to mesenchymal transition. Cell Res. *19*, 156–172.

Xu, J., Wang, F., Van Keymeulen, A., Herzmark, P., Straight, A., Kelly, K., Takuwa, Y., Sugimoto, N., Mitchison, T., and Bourne, H.R. (2003). Divergent signals and cytoskeletal assemblies regulate self-organizing polarity in neutrophils. Cell *114*, 201–214.

Yachida, S., Jones, S., Bozic, I., Antal, T., Leary, R., Fu, B., Kamiyama, M., Hruban, R.H., Eshleman, J.R., Nowak, M.A., et al. (2010). Distant metastasis occurs late during the genetic evolution of pancreatic cancer. Nature *467*, 1114–1117.

Yang, J., Mani, S.A., Donaher, J.L., Ramaswamy, S., Itzykson, R.A., Come, C., Savagner, P., Gitelman, I., Richardson, A., and Weinberg, R.A. (2004). Twist, a master regulator of morphogenesis, plays an essential role in tumor metastasis. Cell *117*, 927–939.

Yang, M., Baranov, E., Wang, J.-W., Jiang, P., Wang, X., Sun, F.-X., Bouvet, M., Moossa, A.R., Penman, S., and Hoffman, R.M. (2002). Direct external imaging of nascent cancer, tumor progression, angiogenesis, and metastasis on internal organs in the fluorescent orthotopic model. Proc. Natl. Acad. Sci. U.S.a. *99*, 3824–3829.

Yang, M.-H., Wu, M.-Z., Chiou, S.-H., Chen, P.-M., Chang, S.-Y., Liu, C.-J., Teng, S.-C., and Wu, K.-J. (2008). Direct regulation of TWIST by HIF-1alpha promotes metastasis. Nat Cell Biol *10*, 295–305.

Ye, X., Brabletz, T., Kang, Y., Longmore, G.D., Nieto, M.A., Stanger, B.Z., Yang, J., and Weinberg, R.A. (2017). Upholding a role for EMT in breast cancer metastasis. Nature *547*, E1–E3.

Yu, M., Bardia, A., Wittner, B.S., Stott, S.L., Smas, M.E., Ting, D.T., Isakoff, S.J., Ciciliano, J.C., Wells, M.N., Shah, A.M., et al. (2013). Circulating breast tumor cells exhibit dynamic changes in epithelial and mesenchymal composition. Science *339*, 580–584.

Yumura, S., Mori, H., and Fukui, Y. (1984). Localization of actin and myosin for the study of ameboid movement in Dictyostelium using improved immunofluorescence. The Journal of Cell Biology *99*, 894–899.

Yurchenco, P.D. (2011). Basement membranes: cell scaffoldings and signaling platforms. Cold Spring Harbor Perspectives in Biology *3*.

Zegers, M.M., and Friedl, P. (2014). Rho GTPases in collective cell migration. Small GTPases *5*, e28997.

Zervantonakis, I.K., Hughes-Alford, S.K., Charest, J.L., Condeelis, J.S., Gertler, F.B., and Kamm, R.D. (2012). Three-dimensional microfluidic model for tumor cell intravasation and endothelial barrier function. Proc. Natl. Acad. Sci. U.S.a. *109*, 13515–13520.

Zhan, T., Rindtorff, N., and Boutros, M. (2017). Wnt signaling in cancer. Oncogene *36*, 1461–1473.

Zhang, B., Shimada, Y., Hirota, T., Ariyoshi, M., Kuroyanagi, J., Nishimura, Y., and Tanaka, T. (2016). Novel immunologic tolerance of human cancer cell xenotransplants in zebrafish. Transl Res *170*, 89–98.e3.

Zhang, B., Shimada, Y., Kuroyanagi, J., Nishimura, Y., Umemoto, N., Nomoto, T., Shintou, T., Miyazaki, T., and Tanaka, T. (2014). Zebrafish xenotransplantation model for cancer stem-like cell study and high-throughput screening of inhibitors. Tumor Biol. *35*, 11861–11869.

Zhang, G., Hoersch, S., Amsterdam, A., Whittaker, C.A., Lees, J.A., and Hopkins, N. (2010a). Highly aneuploid zebrafish malignant peripheral nerve sheath tumors have genetic alterations similar to human cancers. Proc. Natl. Acad. Sci. U.S.a. *107*, 16940–16945.

Zhang, Q., Yang, M., Shen, J., Gerhold, L.M., Hoffman, R.M., and Xing, H.R. (2010b). The role of the intravascular microenvironment in spontaneous metastasis development. Int. J. Cancer *126*, 2534–2541.

Zhou, Z.N., Sharma, V.P., Beaty, B.T., Roh-Johnson, M., Peterson, E.A., van Rooijen, N., Kenny, P.A., Wiley, H.S., Condeelis, J.S., and Segall, J.E. (2014). Autocrine HBEGF expression promotes breast cancer intravasation, metastasis and macrophage-independent invasion in vivo. Oncogene *33*, 3784–3793.

Ziegler, W.H., Liddington, R.C., and Critchley, D.R. (2006). The structure and regulation of vinculin. Trends Cell Biol. *16*, 453–460.

Zinn, K.R., Chaudhuri, T.R., Szafran, A.A., O'Quinn, D., Weaver, C., Dugger, K., Lamar, D., Kesterson, R.A., Wang, X., and Frank, S.J. (2008). Noninvasive bioluminescence imaging in small animals. Ilar J *49*, 103–115.

Zomer, A., Maynard, C., Verweij, F.J., Kamermans, A., Schäfer, R., Beerling, E., Schiffelers, R.M., de Wit, E., Berenguer, J., Ellenbroek, S.I.J., et al. (2015). In Vivo imaging reveals extracellular vesicle-mediated phenocopying of metastatic behavior. Cell *161*, 1046–1057.

Chapter 2.

Intravital Imaging of Metastasis in Adult Zebrafish

The contents of this chapter were written by David Benjamin with editing by Richard Hynes, Adam Amsterdam, and Jess Hebert. The experiments in this chapter were performed by David Benjamin. This chapter is a reproduction of work originally published in BMC Cancer with minor alterations. The original paper can be located using the following reference:

David C. Benjamin and Richard O. Hynes. (2017). Intravital imaging of metastasis in adult Zebrafish. BMC Cancer *17*, 660-672

Introduction

Metastasis is the cause of the overwhelming majority of cancer-related deaths, yet our understanding of the underlying biology remains incomplete (Valastyan and Weinberg, 2011). The events that occur at the metastatic site (namely arrest, extravasation, and growth into a new tumor) are particularly poorly understood (Labelle and Hynes, 2012). These events are in need of further elucidation because they may be rate-limiting steps in the metastatic cascade, as evidenced by the fact that tumors can shed thousands of cells per day into circulation yet only a small fraction of these will go on to form metastases (Chambers et al., 2002). Studies of events at the metastatic site have indicated that dynamic interactions between tumor cells, platelets, leukocytes (Labelle et al., 2011; 2014; Qian et al., 2009; Spicer et al., 2012), and endothelial cells (Laubli et al., 2009) are key in regulating the formation of metastases. These interactions have been challenging to study in mice due to their transient nature and occurrence deep within vital organs (Fein and Egeblad, 2013). The development of intravital imaging techniques has begun to allow the observation of these events.

The current state of the art for intravital imaging in mice involves the surgical implantation of glass windows through which a tissue of interest can be imaged (Pittet and Weissleder, 2011). Protocols have been developed for imaging common sites of metastasis including the lung (Looney et al., 2010), liver (Ritsma et al., 2013), brain (Kienast et al., 2009), and bone marrow (Mazo et al., 1998). Once these windows have been installed, the animal can be imaged repeatedly over multiple weeks. These techniques have been used to study tumor cell arrest (Kienast et al., 2009), interactions with immune cells (Cools-Lartigue et al., 2013; Headley et al., 2016), and their early outgrowth into metastases (Kienast et al., 2009; Ritsma et al., 2012).

While imaging windows have allowed the study of metastatic sites in living mice, some key limitations have restricted their widespread adoption. First, each animal in an experiment requires the surgical implantation of an imaging window. The time required to prepare each animal limits the number that can be used in an experiment. Second, the equipment, expertise and time required to become proficient in the surgical techniques make intravital imaging a far-from-routine technique. Finally, certain tissues present further technical challenges beyond the installation of an imaging window. For example, the lung is one of the best-studied metastatic sites in mice (Nguyen et al., 2009). However, imaging the lung requires additional stabilization techniques to compensate for respiratory movements which reduce the duration of imaging (Alieva et al., 2014). These techniques can involve the *ex vivo* isolation of the lung (Al-Mehdi, AB et al., 2000) or methods to adhere the lung to imaging windows *in vivo* (Kreisel et al., 2010; Looney et al., 2010) to minimize its movement. The additional challenges associated with these techniques have limited the number of intravital imaging studies in murine lungs.

Zebrafish embryos have been extensively used as a model system for the intravital imaging of metastasis (He et al., 2012; Stoletov et al., 2010; Teng et al., 2013) owing to their optical transparency and development outside the mother. In addition, zebrafish share a great deal of homology with humans, with approximately 70% of human genes having an identifiable homolog in zebrafish (Howe et al., 2013). However, it remains unclear how well the embryonic microenvironment and remodeling vasculature recapitulate the situation in an adult fish.

The recent development of a transparent line of zebrafish, *casper* (White et al., 2008), offers an adult model for the intravital imaging of cancer and metastasis. *Casper* fish carry two homozygous mutations that prevent the development of melanophores and iridophores.

Without these two types of pigment cells, zebrafish are transparent even as adults, eliminating the need for any further manipulation of the animal prior to experimentation. *Casper* fish have been used to image the clonal heterogeneity (Moore et al., 2016; Tang et al., 2016) and neovascularization (Tang et al., 2016) of transplanted primary tumors. *Casper* fish have also been used as a quantitative system to study metastasis using fluorescence as a readout (Heilmann et al., 2015). In addition, micrometastases have been detected in tumor-bearing *casper* fish following the transplantation of tumors (Tang et al., 2016). However, the events at the metastatic site have not been studied in adult *casper* fish.

We describe here a protocol for the intravenous injection of tumor cells into young adult *casper* fish that is an improvement on current methods used for adult injections. We then describe a simple protocol for intravital imaging and demonstrate its utility by characterizing the behavior of tumor cells at the metastatic site over the course of two weeks.

Results

Development of adult intravenous injections

Retro-orbital (RO) injections are a common route for injecting cells or reagents directly into circulation in adult zebrafish (Pugach et al., 2009). However, in our hands, these injections have a low efficiency rate in irradiated young adult fish (6 to 10-weeks-old) as determined by the percentage of fish with tumors in the posterior of the animal 14 days post-injection (Fig. 1A and B). The posterior of the animal was chosen for quantification as all injections led to a tumor at the injection site, in the anterior of the animal, but only successful injections disseminated cells to the posterior.

In transparent *casper* fish, the major blood vessels are visible through the skin, allowing direct intravenous (IV) injections. We chose to inject into the common cardinal vein because it is a large target that is easy to locate under a dissecting microscope (Fig. 1C and Additional File 1A). Intravenous injections into the common cardinal vein offered improved efficiency compared to retro-orbital injections in 6 to 10-week-old *casper* fish (Fig. 1A and B). We developed the injection protocol using a GFP-labeled zebrafish melanoma cell line (ZMEL1) that has been previously described (Heilmann et al., 2015). This cell line was chosen as it is one of the few zebrafish cancer cell lines available and its metastatic behavior has been well characterized.

Injection success could be determined immediately following injection by observing GFP-positive cells in the gills and posterior of the fish (Fig. 1D). By 14 days post-injection, tumors were observed growing throughout the fish (Fig. 1A). Histology of fish at this time point

revealed tumors in multiple organs including the kidney, skin, gills, heart, intestine, and liver (Fig. 1E).

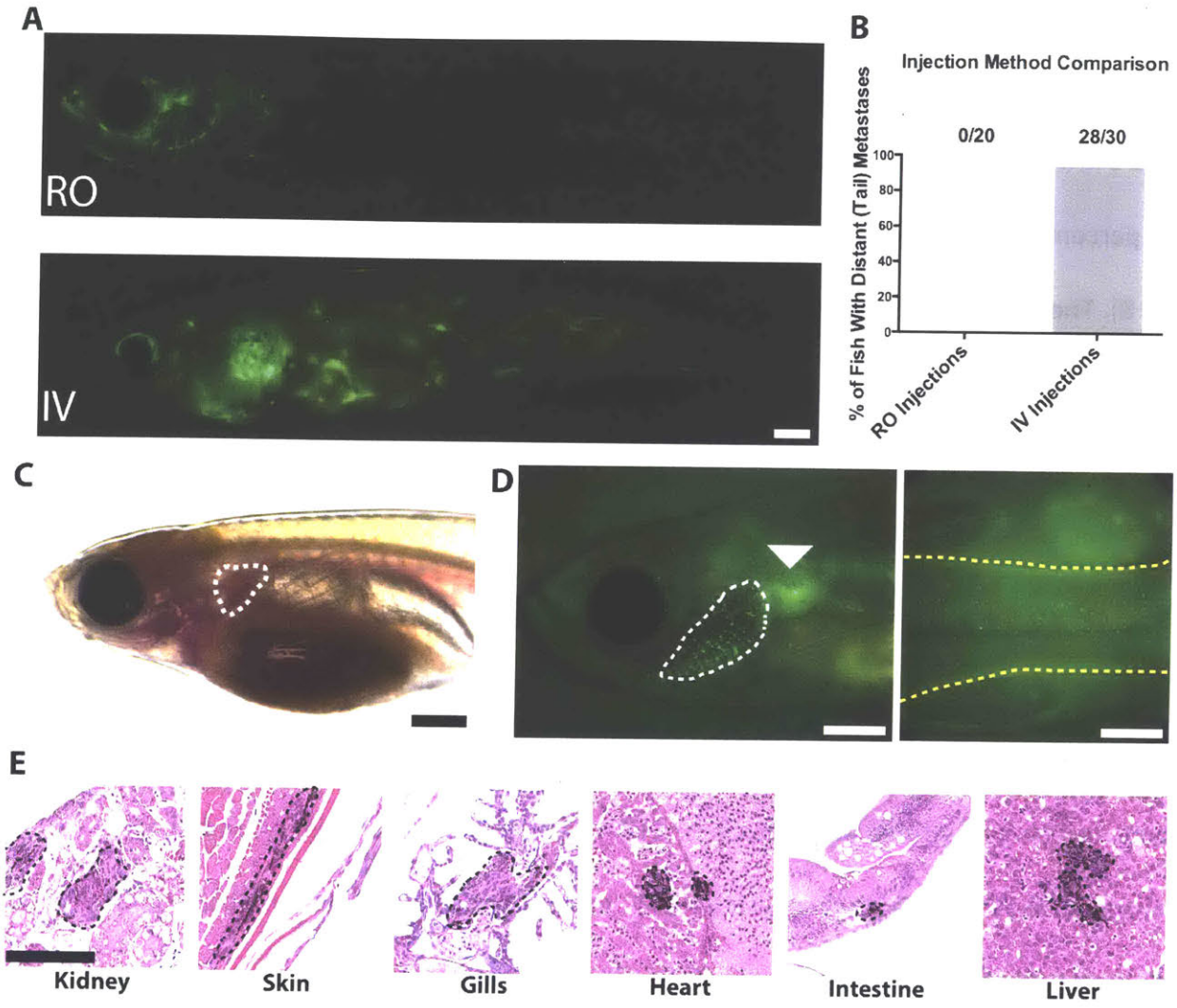

Figure 1 Intravenous injection of zebrafish melanoma cells (ZMEL1) into irradiated adult zebrafish. (**A**) Representative images of irradiated zebrafish injected with GFP-labeled zebrafish ZMEL1 melanoma cells 14 days after retro-orbital (top) and intravenous (bottom) injections. Scale bar is 1mm. (**B**) Quantification of injection efficiency of retro-orbital and intravenous injections as determined by the presence of distant metastases in the posterior of the fish with the success rate indicated. (**C**) 6 to 10-week-old *casper* fish with injection location (common cardinal vein) outlined. Scale bar is 1mm. (**D**) Example of a successful intravenous injection as indicated by GFP-labeled tumor cells in the gills (white dashed line) and posterior of an irradiated *casper* fish (yellow dashed line) 1 hour post-injection. The injection site is indicated with a white arrowhead. Scale bar is 1mm. (**E**) H&E stained transverse sections of irradiated zebrafish 14 days post-injection showing tumors in the indicated organs. Tumors are indicated by black dotted lines. Scale bar is 100μm.

Intravital imaging of adult zebrafish

In mice, intravital imaging requires surgical techniques to gain access to the organs of interest (Pittet and Weissleder, 2011). In contrast, *casper* fish require no surgical intervention prior to imaging. We were able to perform intravital imaging in these fish by simply placing them in a glass-bottom dish and immobilizing them with anesthetic and low-melt agarose (Fig. 2A). *Flk:dsRed2* fish were crossed into the *casper* background to allow visualization of the vasculature and tumor cells in living fish. The vasculature in these fish was clearly visible to a depth of 100μm with confocal microscopy or 200μm using 2-photon microscopy (Fig 2B and C).

The optimal imaging location was determined to be the region just lateral to the spine in the posterior of the fish near the tail fin (Fig. 2C). This region was relatively flat which allowed a large area to be visible in a single focal plane. In addition, this region was far enough from the head to be minimally affected by the fish's opercular movements. ZMEL1 cells could be observed in the vasculature in the skin and sub-dermal musculature in this region shortly following injection (Fig. 2C). In the first few hours following injection, tumor cells were observed flowing through blood vessels (Additional Movie 1) or stably arrested (Additional Movie 2).

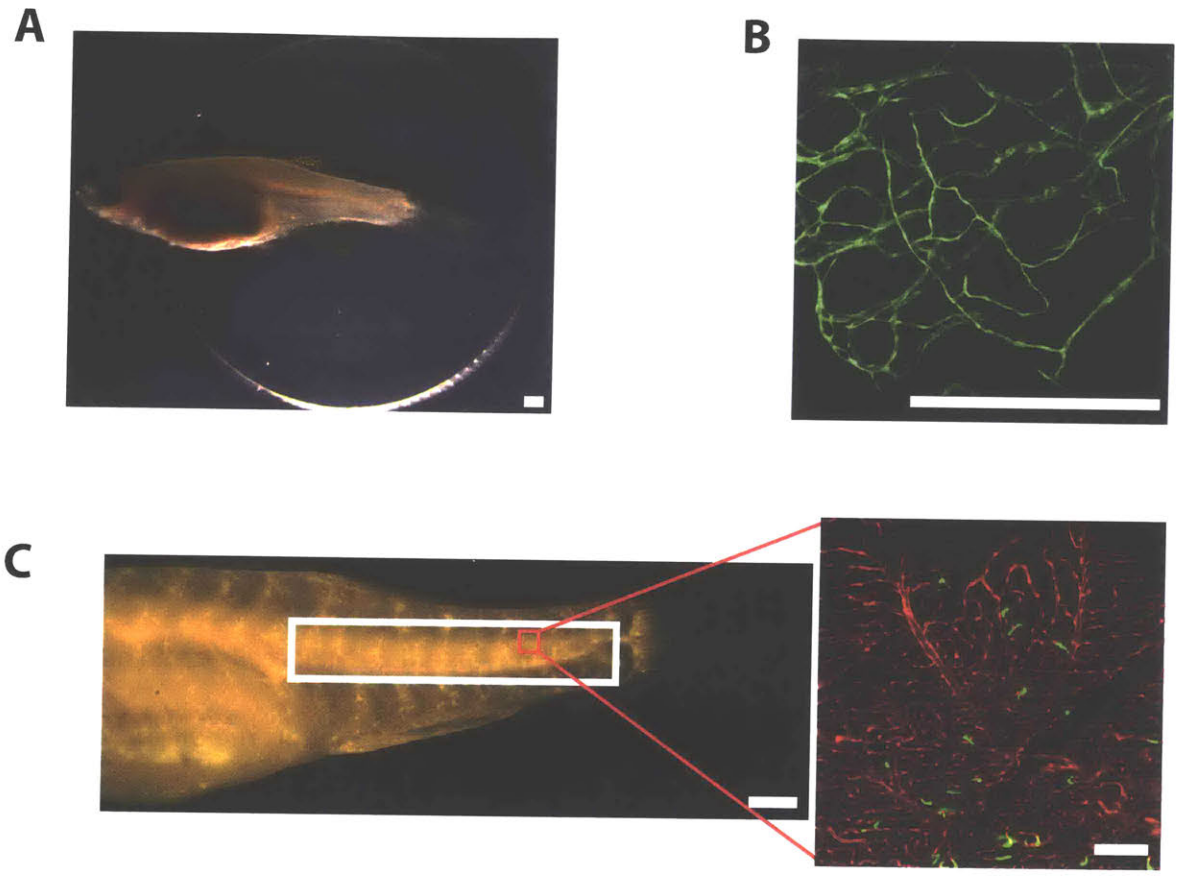

Figure 2 Live imaging of irradiated adult zebrafish following injection of ZMEL1 melanoma cells.

(**A**) Intravital imaging set-up with an adult zebrafish restrained in low-melt agarose in a glass-bottomed 6-well plate. Scale bar is 1mm. (**B**) Maximum intensity projection of a 200um two-photon Z stack showing the vasculature in a *casper;fli1:EGFP* zebrafish. Scale bar is 100um. (**C**) Region of imaging in the posterior of an irradiated *casper;flk:dsRed* zebrafish (white box) and example of a single 20x confocal field (red box). Scale bar for the posterior is 1mm. Scale bar for the 20x field is 100μm.

Studies of the early events at the metastatic site

We next investigated the early events at the metastatic site (namely arrest, extravasation, and early outgrowth of metastases) using intravital imaging. We first characterized the locations where ZMEL1 cells arrested within the first hour following injection. We observed that tumor cells arrested at three categories of locations: bends, branch points, or neither of the two (Fig. 3A). When we compared the relative frequencies of cells at these three locations, we found a majority (73%) of tumor cells arrested at bends and branch points, and the remaining 27% arrested at neither (Fig. 3B). The diameter of tumor cells arrested in vessels was then measured and was found to be larger than the narrowest point in the vessel adjacent to the arrested tumor cell (Fig. 3C). This result suggests that tumor cells in this system arrest once they become lodged in vessels too small for them to travel through.

Following injection with ZMEL1 cells, individual fish were imaged at the time points indicated (Fig. 3E). The non-invasive imaging protocol allowed each fish to be repeatedly imaged without any apparent ill effects. Extravasation was quantified during this time window by scoring cells as intravascular, extravasating, or extravascular (Fig. 3D). Extravasation began at 24 hours post-injection and increased until a peak at 72 hours post-injection. By 6 days post-injection (DPI), all remaining cells had extravasated or were in the process of extravasating (Fig. 3E).

The attrition of tumor cells at the metastatic site was followed at the same time points as above. Cell numbers were quantified as the fraction of cells relative to the first time point (3 hours post-injection). Cell numbers declined initially, reaching a plateau at 48 hours post-injection, after which cell numbers steadily increased until the end of the experiment (Fig. 3F).

During these imaging studies, we observed that many extravascular cells made long protrusions following extravasation (Fig. 3G). Over time these protrusions were observed to be lost (Fig. 3H).

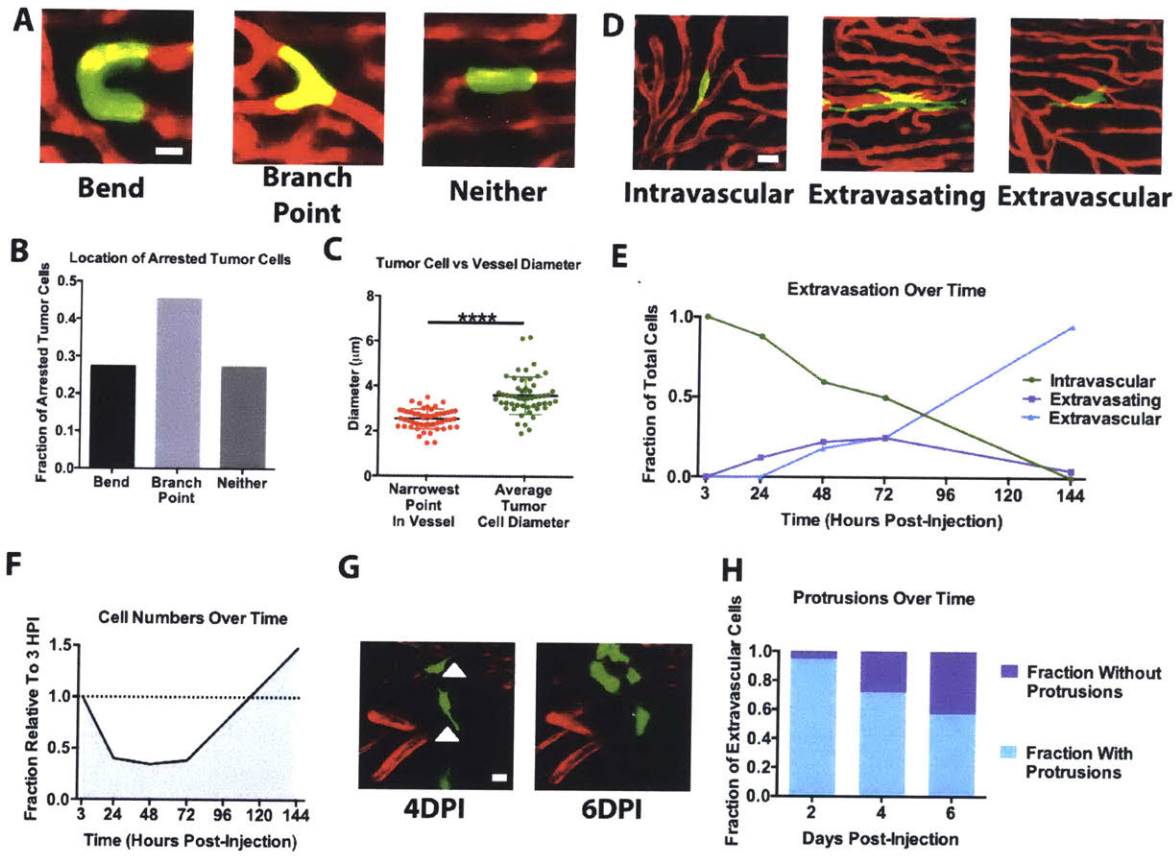

Figure 3 Imaging the early events at the metastatic site in irradiated Casper fish.
(**A**) Example images of ZMEL1 zebrafish melanoma cells arrested at bends, branch points, or neither within 3 hours of injection into *casper;flk:dsRed* fish. Scale bar is 10µm.
(**B**) Quantification of the fraction of ZMEL1 cells arrested at bends, branch points, or neither within three hours of injection. Quantifications are representative of 170 cells in 8 fish. (**C**) Quantifications of the diameter of arrested ZMEL1 cells and the diameter of the vessel in which they are arrested within 3 hours of injection. n= 53 cell and vessel pairs across 5 different fish. $p < 0.0001$ using a two-tailed Student's t test. (**D**) Example images of intravascular, extravasating, and extravascular cells 2 days post-injection. Scale bar is 10µm. (**E**) Quantification of the fraction of zebrafish melanoma cells that are intravascular, extravasating, and extravascular. Data are representative of 141 cells imaged across 8 different fish. (**F**) Quantification of the fraction of ZMEL1 melanoma cells remaining over time following injection. Data are representative of 58 fields in 10 fish. (**G**) Image of ZMEL1 cells 4 and 6 days post-injection showing the loss of protrusions (white arrowheads). Scale bar is 10µm. (**H**) Quantification of the fraction of ZMEL1 cells with protrusions over time. Data are representative of 164 cells in 3 fish.

Following our experiments with the ZMEL1 cell line, we expanded our studies to human tumor cells with well-studied *in vivo* metastatic phenotypes: the MDA-MB-435 melanoma cell line, the LM2 triple-negative breast cancer cell line, and the MA2 melanoma cell line. Following injection into irradiated Casper fish, some cells were observed to have extravasated by 24 hours post-injection (Additional File 2A). However, when the same location was imaged over time, LM2 cells were observed to disappear within two days of injection (Additional File 2B and C). We suspected that these cells were lost due to clearance by the immune system.

We tested various immunosuppression regimes using irradiation, dexamethasone, or a combination of both based on previous studies that have reported success in establishing tumor xenografts in zebrafish (Eden et al., 2014; Stoletov et al., 2007). We also tested two lines of genetically immunocompromised fish: $rag2^{450fs/450fs}$ and $prkdc^{D3612fs/D3612fs}$.

Despite these combinations, our efforts were ultimately unsuccessful (Additional Table 1). It is possible that other methods or cell lines would have been successful as other groups have reported success with different cell lines (Eden et al., 2014; Jung et al., 2016), zebrafish lines(Zhang et al., 2014), and immunotolerization approaches (Zhang et al., 2016). In addition, the continued development of lines of immunocompromised zebrafish suggests that this limitation may be temporary(Langenau, 2016).

It is possible that some of these results could be explained by the inability of these human cell lines to grow in zebrafish. While the MDA-MB-435 cells have previously been shown to grow in immunocompromised 4-week-old zebrafish (Stoletov et al., 2007), LM2 human breast cancer and MA2 human melanoma cells have not. To assay the growth of the LM2 and MA2 cells in zebrafish, these cell lines were injected into 2-day-old embryos. As the embryo

lacks an adaptive immune system, a failure to grow in this context could be the result of an intrinsic inability to grow in zebrafish rather than immune rejection. MA2 metastases in the tail grew between 1 and 4 days post-injection (Additional File 2D). However, LM2 cells were lost during this time period (Additional File 2D). While these results may indicate that the LM2 cells are being lost due to their inability to grow in zebrafish, the fact that MDA-MB-435 and MA2 cells also fail to engraft in adults suggests that immune rejection remains the primary hurdle for successful engraftment.

Studies of metastases over time

Currently, it is technically challenging to study the growth of metastases from single cells to large metastases in a living organism. We followed ZMEL1 cells over the course of two weeks as they formed metastases in irradiated Casper fish. We chose two weeks as the end-point for these studies because ZMEL1 tumors grow rapidly and it becomes difficult to distinguish individual metastases after this time point. Metastases will continue to grow out until 4 weeks post-injection, by which time the fish begin to look unhealthy and must be sacrificed in accordance with animal welfare guidelines (data not shown).

In order to return to the same locations over time, the vasculature was used to provide landmarks. In the region of the fish where imaging was performed, large vessels are seen at regular intervals between muscle segments (Fig. 4A). These vessels form unique patterns that can be recorded and later referenced for navigation. Using these vascular patterns (Fig. 4B), we were able to return to the same spot in the fish over two weeks.

Regions of the fish containing arrested tumor cells were identified shortly after injection. These regions were then imaged at the time points indicated and single, disseminated

tumor cells were followed as they grew into large metastases (Fig. 4C). Following extravasation, cells were quite migratory. Between day 2 and day 4 post-injection, cells rarely remained in the same location (Fig. 4D). Additionally, the morphology of metastases at day 9 post-injection was reminiscent of "pre-micrometastases" observed in early murine liver metastases using intravital imaging (Ritsma et al., 2012). In these "pre-micrometastases," cells were observed to be highly migratory over the course of 6 hours. To test whether the ZMEL1 tumors at day 9 in the zebrafish were also migratory, 9-day post-injection metastases were imaged every 3 hours over the course of 6 hours. During this time interval, minimal migration was observed. However, cells extensively changed shape by extending and retracting protrusions (Fig. 4E).

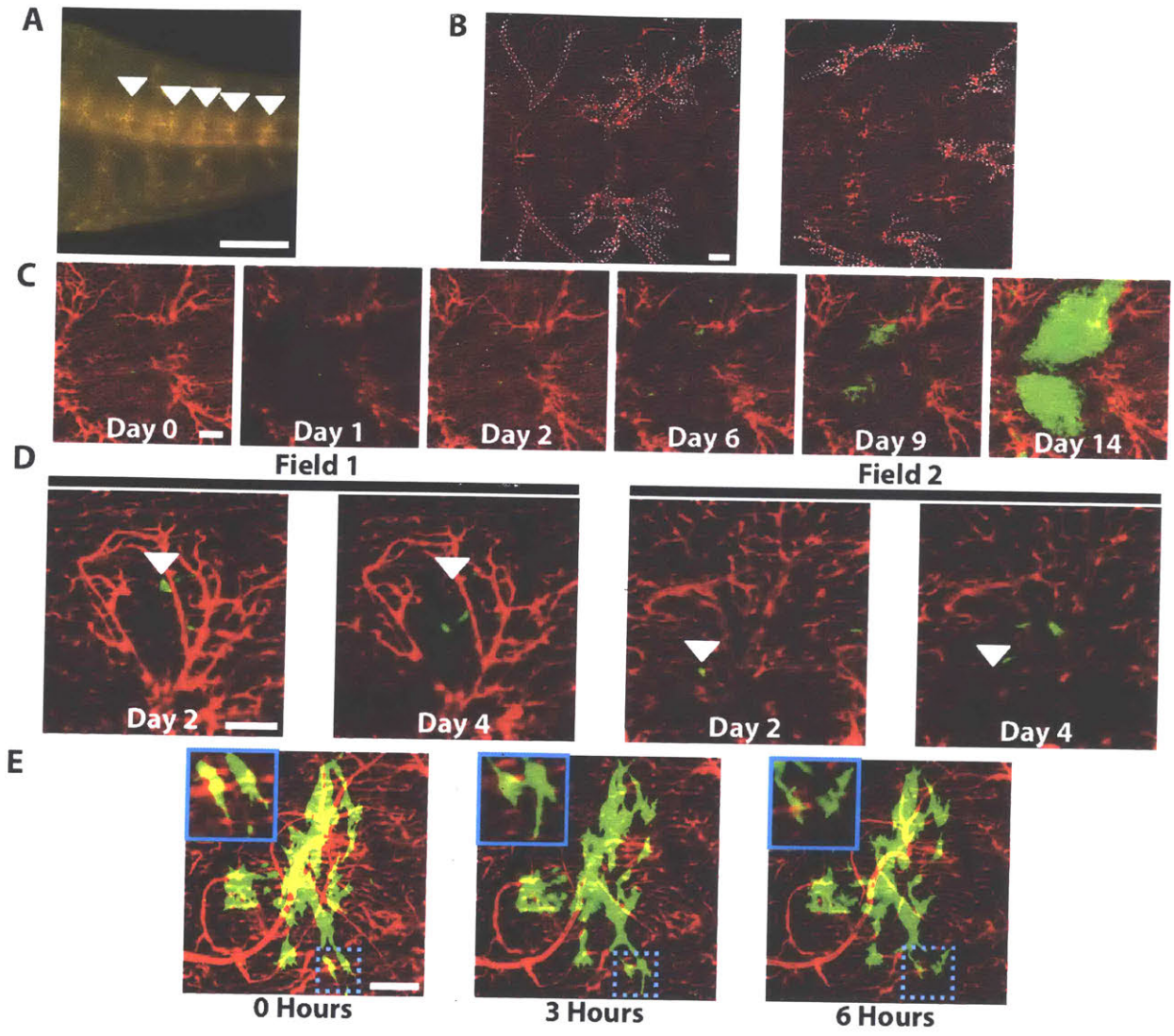

Figure 4 Imaging of disseminated tumor cells over the course of two weeks in irradiated Casper fish.

(**A**) Image of the tail of a *flk:dsRed;casper* fish with the large vessels used as landmarks indicated by white arrowheads. Scale bar is 1mm. (**B**) Example 10x fields with the large vessels used for landmarks (white dotted lines) highlighted to indicate that the vessels in each field are unique. Scale bar is 100μm. (**C**) One field containing ZMEL1 tumor cells imaged over the course of two weeks showing the growth pattern of metastases. Scale bar is 100μm. (**D**) Images of two sites on day 2 and day 4 post-injection showing that individual cells are rarely found in the same location during this time period. Arrowheads indicate the position of selected cells 2 days post-injection. Scale bar is 100μm. (**E**) One field 9 days post-injection that was imaged over the course of 6 hours showing cells extending and retracting protrusions. Inset shows higher magnification of two cells that change shape extensively during the 6 hours of imaging. Scale bar is 100μm.

Discussion

In this study, we report techniques for the intravenous injection of tumor cells into irradiated, young adult zebrafish, as well as an intravital imaging protocol to follow these cells over time as they form metastases. Metastasis is a complex, dynamic process that involves the interactions between tumor cells and many different cell types and factors in the microenvironment (Joyce and Pollard, 2008; Labelle and Hynes, 2012). This complexity is extremely difficult to recapitulate *in vitro*, frequently requiring studies of metastasis to be performed in a live organism, usually a mouse.

Intravital imaging techniques in mice have greatly increased our understanding of these events and the biology underlying them. However, intravital imaging protocols are not trivial, limiting their adoption as a standard laboratory technique. Zebrafish are another a useful model for imaging metastasis in real time *in vivo*. The majority of these experiments have used 2-day-old zebrafish embryos (He et al., 2012; Marques et al., 2009; Stoletov et al., 2010). However, it is unclear how similar the microenvironment and vasculature in the embryo are to those in adult fish. Adult fish have been used to study invasion and intravasation from a primary tumor but not the latter events of the metastatic cascade (Stoletov et al., 2007). We have shown here that adult *casper* zebrafish offer a useful model system for performing intravital imaging studies of the latter steps of the metastatic cascade.

We first demonstrated the reliable delivery of tumor cells throughout the animal following intravenous injections. Histology two weeks post-injection showed delivery to a wide range of organs. This result suggests that this intravenous injection technique could be used to study metastasis to organs besides the skin and muscle, which were chosen in this study for

their ease of imaging. Indeed, while we could not image deep into *casper* fish with confocal microscopy, the fluorescent signal was visible on a dissecting microscope and could be used to assay metastatic burden, potentially allowing zebrafish to be used for rapid, cheap experimental metastasis assays.

Following injection, cells could be imaged traveling in circulation and arresting in the vasculature in the first few hours following injection. The most common method for studying these events has been to sacrifice mice at short time points post-injection and analyze fixed sections (Gil-Bernabé et al., 2012; Labelle et al., 2014; Qian et al., 2009). While these studies have advanced our knowledge considerably, they have rarely been able follow a single cell over time, so these results are summaries of bulk populations. A few intravital imaging studies in mice have followed single cells over extended time periods (Kienast et al., 2009; Ritsma et al., 2012). However, there remains a relative paucity of studies that have monitored the behavior of individual cells over time. Of particular interest would be to track tumor cells following interactions with other cell types and observe the influence of these interactions on those cells' metastatic behavior. A recently developed technique allows for the continuous imaging of an anesthetized zebrafish for up to 24 hours (Richardson et al., 2016; Xu et al., 2014). Combining this technique with our injection method could allow for the study of these events with high temporal resolution.

In addition, the relative contribution of specific adhesion molecules and passive mechanical trapping to arrest remains an area of active research (Labelle and Hynes, 2012). Currently, it remains challenging to perform intravital imaging on more than a few mice in a day. Given that our methods allow the imaging of larger numbers of fish in a day, it would be

possible to screen the contributions of multiple adhesion molecules *in vivo* for their effect on arrest.

Extravasation is similarly a process in which live imaging could provide insight. Currently, most *in vivo* imaging studies of extravasation utilize embryonic systems (either zebrafish embryos or the chicken chorioallantoic membrane) as they provide easy imaging platforms (Leong et al., 2014; Stoletov et al., 2010). It remains unclear how well the remodeling vasculature of an embryo, and the microenvironment in these systems general, recapitulate those of an adult organism. The methods described here can bridge this gap by providing an ease of imaging similar to embryonic systems combined with an adult microenvironment.

The events between extravasation and the emergence of a clinically detectable metastasis remain one of the least well understood events of the metastatic cascade (Massagué and Obenauf, 2016). To date, there have been only a handful of studies that have used intravital imaging to tackle this question (Kienast et al., 2009; Ritsma et al., 2012). The methods presented here can be used to study the events in this time window. We demonstrated this by following single ZMEL1 cells for two weeks following injection. In the first 4 days following extravasation, cells were highly motile. In mice, extravasated tumor cells were also observed to be motile (Kienast et al., 2009; Ritsma et al., 2012) and it has been found that pharmacologic inhibition of this motility can inhibit metastatic outgrowth (Ritsma et al., 2012). These results suggest that a better understanding of motility at the metastatic site would be valuable.

In our experiments, micrometastases 9 days post-injection resembled a previously reported early metastatic phase in the murine liver (Ritsma et al., 2012). However, unlike the

situation in the murine liver, we did not observe rapid migration in the sub-dermal musculature on a similar time scale. Instead, the cells were relatively stationary while continuously extending and retracting protrusions. It would be interesting to see the effect of pharmacological inhibition of this activity on metastatic outgrowth.

We attempted to follow human cells in our system as well but found that they were quickly lost, presumably because of clearance by the immune system. We based our immunosuppression regime on two studies that reported success in growing human cells in adult zebrafish (Eden et al., 2014; Stoletov et al., 2007). Using these studies as a guide, we tested irradiation, treatment with dexamethasone or both in 6 to 10-week-old fish or in younger 4-week-old fish. As the adaptive immune system is still developing in 4 week old fish, it seemed possible that intervention at this time point might be more effective than at a later stage when the immune system is already fully developed (Trede et al., 2004). However, we were unsuccessful in establishing stably growing mammalian tumors.

One possible explanation is that some cell lines are better able to grow in adult zebrafish than others. For example, mouse glioma cells have been reported to grow in adult fish using only dexamethasone immunosuppression (Eden et al., 2014). In another study, DU145, K562, and HepG2 cells were all successfully engrafted using only a single dose of 20Gy of irradiation (Zhang et al., 2014). However, these experiments were performed using a different line of transparent fish (*nacre:rose*) making a direct comparison difficult. The MDA-MB-435 cell line, which we used, has been reported to grow in zebrafish immunosuppressed solely with dexamethasone (Stoletov et al., 2007). We also tested whether the LM2 and MA2 cell lines were able to grow in zebrafish embryos as a test of their ability to grow in a fish environment.

While the LM2 cells failed to grow even in the embryo, the MA2 cells did grow over the course of 4 days. These data potentially indicate that immune clearance (rather than a failure to grow in the fish environment) is the more likely explanation for most of our results.

One piece of evidence further supporting this hypothesis is that the strongest combination of dexamethasone and irradiation did allow some tumor growth before the fish died. To try to solve the problem of immune clearance, we tested two lines of genetically immunocompromised fish. The *rag2*$^{450fs/450fs}$ line of zebrafish contains a frame-shift mutation near the C-terminus of the *rag2* gene resulting in a hypomorphic allele. Fish homozygous for this allele lack T cells but still have B cells (Tang et al., 2014). These residual B cells could be responsible for the observed rejection of human tumor cells in these fish. The *prkdc*$^{D3612fs/D3612fs}$ fish lacks both B and T cells. In addition, there is another *prkdc* mutant line of fish that was developed around the same time (Jung et al., 2016). While the *prkdc*$^{D3612fs/D3612fs}$ line that we used was reported to reject mammalian tumor cells (Moore et al., 2016), this other *prkdc*$^{-/-}$ line was reported to allow the engraftment of multiple human tumor cell lines (Jung et al., 2016). It remains unclear how to reconcile these two conflicting studies. It is possible that differences in the genetic backgrounds or in the *prkdc* mutations themselves are responsible for these differing results.

All of the fish lines mentioned above still have functioning NK cells, which can reject xenotransplanted tumor cells. In mice, it is common to use animals that, in addition to a homozygous *prkdc* mutation, are homozygous for a mutation in the IL2 receptor gamma chain. This mutation serves to eliminate NK cells. Given the rapid development of immunocompromised zebrafish, it seems likely that such fish will soon be available. These or

other genetically immunocompromised lines of zebrafish may soon provide the appropriate background for xenotransplantation experiments.

Another approach to deal with rejection by the immune system is to tolerize fish to human tumor cells prior to transplantation. One such study injected irradiated tumor cells into 2-day-old *casper* embryos (Zhang et al., 2016). The embryos developed normally and these cells were slowly lost over time. However, when adults were later challenged with un-irradiated cells of the same line, tolerized fish developed tumors while naïve fish did not. If this technique can be replicated, it may offer a way around the challenges reported here, albeit, with increased technical complexity.

The above studies show that there is a great deal of heterogeneity in approaches and results of xenotransplantation in adult zebrafish. Recently, allotransplantation has developed into a mature and reproducible technique in adult zebrafish (Heilmann et al., 2015; Moore et al., 2016; Tang et al., 2014). This development coincides with the development of a great number of zebrafish tumor models (White et al., 2013). Cell lines could be derived from these models, which could then be used with the experimental techniques described here. Working with zebrafish tumor cells also has the advantage of avoiding species incompatibilities that could affect studies of a tumor cell's interactions with its microenvironment.

Conclusions

The events at the metastatic site are currently poorly understood. While intravital imaging studies have begun to improve our understanding of them, intravital imaging in mice is a technically challenging and far-from-routine technique. Zebrafish embryos are a common model system for intravital imaging of the metastatic site. However, an adult model system is

more likely to recapitulate the events in human patients. We exhibited here that irradiated, adult *casper* zebrafish provide a simple system for intravital imaging of the metastatic site. We first reported an efficient protocol for the injection of cells into circulation in young adult zebrafish. We then used an intravital imaging protocol to follow individual tumor cells at the metastatic site over the course of two weeks. Our results demonstrate that adult *casper* fish are a useful system for performing intravital imaging of the metastatic site. Furthermore, given the low cost of zebrafish and simplicity of our methods, they offer to increase access to intravital imaging.

Additional Files

A

Additional File 1. Example image of an intravenous injection into the common cardinal vein. (**A**) Example image showing the positioning of the needle and anesthetized zebrafish during intravenous injections.

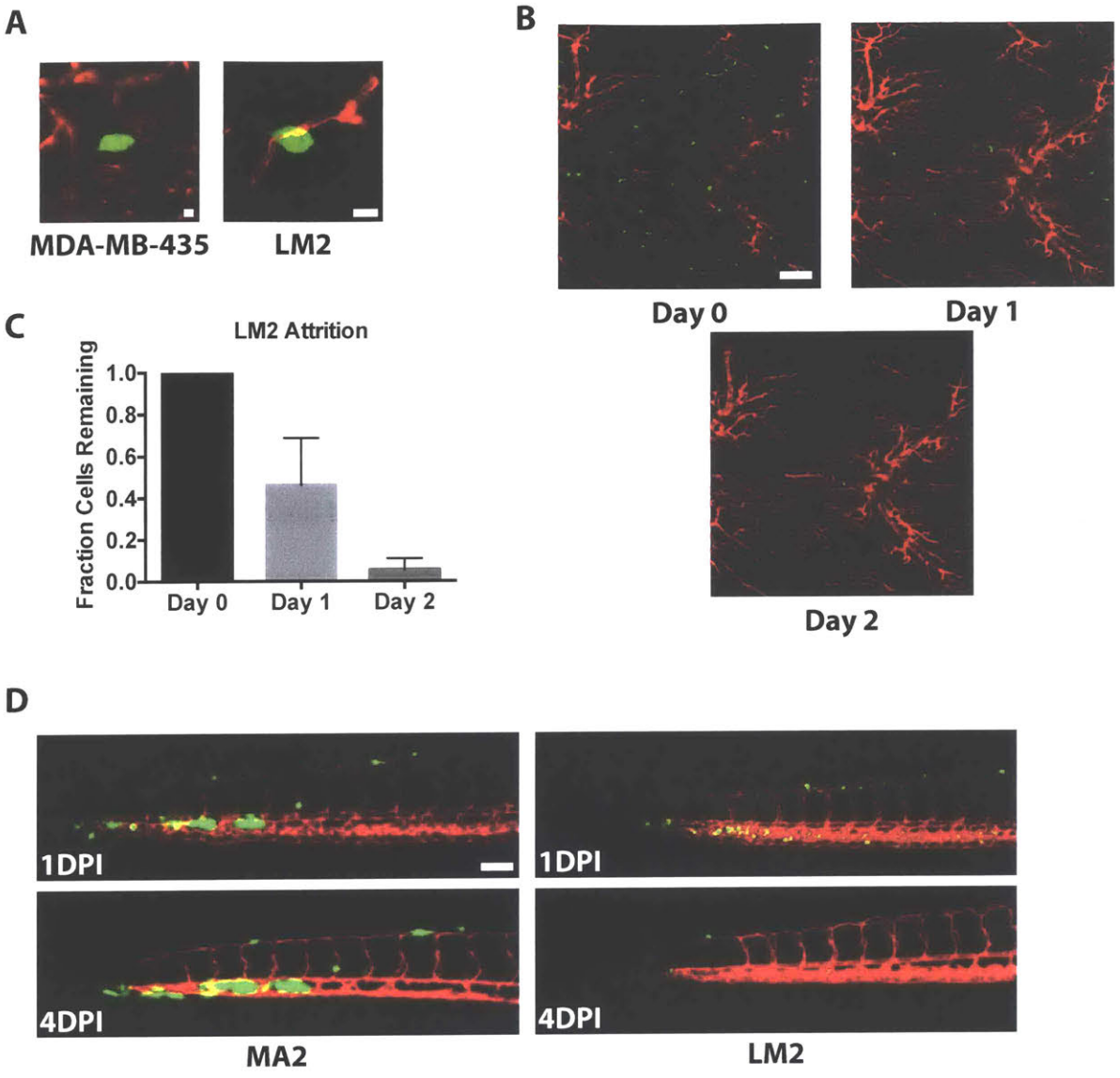

Additional File 2. Human tumor cells arrest and extravasate in irradiated adult zebrafish but fail to form tumors.

(**A**) Images of human melanoma (MDA-MB-435) and breast cancer (LM2) cells that have extravasated in zebrafish 2 days post-injection. Scale bars are 10μm. (**B**) Images showing the attrition of LM2 cells over time in adult zebrafish following injection. Scale bar is 100μm. (**C**) Quantification of the fraction of LM2 cells remaining over time in adult zebrafish. n= 47 fields in 7 different fish. (**D**) Images of the tails of embryos 1 and 4 DPI (3 and 6 days old) injected with LM2 or MA2 cells. Scale bar is 100μm.

Human Cell Xenograft Experiment Results

Age	Immunosuppression Method(s)			Cell Line	Result
	Irradiation	Drug	Fish Line		
6-10 Weeks	15Gy X 2	None	*casper*	MA2	Tumors rejected within 1 week
4 Weeks	15Gy X 2	None	*casper*	MA2	Tumors rejected within 1 week
6-10 Weeks	20Gy X 2	None	*casper*	MA2	Tumors rejected within 1 week
6-10 Weeks	None	Dexamethasone	*casper*	MA2	Tumors rejected within 1 week
4 Weeks	None	Dexamethasone	*casper*	MA2	Tumors rejected within 1 week
6-10 Weeks	20Gy x 2	Dexamethasone	*casper*	MDA-MB-435	Fish died after 3-5 days
6-10 Weeks	15Gy x 2	Dexamethasone	*casper*	MDA-MB-435 and LM2	Tumor grew for 1 week but was rejected by 2 weeks
6-10 Weeks	None	None	*casper*; *rag2* $^{450fs/450fs}$	MA2	Tumors rejected within 1 week
6-10 Weeks	None	None	*casper*; *prkdc* $^{D3612fs/D3612fs}$	MDA-MB-435	Tumors rejected within 1 week

Additional Table 1.
Table summarizing the immunosuppression conditions tested and the results of each method following xenotransplantation.

Additional Movie 1
ZMEL1 cells flowing through the sub-dermal vasculature 56 minutes post-injection. Time code is in seconds. Scale bar is 100μm.
URL:
https://www.ncbi.nlm.nih.gov/pmc/articles/PMC5613480/bin/12885_2017_3647_MOESM2_ESM.avi
Alternative URL: https://www.davidcbenjamin.com/additional-movie-1

Additional Movie 2
ZMEL1 cells stably arrested in the sub-dermal vasculature 140 minutes post-injection. Time code is in seconds. Scale bar is 100μm.
URL:
https://www.ncbi.nlm.nih.gov/pmc/articles/PMC5613480/bin/12885_2017_3647_MOESM3_ESM.avi
Alternative URL: https://www.davidcbenjamin.com/additional-movie-2

References

Al-Mehdi, AB, Tozawa, K., Fisher, AB, Shientag, L., Lee, A., and Muschel, R.J. (2000). Intravascular origin of metastasis from the proliferation of endothelium-attached tumor cells: a new model for metastasis. Nature Medicine *6*, 100–102.

Alieva, M., Ritsma, L., Giedt, R.J., and Weissleder, R. (2014). Imaging windows for long-term intravital imaging: General overview and technical insights. Intravital.

Chambers, A.F., Groom, A.C., and MacDonald, I.C. (2002). Metastasis: Dissemination and growth of cancer cells in metastatic sites. Nat Rev Cancer *2*, 563–572.

Cools-Lartigue, J., Spicer, J., McDonald, B., Gowing, S., Chow, S., Giannias, B., Bourdeau, F., Kubes, P., and Ferri, L. (2013). Neutrophil extracellular traps sequester circulating tumor cells and promote metastasis. J. Clin. Invest. *123*, 3446–3458.

Eden, C.J., Ju, B., Murugesan, M., Phoenix, T.N., Nimmervoll, B., Tong, Y., Ellison, D.W., Finkelstein, D., Wright, K., Boulos, N., et al. (2014). Orthotopic models of pediatric brain tumors in zebrafish. *0*, 1–7.

Fein, M.R., and Egeblad, M. (2013). Caught in the act: revealing the metastatic process by live imaging. Disease Models & Mechanisms *6*, 580–593.

Gil-Bernabé, A.M., Ferjancic, S., Tlalka, M., Zhao, L., Allen, P.D., Im, J.H., Watson, K., Hill, S.A., Amirkhosravi, A., Francis, J.L., et al. (2012). Recruitment of monocytes/macrophages by tissue factor-mediated coagulation is essential for metastatic cell survival and premetastatic niche establishment in mice. Blood *119*, 3164–3175.

He, S., Lamers, G.E., Beenakker, J.-W.M., Cui, C., Ghotra, V.P., Danen, E.H., Meijer, A.H., Spaink, H.P., and Snaar-Jagalska, B.E. (2012). Neutrophil-mediated experimental metastasis is enhanced by VEGFR inhibition in a zebrafish xenograft model. J. Pathol. *227*, 431–445.

Headley, M.B., Bins, A., Nip, A., Roberts, E.W., Looney, M.R., Gerard, A., and Krummel, M.F. (2016). Visualization of immediate immune responses to pioneer metastatic cells in the lung. Nature *531*, 513–517.

Heilmann, S., Ratnakumar, K., Langdon, E.M., Kansler, E.R., Kim, I.S., Campbell, N.R., Perry, E.B., McMahon, A.J., Kaufman, C.K., van Rooijen, E., et al. (2015). A Quantitative System for Studying Metastasis Using Transparent Zebrafish. Cancer Res. *75*, 4272–4282.

Howe, K., Clark, M.D., Torroja, C.F., Torrance, J., Berthelot, C., Muffato, M., Collins, J.E., Humphray, S., McLaren, K., Matthews, L., et al. (2013). The zebrafish reference genome sequence and its relationship to the human genome. Nature *496*, 498–503.

Joyce, J.A., and Pollard, J.W. (2008). Microenvironmental regulation of metastasis. Nat Rev Cancer *9*, 239–252.

Jung, I.H., Chung, Y.-Y., Jung, D.E., Kim, Y.J., Do Hee Kim, Kim, K.-S., and Park, S.W. (2016). Impaired Lymphocytes Development and Xenotransplantation of Gastrointestinal Tumor Cells in Prkdc-Null SCID Zebrafish Model. Neo *18*, 468–479.

Kienast, Y., Baumgarten, von, L., Fuhrmann, M., Klinkert, W.E.F., Goldbrunner, R., Herms, J., and Winkler, F. (2009). Real-time imaging reveals the single steps of brain metastasis formation. Nature Medicine *16*, 116–122.

Kreisel, D., Nava, R.G., Li, W., Zinselmeyer, B.H., Wang, B., Lai, J., Pless, R., Gelman, A.E., Krupnick, A.S., and Miller, M.J. (2010). In vivo two-photon imaging reveals monocyte-dependent neutrophil extravasation during pulmonary inflammation. Proc. Natl. Acad. Sci. U.S.a. *107*, 18073–18078.

Labelle, M., and Hynes, R.O. (2012). The Initial Hours of Metastasis: The Importance of Cooperative Host-Tumor Cell Interactions during Hematogenous Dissemination. Cancer Discovery *2*, 1091–1099.

Labelle, M., Begum, S., and Hynes, R.O. (2011). Direct Signaling between Platelets and Cancer Cells Induces an Epithelial-Mesenchymal-Like Transition and Promotes Metastasis. Cancer Cell *20*, 576–590.

Labelle, M., Begum, S., and Hynes, R.O. (2014). Platelets guide the formation of early metastatic niches. Proc. Natl. Acad. Sci. U.S.a. *111*, E3053–E3061.

Langenau, D.M. (2016). Cancer and Zebrafish.

Laubli, H., Spanaus, K.S., and Borsig, L. (2009). Selectin-mediated activation of endothelial cells induces expression of CCL5 and promotes metastasis through recruitment of monocytes. Blood *114*, 4583–4591.

Leong, H.S., Robertson, A.E., Stoletov, K., Leith, S.J., Chin, C.A., Chien, A.E., Hague, M.N., Ablack, A., Carmine-Simmen, K., McPherson, V.A., et al. (2014). Invadopodia Are Required for Cancer Cell Extravasation and Are a Therapeutic Target for Metastasis. CellReports *8*, 1558–1570.

Looney, M.R., Thornton, E.E., Sen, D., Lamm, W.J., Glenny, R.W., and Krummel, M.F. (2010). Stabilized imaging of immune surveillance in the mouse lung. Nat Meth *8*, 91–96.

Marques, I.J., Weiss, F., Vlecken, D.H., Nitsche, C., Bakkers, J., Lagendijk, A.K., Partecke, L., Heidecke, C.-D., Lerch, M.M., and Bagowski, C.P. (2009). Metastatic behaviour of primary human tumours in a zebrafish xenotransplantation model. BMC Cancer *9*, 128.

Massagué, J., and Obenauf, A.C. (2016). Metastatic colonization by circulating tumour cells. Nature *529*, 298–306.

Mazo, I.B., Gutierrez-Ramos, J.-C., Frenette, P.S., Hynes, R.O., Wagner, D.D., and Andrian, von, U.H. (1998). Hematopoietic Progenitor Cell Rolling in Bone Marrow Microvessels: Parallel Contributions by Endothelial Selectins and Vascular Cell Adhesion Molecule 1. Journal of Experimental Medicine *188*, 465–474.

Moore, J.C., Tang, Q., Yordán, N.T., Moore, F.E., Garcia, E.G., Lobbardi, R., Ramakrishnan, A., Marvin, D.L., Anselmo, A., Sadreyev, R.I., et al. (2016). Single-cell imaging of normal and malignant cell engraftment into optically clear prkdc-null SCID zebrafish. J. Exp. Med. *213*, 2575–2589.

Nguyen, D.X., Bos, P.D., and Massagué, J. (2009). Metastasis: from dissemination to organ-specific colonization. Nat Rev Cancer *9*, 274–284.

Pittet, M.J., and Weissleder, R. (2011). Intravital Imaging. Cell *147*, 983–991.

Pugach, E.K., Li, P., White, R., and Zon, L. (2009). Retro-orbital injection in adult zebrafish. J Vis Exp.

Qian, B., Deng, Y., Im, J.H., Muschel, R.J., Zou, Y., Li, J., Lang, R.A., and Pollard, J.W. (2009). A Distinct Macrophage Population Mediates Metastatic Breast Cancer Cell Extravasation, Establishment and Growth. PLoS ONE *4*, e6562.

Richardson, R., Metzger, M., Knyphausen, P., Ramezani, T., Slanchev, K., Kraus, C., Schmelzer, E., and Hammerschmidt, M. (2016). Re-epithelialization of cutaneous wounds in adult zebrafish combines mechanisms of wound closure in embryonic and adult mammals. Development *143*, 2077–2088.

Ritsma, L., Steller, E.J.A., Beerling, E., Loomans, C.J.M., Zomer, A., Gerlach, C., Vrisekoop, N., Seinstra, D., van Gurp, L., Schäfer, R., et al. (2012). Intravital microscopy through an abdominal imaging window reveals a pre-micrometastasis stage during liver metastasis. Sci Transl Med *4*, 158ra145–158ra145.

Ritsma, L., Steller, E.J.A., Ellenbroek, S.I.J., Kranenburg, O., Rinkes, I.H.M.B., and van Rheenen, J. (2013). Surgical implantation of an abdominal imaging window for intravital microscopy. Nat Protoc *8*, 583–594.

Spicer, J.D., McDonald, B., Cools-Lartigue, J.J., Chow, S.C., Giannias, B., Kubes, P., and Ferri, L.E. (2012). Neutrophils Promote Liver Metastasis via Mac-1-Mediated Interactions with Circulating Tumor Cells. Cancer Research *72*, 3919–3927.

Stoletov, K., Kato, H., Zardouzian, E., Kelber, J., Yang, J., Shattil, S., and Klemke, R. (2010). Visualizing extravasation dynamics of metastatic tumor cells. Journal of Cell Science *123*, 2332–2341.

Stoletov, K., Montel, V., Lester, R.D., Gonias, S.L., and Klemke, R. (2007). High-resolution imaging of the dynamic tumor cell–vascular interface in transparent zebrafish. Proc. Natl. Acad. Sci. U.S.a. *104*, 17406–17411.

Tang, Q., Abdelfattah, N.S., Blackburn, J.S., Moore, J.C., Martinez, S.A., Moore, F.E., Lobbardi, R., Tenente, I.M., Ignatius, M.S., Berman, J.N., et al. (2014). Optimized cell transplantation using adult rag2 mutant zebrafish. Nat Meth *11*, 821–824.

Tang, Q., Moore, J.C., Ignatius, M.S., Tenente, I.E.S.M., Hayes, M.N., Garcia, E.G., n, N.T.Y.A., Bourque, C., He, S., Blackburn, J.S., et al. (2016). Imaging tumour cell heterogeneity following cell transplantation into optically clear immune- deficient zebrafish. Nature Communications *7*, 1–10.

Teng, Y., Xie, X., Walker, S., White, D.T., Mumm, J.S., and Cowell, J.K. (2013). Evaluating human cancer cell metastasis in zebrafish. BMC Cancer *13*, 1–1.

Trede, N.S., Langenau, D.M., Traver, D., Look, A.T., and Zon, L.I. (2004). The use of zebrafish to understand immunity. Immunity *20*, 367–379.

Valastyan, S., and Weinberg, R.A. (2011). Tumor Metastasis: Molecular Insights and Evolving Paradigms. Cell *147*, 275–292.

White, R.M., Sessa, A., Burke, C., Bowman, T., LeBlanc, J., Ceol, C., Bourque, C., Dovey, M., Goessling, W., Burns, C.E., et al. (2008). Transparent Adult Zebrafish as a Tool for In Vivo Transplantation Analysis. Cell Stem Cell *2*, 183–189.

White, R., Rose, K., and Zon, L. (2013). Zebrafish cancer: the state of the art and the path forward. Nature Publishing Group *13*, 624–636.

Wittbrodt, J.N., Liebel, U., and Gehrig, J. (2014). Generation of orientation tools for automated zebrafish screening assays using desktop 3D printing. BMC Biotechnol *14*, 36–36.

Xu, C., Hasan, S.S., Schmidt, I., Rocha, S.F., Pitulescu, M.E., Bussmann, J., Meyen, D., Raz, E., Adams, R.H., and Siekmann, A.F. (2014). Arteries are formed by vein-derived endothelial tip cells. Nature Communications *5*, 1–11.

Xu, L., Shen, S.S., Hoshida, Y., Subramanian, A., Ross, K., Brunet, J.-P., Wagner, S.N., Ramaswamy, S., Mesirov, J.P., and Hynes, R.O. (2008). Gene expression changes in an animal melanoma model correlate with aggressiveness of human melanoma metastases. Molecular Cancer Research *6*, 760–769.

Zhang, B., Shimada, Y., Hirota, T., Ariyoshi, M., Kuroyanagi, J., Nishimura, Y., and Tanaka, T. (2016). Novel immunologic tolerance of human cancer cell xenotransplants in zebrafish. Transl Res *170*, 89–98.e3.

Zhang, B., Shimada, Y., Kuroyanagi, J., Nishimura, Y., Umemoto, N., Nomoto, T., Shintou, T., Miyazaki, T., and Tanaka, T. (2014). Zebrafish xenotransplantation model for cancer stem-like cell study and high-throughput screening of inhibitors. Tumor Biol. *35*, 11861–11869.

Chapter 3.

YAP Enhances Tumor Cell Dissemination by Allowing Transit Through the First Capillary Bed Encountered

The contents of this chapter were written by David Benjamin with editing by John Lamar and Richard Hynes. The experiments described in this chapter were performed by David Benjamin.

Introduction:

YAP (Yes-associated Protein) and TAZ (Transcriptional Co-activator with a PDZ Binding Domain, also known as WWTR1: WW Domain Containing Transcriptional Regulator) are transcriptional co-activators that are aberrantly activated in many human cancers. Our lab became interested in YAP when we discovered that it was a powerful promoter of metastasis (Lamar et al., 2012). However, exactly how it promotes metastasis was not clear as our experiments showed that YAP influenced a number of processes that are important to metastasis. In this chapter, I will first review YAP, TAZ, and the Hippo pathway (which regulates YAP and TAZ) and their role in cancer and metastasis. I will then describe our use of a zebrafish embryo model of metastasis and how that led to the discovery a novel mechanism of how YAP promotes metastasis.

Yorkie, YAP, and TAZ

In Drosophila, the Hippo pathway serves to regulate the activity of the transcriptional co-activator Yorkie (Fig 1A) (Huang et al., 2005). Yorkie cannot bind to DNA on its own but is instead dependent on its interaction with the transcription factor Scalloped to regulate transcription (Goulev et al., 2008; Wu et al., 2008; Zhang et al., 2008). This Yorkie/Scalloped complex is bound to the promoters of target genes and promotes transcription through interactions with mediator as well as chromatin-modifying enzymes (Jin et al., 2013; Oh et al., 2013; Qing et al., 2014).

When Yorkie is repressed, Scalloped is bound to Tondu-domain-containing growth inhibitor (Tgi) which serves to repress Yorkie target genes. When Yorkie is de-repressed, it outcompetes Tgi and binds to Scalloped to regulate transcription (Guo et al., 2013; Koontz et

al., 2013). In mammals the protein VGLL4 (Vestigial Like Family Member 4, an ortholog of Tgi) plays a similar role in negatively regulating YAP/TAZ target genes (Jiao et al., 2014; Zhang et al., 2014).

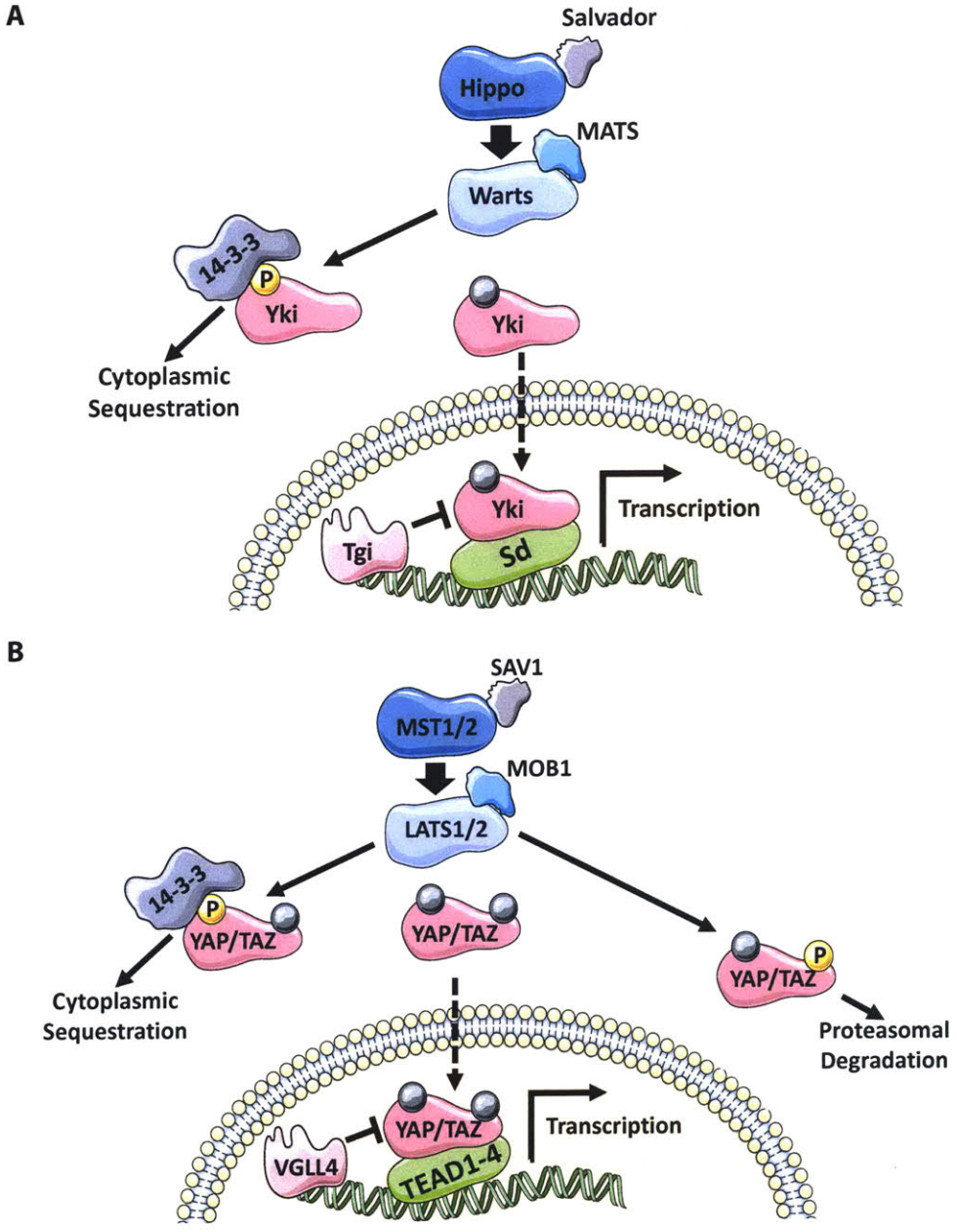

Figure 1. Overview of the Drosophila and mammalian core Hippo Pathways. (**A**) The Drosophila core Hippo pathway. (**B**) The mammalian core Hippo pathway. Figure 1 was generated from modified Servier Medical Art under a Creative Commons 3.0 Unported License (https://smart.servier.com).

In mammals, the Hippo pathway regulates the activity of two orthologs of *Yorkie*: YAP and TAZ (Fig 1B). When they were first discovered, their role in the Hippo pathway was unknown (Kanai et al., 2000; Sudol, 1994). However, since then, it has become clear that they are the major downstream effectors of the Hippo pathway. Like Yorkie, YAP and TAZ cannot bind to DNA. They primarily rely on orthologs of *Scalloped*, the TEAD family of transcription factors (of which there are 4 in humans), to bind to DNA and regulate transcription (Ota and Sasaki, 2008; Stein et al., 2015; Zhao et al., 2008; Zhou et al., 2016). YAP and TAZ can also bind other transcription factors including SMADs, p73, RUNX1/2, NKX2.1, NKX2.5, β-catenin, TBX5, and MRTFA (Cui et al., 2003; Di Palma et al., 2009; Hong and Yaffe, 2006; Kim et al., 2017a; Murakami et al., 2005; Park and Jeong, 2015; Strano et al., 2001; Varelas et al., 2008). However, TEADs appear to be important for most of YAP and TAZ's effects (Chan et al., 2009; Park et al., 2004; Stein et al., 2015; Yu et al., 2015b; Zanconato et al., 2015; Zhao et al., 2008).

YAP and TAZ share most of their core effector domains. For example, both contain a transcriptional activation domain and a TEAD-interacting domain. One difference between the two (apart from their size, YAP is 504AA where as TAZ is only 400AA) is that the primary isoform of YAP contains two WW domains while TAZ contains only one (Varelas, 2014). WW domains mediate protein-protein interactions and have been shown to regulate many of the functions of YAP and TAZ (Zhao et al., 2009). However, it should be noted that splice isoforms of YAP with only one WW domain and TAZ with two WW domains have been found and this alternative splicing can influence their function (Sudol, 2013); (Gaffney et al., 2012; Komuro et al., 2003; Webb et al., 2011).

While the cast of interaction partners for YAP and TAZ are remarkably similar, they clearly play non-redundant roles in mammals (Kohli et al., 2014). This is most strikingly apparently in their knockout phenotypes. YAP knockout in mice is embryonic lethal by day E8.5 (Morin-Kensicki et al., 2006). TAZ knockout mice on the other hand, are viable. They appear mostly normal with the exception of minor skeletal defects and a propensity to develop polycystic kidney disease (Hossain et al., 2007).

While YAP/TEAD and TAZ/TEAD complexes can bind the promoters of genes similarly to Yorkie/Scalloped, the majority of YAP/TAZ in complex with TEADs are bound to distal enhancer elements (Stein et al., 2015; Zanconato et al., 2015). A study of consensus motifs found that binding sites for AP-1 transcription factors are significantly enriched near TEAD-binding motifs in the mammalian genome and that AP-1 and YAP/TAZ/TEADs cooperate to regulate transcription (Zanconato et al., 2015). Given the differences in YAP/TAZ transcriptional targets across cell types, it seems likely that other transcription factors also cooperate with YAP/TAZ/TEADs to regulate target genes (Yu et al., 2015b).

While YAP/TAZ primarily bind distal enhance elements, they can be brought close to promoters through DNA looping (Lian et al., 2010; Stein et al., 2015; Zanconato et al., 2015). YAP/TAZ promote transcription by regulating transcriptional elongation by recruiting the mediator complex (Galli et al., 2015). YAP/TAZ also promote transcription by recruiting chromatin remodeling factors (Lian et al., 2010; Skibinski et al., 2014; Stein et al., 2015). YAP/TAZ can also directly inhibit transcription through recruitment of the NURD complex (Kim et al., 2015b). YAP/TAZ can regulate genes in a non-transcriptional manner as well through control of miRNA biogenesis (Chaulk et al., 2014; Mori et al., 2014).

The Core Hippo Pathway

The Hippo pathway regulates the activity of Yorkie in Drosophila and YAP and TAZ in vertebrates. In 1995, deletion of the gene *Warts* was observed to cause massive tissue overgrowth (Justice et al., 1995; Xu et al., 1995). Subsequently, mutations in *Salvador* (Kango-Singh et al., 2002), *Hippo* (Harvey et al., 2003; Jia et al., 2003a; Pantalacci et al., 2003; Udan et al., 2003; Wu et al., 2003a), and *Mob as tumor suppressor (Mats)* (Lai et al., 2005) were shown to phenocopy mutations in *Warts* as well as to interact genetically (Tapon et al., 2002). These components were placed into a new pathway which was shown to regulate organ size. This new pathway was termed the Hippo pathway after the appearance of the overgrown organs in *Hippo*-mutant Drosophila (Fig 1A) (Yu et al., 2015b).

In Drosophila, the most upstream kinase in the core pathway is Hippo (Harvey et al., 2003; Jia et al., 2003b). When Hippo is activated, it phosphorylates Warts which in turns induces Warts to phosphorylate Yorkie as described above (Wu et al., 2003b). Hippo also phosphorylates two scaffolding proteins Mats and Salvador which serve to aid in the activation of Warts (Fig 1A) (Wei et al., 2007). In mammals, MST1/2 (homologs of Hippo) phosphorylate LATS1/2 as well as the scaffolding proteins Mob1 and Sav1 in a similar mechanism of regulation (Callus et al., 2006; Chan et al., 2005; Praskova et al., 2004; Tapon et al., 2002) (Fig 1B).

Hippo is not the only kinase that can activate Warts. It has been shown that the kinases Misshapen and Happyhour can directly phosphorylate Warts and induce its activation (Li et al., 2014; Zheng et al., 2015). The orthologs of Misshapen and Happyhour in mammals are members of the MAP4K family and multiple members of this family been shown to regulate LATS1/2 through direct phosphorylation (Li et al., 2014; Meng et al., 2015; Zheng et al., 2015).

In recent years, upstream kinases that phosphorylate Hippo to activate the pathway have been identified. In Drosophila, Hippo can be activated by phosphorylation by Tao Kinase 1 in Drosophila (Boggiano et al., 2011; Poon et al., 2011). In Mammals, MST1/2 can also be phosphorylated by Tao kinases to induce Hippo pathway signaling (Poon et al., 2011). Hippo can also dimerize and phosphorylate in trans, leading to its activation without the need for other kinases (Deng et al., 2013; Jin et al., 2012). MST1/2 are also able to dimerize and this dimerization may play a role in their activation as well (Anand et al., 2008; Creasy et al., 1996; Ni et al., 2013).

The localization of Hippo and Warts may also control their activation. Hippo and Warts may be recruited to the apical membrane by Merlin, Expanded, and Kibra to promote their interaction and activation (Baumgartner et al., 2010; Genevet et al., 2010; Hamaratoglu et al., 2006; Yu et al., 2010). In mammals, Merlin can recruit LATS to the plasma membrane for activation by MST1/2 (Yin et al., 2013; Zhang et al., 2010).

In Drosophila, Yorkie activity is principally regulated by its subcellular localization. Yorkie can be phosphorylated by Warts which creates a binding site for 14-3-3 proteins which keep Yorkie sequestered in the cytoplasm (Huang et al., 2005; Oh and Irvine, 2008). In mammals, YAP and TAZ are phosphorylated by LATS1/2 (orthologs of Warts) on five (YAP) or four (TAZ) serine residues (Zhao et al., 2010). Phosphorylation of YAP on S127 (S89 for TAZ) also creates a binding site for 14-3-3 proteins and leads to cytoplasmic sequestration (Dong et al., 2007; Lei et al., 2008; Zhao et al., 2010; 2007). However, YAP/TAZ have additional regulation by phosphorylation that is not conserved with Yorkie. Phosphorylation on S381 of YAP (S311 on TAZ), creates a binding site for Casein Kinase-1 (CK1), which further phosphorylates YAP leading

to the recruitment of E3 ubiquitin ligase $SCF^{-\beta\text{-}TRCP}$, ubiquitylation, and subsequent degradation in the proteasome (Liu et al., 2010; Zhao et al., 2010b). TAZ also contains a second phosphodegron in its N-terminus which is not conserved with YAP (Liu et al., 2010).

Inputs Into The Hippo Pathway And Hippo-Independent Regulation of YAP/TAZ

When one looks at YAP and TAZ in cancer there is an apparent paradox. Despite the fact that many human cancers show aberrant YAP/TAZ activity, mutations in the core Hippo pathway components or YAP and TAZ themselves are rare (Harvey et al., 2013; Zanconato et al., 2016). One potential explanation for this discrepancy is that the sheer number of inputs into the Hippo pathway allows tumor cells to modify YAP/TAZ activity without the need to mutate core pathway components. In this section, I will cover the multitude of mechanisms by which a cell can regulate YAP and TAZ activity. As the inputs that regulate YAP and TAZ are already an exceptionally complex field of study, I will limit this section to mechanisms that have been shown to function in mammalian cells.

It should be pointed out here that the core Hippo kinase cascade (MST1/2 and LATS1/2) is only one mechanism for regulating YAP/TAZ activity. Over the past decade, it has become clear that there are many mechanisms that regulate YAP/TAZ which do not require the Hippo pathway core kinase cascade (Yu and Guan, 2013; Yu et al., 2015b). Indeed, there is debate over whether these may constitute the major mechanism for regulating YAP/TAZ activity in some cases (Zanconato et al., 2016). Adding to the complexity in the field, some inputs can regulate YAP/TAZ both through the core kinase cascade and other mechanisms simultaneously.

One of the first inputs of the Hippo pathway to be discovered was cell-cell adhesion. It was observed that the Hippo pathway was a key player in a phenomenon known as contact inhibition: where cells cease proliferation once they grow to confluence in vitro (Eagle and Levine, 1967; Zhao et al., 2007). Once in contact, epithelial cells form tight junctions (TJs) and adherens junctions (AJs) to connect with their neighbors (Harris and Tepass, 2010; Zihni et al., 2016). These junctions play a key role in mediating the Hippo pathway's regulation of contact inhibition (Varelas et al., 2010).

TJs have been shown to be important regulators of YAP/TAZ activity. For example, knockdown of PALS1 or Crb3 causes YAP/TAZ nuclear localization (Varelas et al., 2010). The Angiomotin family of proteins (AMOT, AMOTL1, and AMOTL2) are key mediators of TJ signaling to the hippo pathway. Angiomotins can induce YAP/TAZ phosphorylation by the Hippo pathway (Paramasivam et al., 2011; Zhao et al., 2011). Angiomotins can also sequester YAP at tight junctions through direct binding and this binding does not require core pathway activity (Chan et al., 2011; Wang et al., 2011; Zhao et al., 2011). ZO-1 has also been shown to sequester TAZ through direct binding (Remue et al., 2010). Conversely, ZO-2 can induce YAP nuclear localization (Oka et al., 2010). Many other TJ proteins including PATJ, MPDZ, and Lin7C can bind to components of the hippo pathway (Varelas et al., 2010; Wang et al., 2011).

Adherens junctions also play a role in regulating YAP/TAZ activity. Adhesions mediated by E-cadherin binding can inactivate YAP through the Hippo pathway (Kim et al., 2011). Many AJ proteins can regulate YAP/TAZ activity. For example, alpha-catenin can bind 14-3-3 proteins and sequester YAP/TAZ in a Hippo-dependent manner (Schlegelmilch et al., 2011; Varelas et al., 2010). The protein Ajuba can interact with LATS1/2 and inhibit YAP/TAZ activity. (Thakur et al.,

2010). Independently from the Hippo pathway, PTPN14 can sequester YAP/TAZ at AJs (Huang et al., 2013; Liu et al., 2013). However the role of its tyrosine phosphatase activity in regulating YAP activity is unclear (Huang et al., 2013; Liu et al., 2013; Wang et al., 2012).

In addition to cell-cell adhesion, YAP/TAZ is also regulated by cell-matrix adhesions. Cells can adhere to the extracellular matrix (ECM) through the integrin family of proteins (Hynes, 2002). In addition to meditating attachment to the ECM, integrins control multiple signaling pathways (Harburger and Calderwood, 2009). Many signaling pathways controlled by integrins rely on signaling through FAK. Consequently, FAK has been shown to be important for promoting YAP/TAZ activity downstream of integrin activation (Guan, 1997;Elbediwy et al., 2016; Fisher et al., 2016; Kim and Gumbiner, 2015). Another class of signaling molecules that can be downstream of integrin activation and FAK signaling are Src family kinases (SFKs) (Yeatman, 2004). In fact one of the SFKs, Yes, was the first interacting partner identified for YAP (Sudol, 1994). More recently, SFKs have been shown to regulate YAP/TAZ activity in both Hippo-dependent and Hippo-independent mechanisms (Ando et al., 2018; Byun et al., 2017; Fisher et al., 2016; Kim and Gumbiner, 2015; Rosenbluh et al., 2012; Si et al., 2017). YAP/TAZ can also be activated through Rho signaling downstream of integrins (Tang et al., 2013).

Cell polarity is another input that regulates YAP/TAZ activity. Apico-basal polarity proteins have been shown to play a role in regulating YAP/TAZ activity. For example, the polarity determinant Scribble, can promote LATS1/2 activation (Cordenonsi et al., 2011; Mohseni et al., 2014). The Crumbs polarity complex also regulates YAP/TAZ phosphorylation levels (Varelas et al., 2010). Planar-cell-polarity (PCP) may also regulate the Hippo pathway in

mammals but this input is not as clearly understood in mammals as in Drosophila (Azzolin et al., 2012; Huang et al., 2012; Yu and Guan, 2013; Yu et al., 2012a).

Another key input into YAP/TAZ activity are physical forces. Cells grown on soft substrates have been shown to have low YAP/TAZ activity, while cells growing on stiff substrates have high YAP/TAZ activity (Dupont et al., 2011). In addition to substrate stiffness, cell-density and the shape of an epithelial sheet can also produce forces that regulate YAP/TAZ activity (Aragona et al., 2013; Wada et al., 2011). Physical force on the nucleus can induce YAP nuclear entry through nuclear pores and this regulation is independent of the Hippo pathway (Elosegui-Artola et al., 2017). Another force that has been shown to regulate YAP/TAZ activity is sheer stress from fluid flow (Kim et al., 2014; Lee et al., 2017; 2018; Nakajima et al., 2017; Wang et al., 2016).

The observations described above have led the recognition of YAP and TAZ as key players in mechanotransduction (Dupont, 2016). Much of the response of YAP/TAZ to physical force is regulated through the cytoskeleton. Studies indicate that the levels of F-Actin and cytoskeletal tension regulate YAP/TAZ transcription. For example, knockdown of actin-capping proteins or actin severing proteins leads to increased YAP/TAZ activity (Aragona et al., 2013). Additionally, inhibition of cytoskeletal tension through inhibition of non-muscle myosin, ROCK, or MLCK decreases YAP/TAZ activity (Dupont et al., 2011; Wada et al., 2011). YAP/TAZ's response to mechanical cues can also be modulated by the composition of the ECM, such as Agrin (Chakraborty et al., 2017). Rho GTPases are also key mediators of YAP/TAZ's response to force (Dupont et al., 2011; Yu et al., 2012a; Zhao et al., 2012). Spectrin, a key constituent of the

cortical actin network, has also been shown to regulate Hippo pathway activity in a strain-dependent manner (Deng et al., 2015; Fletcher et al., 2015; Wong et al., 2015).

Key players in the regulation of YAP by the cytoskeleton are the Angiomotin family of proteins. Angiomotin can physically bind to YAP and sequester it in the cytoplasm when there are low levels of F-actin (Mana-Capelli et al., 2014). When F-actin levels are high, F-actin outcompetes YAP for Angiomotin binding, thereby freeing YAP to enter the nucleus (Mana-Capelli et al., 2014). The cytoskeleton can also regulate signaling through the core Hippo pathway as well through Rho regulation of LATS (Wada et al., 2011; Yu et al., 2012a). Mechanical force may also regulate YAP/TAZ through strain-induced JNK signaling (Codelia et al., 2014).

The Hippo pathway also integrates signals from soluble factors. Lysophosphatidic acid (LPA), Sphingosine-1-phosphate (S1P), Thrombin, Estrogen, and Angiotensin II can activate YAP/TAZ through GNAQ/11 or GNA12/13 repression of LATS1/2 activity (Miller et al., 2012; Mo et al., 2012; Wennmann et al., 2014; Yu et al., 2012b; Zhou et al., 2015). This repression requires the activity of Rho GTPases and the actin cytoskeleton (Yu et al., 2012b; Zhou et al., 2015). GNAQ/11 can also signal through conventional PKC which activates Rho GTPases (and YAP/TAZ activity) whereas novel PKC inhibits Rho GTPases (and inhibits YAP/TAZ activity) (Feng et al., 2014; Gong et al., 2015; Yu et al., 2014). Signals that function through GNAS, such as epinephrine and glucagon, de-repress LATS1/2 to inhibit YAP/TAZ activity (Yu et al., 2012a). These signals function through PKA which inhibits Rho GTPases thereby promoting LATS1/2 activity and YAP/TAZ phosphorylation (Kim et al., 2013b; Yu et al., 2012a; 2013a).

Stress signals are also key inputs into the Hippo pathway. Oxidative stress has been shown to activate MST1/2 activity (Ahn et al., 2005; Lehtinen et al., 2006). Furthermore, YAP/TAZ can induce the expression of genes that mediate the cell's response to oxidative stress to promote survival (Shao et al., 2014). Cellular energy stress can also regulate YAP/TAZ and the Hippo pathway. Under low ATP conditions, AMPK becomes active (Hardie et al., 2012). AMPK can then directly phosphorylate YAP and inhibit its interaction with TEADs (Mo et al., 2015; Wang et al., 2015). AMPK can also promote LATS1/2 phosphorylation of YAP (DeRan et al., 2014; Mo et al., 2015; Wang et al., 2015). Hypoxia also feeds into the Hippo pathway. Under hypoxic conditions, the transcription factor HIF1-α is stabilized and induces the transcription of hypoxia-responsive genes (Semenza, 2012). TAZ is a direct HIF1-α transcriptional target and is thereby transcriptionally up-regulated under hypoxic conditions (Xiang et al., 2014). In addition, other HIF1-α transcriptional targets, the E3 ubiquitin ligases SIAH1/2, ubiquitylate LATS2, targeting it for degradation (Ma et al., 2015).

Finally, there is extensive crosstalk between the Hippo pathway and other signaling pathways. One of the clearest examples of this is crosstalk with the Wnt pathway. YAP/TAZ are targets of the destruction complex and are relieved of their inhibition upon canonical Wnt signaling (Azzolin et al., 2012; 2014). YAP and TAZ can also directly bind to β-catenin to cooperatively regulate transcription (Park and Jeong, 2015). Non-canonical Wnt signaling can also activate YAP/TAZ activity through Frizzled signaling to Rho GTPases (Park et al., 2015). YAP/TAZ also can cooperate with sonic hedgehog (Shh), EGF, IGF, and MAPK signaling (Fan et al., 2013; Fernandez-L et al., 2009; Reddy and Irvine, 2013; Straßburger et al., 2012). The ligands of many signaling pathways including Wnt, Shh, Notch, TGF-β, JAK/STAT, and EGFR are also

regulated by YAP/TAZ (reviewed in (Yu et al., 2015a)). Finally, the cell cycle can also regulate YAP/TAZ activity. LATS1/2 can be phosphorylated by Aurora A and CDK1 to induce their activation (Morisaki et al., 2002; Toji et al., 2004; Yabuta et al., 2011; Zhang et al., 2012). CDK1 can also directly phosphorylate YAP, however, the role of this phosphorylation is unclear (Yang et al., 2013; 2015a; Zhao et al., 2014).

The Hippo Pathway in Cancer

YAP was first identified as a bona fide oncogene in mice when it was determined to be a key driver within a recurrent amplification in human and mouse cancer (Overholtzer et al., 2006). Since then, YAP and TAZ have been shown to be key players in cancer. Mis-regulation of YAP/TAZ activity or increased expression of YAP/TAZ have been seen in virtually every human cancer (Zanconato et al., 2016). Moreover, this aberrant YAP/TAZ expression or activity has been shown to be a poor prognostic indicator (Feng et al., 2016; Sun et al., 2015; Zhang et al., 2011). Numerous studies in mice have shown that, aberrant YAP/TAZ activity promotes tumor development in many different organs.

Given our use of a melanoma cell line in the experiments described in this chapter, I will briefly describe the role of YAP and TAZ in melanoma. For a full review of the role YAP/TAZ across cancer types see (Zanconato et al., 2016). TAZ has been shown to be highly expressed in normal human melanocytes and in human melanoma cell lines. YAP, on the other hand, is less frequently expressed and expressed at much lower levels when present (Kim et al., 2013a; Nallet-Staub et al., 2014). Despite its lower expression, YAP expression has been shown to increase with cutaneous melanoma tumor thickness and YAP expression negatively correlates

with patient survival (Menzel et al., 2014). While TAZ is expressed in human melanomas, it is less clear how its expression changes during tumor progression (Kim et al., 2013a; Nallet-Staub et al., 2014). One study that looked at TAZ using IHC found no correlation between TAZ expression levels and tumor thickness, though this study analyzed relatively few samples (Nallet-Staub et al., 2014). When genetic variants in components of the Hippo pathway were analyzed, SNPs in YAP1, TEAD1, and TEAD4 were shown to be predictive of poor prognosis in cutaneous melanoma patients (Yuan et al., 2015). Additionally, the upstream activator of the Hippo pathway Merlin has been shown to be a negative regulator of melanoma growth (Murray et al., 2012). Key driver mutations in a rare subtype of melanoma called uveal melanoma have recently been shown to function through YAP. As our work was with cutaneous melanoma, these uveal melanoma mutations will be described at the end of this section where I describe the known Hippo pathway mutations across human cancers.

Experiments have shown that YAP and TAZ play important roles in cutaneous melanoma. Knockdown of either YAP or TAZ inhibits invasion, anchorage-independent growth, and metastasis (Lamar et al., 2012; Nallet-Staub et al., 2014). Furthermore, the TEADs themselves have been shown to be key regulators of melanoma cell invasion (Verfaillie et al., 2015a). YAP has also been shown to promote resistance to BRAF inhibition and this inhibition is dependent on TEAD-mediated transcription (Fisher et al., 2017). One way that YAP contributes to resistance to BRAF inhibition is by promoting immune evasion through the regulation of PD-L1 in BRAF inhibition-resistant cells (Kim et al., 2018).

When all tumor types are considered, YAP/TAZ promote cancer development through three main mechanisms. First, YAP/TAZ promote proliferation by regulating many genes

involved in cell cycle progression (Kapoor et al., 2014; Santinon et al., 2018; Zanconato et al., 2015). In addition, YAP/TAZ can upregulate the transcription of other pro-proliferative oncogenes such as Myc (Zanconato et al., 2015). Second, YAP/TAZ provide resistance to apoptosis and senescence. YAP/TAZ can prevent apoptosis through upregulating anti-apoptotic proteins such as Bcl2 family members (Rosenbluh et al., 2012). YAP/TAZ prevent senescence by similarly upregulating proteins that oppose senescence such as Cdk6 (Dong et al., 2007; Xie et al., 2013). Finally, YAP/TAZ regulate transcriptional programs that endow tumor cells with cancer stem cell traits (Cordenonsi et al., 2011b; Park et al., 2018).

As mentioned earlier, mutations in YAP/TAZ themselves or core components of the Hippo pathway are relatively rare in human cancers (Harvey et al., 2013; Zanconato et al., 2016). However, there are a few tumor types that do have recurrent mutations in the Hippo pathway. Inactivating mutations in the gene NF2 (which encodes the protein Merlin) were identified as the cause of neurofibromatosis type 2, an inherited disease that causes numerous tumors including schwannomas and meningiomas (Agnihotri et al., 2016; Oh et al., 2015; Striedinger et al., 2008). Mesothelioma is another cancer type in which Hippo pathway component mutations have been discovered. NF2 is the most commonly affected pathway component in this tumor type with 40% of samples showing NF2 loss or mutations. LATS1 and MST1 are lost or mutated in 21% and 16% of mesotheliomas respectively. A non-functional LATS1-PSEN1 fusion gene has also been reported in mesothelioma samples (Miyanaga et al., 2015). Mutations are also seen in SAV1, LATS2, and MST2 at lower frequencies (Bueno et al., 2016). Core Hippo pathway component mutations are sporadically seen in other tumor types. LATS1/2 have been estimated to be mutated in 1-2% of human cancers based on data from the

COSMIC database (Yu et al., 2013b). MST1/2 mutations are similarly rare (Forbes et al., 2017). Sporadic mutations in MOB1 and SAV1 have also been reported.

YAP itself lies in a region of chromosome 11q22 that has been shown to be amplified in a number of cancers including hepatocellular carcinoma, medulloblastoma, and lung cancer although these amplifications are not enough to explain the broad activation of YAP activity across human cancers (Fernandez-L et al., 2009; Lorenzetto et al., 2014; Overholtzer et al., 2006; Zender et al., 2006). To date, activating mutations in YAP have not been identified in human cancers. However, a single germline point mutation in YAP has been shown to increase the risk of lung adenocarcinoma in carriers (Chen et al., 2015). There are also a few cancers where YAP fusion genes have been identified (Antonescu et al., 2013; Pajtler et al., 2015; Parker et al., 2014). TAZ mutations in cancer are rare with only TAZ-CAMTA1 and TAZ-FOSB fusion genes being observed in epithelioid hemangioendothelioma, a rare vascular tumor (Antonescu et al., 2014; Tanas et al., 2011).

Conversely, YAP has been found to be deleted in multiple myeloma (Cottini et al., 2014). Intriguingly, YAP has been suggested to be a tumor suppressor in the context of hematological malignancies (Cottini et al., 2014). However, YAP's role in this context is still far from clear and there are also data that YAP is not involved in tumorigenesis in these malignancies at all (Donato et al., 2018).

The lack of mutations in YAP/TAZ or core Hippo pathway components suggests that other cancer-promoting mutations can influence YAP/TAZ. Indeed, uveal melanoma, a rare subtype of malignant melanoma, has also been shown to involve the Hippo pathway. It has been observed that ~80% of uveal melanomas have mutations in GNAQ or GNA11 (Van

Raamsdonk et al., 2009; 2010). Recent work has shown that these mutations can induce YAP/TAZ activation (Feng et al., 2014). The mechanism behind YAP/TAZ activation by these mutations highlight how the field has attempted to reconcile the fact that YAP and TAZ seem to play a key role in cancer with the apparent lack of mutations in components of the core Hippo pathway. As described earlier, the YAP/TAZ activity is regulated by an extensive assortment of inputs. The current hypothesis is that the sheer number of inputs into the Hippo pathway allows for YAP/TAZ activity to be modified without the need to mutate core hippo pathway components. In the case of GNAQ/GNA11, activation of these genes activate YAP/TAZ through both inactivating the Hippo pathway and a Hippo-independent mechanism thus showing how mutations outside the core pathway can activate YAP/TAZ (Feng et al., 2014; Yu et al., 2012a).

The Hippo Pathway in Metastasis

YAP was first shown directly to promote metastasis by our lab. Over-expression of a Hippo-insensitive mutant of YAP enhanced metastasis in a number of breast cancer and a melanoma cell line (Lamar et al., 2012). In this work, YAP was shown enhance a number of cellular mechanisms which correlate with metastatic ability including invasion, migration, anchorage independent growth, and growth in 3D *in vitro* (Lamar et al., 2012). Since then, YAP and TAZ have been shown to play a role in every step of the metastatic cascade (Janse van Rensburg and Yang, 2016; Warren et al., 2018). In most cases, YAP/TAZ's promotion of metastasis or metastasis-associated traits are dependent on their ability to regulate transcription and interaction with the TEAD family of transcription factors (Warren et al., 2018). A current challenge in the field is determining which YAP/TAZ transcriptional target genes are

responsible for mediating YAP/TAZ's promotion of metastasis. This is complicated by the sheer number of genes that YAP/TAZ regulate, the fact that the set of YAP/TAZ target genes varies considerably across cell and tissue types, and the fact that YAP/TAZ play a role in multiple steps of the metastatic cascade (Hao et al., 2008; Warren et al., 2018; Yu et al., 2015b; Zhao et al., 2007).

The first hint that YAP/TAZ might be involved in metastasis was the observation that YAP over-expression promoted EMT in MCF10A cells (Overholtzer et al., 2006). Since then, YAP and TAZ have both been shown to induce EMT in a number of tumor types (Janse van Rensburg and Yang, 2016; Warren et al., 2018; Zanconato et al., 2016). Mechanistically, several key EMT transcription factors such as Foxc2, Twist, Snail, Slug, and Zeb1 are induced transcriptionally by YAP/TAZ (Lei et al., 2008; Li et al., 2015; Matteucci et al., 2013; Xiao et al., 2015) . YAP can also directly bind to the EMT-promoting transcription factor Zeb1 to cooperatively regulate transcription (Lehmann et al., 2016). This observation suggests that direct interactions with EMT transcription factors may also play a role in YAP's promotion of EMT.

YAP/TAZ expression levels are correlated with invasion in human patients and have been shown to promote migration and invasion in a number of tumor types (Bartucci et al., 2015; Ge et al., 2011; Kim et al., 2015a; Lamar et al., 2012; Verfaillie et al., 2015b; Vlug et al., 2013; Zhang et al., 2011). Some of the YAP/TAZ target genes regulating motility and invasion have been identified. In gastric cancer, YAP regulates motility by upregulating the Rho-GAP ARHGAP29 which leads to increased cofilin activity. In breast cancer YAP/TAZ can promote motility and invasion through the upregulation of Zyxin and BMP4 and the downregulation of ΔNp63 (Diepenbruck et al., 2014; Lai and Yang, 2013; Valencia-Sama et al., 2015). In

mesothelioma and breast cancer YAP/TAZ regulate motility and invasion through RHAMM (Shigeeda et al., 2017; Wang et al., 2014). In pancreatic cancer, YAP/TAZ can promote motility and invasion through upregulating LPAR3 (Yang et al., 2015b; Zhou et al., 2017). Many more YAP/TAZ target genes involved regulating motility and invasion likely remain to be discovered. Intriguingly, YAP may also be able to regulate invasion in a non-transcriptional manner. YAP has been reported to be localized to invadopodia, specialized membrane protrusions which degrade the ECM and promote invasion (Daszczuk and Proszynski, 2016; Eddy et al., 2017). However, the functional significance of this observation is unknown.

YAP/TAZ also play a role once tumor cells reach blood vessels and intravasate. YAP/TAZ activation by GNAQ has been shown to enhance intravasation in uveal melanoma (Huang et al., 2015). De-repressed YAP can also promote intravasation in breast cancer (Sharif et al., 2015). Many genes involved in motility are involved in intravasation as well suggesting that YAP's regulation of motility may also influence intravasation (Reymond et al., 2013).

Once in the circulation, tumor cells face multiple barriers to their survival. One such barrier is believed to be anoikis, which is a form of programmed cell death upon detachment from the ECM. YAP inactivation has been shown to be a requirement for activation of anoikis and YAP/TAZ activity resists anoikis in cancer cells (Zhao et al., 2012). Recent work has shown that shear stress from fluid flow can activate the Hippo pathway suggesting that blood flow could induce protective YAP/TAZ activity (Lee et al., 2017; 2018). Another mechanism of intravascular YAP/TAZ activation depends on interactions with platelets. Platelets are important mediators of metastases (Labelle and Hynes, 2012) and have recently been shown to activate

YAP/TAZ in tumor cells through RhoA to promote resistance to anoikis (Haemmerle et al., 2017).

Escaping the harsh intravascular environment by extravasating is a key requirement for successful metastasis. Consequently, YAP/TAZ have been shown to promote extravasation in breast and lung cancer cells lines (Gu et al., 2016; Sharif et al., 2015). Once again activation of YAP/TAZ by fluid shear stress may play a role in extravasation. Shear stress from fluid flow has been shown to regulate YAP and TAZ activity to promote cancer cell motility (Lee et al., 2017). Other metastasis enhancing genes have been observed to promote intravascular motility and this has been associated with enhanced extravasation (Stoletov et al., 2010). Shear stress activation may also prime metastasizing tumor cells for proliferation following extravasation. For example, TAZ activation by shear stress has been shown to promote tumor cell proliferation (Lee et al., 2018).

Once out of blood vessels, tumor cells face a number of challenges to their survival and proliferation at the metastatic site. Attachment to the ECM, and overcoming anoikis, is key requirement for outgrowth at the metastatic site (Shibue et al., 2013; 2012). Given YAP's role in resisting anoikis, it is unsurprising that YAP/TAZ have been suggested to promote outgrowth at the metastatic site in multiple tumor types (Kim et al., 2017b; Lamar et al., 2012; Liu et al., 2018; Yin et al., 2018; Zhao et al., 2012). In addition to survival, YAP/TAZ also promotes proliferation at the metastatic site (Hsu et al., 2015). Oxidative stress at the metastatic site is another barrier to metastasis (Piskounova et al., 2015). YAP/TAZ have been shown to regulate genes that respond to oxidative stress and could promote tumor cell survival under these conditions (Shao et al., 2014).

As described above, YAP/TAZ drive metastasis in multiple tumor types. Their role at the primary tumor and during the early steps of the metastatic cascade have been extensively studied (Janse van Rensburg and Yang, 2016; Warren et al., 2018; Zanconato et al., 2016). However, it is less clear how YAP/TAZ activation influence tumor cells at the metastatic site. To date, intravital imaging has not been applied to look at how activation of YAP/TAZ changes the behavior of tumor cells during metastasis. As reviewed in chapter 1, zebrafish embryos are a powerful system for the intravital imaging of metastasis. Therefore, we decided to use intravital imaging in zebrafish embryos to study how YAP activation influenced tumor cell behavior in circulation and at the metastatic site. This section of the thesis will describe these experiments and the novel observations that resulted.

Results:

To study tumor cells in circulation and at the metastatic site we chose to inject cells directly into circulation. We took advantage of a well-established experimental metastasis protocol where tumor cells are injected intravenously via the Duct of Cuvier (DoC) of 2-day-old embryos (Fig 2A) (Stoletov et al., 2010). The Duct of Cuvier is a large vessel that drains directly into the heart and provides a large target for these injections (Supplemental Movie 1). While many tumor cells are seen in the tail following this type of injection, few cells are seen in the brain of the embryo. This suggested that the brain would be a good location to look for enhancement of metastasis in the embryo system. Furthermore, brain metastasis is a major clinical problem with limited options for treatment or prevention (Maher et al., 2009). We

chose to assay metastasis 4 days post-injection(DPI) to allow cells time to extravasate and proliferate within the brain before imaging (Fig 2A).

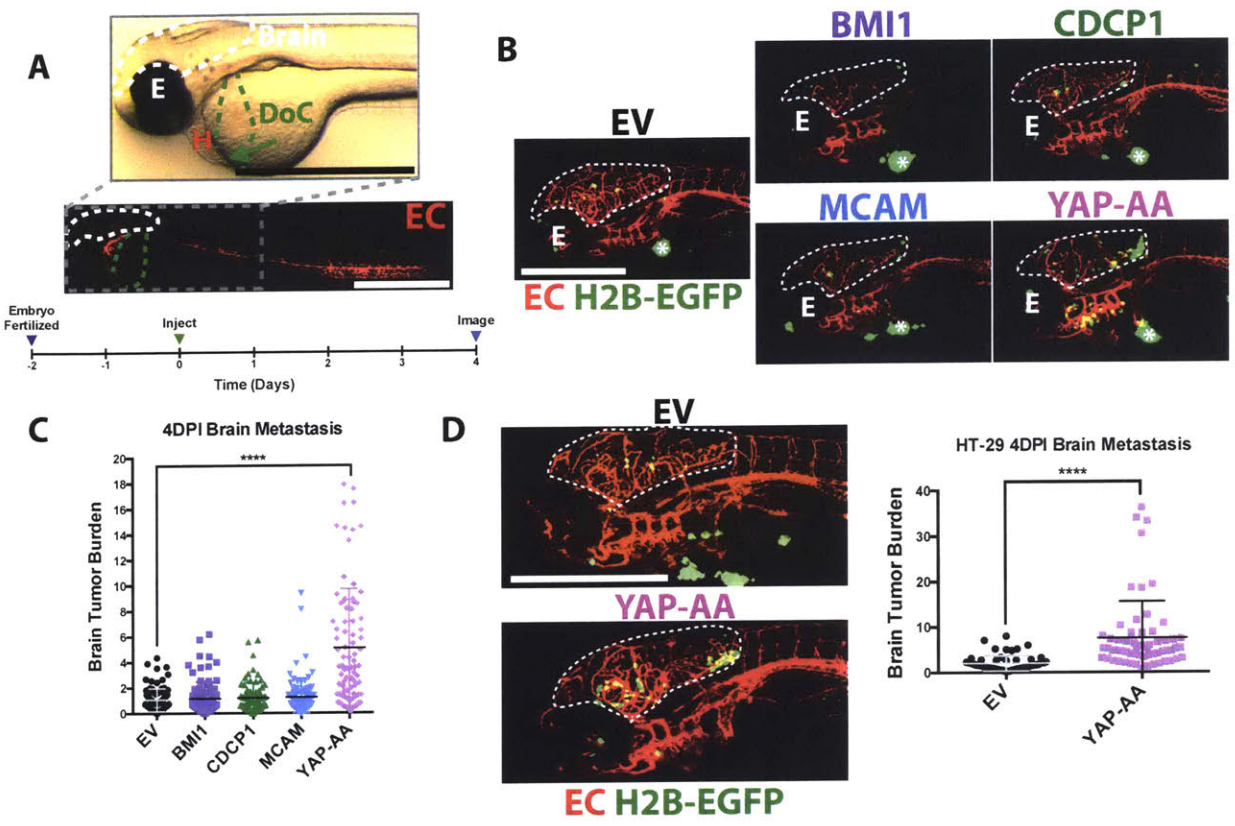

Figure 2. YAP-AA promotes brain metastasis in zebrafish embryos. (**A**) Overview images of a 2dpf flk:dsRed transgenic embryo imaged in brightfield (top) and fluorescence (bottom) to provide an overview of the experimental system. The target vessel, the Duct of Cuvier (DoC) is highlighted in green. An arrow indicates the location of injection site. The site of metastasis, the brain, is outlined in white. The eye and heart of the embryo are indicated with E and H respectively. The timeline below outlines the course of the experiment. Scale bars are 1mm. (**B**) Representative images of the heads of flk:dsred zebrafish injected with A375 cells 4 days post-injection with the brain outlined in white. The eye is indicated by an E. The tumor at the injection site is indicated with an *. Scale bar is 500μm. (**C**) Quantification of the images in B. $p<0.0001$ using ANOVA with Dunnett's correction for multiple hypothesis testing. n= 90 embryos per condition across 3 independent experiments (**D**) Representative images of embryos 4 days after injection with HT-29 cells. Scale bar is 500μm. The brain is outlined by a white dotted line. (left) Quantification of images $p<0.0001$ using a two-tailed student's t-test. n=60 embryos per condition across 2 independent experiments. EC, endothelial cell. H2B-EGFP, A375 and HT-29 cells over-express histone H2B fused to EGFP.

Cells were injected into flk1:dsRed transgenic embryos which express dsRed in endothelial cells. This allowed the endothelium to be used as a landmark to determine where tumor cells were located. We generated A375 human melanoma and HT-29 human colon cancer cells which expressed H2B-EGFP and iRFP670 to label the nucleus and cytoplasm respectively. These two labels allowed cell behaviors to be monitored through confocal microscopy.

Four genes known to promote melanoma metastasis in mice, BMI1,CDCP1,MCAM, and YAP, were over-expressed in tumor cells using a lentiviral expression system (Fig S1A) (Ferretti et al., 2016; Lamar et al., 2012; Liu et al., 2011; Xie et al., 1997). BMI1, CDCP1, and MCAM were all wild-type proteins whereas YAP was a mutated form that is insensitive to the Hippo pathway (YAP S127A,S381A, labeled as YAP-AA in this study).

These genes were assayed in the zebrafish system to see if they promoted brain metastasis when compared to an empty vector (EV) control. Metastatic burden was calculated as the percent area of the brain that was taken up by tumor cell nuclei using the H2B-EGFP signal (see methods for a detailed description of how this was calculated). Only YAP-AA promoted brain metastasis by A375 cells in this system (Fig 2B and C). YAP-AA promoted a statistically significant increase in brain metastasis regardless of quantification method (Fig S1B and C) so brain tumor burden was used for the rest of the study as it was the easiest to compute. YAP-AA also promoted brain metastasis by the HT-29 cell line in zebrafish embryos (Fig 2D and S1E). YAP-AA also enhanced brain metastasis by 8DPI in A375 cells (Fig S1D). However, by this time, there was significant mortality. For this reason, the 4DPI time point was

the final time point used in future experiments. Wild-type YAP (YAP-Wt) was over-expressed in the A375 cell line and assayed for metastasis (Fig S2A). Wild-type YAP did not promote metastasis in the zebrafish system (Fig S2B).

YAP Promotes Metastasis Within 10 Hours Of Injection

YAP regulates many properties that can influence metastasis such as proliferation, survival, and extravasation (Warren et al., 2018). In order to determine how YAP-AA was enhancing metastasis in this system, we first set out to determine when YAP-AA's promotion of metastasis was occurring. One of the strengths of the zebrafish embryo system is that individual embryos can be imaged over time with single-cell resolution. Zebrafish embryos were imaged at 10 hours post-injection, 1DPI, 2DPI, and 4DPI (Fig 3A). At the earliest time point, 10 hours post-injection, there was already a statistically significant difference between YAP-AA and EV control brain tumor cell burden (Fig 3B). It also appeared that the magnitude of the difference in brain tumor cell burden between the YAP-AA cells and the control cells did not change over time. To confirm that all of YAP-AA's effect on metastasis occurred in the first 10 hours, the data for each fish were normalized to the 10-hour time point. When the data were analyzed this way, there was no difference between YAP-AA and control cells indicating that all of YAP-AA's enhancement of metastasis was occurring in the first 10 hours following injection (Fig 3C). YAP-AA also enhanced brain metastasis in HT-29 cells within the first 10 hours (Fig 3D).

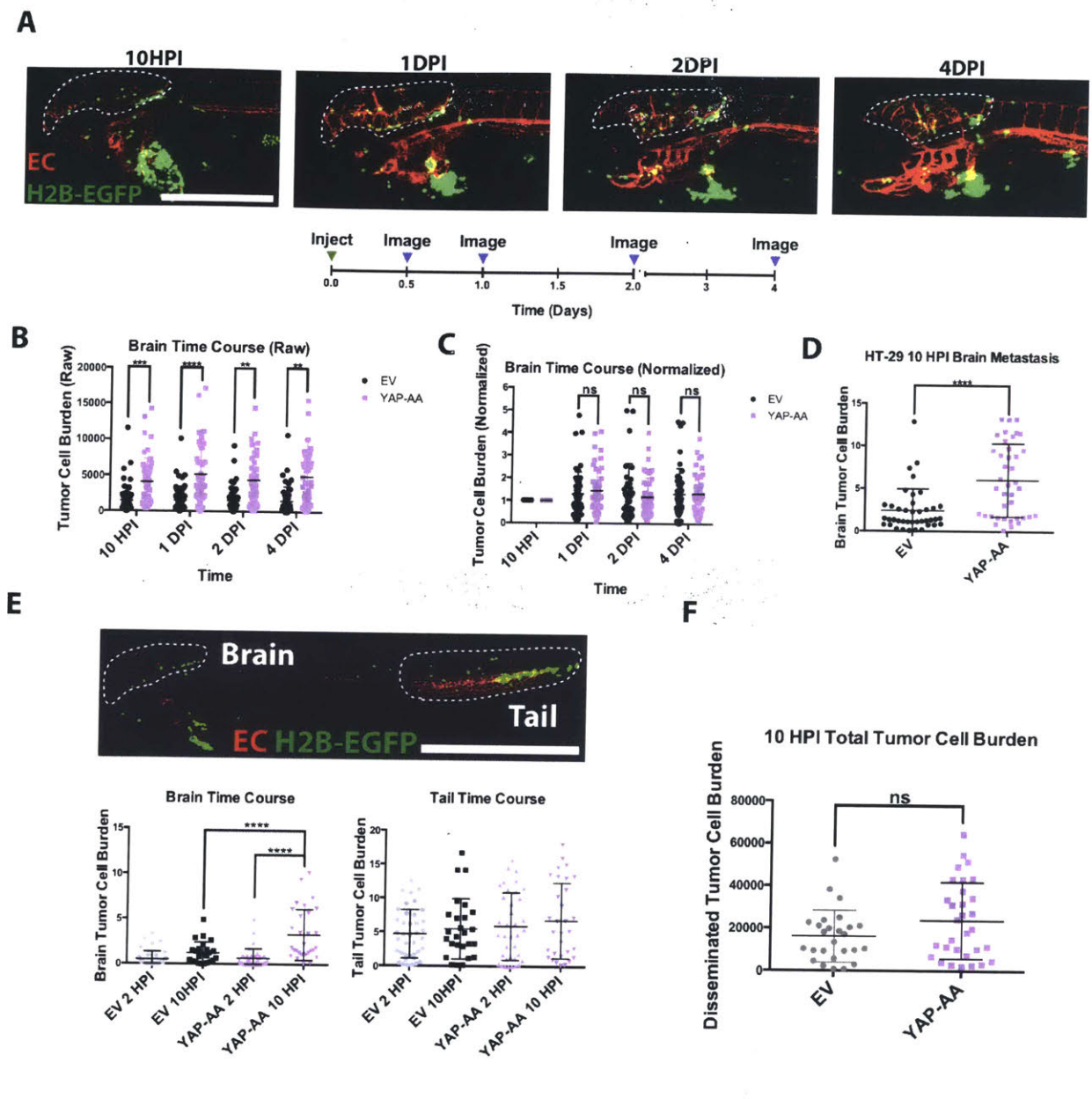

Figure 3. YAP-AA promotes metastasis within the first 10 hours of injection. (**A**) Representative images of a single embryo injected with A375 cells imaged at the indicated time points. Scale bar is 500μm. (**B**) Quantification of the raw tumor cell burden in the brain at the indicated time points. $p=2.78x10^{-6}$,$1.77x10^{-6}$,$3x10^{-4}$, and $7.16x10^{-5}$ for each time point respectively using a two-tailed student's t-test at each time point with the Holm-Šídák correction for multiple hypothesis testing. n=52 embryos per condition across 2 independent experiments (**C**) Quantification of the same data as in (B) but the tumor cell burden for each embryo was normalized to the first time point for that embryo. Statistics were calculated using a two-tailed student's t-test for each time point with the Holm-Šídák correction for multiple hypothesis testing. (**D**) Quantification of HT-29 tumor cell burden in the brain 10 hours post-

injection. $p<0.0001$ using a student's t-test. n= 40 embryos per condition over 2 independent experiments. (**E**) Overview image of a flk:dsRed embryo showing that most tumor cells (H2B-EGFP) in circulation arrest in the brain and tail. Scale bar is 1mm. Quantifications are shown of tumor cell burden in the indicated organ at the indicated time points. $p<0.0001$ using one-way ANOVA with Dunnett's test for multiple hypothesis. corrections. n=31 embryos per condition over two independent experiments. Scale bar is 1mm. (**F**) Sum of the raw data from (E) in the brain and tail at the 10-hour time points indicating that the YAP-AA does not increase the total disseminated tumor cell burden. Statistics were done with a two-tailed student's t-test. EC, endothelial cell. H2B-EGFP, tumor cell H2B-EGFP.

Following injection, there is often a bolus of cells at the injection site that can shed cells into circulation over time. Therefore, one possibility was that YAP-AA was leading to more brain metastasis by promoting more cells entering circulation from the injection bolus. To address this possibility, the size of the injection site bolus was determined at 10HPI for EV and YAP-AA injected embryos. The size of the injection site bolus was not significantly different between EV and YAP-AA cells suggesting YAP-AA was not promoting the shedding of cells into circulation from the injection bolus (Fig S3A and B).

To further study this question, we compared the disseminated tumor cell burden in EV and YAP-AA injected embryos. Following entry into circulation, most tumor cells are lodged in the brain or tail of the fish (Fig 3E). Therefore, the tumor cell burden in the brain and tail were determined 2HPI and 10HPI. At 2HPI, there was no difference in EV and YAP-AA tumor cell burden in the brain. Consistent with previous experiments, by 10HPI, there was a significant difference between EV and YAP-AA tumor cell burden in the brain (Fig 3E). In the tail, there was a slight increase in the tumor cell burden between EV and YAP-AA injected fish by 10HPI. However, this difference was not significant (Fig 3E). When the sum of the tumor cell burden in the brain and tail (representing the overwhelming majority of disseminated tumor cells in the fish) was calculated, there was a slight increase in the total disseminated tumor cell burden in

the YAP-AA embryos (Fig 3F). However, this difference was not significant leading us to believe that enhanced entry into circulation could not explain the dramatic enhancement of brain metastasis observed. Rather, YAP-AA seemed to be primarily enhancing brain metastasis while having only a slight effect on tail metastasis and total disseminated tumor cell burden.

Given that YAP-AA seemed to be specifically enhancing brain metastasis, we hypothesized that YAP-AA might be affecting arrest in the brain, extravasation in the brain, or survival in circulation. To study these processes, we took advantage of the ability to perform time lapse imaging in living embryos. Following injection, the heads of embryos were imaged every 2 minutes for 12 hours. The time cells were seen to spend in the same spot in within the brain vasculature was used as a proxy for the ability of cells to arrest in the brain. YAP-AA slightly increased the time that tumor cells remained in the same location in the vasculature, however, this difference was not significant (Fig S4A). This slight increase in the time spent in the same location within the vasculature did not seem to be enough to explain YAP's robust promotion of brain metastasis in this system.

We next evaluated extravasation in the brains of these embryos. Surprisingly, when the fraction of tumor cells that had extravasated at 10HPI was calculated, YAP-AA appeared to decrease the fraction of cells that had extravasated, although this difference was not significant (Fig S4B). Consistent with this result, YAP-AA cells degraded less fluorescent gelatin than control cells in a gelatin degradation assay (Fig S4C). This assay is commonly used as a proxy for the activity of invadopodia, invasive structures that are required for extravasation (Leong et al., 2014). These results suggested that YAP-AA was not enhancing extravasation.

Finally, the survival of cells in circulation was studied during 12 hour movies. During programmed cell death, the nuclei of dying cells are seen to fragment into small pieces (Fuchs and Steller, 2015). Using the H2B-EGFP label in our cells, we were able to monitor nuclear fragmentation by cells within the vasculature. Over the 12 hours the embryos were imaged, approximately 4% cells were seen to undergo nuclear fragmentation and disappear. No significant difference was observed when EV and YAP-AA cells were compared (Fig S4D). These results implied that YAP-AA was not promoting brain metastasis by enhancing arrest, extravasation, or survival in circulation in our system although we cannot entirely rule out arrest or survival in circulation. Another possibility for YAP-AA's enhancement of metastasis is through enhancing proliferation. However, given that mammalian cells take around 24 hours to divide, it seems unlikely that the difference in tumor cell burden that we see at 10 hours could be due to cell division.

During the generation of the movies which were used to gather the data described above, it was observed that there appeared to be more tumor cells arriving in the brain (Fig 4A and Supplemental Movies 2 and 3). When the cells in the brain were quantified over time, a steady influx of YAP-AA cells was observed while few EV cells were seen to arrive (Fig 4B). By 4.5HPI there was a statistically significant increase in the number of YAP-AA cells in the brain compared to control cells. The difference in number between control and YAP-AA cells continued to increase throughout the duration of the movies (Fig 4B).

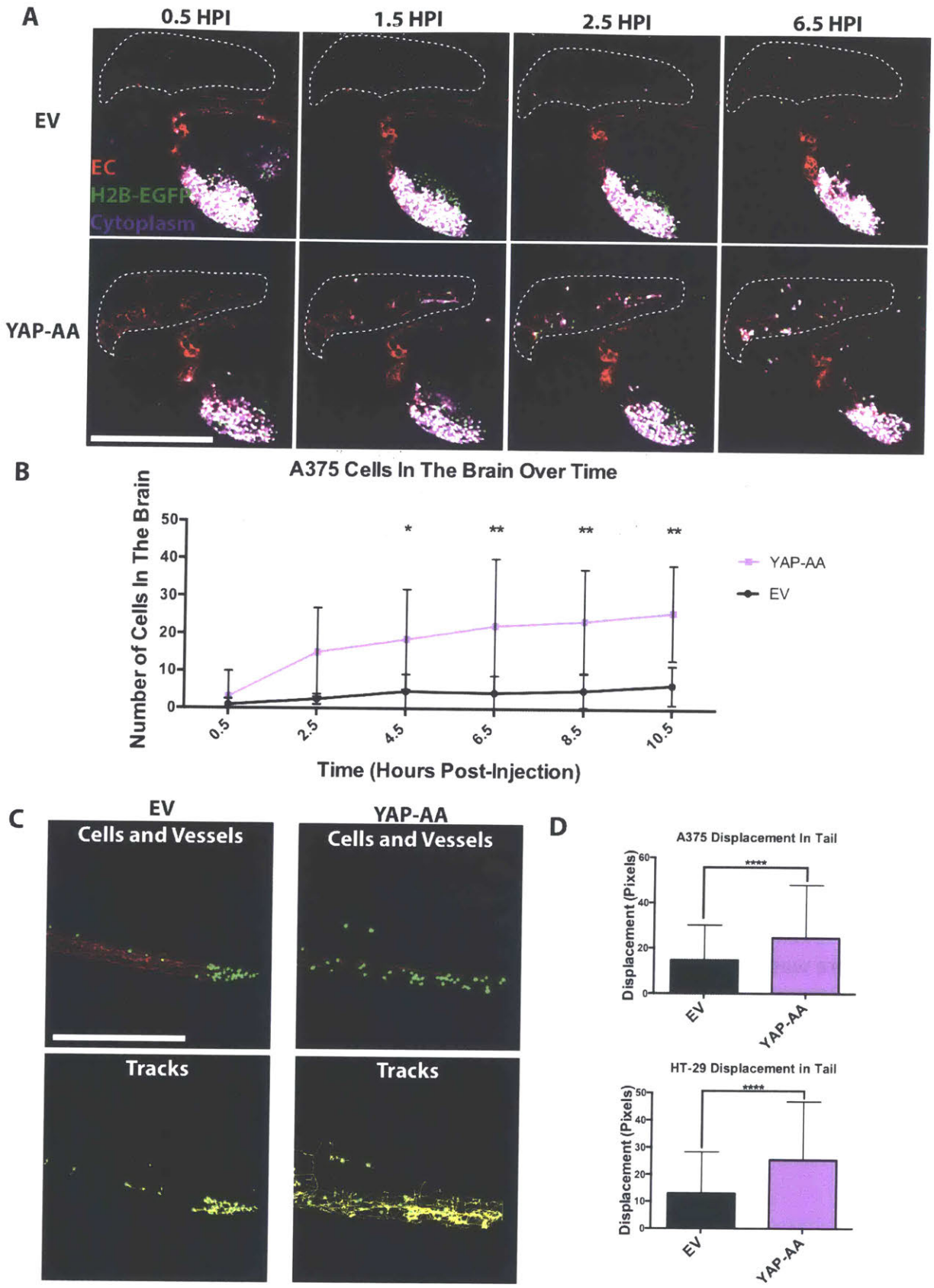
A
0.5 HPI
1.5 HPI
2.5 HPI
6.5 HPI
EV
EC
H2B-EGFP
Cytoplasm
YAP-AA
B
A375 Cells In The Brain Over Time
Number of Cells In The Brain
50
40
30
20
10
0
*
**
**
**
YAP-AA
EV
0.5
2.5
4.5
6.5
8.5
10.5
Time (Hours Post-Injection)
C
EV
Cells and Vessels
YAP-AA
Cells and Vessels
Tracks
Tracks
D
A375 Displacement In Tail
Displacement (Pixels)
60
40
20
0
****
EV
YAP-AA
HT-29 Displacement in Tail
Displacement (Pixels)
50
40
30
20
10
0
****
EV
YAP-AA

Figure 4. YAP-AA causes more cells to arrive in the brain. (**A**) Representative still images from a movie of the heads of embryos injected with EV or YAP-AA cells showing more YAP-AA cells arriving in the brain over time. Scale bar is 500μm. (**B**) Quantification of the number of A375 cells observed in the brain over time following injection. p=0.016 at 4.5HPI, p=0.0023 at 6.5HPI, p=0.0016 at 8.5HPI, and p= 0.001 at 10.5HPI. Statistics were calculated using a two-tailed student's t-test at each time point with the Holm-Šídák correction for multiple hypothesis testing. n= 6 embryos per condition across 3 independent experiments. (**C**) Representative images of 7-hour A375 cell tracks in the tail generated in ImageJ from 12-hour movies. Scale bar is 500μm. (**D**) Quantification of 7-hour cell displacement in the tail for the indicated cell line. p<0.0001 for both cell lines. Statistics were calculated using a two-tailed student's t-test. A375, n=1035 tracks per condition which were generated from movies of 6 embryos per condition. HT-29, n=724 tracks per condition generated from movies of 9 embryos per condition.

EC, endothelial cell. Tumor cells express H2B-EGFP (green) and cytoplasmic iRFP670 (purple). Overlap between these two channels appears white.

These observations suggested that YAP-AA was promoting brain metastasis by greatly increasing the numbers of cells that arrive in the brain in the first 10 hours. Given that we already showed that YAP-AA only slightly enhanced the total number of cells in circulation, we wondered where these extra cells might be coming from. We took advantage of the small size of zebrafish embryos to image entire embryos to track all the cells in circulation over time. It was observed that tumor cells were primarily clustered in the tail immediately following injection (Supplemental Movies 4 and 5). The EV control cells primarily remained in the tail during the course of these movies. However, over time, YAP-AA cells were seen moving in the tail and rapidly disappearing (presumably after becoming dislodged and swept away by circulation). Shortly thereafter, YAP-AA cells were observed to arrive at the brain. Given these observations and the observations that 1) YAP-AA only slightly increased the total number of cells in circulation 2) more YAP-AA cells arrive in the brain than control cells, we hypothesized that YAP-AA was redistributing where cells end up in the animal by causing cells to leave the tail and travel to the brain.

YAP-AA Promotes Tumor Cell Travel From The Tail To The Brain

To determine if YAP-AA was causing tumor cells to leave the tail, the tails of embryos were imaged every 2 minutes for 12 hours following injection. While EV control cells mostly remained in the same spot following arrest in the tail, YAP-AA cells moved around within in the tail vasculature and eventually disappeared (presumably after being swept back into circulation) (Fig 4C and D and Supplemental Movies 6 and 7). Given that these results suggested that YAP-AA was promoting escape from the tail, this led to the question of why YAP-AA-injected embryos do not seem to have fewer cells in the tail than EV control-injected embryos (Fig 3F). When the fraction of cell burden in the tail and brain were compared, more than 80% of the EV tumor cell burden was in the tail (Fig S5A). In embryos injected with YAP-AA cells, there was a small increase in the fraction of cell burden in the brain but this shift is still small relative to the cell burden in the tail (Fig S5A). This indicates that even a small decrease in the tail tumor cell burden could lead to a large increase in the brain tumor cell burden.

We next sought to determine if the cells seen disappearing from the tail in our movies were indeed traveling to the brain. To determine if cells that leave the tail can travel to the brain we took advantage of the photoconvertible protein Dendra2. Dendra2 is a green-to-red photoconvertible protein that converts upon intense illumination with a 405nm laser. A375 YAP-AA or EV control cells were made to express Dendra2 and iRFP670. iRFP670 is constitutively fluorescent and served as a control to label all tumor cells. These cells were injected into Fli1:EGFP embryos which have green fluorescent vasculature.

In this experiment, cells lodged in the tail were photoconverted within 2 hours of injection (Fig 5A). If YAP-AA causes tumor cells to leave the tail and travel to the brain, there

should be more photoconverted YAP-AA cells in the brain than EV photoconverted cells at 10HPI. As a control, we first confirmed that only the cells in the tail were photoconverted at the 2HPI time point immediately following conversion (Fig 5B). At 10HPI, there were more photoconverted YAP-AA cells in the brains than EV control cells (Fig 5C). Both the number and the fraction of photoconverted cells in the brains were statistically significant in the YAP-AA embryos (Fig 5D). These results fit with our hypothesis that YAP-AA promotes tumor cell travel from the tail to the brain.

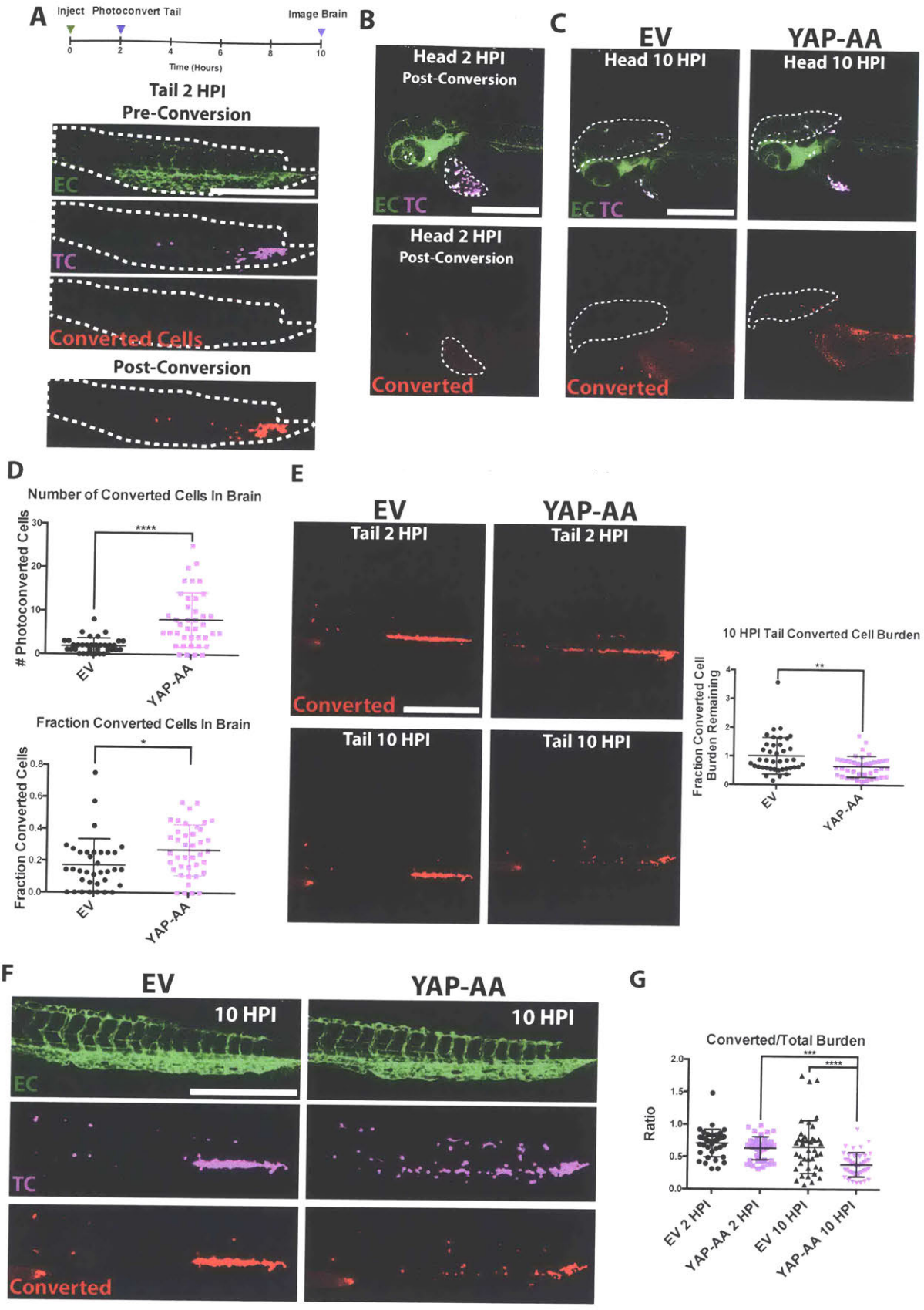
A
Inject
Photoconvert Tail
Image Brain
0
2
4
6
8
10
Time (Hours)
Tail 2 HPI
Pre-Conversion
EC
TC
Converted Cells
Post-Conversion
B
Head 2 HPI
Post-Conversion
EC TC
Head 2 HPI
Post-Conversion
Converted
C
EV
YAP-AA
Head 10 HPI
Head 10 HPI
EC TC
Converted
Converted
D
Number of Converted Cells In Brain
Photoconverted Cells
****
EV
YAP-AA
Fraction Converted Cells In Brain
Fraction Converted Cells
*
EV
YAP-AA
E
EV
YAP-AA
Tail 2 HPI
Tail 2 HPI
Converted
Tail 10 HPI
Tail 10 HPI
10 HPI Tail Converted Cell Burden
Fraction Converted Cell Burden Remaining
**
EV
YAP-AA
F
EV
YAP-AA
10 HPI
10 HPI
EC
TC
Converted
G
Converted/Total Burden
Ratio
***
****
EV 2 HPI
YAP-AA 2 HPI
EV 10 HPI
YAP-AA 10 HPI

Figure 5. YAP-AA promotes tumor cell mobilization from the tail to seed the brain. (**A**) (Upper) Experimental overview indicating that Dendra2 expressing A375 cells in the tail are photoconverted within 2 hours of injection. The brain is then imaged at 10HPI to look for photoconverted cells. (Lower) A375 cells constitutively express iRFP670 (purple) allowing unconverted tumor cells to be identified. Upon photoconversion, A375 cells fluoresce red. The tail is outlined with a white dotted line. Scale bar is 500μm. (**B**) Image of the head at 2HPI after the cells in the tail have been photoconverted showing that cells in the head or injection site were not photoconverted. A bolus of A375 cells at the injection site is indicated with a white dotted line. Scale bar is 500μm. (**C**) Image of the head at 10HPI showing more photoconverted YAP-AA cells in the brain (white dotted line). Scale bar is 500μm. (**D**) Quantification of the number and fraction of photoconverted cells in the brain. $P<0.0001$ for the number of converted cells and $p=0.012$ for the fraction of converted cells. n= 35 embryos per condition across 3 independent experiments. (**E**) Image of photoconverted cells in the tail at the indicated time points showing that YAP-AA cells are lost from the tail over time. $p=0.003$ using a two-tailed student's t-test. n= 35 embryos per condition across 3 independent experiments. Scale bar is 500μm. (**F**) Representative images of the tails of fli1:EGFP zebrafish embryos 10HPI showing iRFP670 (purple) labeling all A375 cells and Dendra2 (red) labeling cells photoconverted at 2HPI. Scale bar is 500μm. (**G**) Quantification of the ratio of converted tumor cell burden to total tumor cell burden of the images in F. $p<0.001$ for YAP2HPI->YAP 10HPI, and $p<0.0001$ for EV10HPI->YAP10HPI using one-way ANOVA with Tukey's test for multiple comparisons. n=40 embryos per condition across 2 independent experiments. EC, endothelial cell. TC, tumor cell

We then looked at the behavior of the photoconverted cells in the tail. Given that YAP-AA does not appear to affect survival in circulation in our system, if YAP-AA is promoting tumor cells to leave the tail, then one would expect the photoconverted YAP-AA tumor cell burden in the tail to decrease over time while the EV photoconverted tumor cell burden in the tail would remain about the same.

When the photoconverted cells in the tail were followed over time, the EV control cell burden remained about the same (Fig 5E). However, the YAP-AA tumor cell burden decreased over time (Fig 5E). This loss was quantified by calculating the ratio of the photoconverted tumor cell burden at 2HPI and 10HPI. Interestingly, at 10HPI there were many YAP-AA cells in the tail that were not photoconverted while almost all the EV control cells in the tail at this time point

were photoconverted (Fig 5F). Unconverted cells in the tail at the 10HPI time point are cells that arrived in the tail following photoconversion as our photoconversion was highly efficient (Fig 5A).

When the ratio of the converted to unconverted tumor cell burden in the tail was calculated, it is near 1 at the 2HPI time point for both EV and YAP-AA cells (Fig 5G). This ratio is not equal to 1 because photoconverted Dendra2 is dimmer than iRFP670. By 10 hours, this ratio has dropped for the YAP-AA cells while remaining essentially unchanged for EV control cells again indicating that unconverted YAP-AA cells are arriving in the tail after photoconversion (Fig 5G). This observation fits with the model that YAP-AA cells are better at dispersing throughout the embryo. This observation suggests that YAP-AA might also be promoting cells to leave the brain as well. During our brain time-lapse imaging, cells were observed leaving brain. However, there also appeared to be areas where cells remained sequestered for the duration of our imaging (Movie S2 and S3). The vessels in the brain are generally narrower than the ones in the tail. We suspect that this difference accounts for tumor cells remaining sequestered in the brain following their arrival but escaping from the tail.

YAP May Be Enhancing Escape From The Tail Through Intravascular Migration

Once it became apparent that YAP-AA was enhancing tumor cell escape from the tail and that these escaping cells could travel to the brain, we set out to determine how YAP-AA was promoting escape from the tail. We hypothesized that YAP-AA might be helping tumor cells dislodge within the vasculature through decreased adhesion to the endothelium or to other tumor cells. To test these hypotheses, we first assayed the adhesion of EV or YAP-AA cells to human endothelial cells *in vitro*. Surprisingly, YAP-AA cells were more adherent to the human

endothelial cells than the EV control cells (Fig 6A). Next, the ability of cells to undergo homotypic adhesion was assayed using an *in vitro* cell aggregation assay (Fig 6B). The YAP-AA over-expressing cells formed larger aggregates in this assay leading us to conclude that they were more self-adhesive than control cells (Fig 6B). These observations suggested that YAP was not enhancing escape from the tail by decreasing cell adhesion.

We next tested whether YAP-AA's promotion of metastasis was a cell autonomous process. Control A375 cells or YAP-AA cells were made to express Cerulean or iRFP670. Control and YAP-AA cells were injected into zebrafish embryos separately or mixed together in a 1:1 ratio. When co-injected, the YAP-AA cells showed enhanced brain metastasis by 4 days post-injection (Fig 6C). Co-injection did not enhance control cell metastasis indicating that YAP's enhancement of metastasis was confined to the YAP-AA cells (Fig 6C).

The fact that YAP-AA's enhancement of metastasis was a cell autonomous process suggested that it might be an active process. YAP is well known to promote cell migration so YAP-AA cells and control cells were assayed in transwell migration assays. YAP-AA greatly enhanced the fraction of transmigrated cells in both the A375 cell line and the HT-29 cell line (Fig 6D). The observations that 1) YAP-AA enhanced adhesion to the endothelium 2) YAP-AA enhanced brain metastasis in a cell-autonomous manner and 3) YAP-AA greatly enhanced migration *in vitro* hinted that YAP-AA might be promoting escape from the tail through intravascular migration. This would not be the first time that an oncogene had been shown to promote intravascular migration in this location in zebrafish embryos (Stoletov et al., 2010). In this work, tumor cells were observed to adopt a rounded morphology and crawl along the

luminal surface of the endothelium and, in some cases, to move against blood flow (Stoletov et al., 2010).

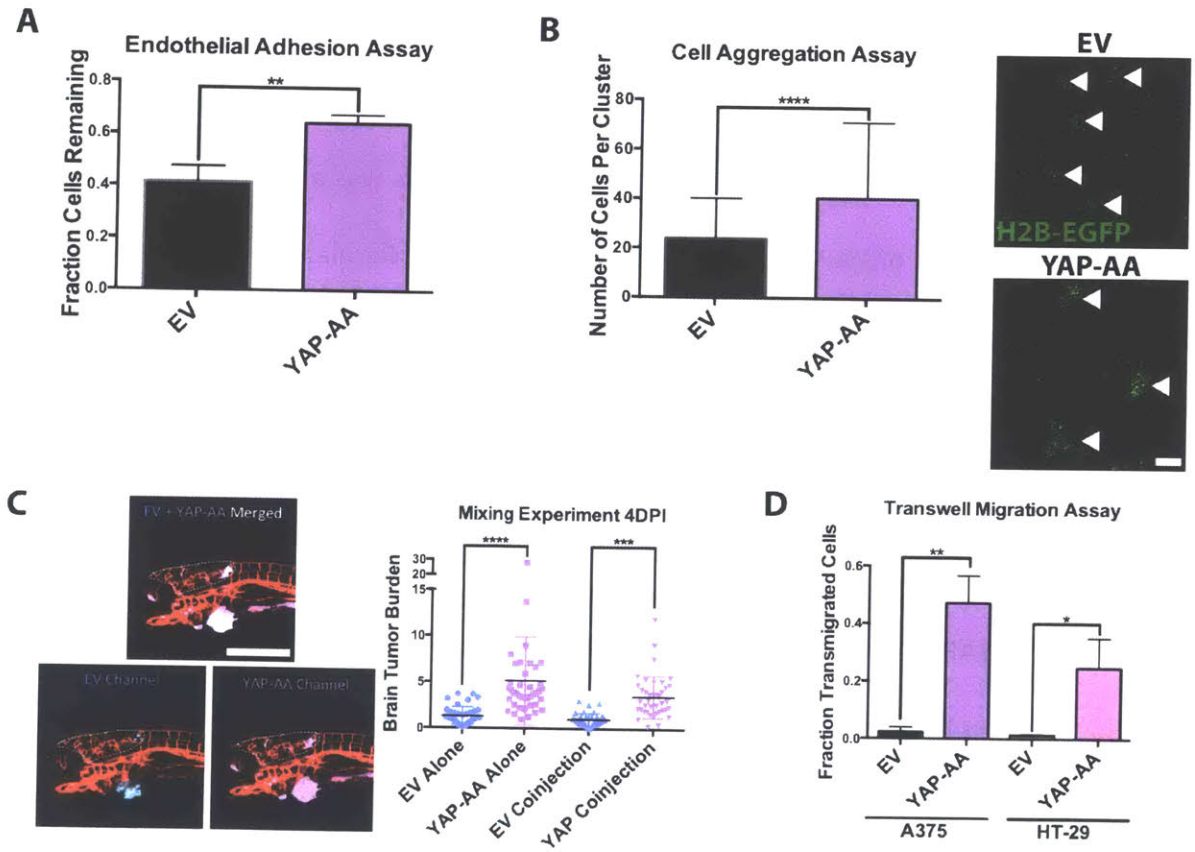

Figure 6. YAP-AA may promote tumor cell intravascular migration. (**A**) Endothelial adhesion assay indicating that YAP-AA A375 cells are more adhesive to an endothelial monolayer. p=0.004 using a two-tailed student's t-test on data from 3 independent experiments. (**B**) Cell aggregation assay indicating that YAP-over-expressing A375 cells form larger aggregates *in vitro*. p<0.0001 using a two-tailed student's t-test n=117 aggregates per condition analyzed from two independent experiments. Arrowheads indicate example aggregates in an image of H2B-EGFP-expressing A375 cells following aggregation. Scale bar is 100μm. (**C**) Brain tumor burden of EV control and YAP-AA cells at 4DPI from a co-injection experiment. p<0.0001 for cell types alone. p=0.0004 for co-injected cells. Statistics were calculated using one-way ANOVA with Dunnett's test for multiple hypothesis corrections. n=40 embryos per condition (EV alone, YAP-AA alone, and co-injection) across two independent experiments. Scale bar is 500μm. (**D**) Transwell migrations assays for A375 and HT-29 cells indicating that YAP-AA promotes cell migration *in vitro*. A375, p=0.0013 HT-29 p=0.017. Statistics were calculated using a two-tailed student's t-test on the averages of 3 independent experiments for each cell line.

Since we suspected that YAP-AA's promotion of escape from the tail might be due to enhanced migration, we wanted to determine how YAP might be enhancing migration in these cells. We first assayed whether YAP-AA's promotion of metastasis in this system was dependent on its ability to regulate transcription and interact with the TEAD family of transcription factors. We over-expressed YAP-AA or YAP-AA with mutations that inactivate the TEAD-binding domain (AA-S94A), the two WW domains (AA-WW), or delete the transactivation domain (A-TA) (Fig 7A). The S94A (AA-S94A) and transactivation domain deletions (A-TA) abrogate YAP's ability to promote transcription. The WW domains mutations disrupt some protein-protein interactions but do not affect TEAD-dependent transcription. The YAP-AA-WW construct promoted brain metastasis by 4 days post-injection (Fig 7A). However, the YAP-AA-S94A and the YAP-A-TA mutants did not promote metastasis indicating that YAP's ability to regulate transcription and interact with the TEAD family of transcription factors was required to enhance metastasis in this system (Fig 7A).

A recent paper has shown that YAP can promote migration through TEAD-dependent transcriptional upregulation of the Rho GAP ARHGAP29. Mechanistically, ARHGAP29 promotes migration through increased cofilin activity due to a decrease in cofilin phosphorylation. When levels of phosphorylated cofilin were assayed, there was no difference between EV control or YAP-AA over-expressing A375 cells (Fig 7B). Qiao et al. also described that YAP promotes a decrease in the F:G actin ratio. However, YAP-AA over-expression in A375 cells leads to an increase in F actin and consequently a higher F:G actin ratio (Fig 7C). These results indicated that YAP promoted motility in A375 cells through actin polymerization in a mechanism which may be distinct from those previously reported.

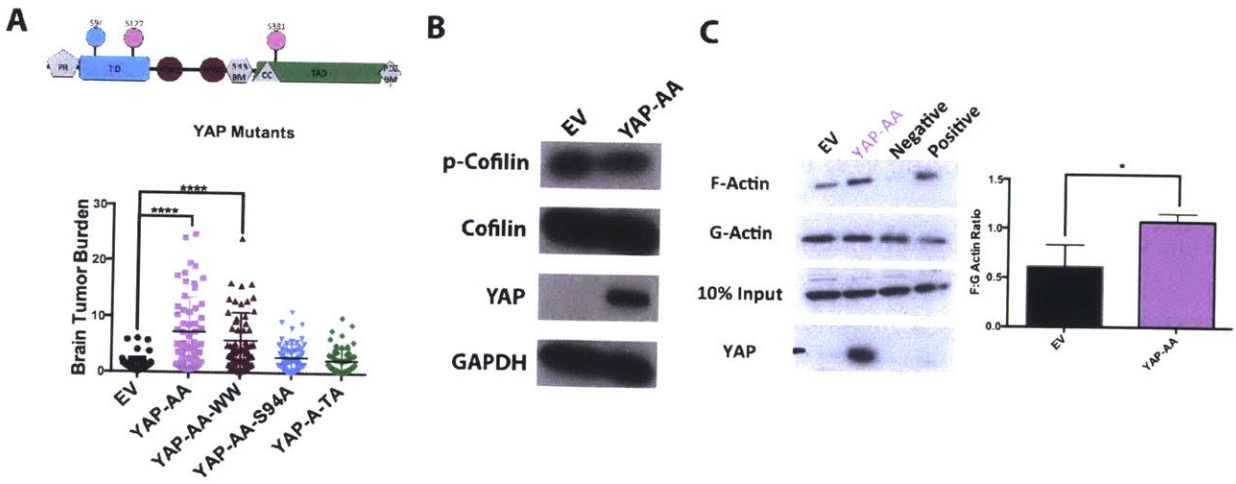

Figure 7. YAP-AA promotes migration through enhancing actin polymerization. (**A**) (Upper) Domain map of YAP indicating the locations of the mutations in the mutant constructs used. (Lower) Quantification of brain metastasis formation 4DPI by A375 cells over-expressing the indicated mutant YAP constructs. (**B**) Western blot of A375 cell lysate showing that YAP-AA does not change phospho-cofilin levels (**C**) (Left) Western blot of A375 cell F and G-actin pools in control and YAP-AA cells. (Right) Densitometry quantification of the F:G actin ratio indicating that this ratio is elevated in YAP-AA cells. p= 0.028 using a two-tailed student's t-test on data from 3 independent experiments.

Discussion:

In this chapter, we set out to use zebrafish embryos as a system to study how specific genes modulate the behavior of tumor cells in circulation and at the metastatic site. The events that occur in these locations are rate-limiting for metastasis, indicating that a better understanding of these barriers could uncover opportunities for therapeutic intervention (Massagué and Obenauf, 2016). The events in circulation and at the metastatic site are dynamic and so require the use of intravital imaging to fully comprehend them. A number of intravital imaging studies have catalogued the behavior of tumor cells at the metastatic site in detail (Entenberg et al., 2017; Follain et al., 2018; Kienast et al., 2009; Ritsma et al., 2012; Stoletov et al., 2010). These studies have identified novel steps in metastasis at which therapeutic intervention may be possible. For example, in the liver, tumor cells were observed to migrate extensively while forming micro-metastases and this migration was shown to be required for their metastatic outgrowth (Ritsma et al., 2012). In the brain, solitary disseminated tumor cells required interactions with endothelial cells for survival, suggesting that disrupting these interactions would prevent metastatic outgrowth (Kienast et al., 2009). However, few studies have used intravital imaging to investigate how known metastasis-promoting genes influence the behavior of tumor cells in circulation and at the metastatic site.

Our work also illustrates the utility of zebrafish embryos to study metastasis. The ability to inject hundreds of embryos in a day allows large scale *in vivo* screens of metastasis to be conducted. While we only used 4 genes in this study, many more could have been looked at had we not focused on YAP early on. Another key reason that zebrafish embryos are so powerful is that they are simple to use for time-lapse imaging over time scales from seconds to

days. Time lapse imaging also allowed us to rapidly assay YAP's influence on multiple phenotypes such as arrest, extravasation, and survival in circulation. While there are *in vitro* assays that can be used as proxies for these processes, they involve complex interactions between tumor cells and the microenvironment that are impossible to wholly replicate *in vitro*.

The ability to follow tumor cells in individual embryos over the course of 4 days allowed us to easily determine exactly when YAP was promoting metastasis in this system. The ability to image the entire embryo also allowed us to account for every cell that had entered circulation in the animal as well as the cells that remained at the injection site. This accounting proved critical for us to be able to identify how YAP was influencing the distribution of tumor cells throughout the embryo.

Our results from this study have some implications for the YAP field as well. Our initial observation that YAP-AA promoted brain metastasis in the zebrafish system is noteworthy because there has been little data to date connecting YAP to brain metastasis specifically (Hsu et al., 2018). YAP activity has been shown to promote metastasis in multiple tumor types and can regulate many processes associated with metastasis such as invasion, migration, extravasation, anchorage independent growth (Janse van Rensburg and Yang, 2016; Lamar et al., 2012; Warren et al., 2018). Given these data showing that YAP is a strong promoter of metastasis, at first glance, it may not be surprising that YAP promoted brain metastasis in our system. However, studies of cells with a propensity to metastasize to the brain indicate that there are specific barriers in the brain that metastasizing tumor cells must be overcome (Bos et al., 2009; Valiente et al., 2014). Not all metastasis promoting genes would be expected to allow metastasizing tumor cells to overcome these barriers. The fact that YAP promoted brain

metastasis in our system suggests that YAP might be among the scarce set of genes that promotes brain metastasis. Given that brain metastasis is a devastating condition with few treatment options (Maher et al., 2009), our observation suggests that further studies of YAP in the context of brain metastasis are warranted.

Our results also highlight how YAP can function at different steps in the metastatic cascade in different tumor types. It has been apparent for some time that the set of genes regulated by YAP varies considerably across cell types (Hao et al., 2008; Yu et al., 2015b; Zhao et al., 2007). Despite this fact, YAP seems to regulate many of the same processes in different tumor types. For example YAP has been shown to promote extravasation and resistance to anoikis in multiple tumor types including breast and lung cancer (Gu et al., 2016; Lamar et al., 2012; Liu et al., 2018; Nallet-Staub et al., 2014; Sharif et al., 2015; Warren et al., 2018).

In our system, we saw no evidence that that YAP had any effect of either of these processes in A375 melanoma cells. Our result that YAP did not enhance extravasation was particularly surprising because YAP-AA cells seemed to have a lower proportion of extravascular cells at 10 HPI suggesting that YAP-AA may even be inhibiting extravasation (though this difference was not statistically significant). One potential explanation is that extravasation in a zebrafish system is not representative of extravasation in a mammalian system. However, the fact that YAP-AA cells also degraded less gelatin in a gelatin degradation assay (a proxy for invadopodia activity) fits with a model where YAP-AA does not enhance extravasation. Furthermore, in breast cancer, YAP was shown to enhance extravasation in zebrafish suggesting that our lack of enhancement is not due to our model system but a real YAP phenotype in these cells (Sharif et al., 2015).

The fact that we did have any evidence to suggest that YAP-AA affected survival in circulation was also rather surprising given YAP's known role in resisting anoikis (Haemmerle et al., 2017; Zhao et al., 2012). One possibility, is that our assay is just not detecting most dying cells. TUNEL assays on whole mount embryos following injection could be a more reliable method assay YAP's effect on tumor cell survival in this system. However, survival in circulation may not play much of a role in this system. In support of this view, we only saw about 4% of cells in circulation dying during 12 hours of imaging (Fig S4). Compared to survival in circulation in mice, the zebrafish embryo seems to be a much more hospitable environment suggesting that anoikis in circulation may not pose much of a barrier to metastasis in our system (Fidler, 1970). We also have not formally ruled out proliferation as a mechanism by which YAP might be enhancing metastasis in this system. While the fact that YAP promotes metastasis by 10HPI suggests that proliferation is not playing a role, further experiments are necessary to formally rule this out.

The fact that YAP seems to have no effect on some processes in our hands may suggest that YAP regulates different steps of the metastatic cascade in different tumor types. Therefore, in order to fully understand how YAP (and TAZ) are involved in metastasis, it might be necessary to look at every step of the metastatic cascade in each tumor type of interest. Zebrafish embryos could provide a useful system for performing these experiments as we have demonstrated how one can use them to rapidly studying multiple aspects of the metastatic cascade.

Our observation that YAP-AA redistributes tumor cells by inducing cells arrested in the vasculature to re-enter circulatory flow was also quite interesting. It has generally been

assumed that metastasizing tumor cells take a direct route through circulation to the metastatic site. Arrest in the capillaries of a distant organ is seen as the end of their trip with cells either extravasating or dying. However other studies, and our results, suggest that tumor cells might take a more circuitous route. In some cases, tumor cells might be able to re-enter circulatory flow following arrest and travel to other organs.

Intravital imaging studies have shown that tumor cell arrest in the vasculature is dynamic. Tumor cells often arrest temporarily before being carried back into circulation (Benjamin and Hynes, 2017; Kienast et al., 2009; Morris et al., 1993; Spicer et al., 2012). Early studies, which tracked tumor cells in circulation in mice, suggest that cells seen departing following stable arrest in one organ can transit through the circulatory system to other organs over the course of a few hours (Fidler, 1970; Fidler and Nicolson, 1977). At longer time scales, experiments have shown that tumor cell transit in animal models is more complex than just a linear stream from primary tumor to metastasis. Instead, tumor cells can metastasize from one primary tumor to another contralateral tumor or from a metastasis back to the primary tumor in a process called re-seeding (Kim et al., 2009).

The ability to move through the first capillary bed encountered to travel to other organs may also be required to account for metastasis to some organs. For example, colon cancer often metastasizes to the liver which is the first capillary bed downstream through the circulatory system (Budczies et al., 2015). However, colon cancer can also metastasize to the lungs. Given the layout of the circulatory system and the liver vasculature, it seems likely that in order to reach the lungs, tumor cells would have to first transit through capillaries in the liver

(Aird, 2007). Genes that aid in transit through the liver vasculature transit could therefore promote metastasis to other organs such as the lung.

A number of observations led to our hypothesis that YAP-AA was promoting intravascular migration. First, YAP-AA enhanced adhesion to the endothelium in *in vitro* endothelial adhesion assays. Second, YAP-AA greatly enhanced migration in *in vitro* transwell migration assays. Finally, YAP-AA enhanced migration when YAP-AA cells were mixed with EV control cells. This result suggested that the YAP-AA cells were leaving the trail through an active process. If YAP-AA were promoting escape from the tail through a passive process, we would have expected the EV control cells to block the vessels and prevent the YAP-AA cells from leaving. Instead the YAP-AA cells were still able to spread to the brain when co-injected with the EV control cells.

If YAP-AA is promoting this redistribution of tumor cells through promoting intravascular migration as we currently hypothesize, this would not be the first reported case of intravascular migration in zebrafish embryos. Tumor cell intravascular migration has previously been reported to occur in zebrafish embryos following over-expression of the EMT-promoting transcription factor Twist1 (Stoletov et al., 2010). This study used time lapse imaging in zebrafish embryos to observe individual tumor cells which used a rounded morphology to actively crawl within the vasculature. This crawling was confirmed to be an active process as it could occur against the direction of blood flow (Stoletov et al., 2010). Further imaging in our system with higher temporal resolution may be useful to determine if our cells are behaving similarly. A key observation in Stoletov et al. was that Twist1-induced intravascular migration was dependent on integrin-β1. In our system, YAP-AA enhanced tumor cell adhesion to

endothelial cells which is consistent with intravascular migration requiring adhesion to the endothelium. It would therefore seem that, a key experiment in our system would be to see if YAP-AA could still enhance tumor cell travel to the brain in integrin-β1 knockdown cells.

Finally, a caveat of our experiments is that they were performed by over-expressing a constitutively active form of YAP. In our experiments, YAP transcriptional activity was high regardless of the state of the Hippo pathway. Given the failure of wild-type YAP to promote brain metastasis in our hands, it seems likely that YAP is normally repressed by the Hippo pathway within the vasculature in our system. However, there are a number of mechanisms that might activate YAP activity within the vasculature in other cell types. For example, YAP and TAZ have been shown to be able to be activated by fluid shear stress (Lee et al., 2017; 2018) and this activation can promote tumor cell motility (Lee et al., 2017). It is possible that the cells we tested were not responsive to this mode of YAP regulation. Cells that are more responsive to fluid flow could potentially disseminate from the tail following induction of YAP activity through this mechanism.

Another way YAP could be activated within the vasculature is through physical force on the nucleus. Recently, force acting on the nucleus has been shown to promote YAP nuclear entry and activity (Elosegui-Artola et al., 2017). It has been observed that tumor cells arrested in the vasculature undergo large deformations of their nuclei as they are pushed into narrow vessels by the blood flow. These observations suggest that the force exerted on the nucleus during arrest could activate YAP (Tsuji et al., 2006; Yamamoto et al., 2004; Yamauchi et al., 2006; 2005).

Finally, tumor cells arrested at the metastatic site are frequently seen interacting with platelets (Labelle and Hynes, 2012). Recently, platelets have been shown to be able to activate YAP, suggesting that this might be another way to activate YAP in circulation (Haemmerle et al., 2017). During the period when we see our YAP phenotype, the first thrombocytes (the zebrafish equivalent of platelets) begin to appear in the embryo (Khandekar et al., 2012). It is possible that there are not enough of them or the early thrombocytes present during our experiments were not yet capable of activating YAP activity. It would be interesting to perform our experiments in 3DPF embryos, which have many circulating thrombocytes, to see if wild-type YAP can promote brain metastasis in this context.

In summary, we found that YAP-AA promoted brain metastasis in zebrafish embryos. Through time lapse imaging, we were able to rapidly assess YAP-AA's influence on arrest, extravasation, survival in circulation, and travel in circulation to determine how it was promoting metastasis in this system. We found that, while control cells arrest in the tail vasculature after injection and remain trapped there, YAP-AA induces cells to dislodge, re-enter circulatory flow, and travel to the brain. We suspect that YAP-AA may be promoting this escape from the tail through intravascular migration. The ability to transit through the first capillary bed encountered in circulation represents a novel mechanism for tumor cells to increase their dissemination through an organism.

Supplemental Figures

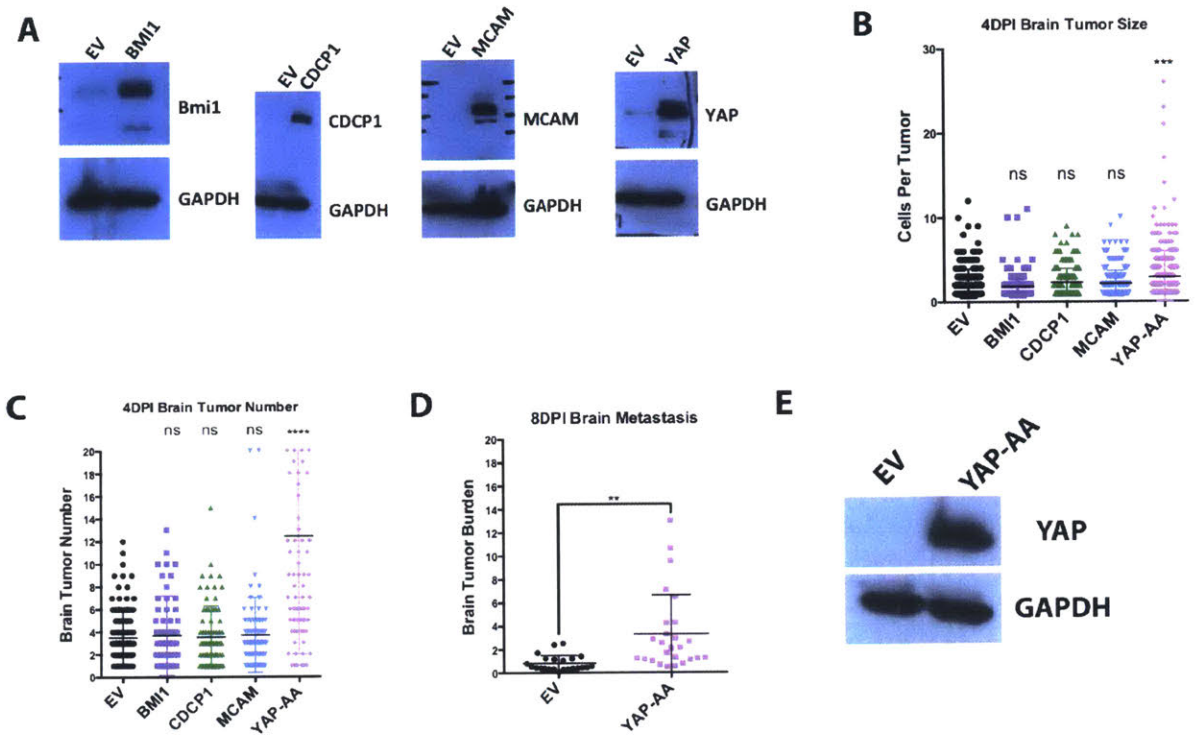

Figure S1. YAP-AA enhances metastasis using multiple quantification methods and as late as 8DPI. (**A**) Western blots indicating over-expression of the labeled genes. (**B**) Quantification of the number of cells per tumor in the brain at 4DPI. $p<0.001$. n=345 tumors per condition in 90 fish per condition. Statistics were calculated using one-way ANOVA with Dunnett's test for multiple hypothesis correction. (**C**) Quantification of the number of brain tumors in the brain of embryos at 4DPI. $p<0.0001$. Statistics were calculated using one-way ANOVA with Dunnett's test for multiple hypothesis correction. n= 90 fish per condition across 3 independent experiments. (**D**) Quantification of brain metastases in fish 8DPI. $p=0.001$ using a two-tailed student's t-test. n=23 fish per condition across 2 independent experiments. (**E**) Western blot of control or YAP-AA over-expressing HT-29 cells.

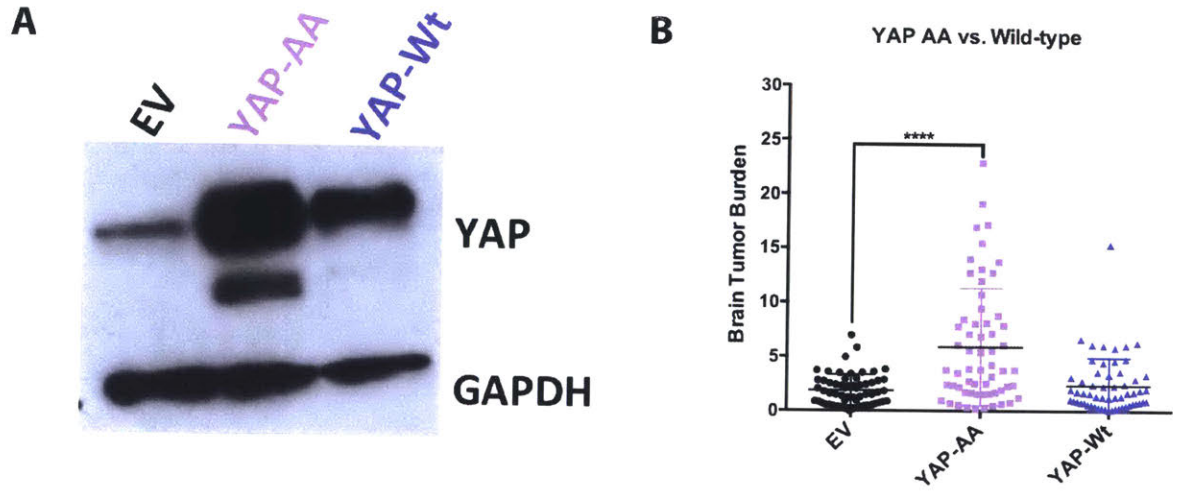

Figure S2. Wild-type YAP does not enhance metastasis in zebrafish embryos. (**A**) Western blot showing Wild-type and YAP-AA expression in the cell lines used for experiments. (**B**) Quantification of brain metastases in embryos 4DPI. $p < 0.0001$ using one-way ANOVA with Dunnett's test for multiple hypothesis testing. n=60 embryos per condition across 2 independent experiments.

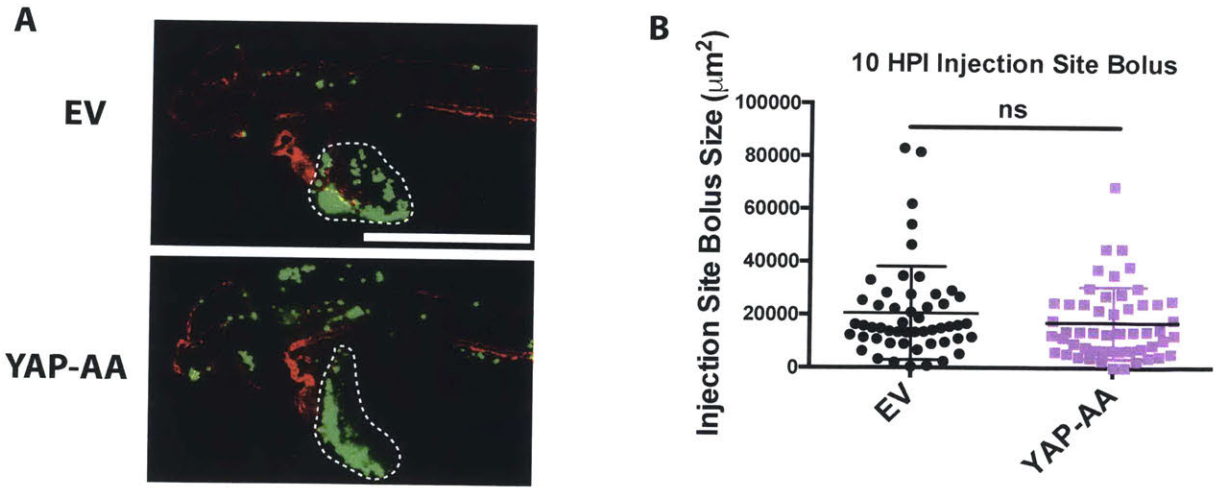

Figure S3. YAP-AA does not enhance entry into circulation from the injection site by 10HPI. (**A**) Representative images of injection site tumors at 10HPI. Scale bar is 500μm. (**B**) Quantification of the area of injection site tumors at 10HPI. p=0.25. n=52 embryos per condition across 2 independent experiments.

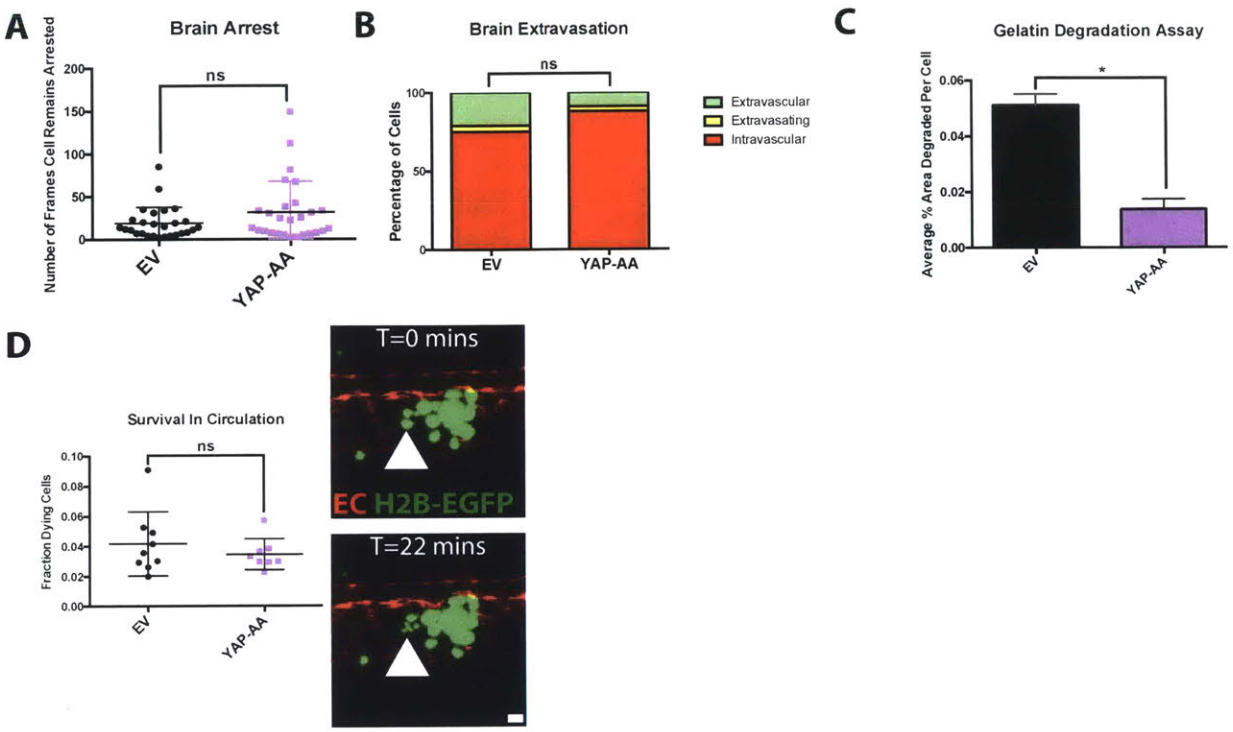

Figure S4. YAP-AA does not enhance arrest, extravasation, or survival in circulation. (**A**) Quantification of the time cells are observed to be arrested at the same spot in the brain vasculature before moving. (**B**) Quantification of the fraction of cells observed to be intravascular, extravasating, or extravasascular at 10HPI. p=0.05 using a chi squared test. n=53 cells per condition in 5 embryos per condition. (**C**) Quantification of fluorescent gelatin degradation by control and YAP-AA cells *in vitro*. p=0.01 using a two-tailed student's t-test on the averages of two independent experiments. n= 45 fields per condition per experiment (**D**) (left) Quantification of the fraction of cells observed to die during 12-hour movies of the tail of embryos. p=0.4 using a two-tailed student's t-test. n=8 embryos per condition. (right) Representative images showing a cell dying within the vasculature over the course of 22 minutes. Scale bar is 10μm.

A

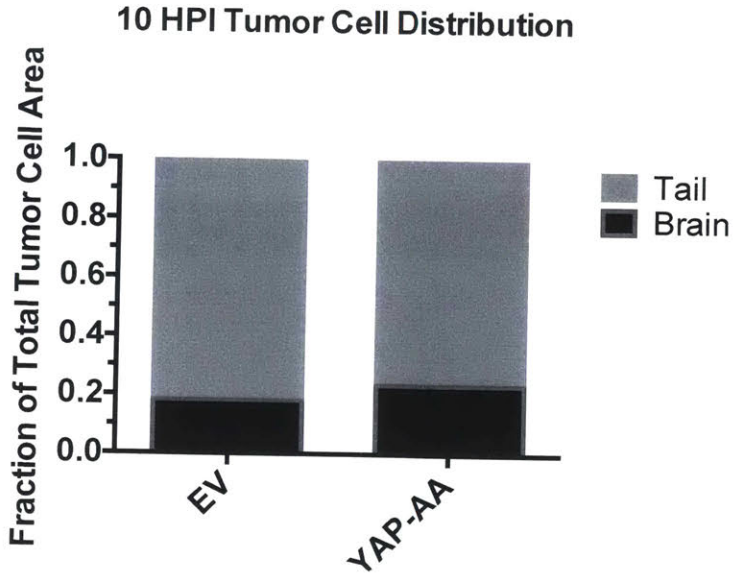

Figure S5. Most tumor cells are arrested in the tail at 10 hours post-injection. (**A**) Graph plotting the fractional area of tumor cells in the brain and tail relative to the sum of the total area from the sum of both those locations. Data were generated from analysis of 31 embryos per condition across two independent experiments.

A

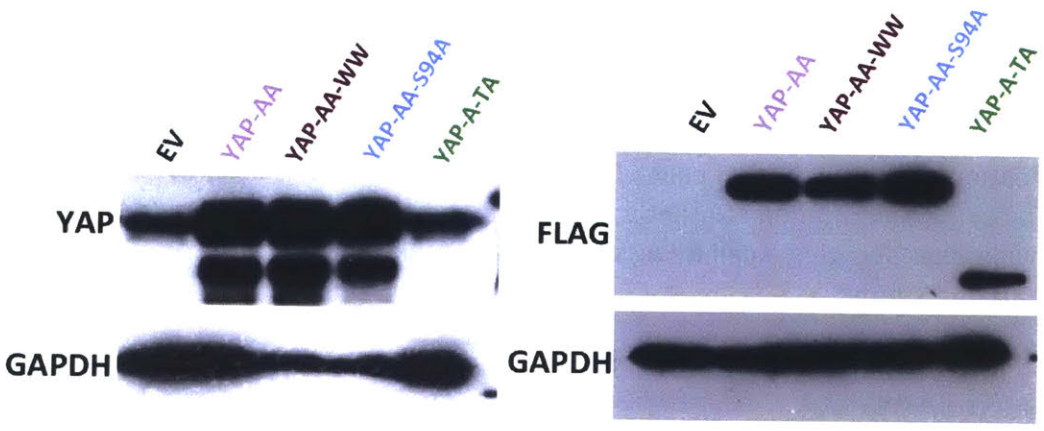

Figure S6. Expression of YAP mutants. (**A**) Western blots of cells over-expressing the indicated YAP mutants. Note that the binding site for the YAP antibody is contained in the region deleted in the YAP-A-TA mutant so is not detected in the total YAP blot. All mutants are FLAG-tagged and can be detected with a FLAG antibody.

Supplemental Movie 1. Movie showing blood flow through the Duct of Cuvier of a 2-day-old zebrafish embryo. The Duct of Cuvier provides a large target for the injection of tumor cells. Following injection, the cells are exposed to blood flow and are carried into circulation and can disperse throughout the embryo. Scale bar is 1mm. Timecode is in seconds.

URL: https://youtu.be/DfwSZvMWitU
Alternative URL: https://www.davidcbenjamin.com/movie-s1

Supplemental Movie 2. Movie of the head of a zebrafish embryo injected with EV control A375 cells over 12 hours. A375 cells express cytoplasmic iRFP670 (magenta) and nuclear EGFP (H2B-EGFP). Endothelial cells express dsRed. Scale bar is 500μm. Timecode is in hours.

URL: https://youtu.be/zbsG7Dc9l8E
Alternative URL: https://www.davidcbenjamin.com/movie-s2

Supplemental Movie 3. Movie of the head of a zebrafish embryo injected with YAP-AA over-expressing A375 cells over 12 hours. A375 cells express cytoplasmic iRFP670 (magenta) and nuclear EGFP (H2B-EGFP). Endothelial cells express dsRed. Scale bar is 500μm. Timecode is in hours.

URL: https://youtu.be/1dfm2R702OQ
Alternative URL: https://www.davidcbenjamin.com/movie-s3

Supplemental Movie 4. Movie of a whole zebrafish embryo injected with EC control A375 cells over 12 hours. A375 cells express cytoplasmic iRFP670 (magenta) and nuclear EGFP (H2B-EGFP). Endothelial cells express dsRed. Scale bar is 1mm. Timecode is in hours.

URL: https://youtu.be/s8kY9K5EIaM
Alternative URL: https://www.davidcbenjamin.com/movie-s4

Supplemental Movie 5. Movie of a whole zebrafish embryo injected with YAP-AA over-expressing A375 cells over 12 hours. A375 cells express cytoplasmic iRFP670 (magenta) and nuclear EGFP (H2B-EGFP). Endothelial cells express dsRed. Scale bar is 1mm. Timecode is in hours.

URL: https://youtu.be/PxI_icJWNiA
Alternative URL: https://www.davidcbenjamin.com/movie-s5

Supplemental Movie 6. Movie of A375 control cells in the tail over the course of 12 hours following injection. A375 cells express cytoplasmic iRFP670 (magenta) and nuclear EGFP (H2B-EGFP). Endothelial cells express dsRed. Scale bar is 500μm. Time code is in hours.

URL: https://youtu.be/H51oqPL7iqc
Alternative URL: https://www.davidcbenjamin.com/movie-s6

Supplemental Movie 7. Movie of A375 cells over-expressing YAP-AA in the tail over the course of 12 hours following injection. Scale bar is 500μm. Time code is in hours. A375 cells express cytoplasmic iRFP670 (magenta) and nuclear EGFP (H2B-EGFP. Endothelial cells express dsRed. Scale bar is 500μm. Time code is in hours.

URL: https://youtu.be/MHyWwm_8TsE
Alternative URL: https://www.davidcbenjamin.com/movie-s7

References:

Ahn, S.-H., Cheung, W.L., Hsu, J.-Y., Diaz, R.L., Smith, M.M., and Allis, C.D. (2005). Sterile 20 kinase phosphorylates histone H2B at serine 10 during hydrogen peroxide-induced apoptosis in S. cerevisiae. Cell *120*, 25–36.

Aird, W.C. (2007). Phenotypic heterogeneity of the endothelium: II. Representative vascular beds. Circulation Research *100*, 174–190.

Anand, R., Kim, A.-Y., Brent, M., and Marmorstein, R. (2008). Biochemical analysis of MST1 kinase: elucidation of a C-terminal regulatory region. Biochemistry *47*, 6719–6726.

Ando, T., Charindra, D., Shrestha, M., Umehara, H., Ogawa, I., Miyauchi, M., and Takata, T. (2018). Tissue inhibitor of metalloproteinase-1 promotes cell proliferation through YAP/TAZ activation in cancer. Oncogene *37*, 263–270.

Aragona, M., Panciera, T., Manfrin, A., Giulitti, S., Michielin, F., Elvassore, N., Dupont, S., and Piccolo, S. (2013). A mechanical checkpoint controls multicellular growth through YAP/TAZ regulation by actin-processing factors. Cell *154*, 1047–1059.

Azzolin, L., Panciera, T., Soligo, S., Enzo, E., Bicciato, S., Dupont, S., Bresolin, S., Frasson, C., Basso, G., Guzzardo, V., et al. (2014). YAP/TAZ incorporation in the β-catenin destruction complex orchestrates the Wnt response. Cell *158*, 157–170.

Azzolin, L., Zanconato, F., Bresolin, S., Forcato, M., Basso, G., Bicciato, S., Cordenonsi, M., and Piccolo, S. (2012). Role of TAZ as mediator of Wnt signaling. Cell *151*, 1443–1456.

Bartucci, M., Dattilo, R., Moriconi, C., Pagliuca, A., Mottolese, M., Federici, G., Benedetto, A.D., Todaro, M., Stassi, G., Sperati, F., et al. (2015). TAZ is required for metastatic activity and chemoresistance of breast cancer stem cells. Oncogene *34*, 681–690.

Baumgartner, R., Poernbacher, I., Buser, N., Hafen, E., and Stocker, H. (2010). The WW domain protein Kibra acts upstream of Hippo in Drosophila. Developmental Cell *18*, 309–316.

Benjamin, D.C., and Hynes, R.O. (2017). Intravital imaging of metastasis in adult Zebrafish. 1–12.

Boggiano, J.C., Vanderzalm, P.J., and Fehon, R.G. (2011). Tao-1 phosphorylates Hippo/MST kinases to regulate the Hippo-Salvador-Warts tumor suppressor pathway. Developmental Cell *21*, 888–895.

Bos, P.D., Zhang, X.H.F., Nadal, C., Shu, W., Gomis, R.R., Nguyen, D.X., Minn, A.J., van de Vijver, M.J., Gerald, W.L., Foekens, J.A., et al. (2009). Genes that mediate breast cancer metastasis to the brain. Nature *459*, 1005–1009.

Budczies, J., Winterfeld, von, M., Klauschen, F., Bockmayr, M., Lennerz, J.K., Denkert, C., Wolf, T., Warth, A., Dietel, M., Anagnostopoulos, I., et al. (2015). The landscape of metastatic progression patterns across major human cancers. Oncotarget *6*, 570–583.

Bueno, R., Stawiski, E.W., Goldstein, L.D., Durinck, S., De Rienzo, A., Modrusan, Z., Gnad, F., Nguyen, T.T., Jaiswal, B.S., Chirieac, L.R., et al. (2016). Comprehensive genomic analysis of malignant pleural mesothelioma identifies recurrent mutations, gene fusions and splicing alterations. Nat Genet *48*, 407–416.

Byun, M.R., Hwang, J.-H., Kim, A.R., Kim, K.M., Park, J.I., Oh, H.T., Hwang, E.S., and Hong, J.-H. (2017). SRC activates TAZ for intestinal tumorigenesis and regeneration. Cancer Letters *410*, 32–40.

Callus, B.A., Verhagen, A.M., and Vaux, D.L. (2006). Association of mammalian sterile twenty kinases, Mst1 and Mst2, with hSalvador via C-terminal coiled-coil domains, leads to its stabilization and phosphorylation. Febs J. *273*, 4264–4276.

Chakraborty, S., Njah, K., Pobbati, A.V., Lim, Y.B., Raju, A., Lakshmanan, M., Tergaonkar, V., Lim, C.T., and Hong, W. (2017). Agrin as a Mechanotransduction Signal Regulating YAP through the Hippo Pathway. CellReports *18*, 2464–2479.

Chan, E.H.Y., Nousiainen, M., Chalamalasetty, R.B., Schäfer, A., Nigg, E.A., and Silljé, H.H.W. (2005). The Ste20-like kinase Mst2 activates the human large tumor suppressor kinase Lats1. Oncogene *24*, 2076–2086.

Chan, S.W., Lim, C.J., Chong, Y.F., Pobbati, A.V., Huang, C., and Hong, W. (2011). Hippo pathway-independent restriction of TAZ and YAP by angiomotin. J. Biol. Chem. *286*, 7018–7026.

Chan, S.W., Lim, C.J., Loo, L.S., Chong, Y.F., Huang, C., and Hong, W. (2009). TEADs mediate nuclear retention of TAZ to promote oncogenic transformation. Journal of Biological Chemistry *284*, 14347–14358.

Chaulk, S.G., Lattanzi, V.J., Hiemer, S.E., Fahlman, R.P., and Varelas, X. (2014). The Hippo pathway effectors TAZ/YAP regulate dicer expression and microRNA biogenesis through Let-7. J. Biol. Chem. *289*, 1886–1891.

Chen, H.-Y., Yu, S.-L., Ho, B.-C., Su, K.-Y., Hsu, Y.-C., Chang, C.-S., Li, Y.-C., Yang, S.-Y., Hsu, P.-Y., Ho, H., et al. (2015). R331W Missense Mutation of Oncogene YAP1Is a Germline Risk Allele for Lung Adenocarcinoma With Medical Actionability. Journal of Clinical Oncology *33*, 2303–2310.

Codelia, V.A., Sun, G., and Irvine, K.D. (2014). Regulation of YAP by mechanical strain through Jnk and Hippo signaling. Curr. Biol. *24*, 2012–2017.

Cordenonsi, M., Zanconato, F., Azzolin, L., Forcato, M., Rosato, A., Frasson, C., Inui, M., Montagner, M., Parenti, A.R., Poletti, A., et al. (2011). The Hippo transducer TAZ confers cancer stem cell-related traits on breast cancer cells. Cell *147*, 759–772.

Cottini, F., Hideshima, T., Xu, C., Sattler, M., Dori, M., Agnelli, L., Hacken, ten, E., Bertilaccio, M.T., Antonini, E., Neri, A., et al. (2014). Rescue of Hippo coactivator YAP1 triggers DNA damage-induced apoptosis in hematological cancers. Nature Medicine *20*, 599–606.

Creasy, C.L., Ambrose, D.M., and Chernoff, J. (1996). The Ste20-like protein kinase, Mst1, dimerizes and contains an inhibitory domain. Journal of Biological Chemistry *271*, 21049–21053.

Cui, C.B., Cooper, L.F., Yang, X., Karsenty, G., and Aukhil, I. (2003). Transcriptional coactivation of bone-specific transcription factor Cbfa1 by TAZ. Molecular and Cellular Biology *23*, 1004–1013.

Daszczuk, P.E., and Proszynski, T.J. (2016). Hippo signaling pathway transcription co-activator YAP is localized to podosomes/invadopodia in Src-transformed NIH-3T3 fibroblasts. Matters 1–4.

Deng, H., Wang, W., Yu, J., Zheng, Y., Qing, Y., and Pan, D. (2015). Spectrin regulates Hippo signaling by modulating cortical actomyosin activity. Elife *4*, e06567.

Deng, Y., Matsui, Y., Zhang, Y., and Lai, Z.-C. (2013). Hippo activation through homodimerization and membrane association for growth inhibition and organ size control. Developmental Biology *375*, 152–159.

DeRan, M., Yang, J., Shen, C.-H., Peters, E.C., Fitamant, J., Chan, P., Hsieh, M., Zhu, S., Asara, J.M., Zheng, B., et al. (2014). Energy stress regulates hippo-YAP signaling involving AMPK-mediated regulation of angiomotin-like 1 protein. CellReports *9*, 495–503.

Di Palma, T., D'Andrea, B., Liguori, G.L., Liguoro, A., de Cristofaro, T., Del Prete, D., Pappalardo, A., Mascia, A., and Zannini, M. (2009). TAZ is a coactivator for Pax8 and TTF-1, two transcription factors involved in thyroid differentiation. Exp Cell Res. *315*, 162–175.

Diepenbruck, M., Waldmeier, L., Ivanek, R., Berninger, P., Arnold, P., van Nimwegen, E., and Christofori, G. (2014). Tead2 expression levels control the subcellular distribution of Yap and Taz, zyxin expression and epithelial-mesenchymal transition. Journal of Cell Science *127*, 1523–1536.

Donato, E., Biagioni, F., Bisso, A., Caganova, M., Amati, B., and Campaner, S. (2018). YAP and TAZ are dispensable for physiological and malignant haematopoiesis. Leukemia 1–0.

Dong, J., Feldmann, G., Huang, J., Wu, S., Zhang, N., Comerford, S.A., Gayyed, M.F., Anders, R.A., Maitra, A., and Pan, D. (2007). Elucidation of a universal size-control mechanism in Drosophila and mammals. Cell *130*, 1120–1133.

Dupont, S. (2016). Role of YAP/TAZ in cell-matrix adhesion-mediated signalling and mechanotransduction. Exp Cell Res. *343*, 42–53.

Dupont, S., Morsut, L., Aragona, M., Enzo, E., Giulitti, S., Cordenonsi, M., Zanconato, F., Le Digabel, J., Forcato, M., Bicciato, S., et al. (2011). Role of YAP/TAZ in mechanotransduction. Nature *474*, 179–183.

Eagle, H., and Levine, E.M. (1967). Growth regulatory effects of cellular interaction. Nature *213*, 1102–1106.

Eddy, R.J., Weidmann, M.D., Sharma, V.P., and Condeelis, J.S. (2017). Tumor Cell Invadopodia: Invasive Protrusions that Orchestrate Metastasis. Trends Cell Biol. *27*, 595–607.

Elbediwy, A., Vincent-Mistiaen, Z.I., Spencer-Dene, B., Stone, R.K., Boeing, S., Wculek, S.K., Cordero, J., Tan, E.H., Ridgway, R., Brunton, V.G., et al. (2016). Integrin signalling regulates YAP and TAZ to control skin homeostasis. Development *143*, 1674–1687.

Elosegui-Artola, A., Andreu, I., Beedle, A.E.M., Lezamiz, A., Uroz, M., Kosmalska, A.J., Oria, R., Kechagia, J.Z., Rico-Lastres, P., Le Roux, A.-L., et al. (2017). Force Triggers YAP Nuclear Entry by Regulating Transport across Nuclear Pores. Cell *171*, 1397–1410.e14.

Entenberg, D., Voiculescu, S., Guo, P., Borriello, L., Wang, Y., Karagiannis, G.S., Jones, J., Baccay, F., Oktay, M., and Condeelis, J. (2017). A permanent window for the murine lung enables high-resolution imaging of cancer metastasis. Nat Meth *15*, 73–80.

Fan, R., Kim, N.-G., and Gumbiner, B.M. (2013). Regulation of Hippo pathway by mitogenic growth factors via phosphoinositide 3-kinase and phosphoinositide-dependent kinase-1. Proc. Natl. Acad. Sci. U.S.a. *110*, 2569–2574.

Feng, X., Degese, M.S., Iglesias-Bartolome, R., Vaque, J.P., Molinolo, A.A., Rodrigues, M., Zaidi, M.R., Ksander, B.R., Merlino, G., Sodhi, A., et al. (2014). Hippo-independent activation of YAP by the GNAQ uveal melanoma oncogene through a trio-regulated rho GTPase signaling circuitry. Cancer Cell *25*, 831–845.

Fernandez-L, A., Northcott, P.A., Dalton, J., Fraga, C., Ellison, D., Angers, S., Taylor, M.D., and Kenney, A.M. (2009). YAP1 is amplified and up-regulated in hedgehog-associated medulloblastomas and mediates Sonic hedgehog-driven neural precursor proliferation. Genes & Development *23*, 2729–2741.

Ferretti, R., Bhutkar, A., McNamara, M.C., and Lees, J.A. (2016). BMI1 induces an invasive signature in melanoma that promotes metastasis and chemoresistance. Genes & Development *30*, 18–33.

Fidler, I.J. (1970). Metastasis: quantitative analysis of distribution and fate of tumor emboli labeled with 125 I-5-iodo-2'-deoxyuridine. J. Natl. Cancer Inst. *45*, 773–782.

Fidler, I.J., and Nicolson, G.L. (1977). Fate of recirculating B16 melanoma metastatic variant cells in parabiotic syngeneic recipients. J. Natl. Cancer Inst. *58*, 1867–1872.

Fisher, M.L., Grun, D., Adhikary, G., Xu, W., and Eckert, R.L. (2017). Inhibition of YAP function overcomes BRAF inhibitor resistance in melanoma cancer stem cells. Oncotarget *8*, 110257–110272.

Fisher, M.L., Kerr, C., Adhikary, G., Grun, D., Xu, W., Keillor, J.W., and Eckert, R.L. (2016). Transglutaminase Interaction with α6/β4-Integrin Stimulates YAP1-Dependent ΔNp63α Stabilization and Leads to Enhanced Cancer Stem Cell Survival and Tumor Formation. Cancer Research *76*, 7265–7276.

Fletcher, G.C., Elbediwy, A., Khanal, I., Ribeiro, P.S., Tapon, N., and Thompson, B.J. (2015). The Spectrin cytoskeleton regulates the Hippo signalling pathway. Embo J. *34*, 940–954.

Follain, G., Osmani, N., Azevedo, A.S., Allio, G., Mercier, L., Karreman, M.A., Solecki, G., Garcia Leòn, M.J., Lefebvre, O., Fekonja, N., et al. (2018). Hemodynamic Forces Tune the Arrest, Adhesion, and Extravasation of Circulating Tumor Cells. Developmental Cell *45*, 33–52.e12.

Forbes, S.A., Beare, D., Boutselakis, H., Bamford, S., Bindal, N., Tate, J., Cole, C.G., Ward, S., Dawson, E., Ponting, L., et al. (2017). COSMIC: somatic cancer genetics at high-resolution. Nucleic Acids Res. *45*, D777–D783.

Fuchs, Y., and Steller, H. (2015). Live to die another way: modes of programmed cell death and the signals emanating from dying cells. Nat Rev Mol Cell Biol *16*, 329–344.

Gaffney, C.J., Oka, T., Mazack, V., Hilman, D., Gat, U., Muramatsu, T., Inazawa, J., Golden, A., Carey, D.J., Farooq, A., et al. (2012). Identification, basic characterization and evolutionary analysis of differentially spliced mRNA isoforms of human YAP1 gene. Gene *509*, 215–222.

Galli, G.G., Carrara, M., Yuan, W.-C., Valdes-Quezada, C., Gurung, B., Pepe-Mooney, B., Zhang, T., Geeven, G., Gray, N.S., de Laat, W., et al. (2015). YAP Drives Growth by Controlling Transcriptional Pause Release from Dynamic Enhancers. Molecular Cell *60*, 328–337.

Ge, L., Smail, M., Meng, W., Shyr, Y., Ye, F., Fan, K.-H., Li, X., Zhou, H.-M., and Bhowmick, N.A. (2011). Yes-associated protein expression in head and neck squamous cell carcinoma nodal metastasis. PLoS ONE *6*, e27529.

Genevet, A., Wehr, M.C., Brain, R., Thompson, B.J., and Tapon, N. (2010). Kibra is a regulator of the Salvador/Warts/Hippo signaling network. Developmental Cell *18*, 300–308.

Gong, R., Hong, A.W., Plouffe, S.W., Zhao, B., Liu, G., Yu, F.-X., Xu, Y., and Guan, K.-L. (2015). Opposing roles of conventional and novel PKC isoforms in Hippo-YAP pathway regulation. Cell Res. *25*, 985–988.

Goulev, Y., Fauny, J.D., Gonzalez-Marti, B., Flagiello, D., Silber, J., and Zider, A. (2008). SCALLOPED interacts with YORKIE, the nuclear effector of the hippo tumor-suppressor pathway in Drosophila. Curr. Biol. *18*, 435–441.

Gu, J.J., Rouse, C., Xu, X., Wang, J., Onaitis, M.W., and Pendergast, A.M. (2016). Inactivation of ABL kinases suppresses non-small cell lung cancer metastasis. JCI Insight *1*, e89647.

Guan, J.L. (1997). Role of focal adhesion kinase in integrin signaling. Int. J. Biochem. Cell Biol. *29*, 1085–1096.

Guo, T., Lu, Y., Li, P., Yin, M.-X., Lv, D., Zhang, W., Wang, H., Zhou, Z., Ji, H., Zhao, Y., et al. (2013). A novel partner of Scalloped regulates Hippo signaling via antagonizing Scalloped-Yorkie activity. Cell Res. *23*, 1201–1214.

Haemmerle, M., Taylor, M.L., Gutschner, T., Pradeep, S., Cho, M.S., Sheng, J., Lyons, Y.M., Nagaraja, A.S., Dood, R.L., Wen, Y., et al. (2017). Platelets reduce anoikis and promote metastasis by activating YAP1 signaling. Nature Communications *8*, 310.

Hamaratoglu, F., Willecke, M., Kango-Singh, M., Nolo, R., Hyun, E., Tao, C., Jafar-Nejad, H., and Halder, G. (2006). The tumour-suppressor genes NF2/Merlin and Expanded act through Hippo signalling to regulate cell proliferation and apoptosis. Nat Cell Biol *8*, 27–36.

Hao, Y., Chun, A., Cheung, K., Rashidi, B., and Yang, X. (2008). Tumor suppressor LATS1 is a negative regulator of oncogene YAP. Journal of Biological Chemistry *283*, 5496–5509.

Harburger, D.S., and Calderwood, D.A. (2009). Integrin signalling at a glance. Journal of Cell Science *122*, 159–163.

Hardie, D.G., Ross, F.A., and Hawley, S.A. (2012). AMPK: a nutrient and energy sensor that maintains energy homeostasis. Nature Reviews Drug Discovery *13*, 251–262.

Harris, T.J.C., and Tepass, U. (2010). Adherens junctions: from molecules to morphogenesis. Nature Reviews Drug Discovery *11*, 502–514.

Harvey, K.F., Pfleger, C.M., and Hariharan, I.K. (2003). The Drosophila Mst ortholog, hippo, restricts growth and cell proliferation and promotes apoptosis. Cell *114*, 457–467.

Harvey, K.F., Zhang, X., and Thomas, D.M. (2013). The Hippo pathway and human cancer. Nat Rev Cancer *13*, 246–257.

Hong, J.-H., and Yaffe, M.B. (2006). TAZ: a beta-catenin-like molecule that regulates mesenchymal stem cell differentiation. Cell Cycle *5*, 176–179.

Hossain, Z., Ali, S.M., Ko, H.L., Xu, J., Ng, C.P., Guo, K., Qi, Z., Ponniah, S., Hong, W., and Hunziker, W. (2007). Glomerulocystic kidney disease in mice with a targeted inactivation of Wwtr1. Proc. Natl. Acad. Sci. U.S.a. *104*, 1631–1636.

Hsu, P.-C., Miao, J., Huang, Z., Yang, Y.-L., Xu, Z., You, J., Dai, Y., Yeh, C.-C., Chan, G., Liu, S., et al. (2018). Inhibition of yes-associated protein suppresses brain metastasis of human lung adenocarcinoma in a murine model. J. Cell. Mol. Med.

Hsu, Y.-L., Hung, J.-Y., Chou, S.-H., Huang, M.-S., Tsai, M.-J., Lin, Y.-S., Chiang, S.-Y., Ho, Y.-W., Wu, C.-Y., and Kuo, P.-L. (2015). Angiomotin decreases lung cancer progression by sequestering oncogenic YAP/TAZ and decreasing Cyr61 expression. Oncogene *34*, 4056–4068.

Huang, J.-M., Nagatomo, I., Suzuki, E., Mizuno, T., Kumagai, T., Berezov, A., Zhang, H., Karlan, B., Greene, M.I., and Wang, Q. (2013). YAP modifies cancer cell sensitivity to EGFR and survivin inhibitors and is negatively regulated by the non-receptor type protein tyrosine phosphatase 14. Oncogene *32*, 2220–2229.

Huang, J.L.-Y., Urtatiz, O., and Van Raamsdonk, C.D. (2015). Oncogenic G Protein GNAQ Induces Uveal Melanoma and Intravasation in Mice. Cancer Research *75*, 3384–3397.

Huang, J., Wu, S., Barrera, J., Matthews, K., and Pan, D. (2005). The Hippo signaling pathway coordinately regulates cell proliferation and apoptosis by inactivating Yorkie, the Drosophila Homolog of YAP. Cell *122*, 421–434.

Huang, W., Lv, X., Liu, C., Zha, Z., Zhang, H., Jiang, Y., Xiong, Y., Lei, Q.-Y., and Guan, K.-L. (2012). The N-terminal phosphodegron targets TAZ/WWTR1 protein for SCFβ-TrCP-dependent degradation in response to phosphatidylinositol 3-kinase inhibition. J. Biol. Chem. *287*, 26245–26253.

Hynes, R.O. (2002). Integrins: bidirectional, allosteric signaling machines. Cell *110*, 673–687.

Janse van Rensburg, H.J., and Yang, X. (2016). The roles of the Hippo pathway in cancer metastasis. Cell. Signal. *28*, 1761–1772.

Jia, J., Zhang, W., Wang, B., Trinko, R., and Jiang, J. (2003a). The Drosophila Ste20 family kinase dMST functions as a tumor suppressor by restricting cell proliferation and promoting apoptosis. Genes & Development *17*, 2514–2519.

Jia, J., Zhang, W., Wang, B., Trinko, R., and Jiang, J. (2003b). The Drosophila Ste20 family kinase dMST functions as a tumor suppressor by restricting cell proliferation and promoting apoptosis. Genes & Development *17*, 2514–2519.

Jiao, S., Wang, H., Shi, Z., Dong, A., Zhang, W., Song, X., He, F., Wang, Y., Zhang, Z., Wang, W., et al. (2014). A peptide mimicking VGLL4 function acts as a YAP antagonist therapy against gastric cancer. Cancer Cell *25*, 166–180.

Jin, Y., Dong, L., Lu, Y., Wu, W., Hao, Q., Zhou, Z., Jiang, J., Zhao, Y., and Zhang, L. (2012). Dimerization and cytoplasmic localization regulate Hippo kinase signaling activity in organ size control. J. Biol. Chem. *287*, 5784–5796.

Jin, Y., Xu, J., Yin, M.-X., Lu, Y., Hu, L., Li, P., Zhang, P., Yuan, Z., Ho, M.S., Ji, H., et al. (2013). Brahma is essential for Drosophila intestinal stem cell proliferation and regulated by Hippo signaling. Elife *2*, e00999.

Justice, R.W., Zilian, O., Woods, D.F., Noll, M., and Bryant, P.J. (1995). The Drosophila tumor suppressor gene warts encodes a homolog of human myotonic dystrophy kinase and is required for the control of cell shape and proliferation. Genes & Development *9*, 534–546.

Kango-Singh, M., Nolo, R., Tao, C., Verstreken, P., Hiesinger, P.R., Bellen, H.J., and Halder, G. (2002). Shar-pei mediates cell proliferation arrest during imaginal disc growth in Drosophila. Development *129*, 5719–5730.

Kapoor, A., Yao, W., Ying, H., Hua, S., Liewen, A., Wang, Q., Zhong, Y., Wu, C.-J., Sadanandam, A., Hu, B., et al. (2014). Yap1 activation enables bypass of oncogenic Kras addiction in pancreatic cancer. Cell *158*, 185–197.

Khandekar, G., Kim, S., and Jagadeeswaran, P. (2012). Zebrafish thrombocytes: functions and origins. Advances in Hematology *2012*, 857058.

Kienast, Y., Baumgarten, von, L., Fuhrmann, M., Klinkert, W.E.F., Goldbrunner, R., Herms, J., and Winkler, F. (2009). Real-time imaging reveals the single steps of brain metastasis formation. Nature Medicine *16*, 116–122.

Kim, H.M., Jung, W.H., and Koo, J.S. (2015a). Expression of Yes-associated protein (YAP) in metastatic breast cancer. Int J Clin Exp Pathol *8*, 11248–11257.

Kim, J.E., Finlay, G.J., and Baguley, B.C. (2013a). The role of the hippo pathway in melanocytes and melanoma. Front Oncol *3*, 123.

Kim, K.M., Choi, Y.J., Hwang, J.-H., Kim, A.R., Cho, H.J., Hwang, E.S., Park, J.Y., Lee, S.-H., and Hong, J.-H. (2014). Shear stress induced by an interstitial level of slow flow increases the osteogenic differentiation of mesenchymal stem cells through TAZ activation. PLoS ONE *9*, e92427.

Kim, M.-Y., Oskarsson, T., Acharyya, S., Nguyen, D.X., Zhang, X.H.F., Norton, L., and Massagué, J. (2009). Tumor self-seeding by circulating cancer cells. Cell *139*, 1315–1326.

Kim, M.H., Kim, C.G., Kim, S.-K., Shin, S.J., Choe, E.A., Park, S.-H., Shin, E.-C., and Kim, J. (2018). YAP-Induced PD-L1 Expression Drives Immune Evasion in BRAFi-Resistant Melanoma. Cancer Immunol Res *6*, 255–266.

Kim, M., Kim, M., Lee, S., Kuninaka, S., Saya, H., Lee, H., Lee, S., and Lim, D.-S. (2013b). cAMP/PKA signalling reinforces the LATS-YAP pathway to fully suppress YAP in response to actin cytoskeletal changes. Embo J. *32*, 1543–1555.

Kim, M., Kim, T., Johnson, R.L., and Lim, D.-S. (2015b). Transcriptional co-repressor function of the hippo pathway transducers YAP and TAZ. CellReports *11*, 270–282.

Kim, N.-G., and Gumbiner, B.M. (2015). Adhesion to fibronectin regulates Hippo signaling via the FAK-Src-PI3K pathway. The Journal of Cell Biology *210*, 503–515.

Kim, N.-G., Koh, E., Chen, X., and Gumbiner, B.M. (2011). E-cadherin mediates contact inhibition of proliferation through Hippo signaling-pathway components. Proc. Natl. Acad. Sci. U.S.a. *108*, 11930–11935.

Kim, T., Hwang, D., Lee, D., Kim, J.-H., Kim, S.-Y., and Lim, D.-S. (2017a). MRTF potentiates TEAD-YAP transcriptional activity causing metastasis. Embo J. *36*, 520–535.

Kim, T., Hwang, D., Lee, D., Kim, J.-H., Kim, S.-Y., and Lim, D.-S. (2017b). MRTF potentiates TEAD-YAP transcriptional activity causing metastasis. Embo J. *36*, 520–535.

Kohli, P., Bartram, M.P., Habbig, S., Pahmeyer, C., Lamkemeyer, T., Benzing, T., Schermer, B., and Rinschen, M.M. (2014). Label-free quantitative proteomic analysis of the YAP/TAZ interactome. Am. J. Physiol., Cell Physiol. *306*, C805–C818.

Komuro, A., Nagai, M., Navin, N.E., and Sudol, M. (2003). WW domain-containing protein YAP associates with ErbB-4 and acts as a co-transcriptional activator for the carboxyl-terminal fragment of ErbB-4 that translocates to the nucleus. Journal of Biological Chemistry *278*, 33334–33341.

Koontz, L.M., Liu-Chittenden, Y., Yin, F., Zheng, Y., Yu, J., Huang, B., Chen, Q., Wu, S., and Pan, D. (2013). The Hippo effector Yorkie controls normal tissue growth by antagonizing scalloped-mediated default repression. Developmental Cell *25*, 388–401.

Labelle, M., and Hynes, R.O. (2012). The Initial Hours of Metastasis: The Importance of Cooperative Host-Tumor Cell Interactions during Hematogenous Dissemination. Cancer Discovery *2*, 1091–1099.

Lai, D., and Yang, X. (2013). BMP4 is a novel transcriptional target and mediator of mammary cell migration downstream of the Hippo pathway component TAZ. Cell. Signal. *25*, 1720–1728.

Lai, Z.-C., Wei, X., Shimizu, T., Ramos, E., Rohrbaugh, M., Nikolaidis, N., Ho, L.-L., and Li, Y. (2005). Control of cell proliferation and apoptosis by mob as tumor suppressor, mats. Cell *120*, 675–685.

Lamar, J.M., Stern, P., Liu, H., Schindler, J.W., Jiang, Z.-G., and Hynes, R.O. (2012). The Hippo pathway target, YAP, promotes metastasis through its TEAD-interaction domain. Proc. Natl. Acad. Sci. U.S.a. *109*, E2441–E2450.

Lee, H.J., Diaz, M.F., Price, K.M., Ozuna, J.A., Zhang, S., Sevick-Muraca, E.M., Hagan, J.P., and Wenzel, P.L. (2017). Fluid shear stress activates YAP1 to promote cancer cell motility. Nature Communications *8*, 14122.

Lee, H.J., Ewere, A., Diaz, M.F., and Wenzel, P.L. (2018). TAZ responds to fluid shear stress to regulate the cell cycle. Cell Cycle *17*, 147–153.

Lehmann, W., Mossmann, D., Kleemann, J., Mock, K., Meisinger, C., Brummer, T., Herr, R., Brabletz, S., Stemmler, M.P., and Brabletz, T. (2016). ZEB1 turns into a transcriptional activator by interacting with YAP1 in aggressive cancer types. Nature Communications *7*, 10498.

Lehtinen, M.K., Yuan, Z., Boag, P.R., Yang, Y., Villén, J., Becker, E.B.E., DiBacco, S., la Iglesia, de, N., Gygi, S., Blackwell, T.K., et al. (2006). A conserved MST-FOXO signaling pathway mediates oxidative-stress responses and extends life span. Cell *125*, 987–1001.

Lei, Q.-Y., Zhang, H., Zhao, B., Zha, Z.-Y., Bai, F., Pei, X.-H., Zhao, S., Xiong, Y., and Guan, K.-L. (2008). TAZ promotes cell proliferation and epithelial-mesenchymal transition and is inhibited by the hippo pathway. Molecular and Cellular Biology *28*, 2426–2436.

Leong, H.S., Robertson, A.E., Stoletov, K., Leith, S.J., Chin, C.A., Chien, A.E., Hague, M.N., Ablack, A., Carmine-Simmen, K., McPherson, V.A., et al. (2014). Invadopodia Are Required for Cancer Cell Extravasation and Are a Therapeutic Target for Metastasis. CellReports *8*, 1558–1570.

Li, Q., Li, S., Mana-Capelli, S., Roth Flach, R.J., Danai, L.V., Amcheslavsky, A., Nie, Y., Kaneko, S., Yao, X., Chen, X., et al. (2014). The conserved misshapen-warts-Yorkie pathway acts in enteroblasts to regulate intestinal stem cells in Drosophila. Developmental Cell *31*, 291–304.

Li, Z., Wang, Y., Zhu, Y., Yuan, C., Wang, D., Zhang, W., Qi, B., Qiu, J., Song, X., Ye, J., et al. (2015). The Hippo transducer TAZ promotes epithelial to mesenchymal transition and cancer stem cell maintenance in oral cancer. Mol Oncol *9*, 1091–1105.

Lian, I., Kim, J., Okazawa, H., Zhao, J., Zhao, B., Yu, J., Chinnaiyan, A., Israel, M.A., Goldstein, L.S.B., Abujarour, R., et al. (2010). The role of YAP transcription coactivator in regulating stem cell self-renewal and differentiation. Genes & Development *24*, 1106–1118.

Liu, C.-Y., Zha, Z.-Y., Zhou, X., Zhang, H., Huang, W., Zhao, D., Li, T., Chan, S.W., Lim, C.J., Hong, W., et al. (2010). The hippo tumor pathway promotes TAZ degradation by phosphorylating a phosphodegron and recruiting the SCF{beta}-TrCP E3 ligase. J. Biol. Chem. *285*, 37159–37169.

Liu, H., Ong, S.-E., Badu-Nkansah, K., Schindler, J., White, F.M., and Hynes, R.O. (2011). CUB-domain-containing protein 1 (CDCP1) activates Src to promote melanoma metastasis. Proc. Natl. Acad. Sci. U.S.a. *108*, 1379–1384.

Liu, J., Ye, L., Li, Q., Wu, X., Wang, B., Ouyang, Y., Yuan, Z., Li, J., and Lin, C. (2018). Synaptopodin-2 suppresses metastasis of triple-negative breast cancer via inhibition of YAP/TAZ activity. J. Pathol. *244*, 71–83.

Liu, X., Yang, N., Figel, S.A., Wilson, K.E., Morrison, C.D., Gelman, I.H., and Zhang, J. (2013). PTPN14 interacts with and negatively regulates the oncogenic function of YAP. Oncogene *32*, 1266–1273.

Ma, B., Chen, Y., Chen, L., Cheng, H., Mu, C., Li, J., Gao, R., Zhou, C., Cao, L., Liu, J., et al. (2015). Hypoxia regulates Hippo signalling through the SIAH2 ubiquitin E3 ligase. Nat Cell Biol *17*, 95–103.

Maher, E.A., Mietz, J., Arteaga, C.L., DePinho, R.A., and Mohla, S. (2009). Brain metastasis: opportunities in basic and translational research. pp. 6015–6020.

Mana-Capelli, S., Paramasivam, M., Dutta, S., and McCollum, D. (2014). Angiomotins link F-actin architecture to Hippo pathway signaling. Mol. Biol. Cell *25*, 1676–1685.

Massagué, J., and Obenauf, A.C. (2016). Metastatic colonization by circulating tumour cells. Nature *529*, 298–306.

Matteucci, E., Maroni, P., Luzzati, A., Perrucchini, G., Bendinelli, P., and Desiderio, M.A. (2013). Bone metastatic process of breast cancer involves methylation state affecting E-cadherin expression through TAZ and WWOX nuclear effectors. Eur. J. Cancer *49*, 231–244.

Meng, Z., Moroishi, T., Mottier-Pavie, V., Plouffe, S.W., Hansen, C.G., Hong, A.W., Park, H.W., Mo, J.-S., Lu, W., Lu, S., et al. (2015). MAP4K family kinases act in parallel to MST1/2 to activate LATS1/2 in the Hippo pathway. Nature Communications *6*, 8357.

Menzel, M., Meckbach, D., Weide, B., Toussaint, N.C., Schilbach, K., Noor, S., Eigentler, T., Ikenberg, K., Busch, C., Quintanilla-Martinez, L., et al. (2014). In melanoma, Hippo signaling is affected by copy number alterations and YAP1 overexpression impairs patient survival. Pigment Cell & Melanoma Research *27*, 671–673.

Miller, E., Yang, J., DeRan, M., Wu, C., Su, A.I., Bonamy, G.M.C., Liu, J., Peters, E.C., and Wu, X. (2012). Identification of serum-derived sphingosine-1-phosphate as a small molecule regulator of YAP. Chemistry & Biology *19*, 955–962.

Miyanaga, A., Masuda, M., Tsuta, K., Kawasaki, K., Nakamura, Y., Sakuma, T., Asamura, H., Gemma, A., and Yamada, T. (2015). Hippo pathway gene mutations in malignant mesothelioma: revealed by RNA and targeted exon sequencing. J Thorac Oncol *10*, 844–851.

Mo, J.-S., Meng, Z., Kim, Y.C., Park, H.W., Hansen, C.G., Kim, S., Lim, D.-S., and Guan, K.-L. (2015). Cellular energy stress induces AMPK-mediated regulation of YAP and the Hippo pathway. Nat Cell Biol *17*, 500–510.

Mo, J.-S., Yu, F.-X., Gong, R., Brown, J.H., and Guan, K.-L. (2012). Regulation of the Hippo-YAP pathway by protease-activated receptors (PARs). Genes & Development *26*, 2138–2143.

Mohseni, M., Sun, J., Lau, A., Curtis, S., Goldsmith, J., Fox, V.L., Wei, C., Frazier, M., Samson, O., Wong, K.-K., et al. (2014). A genetic screen identifies an LKB1-MARK signalling axis controlling the Hippo-YAP pathway. Nat Cell Biol *16*, 108–117.

Mori, M., Triboulet, R., Mohseni, M., Schlegelmilch, K., Shrestha, K., Camargo, F.D., and Gregory, R.I. (2014). Hippo signaling regulates microprocessor and links cell-density-dependent miRNA biogenesis to cancer. Cell *156*, 893–906.

Morin-Kensicki, E.M., Boone, B.N., Howell, M., Stonebraker, J.R., Teed, J., Alb, J.G., Magnuson, T.R., O'Neal, W., and Milgram, S.L. (2006). Defects in yolk sac vasculogenesis, chorioallantoic fusion, and embryonic axis elongation in mice with targeted disruption of Yap65. Molecular and Cellular Biology *26*, 77–87.

Morisaki, T., Hirota, T., Iida, S.-I., Marumoto, T., Hara, T., Nishiyama, Y., Kawasuzi, M., Hiraoka, T., Mimori, T., Araki, N., et al. (2002). WARTS tumor suppressor is phosphorylated by Cdc2/cyclin B at spindle poles during mitosis. FEBS Lett. *529*, 319–324.

Morris, V.L., MacDonald, I.C., Koop, S., Schmidt, E.E., Chambers, A.F., and Groom, A.C. (1993). Early interactions of cancer cells with the microvasculature in mouse liver and muscle during hematogenous metastasis: videomicroscopic analysis. Clin. Exp. Metastasis *11*, 377–390.

Murakami, M., Nakagawa, M., Olson, E.N., and Nakagawa, O. (2005). A WW domain protein TAZ is a critical coactivator for TBX5, a transcription factor implicated in Holt-Oram syndrome. Proc. Natl. Acad. Sci. U.S.a. *102*, 18034–18039.

Murray, L.B., Lau, Y.-K.I., and Yu, Q. (2012). Merlin is a negative regulator of human melanoma growth. PLoS ONE *7*, e43295.

Nakajima, H., Yamamoto, K., Agarwala, S., Terai, K., Fukui, H., Fukuhara, S., Ando, K., Miyazaki, T., Yokota, Y., Schmelzer, E., et al. (2017). Flow-Dependent Endothelial YAP Regulation Contributes to Vessel Maintenance. Developmental Cell *40*, 523–536.e526.

Nallet-Staub, F., Marsaud, V., Li, L., Gilbert, C., Dodier, S., Bataille, V., Sudol, M., Herlyn, M., and Mauviel, A. (2014). Pro-invasive activity of the Hippo pathway effectors YAP and TAZ in cutaneous melanoma. J. Invest. Dermatol. *134*, 123–132.

Ni, L., Li, S., Yu, J., Min, J., Brautigam, C.A., Tomchick, D.R., Pan, D., and Luo, X. (2013). Structural basis for autoactivation of human Mst2 kinase and its regulation by RASSF5. Structure *21*, 1757–1768.

Oh, H., and Irvine, K.D. (2008). In vivo regulation of Yorkie phosphorylation and localization. Development *135*, 1081–1088.

Oh, H., Slattery, M., Ma, L., Crofts, A., White, K.P., Mann, R.S., and Irvine, K.D. (2013). Genome-wide association of Yorkie with chromatin and chromatin-remodeling complexes. CellReports *3*, 309–318.

Oka, T., Remue, E., Meerschaert, K., Vanloo, B., Boucherie, C., Gfeller, D., Bader, G.D., Sidhu, S.S., Vandekerckhove, J., Gettemans, J., et al. (2010). Functional complexes between YAP2 and

ZO-2 are PDZ domain-dependent, and regulate YAP2 nuclear localization and signalling. Biochem. J. *432*, 461–472.

Ota, M., and Sasaki, H. (2008). Mammalian Tead proteins regulate cell proliferation and contact inhibition as transcriptional mediators of Hippo signaling. Development *135*, 4059–4069.

Overholtzer, M., Zhang, J., Smolen, G.A., Muir, B., Li, W., Sgroi, D.C., Deng, C.-X., Brugge, J.S., and Haber, D.A. (2006). Transforming properties of YAP, a candidate oncogene on the chromosome 11q22 amplicon. Proc. Natl. Acad. Sci. U.S.a. *103*, 12405–12410.

Pantalacci, S., Tapon, N., and Léopold, P. (2003). The Salvador partner Hippo promotes apoptosis and cell-cycle exit in Drosophila. Nat Cell Biol *5*, 921–927.

Paramasivam, M., Sarkeshik, A., Yates, J.R., Fernandes, M.J.G., and McCollum, D. (2011). Angiomotin family proteins are novel activators of the LATS2 kinase tumor suppressor. Mol. Biol. Cell *22*, 3725–3733.

Park, H.W., Kim, Y.C., Yu, B., Moroishi, T., Mo, J.-S., Plouffe, S.W., Meng, Z., Lin, K.C., Yu, F.-X., Alexander, C.M., et al. (2015). Alternative Wnt Signaling Activates YAP/TAZ. Cell *162*, 780–794.

Park, J., and Jeong, S. (2015). Wnt activated β-catenin and YAP proteins enhance the expression of non-coding RNA component of RNase MRP in colon cancer cells. Oncotarget *6*, 34658–34668.

Park, K.-S., Whitsett, J.A., Di Palma, T., Hong, J.-H., Yaffe, M.B., and Zannini, M. (2004). TAZ interacts with TTF-1 and regulates expression of surfactant protein-C. Journal of Biological Chemistry *279*, 17384–17390.

Piskounova, E., Agathocleous, M., Murphy, M.M., Hu, Z., Huddlestun, S.E., Zhao, Z., Leitch, A.M., Johnson, T.M., DeBerardinis, R.J., and Morrison, S.J. (2015). Oxidative stress inhibits distant metastasis by human melanoma cells. Nature *527*, 186–191.

Poon, C.L.C., Lin, J.I., Zhang, X., and Harvey, K.F. (2011). The sterile 20-like kinase Tao-1 controls tissue growth by regulating the Salvador-Warts-Hippo pathway. Developmental Cell *21*, 896–906.

Praskova, M., Khoklatchev, A., Ortiz-Vega, S., and Avruch, J. (2004). Regulation of the MST1 kinase by autophosphorylation, by the growth inhibitory proteins, RASSF1 and NORE1, and by Ras. Biochem. J. *381*, 453–462.

Qing, Y., Yin, F., Wang, W., Zheng, Y., Guo, P., Schozer, F., Deng, H., and Pan, D. (2014). The Hippo effector Yorkie activates transcription by interacting with a histone methyltransferase complex through Ncoa6. Elife *3*.

Reddy, B.V.V.G., and Irvine, K.D. (2013). Regulation of Hippo signaling by EGFR-MAPK signaling through Ajuba family proteins. Developmental Cell *24*, 459–471.

Remue, E., Meerschaert, K., Oka, T., Boucherie, C., Vandekerckhove, J., Sudol, M., and Gettemans, J. (2010). TAZ interacts with zonula occludens-1 and -2 proteins in a PDZ-1 dependent manner. FEBS Lett. *584*, 4175–4180.

Reymond, N., d'Água, B.B., and Ridley, A.J. (2013). Crossing the endothelial barrier during metastasis. Nat Rev Cancer *13*, 858–870.

Ritsma, L., Steller, E.J.A., Beerling, E., Loomans, C.J.M., Zomer, A., Gerlach, C., Vrisekoop, N., Seinstra, D., van Gurp, L., Schäfer, R., et al. (2012). Intravital microscopy through an abdominal imaging window reveals a pre-micrometastasis stage during liver metastasis. Sci Transl Med *4*, 158ra145–158ra145.

Rosenbluh, J., Nijhawan, D., Cox, A.G., Li, X., Neal, J.T., Schafer, E.J., Zack, T.I., Wang, X., Tsherniak, A., Schinzel, A.C., et al. (2012). β-Catenin-driven cancers require a YAP1 transcriptional complex for survival and tumorigenesis. Cell *151*, 1457–1473.

Santinon, G., Brian, I., Pocaterra, A., Romani, P., Franzolin, E., Rampazzo, C., Bicciato, S., and Dupont, S. (2018). dNTP metabolism links mechanical cues and YAP/TAZ to cell growth and oncogene-induced senescence. Embo J.

Schlegelmilch, K., Mohseni, M., Kirak, O., Pruszak, J., Rodriguez, J.R., Zhou, D., Kreger, B.T., Vasioukhin, V., Avruch, J., Brummelkamp, T.R., et al. (2011). Yap1 acts downstream of α-catenin to control epidermal proliferation. Cell *144*, 782–795.

Semenza, G.L. (2012). Hypoxia-inducible factors in physiology and medicine. Cell *148*, 399–408.

Shao, D., Zhai, P., Del Re, D.P., Sciarretta, S., Yabuta, N., Nojima, H., Lim, D.-S., Pan, D., and Sadoshima, J. (2014). A functional interaction between Hippo-YAP signalling and FoxO1 mediates the oxidative stress response. Nature Communications *5*, 3315.

Sharif, G.M., Schmidt, M.O., Yi, C., Hu, Z., Haddad, B.R., Glasgow, E., Riegel, A.T., and Wellstein, A. (2015). Cell growth density modulates cancer cell vascular invasion via Hippo pathway activity and CXCR2 signaling. 1–11.

Shibue, T., Brooks, M.W., and Weinberg, R.A. (2013). An integrin-linked machinery of cytoskeletal regulation that enables experimental tumor initiation and metastatic colonization. Cancer Cell *24*, 481–498.

Shibue, T., Brooks, M.W., Inan, M.F., Reinhardt, F., and Weinberg, R.A. (2012). The outgrowth of micrometastases is enabled by the formation of filopodium-like protrusions. Cancer Discovery *2*, 706–721.

Shigeeda, W., Shibazaki, M., Yasuhira, S., Masuda, T., Tanita, T., Kaneko, Y., Sato, T., Sekido, Y., and Maesawa, C. (2017). Hyaluronic acid enhances cell migration and invasion via the YAP1/TAZ-RHAMM axis in malignant pleural mesothelioma. Oncotarget *8*, 93729–93740.

Si, Y., Ji, X., Cao, X., Dai, X., Xu, L., Zhao, H., Guo, X., Yan, H., Zhang, H., Zhu, C., et al. (2017). Src Inhibits the Hippo Tumor Suppressor Pathway through Tyrosine Phosphorylation of Lats1. Cancer Research *77*, 4868–4880.

Skibinski, A., Breindel, J.L., Prat, A., Galván, P., Smith, E., Rolfs, A., Gupta, P.B., LaBaer, J., and Kuperwasser, C. (2014). The Hippo transducer TAZ interacts with the SWI/SNF complex to regulate breast epithelial lineage commitment. CellReports *6*, 1059–1072.

Spicer, J.D., McDonald, B., Cools-Lartigue, J.J., Chow, S.C., Giannias, B., Kubes, P., and Ferri, L.E. (2012). Neutrophils Promote Liver Metastasis via Mac-1-Mediated Interactions with Circulating Tumor Cells. Cancer Research *72*, 3919–3927.

Stein, C., Bardet, A.F., Roma, G., Bergling, S., Clay, I., Ruchti, A., Agarinis, C., Schmelzle, T., Bouwmeester, T., Schübeler, D., et al. (2015). YAP1 Exerts Its Transcriptional Control via TEAD-Mediated Activation of Enhancers. PLoS Genet. *11*, e1005465.

Stoletov, K., Kato, H., Zardouzian, E., Kelber, J., Yang, J., Shattil, S., and Klemke, R. (2010). Visualizing extravasation dynamics of metastatic tumor cells. Journal of Cell Science *123*, 2332–2341.

Strano, S., Munarriz, E., Rossi, M., Castagnoli, L., Shaul, Y., Sacchi, A., Oren, M., Sudol, M., Cesareni, G., and Blandino, G. (2001). Physical interaction with Yes-associated protein enhances p73 transcriptional activity. Journal of Biological Chemistry *276*, 15164–15173.

Straßburger, K., Tiebe, M., Pinna, F., Breuhahn, K., and Teleman, A.A. (2012). Insulin/IGF signaling drives cell proliferation in part via Yorkie/YAP. Developmental Biology *367*, 187–196.

Sudol, M. (1994). Yes-associated protein (YAP65) is a proline-rich phosphoprotein that binds to the SH3 domain of the Yes proto-oncogene product. Oncogene *9*, 2145–2152.

Sudol, M. (2013). YAP1 oncogene and its eight isoforms. Oncogene *32*, 3922–3922.

Tang, Y., Rowe, R.G., Botvinick, E.L., Kurup, A., Putnam, A.J., Seiki, M., Weaver, V.M., Keller, E.T., Goldstein, S., Dai, J., et al. (2013). MT1-MMP-dependent control of skeletal stem cell commitment via a β1-integrin/YAP/TAZ signaling axis. Developmental Cell *25*, 402–416.

Tapon, N., Harvey, K.F., Bell, D.W., Wahrer, D.C.R., Schiripo, T.A., Haber, D.A., and Hariharan, I.K. (2002). salvador Promotes both cell cycle exit and apoptosis in Drosophila and is mutated in human cancer cell lines. Cell *110*, 467–478.

Thakur, Das, M., Feng, Y., Jagannathan, R., Seppa, M.J., Skeath, J.B., and Longmore, G.D. (2010). Ajuba LIM proteins are negative regulators of the Hippo signaling pathway. Curr. Biol. *20*, 657–662.

Toji, S., Yabuta, N., Hosomi, T., Nishihara, S., Kobayashi, T., Suzuki, S., Tamai, K., and Nojima, H. (2004). The centrosomal protein Lats2 is a phosphorylation target of Aurora-A kinase. Genes Cells *9*, 383–397.

Tsuji, K., Yamauchi, K., Yang, M., Jiang, P., Bouvet, M., Endo, H., Kanai, Y., Yamashita, K., Moossa, A.R., and Hoffman, R.M. (2006). Dual-color imaging of nuclear-cytoplasmic dynamics, viability, and proliferation of cancer cells in the portal vein area. Cancer Res. *66*, 303–306.

Udan, R.S., Kango-Singh, M., Nolo, R., Tao, C., and Halder, G. (2003). Hippo promotes proliferation arrest and apoptosis in the Salvador/Warts pathway. Nat Cell Biol *5*, 914–920.

Valencia-Sama, I., Zhao, Y., Lai, D., Janse van Rensburg, H.J., Hao, Y., and Yang, X. (2015). Hippo Component TAZ Functions as a Co-repressor and Negatively Regulates ΔNp63 Transcription through TEA Domain (TEAD) Transcription Factor. J. Biol. Chem. *290*, 16906–16917.

Valiente, M., Obenauf, A.C., Jin, X., Chen, Q., Zhang, X.H.F., Lee, D.J., Chaft, J.E., Kris, M.G., Huse, J.T., Brogi, E., et al. (2014). Serpins promote cancer cell survival and vascular co-option in brain metastasis. Cell *156*, 1002–1016.

Varelas, X. (2014). The Hippo pathway effectors TAZ and YAP in development, homeostasis and disease. Development *141*, 1614–1626.

Varelas, X., Sakuma, R., Samavarchi-Tehrani, P., Peerani, R., Rao, B.M., Dembowy, J., Yaffe, M.B., Zandstra, P.W., and Wrana, J.L. (2008). TAZ controls Smad nucleocytoplasmic shuttling and regulates human embryonic stem-cell self-renewal. Nat Cell Biol *10*, 837–848.

Varelas, X., Samavarchi-Tehrani, P., Narimatsu, M., Weiss, A., Cockburn, K., Larsen, B.G., Rossant, J., and Wrana, J.L. (2010). The Crumbs complex couples cell density sensing to Hippo-dependent control of the TGF-β-SMAD pathway. Developmental Cell *19*, 831–844.

Verfaillie, A., Imrichova, H., Atak, Z.K., Dewaele, M., Rambow, F., Hulselmans, G., Christiaens, V., Svetlichnyy, D., Luciani, F., Van den Mooter, L., et al. (2015a). Decoding the regulatory landscape of melanoma reveals TEADS as regulators of the invasive cell state. Nature Communications *6*, 6683.

Verfaillie, A., Imrichova, H., Atak, Z.K., Dewaele, M., Rambow, F., Hulselmans, G., Christiaens, V., Svetlichnyy, D., Luciani, F., Van den Mooter, L., et al. (2015b). Decoding the regulatory landscape of melanoma reveals TEADS as regulators of the invasive cell state. Nature Communications *6*, 6683.

Vlug, E.J., van de Ven, R.A.H., Vermeulen, J.F., Bult, P., van Diest, P.J., and Derksen, P.W.B. (2013). Nuclear localization of the transcriptional coactivator YAP is associated with invasive lobular breast cancer. Cell Oncol (Dordr) *36*, 375–384.

Wada, K.-I., Itoga, K., Okano, T., Yonemura, S., and Sasaki, H. (2011). Hippo pathway regulation by cell morphology and stress fibers. Development *138*, 3907–3914.

Wang, K.-C., Yeh, Y.-T., Nguyen, P., Limqueco, E., Lopez, J., Thorossian, S., Guan, K.-L., Li, Y.-S.J., and Chien, S. (2016). Flow-dependent YAP/TAZ activities regulate endothelial phenotypes and atherosclerosis. Proc. Natl. Acad. Sci. U.S.a. *113*, 11525–11530.

Wang, W., Huang, J., and Chen, J. (2011). Angiomotin-like proteins associate with and negatively regulate YAP1. J. Biol. Chem. *286*, 4364–4370.

Wang, W., Huang, J., Wang, X., Yuan, J., Li, X., Feng, L., Park, J.-I., and Chen, J. (2012). PTPN14 is required for the density-dependent control of YAP1. Genes & Development *26*, 1959–1971.

Wang, W., Xiao, Z.-D., Li, X., Aziz, K.E., Gan, B., Johnson, R.L., and Chen, J. (2015). AMPK modulates Hippo pathway activity to regulate energy homeostasis. Nat Cell Biol *17*, 490–499.

Wang, Z., Wu, Y., Wang, H., Zhang, Y., Mei, L., Fang, X., Zhang, X., Zhang, F., Chen, H., Liu, Y., et al. (2014). Interplay of mevalonate and Hippo pathways regulates RHAMM transcription via YAP to modulate breast cancer cell motility. Proc. Natl. Acad. Sci. U.S.a. *111*, E89–E98.

Warren, J., Xiao, Y., and Lamar, J. (2018). YAP/TAZ Activation as a Target for Treating Metastatic Cancer. Cancers *10*, 115–137.

Webb, C., Upadhyay, A., Giuntini, F., Eggleston, I., Furutani-Seiki, M., Ishima, R., and Bagby, S. (2011). Structural features and ligand binding properties of tandem WW domains from YAP and TAZ, nuclear effectors of the Hippo pathway. Biochemistry *50*, 3300–3309.

Wei, X., Shimizu, T., and Lai, Z.-C. (2007). Mob as tumor suppressor is activated by Hippo kinase for growth inhibition in Drosophila. Embo J. *26*, 1772–1781.

Wennmann, D.O., Vollenbröker, B., Eckart, A.K., Bonse, J., Erdmann, F., Wolters, D.A., Schenk, L.K., Schulze, U., Kremerskothen, J., Weide, T., et al. (2014). The Hippo pathway is controlled by Angiotensin II signaling and its reactivation induces apoptosis in podocytes. Cell Death Dis *5*, e1519–e1519.

Wong, K.K.L., Li, W., An, Y., Duan, Y., Li, Z., Kang, Y., and Yan, Y. (2015). β-Spectrin regulates the hippo signaling pathway and modulates the basal actin network. J. Biol. Chem. *290*, 6397–6407.

Wu, S., Huang, J., Dong, J., and Pan, D. (2003a). hippo encodes a Ste-20 family protein kinase that restricts cell proliferation and promotes apoptosis in conjunction with salvador and warts. Cell *114*, 445–456.

Wu, S., Huang, J., Dong, J., and Pan, D. (2003b). hippo encodes a Ste-20 family protein kinase that restricts cell proliferation and promotes apoptosis in conjunction with salvador and warts. Cell *114*, 445–456.

Wu, S., Liu, Y., Zheng, Y., Dong, J., and Pan, D. (2008). The TEAD/TEF family protein Scalloped mediates transcriptional output of the Hippo growth-regulatory pathway. Developmental Cell *14*, 388–398.

Xiang, L., Gilkes, D.M., Hu, H., Takano, N., Luo, W., Lu, H., Bullen, J.W., Samanta, D., Liang, H., and Semenza, G.L. (2014). Hypoxia-inducible factor 1 mediates TAZ expression and nuclear localization to induce the breast cancer stem cell phenotype. Oncotarget *5*, 12509–12527.

Xiao, H., Jiang, N., Zhou, B., Liu, Q., and Du, C. (2015). TAZ regulates cell proliferation and epithelial-mesenchymal transition of human hepatocellular carcinoma. Cancer Science *106*, 151–159.

Xie, S., Luca, M., Huang, S., Gutman, M., Reich, R., Johnson, J.P., and Bar-Eli, M. (1997). Expression of MCAM/MUC18 by human melanoma cells leads to increased tumor growth and metastasis. Cancer Res. *57*, 2295–2303.

Xu, T., Wang, W., Zhang, S., Stewart, R.A., and Yu, W. (1995). Identifying tumor suppressors in genetic mosaics: the Drosophila lats gene encodes a putative protein kinase. Development *121*, 1053–1063.

Yabuta, N., Mukai, S., Okada, N., Aylon, Y., and Nojima, H. (2011). The tumor suppressor Lats2 is pivotal in Aurora A and Aurora B signaling during mitosis. Cell Cycle *10*, 2724–2736.

Yamamoto, N., Jiang, P., Yang, M., Xu, M., Yamauchi, K., Tsuchiya, H., Tomita, K., Wahl, G.M., Moossa, A.R., and Hoffman, R.M. (2004). Cellular dynamics visualized in live cells in vitro and in vivo by differential dual-color nuclear-cytoplasmic fluorescent-protein expression. Cancer Res. *64*, 4251–4256.

Yamauchi, K., Yang, M., Jiang, P., Xu, M., Yamamoto, N., Tsuchiya, H., Tomita, K., Moossa, A.R., Bouvet, M., and Hoffman, R.M. (2006). Development of real-time subcellular dynamic multicolor imaging of cancer-cell trafficking in live mice with a variable-magnification whole-mouse imaging system. Cancer Res. *66*, 4208–4214.

Yamauchi, K., Yang, M., Jiang, P., Yamamoto, N., Xu, M., Amoh, Y., Tsuji, K., Bouvet, M., Tsuchiya, H., Tomita, K., et al. (2005). Real-time in vivo dual-color imaging of intracapillary cancer cell and nucleus deformation and migration. Cancer Res. *65*, 4246–4252.

Yang, S., Zhang, L., Liu, M., Chong, R., Ding, S.-J., Chen, Y., and Dong, J. (2013). CDK1 phosphorylation of YAP promotes mitotic defects and cell motility and is essential for neoplastic transformation. Cancer Research *73*, 6722–6733.

Yang, S., Zhang, L., Purohit, V., Shukla, S.K., Chen, X., Yu, F., Fu, K., Chen, Y., Solheim, J., Singh, P.K., et al. (2015a). Active YAP promotes pancreatic cancer cell motility, invasion and tumorigenesis in a mitotic phosphorylation-dependent manner through LPAR3. Oncotarget *6*, 36019–36031.

Yang, S., Zhang, L., Purohit, V., Shukla, S.K., Chen, X., Yu, F., Fu, K., Chen, Y., Solheim, J., Singh, P.K., et al. (2015b). Active YAP promotes pancreatic cancer cell motility, invasion and tumorigenesis in a mitotic phosphorylation-dependent manner through LPAR3. Oncotarget *6*, 36019–36031.

Yeatman, T.J. (2004). A renaissance for SRC. Nat Rev Cancer *4*, 470–480.

Yin, F., Yu, J., Zheng, Y., Chen, Q., Zhang, N., and Pan, D. (2013). Spatial organization of Hippo signaling at the plasma membrane mediated by the tumor suppressor Merlin/NF2. Cell *154*, 1342–1355.

Yin, K., Dang, S., Cui, L., Fan, X., Wang, L., Xie, R., Qu, J., Shang, M., Chen, J., and Xu, Z. (2018). Netrin-1 promotes metastasis of gastric cancer by regulating YAP activity. Biochemical and Biophysical Research Communications *496*, 76–82.

Yu, F.X., and Guan, K.L. (2013). The Hippo pathway: regulators and regulations. Genes & Development *27*, 355–371.

Yu, F.-X., Luo, J., Mo, J.-S., Liu, G., Kim, Y.C., Meng, Z., Zhao, L., Peyman, G., Ouyang, H., Jiang, W., et al. (2014). Mutant Gq/11 promote uveal melanoma tumorigenesis by activating YAP. Cancer Cell *25*, 822–830.

Yu, F.-X., Meng, Z., Plouffe, S.W., and Guan, K.-L. (2015a). Hippo pathway regulation of gastrointestinal tissues. Annu. Rev. Physiol. *77*, 201–227.

Yu, F.-X., Zhang, Y., Park, H.W., Jewell, J.L., Chen, Q., Deng, Y., Pan, D., Taylor, S.S., Lai, Z.-C., and Guan, K.-L. (2013a). Protein kinase A activates the Hippo pathway to modulate cell proliferation and differentiation. Genes & Development *27*, 1223–1232.

Yu, F.-X., Zhao, B., and Guan, K.-L. (2015b). Hippo Pathway in Organ Size Control, Tissue Homeostasis, and Cancer. Cell *163*, 811–828.

Yu, F.-X., Zhao, B., Panupinthu, N., Jewell, J.L., Lian, I., Wang, L.H., Zhao, J., Yuan, H., Tumaneng, K., Li, H., et al. (2012a). Regulation of the Hippo-YAP pathway by G-protein-coupled receptor signaling. Cell *150*, 780–791.

Yu, F.-X., Zhao, B., Panupinthu, N., Jewell, J.L., Lian, I., Wang, L.H., Zhao, J., Yuan, H., Tumaneng, K., Li, H., et al. (2012b). Regulation of the Hippo-YAP pathway by G-protein-coupled receptor signaling. Cell *150*, 780–791.

Yu, J., Zheng, Y., Dong, J., Klusza, S., Deng, W.-M., and Pan, D. (2010). Kibra functions as a tumor suppressor protein that regulates Hippo signaling in conjunction with Merlin and Expanded. Developmental Cell *18*, 288–299.

Yu, T., Bachman, J., and Lai, Z.-C. (2013b). Evidence for a tumor suppressor role for the large tumor suppressor genes LATS1 and LATS2 in human cancer. Genetics *195*, 1193–1196.

Yuan, H., Liu, H., Liu, Z., Zhu, D., Amos, C.I., Fang, S., Lee, J.E., and Wei, Q. (2015). Genetic variants in Hippo pathway genes YAP1, TEAD1 and TEAD4 are associated with melanoma-specific survival. Int. J. Cancer *137*, 638–645.

Zanconato, F., Cordenonsi, M., and Piccolo, S. (2016). YAP/TAZ at the Roots of Cancer. Cancer Cell *29*, 783–803.

Zanconato, F., Forcato, M., Battilana, G., Azzolin, L., Quaranta, E., Bodega, B., Rosato, A., Bicciato, S., Cordenonsi, M., and Piccolo, S. (2015). Genome-wide association between YAP/TAZ/TEAD and AP-1 at enhancers drives oncogenic growth. Nat Cell Biol *17*, 1218–1227.

Zhang, L., Ren, F., Zhang, Q., Chen, Y., Wang, B., and Jiang, J. (2008). The TEAD/TEF family of transcription factor Scalloped mediates Hippo signaling in organ size control. Developmental Cell *14*, 377–387.

Zhang, L., Iyer, J., Chowdhury, A., Ji, M., Xiao, L., Yang, S., Chen, Y., Tsai, M.-Y., and Dong, J. (2012). KIBRA regulates aurora kinase activity and is required for precise chromosome alignment during mitosis. J. Biol. Chem. *287*, 34069–34077.

Zhang, N., Bai, H., David, K.K., Dong, J., Zheng, Y., Cai, J., Giovannini, M., Liu, P., Anders, R.A., and Pan, D. (2010). The Merlin/NF2 tumor suppressor functions through the YAP oncoprotein to regulate tissue homeostasis in mammals. Developmental Cell *19*, 27–38.

Zhang, W., Gao, Y., Li, P., Shi, Z., Guo, T., Li, F., Han, X., Feng, Y., Zheng, C., Wang, Z., et al. (2014). VGLL4 functions as a new tumor suppressor in lung cancer by negatively regulating the YAP-TEAD transcriptional complex. Cell Res. *24*, 331–343.

Zhang, X., George, J., Deb, S., Degoutin, J.L., Takano, E.A., Fox, S.B., AOCS Study group, Bowtell, D.D.L., and Harvey, K.F. (2011). The Hippo pathway transcriptional co-activator, YAP, is an ovarian cancer oncogene. Oncogene *30*, 2810–2822.

Zhao, B., Li, L., Tumaneng, K., Wang, C.Y., and Guan, K.L. (2010). A coordinated phosphorylation by Lats and CK1 regulates YAP stability through SCF -TRCP. Genes & Development *24*, 72–85.

Zhao, B., Kim, J., Ye, X., Lai, Z.-C., and Guan, K.-L. (2009). Both TEAD-binding and WW domains are required for the growth stimulation and oncogenic transformation activity of yes-associated protein. Cancer Research *69*, 1089–1098.

Zhao, B., Li, L., Lu, Q., Wang, L.H., Liu, C.-Y., Lei, Q., and Guan, K.-L. (2011). Angiomotin is a novel Hippo pathway component that inhibits YAP oncoprotein. Genes & Development *25*, 51–63.

Zhao, B., Li, L., Wang, L., Wang, C.-Y., Yu, J., and Guan, K.-L. (2012). Cell detachment activates the Hippo pathway via cytoskeleton reorganization to induce anoikis. Genes & Development *26*, 54–68.

Zhao, B., Wei, X., Li, W., Udan, R.S., Yang, Q., Kim, J., Xie, J., Ikenoue, T., Yu, J., Li, L., et al. (2007). Inactivation of YAP oncoprotein by the Hippo pathway is involved in cell contact inhibition and tissue growth control. Genes & Development *21*, 2747–2761.

Zhao, B., Ye, X., Yu, J., Li, L., Li, W., Li, S., Yu, J., Yu, J., Lin, J.D., Wang, C.-Y., et al. (2008). TEAD mediates YAP-dependent gene induction and growth control. Genes & Development *22*, 1962–1971.

Zhao, Y., Khanal, P., Savage, P., She, Y.-M., Cyr, T.D., and Yang, X. (2014). YAP-induced resistance of cancer cells to antitubulin drugs is modulated by a Hippo-independent pathway. Cancer Research *74*, 4493–4503.

Zheng, Y., Wang, W., Liu, B., Deng, H., Uster, E., and Pan, D. (2015). Identification of Happyhour/MAP4K as Alternative Hpo/Mst-like Kinases in the Hippo Kinase Cascade. Developmental Cell *34*, 642–655.

Zhou, P.-J., Xue, W., Peng, J., Wang, Y., Wei, L., Yang, Z., Zhu, H.H., Fang, Y.-X., and Gao, W.-Q. (2017). Elevated expression of Par3 promotes prostate cancer metastasis by forming a Par3/aPKC/KIBRA complex and inactivating the hippo pathway. J. Exp. Clin. Cancer Res. *36*, 139.

Zhou, X., Wang, S., Wang, Z., Feng, X., Liu, P., Lv, X.-B., Li, F., Yu, F.-X., Sun, Y., Yuan, H., et al. (2015). Estrogen regulates Hippo signaling via GPER in breast cancer. J. Clin. Invest. *125*, 2123–2135.

Zhou, Y., Huang, T., Cheng, A.S.L., Yu, J., Kang, W., and To, K.F. (2016). The TEAD Family and Its Oncogenic Role in Promoting Tumorigenesis. Int J Mol Sci *17*.

Zihni, C., Mills, C., Matter, K., and Balda, M.S. (2016). Tight junctions: from simple barriers to multifunctional molecular gates. Nature Reviews Drug Discovery *17*, 564–580.

Chapter 4.

Conclusion

The contents of this chapter were written by David Benjamin with editing by Jess Hebert and Richard Hynes.

Summary of Results

Metastasis is the cause of the overwhelming majority of cancer-related mortality, yet our understanding of this process is incomplete. In particular the events at the metastatic site remain poorly understood. A complete understanding of these events is critical because they may rate-limiting for metastasis (Fidler, 1970; Luzzi et al., 1998; Massagué and Obenauf, 2016). While intravital imaging studies in mice provided insights, intravital imaging in mice remains a technically challenging technique whose use is far from routine.

We thought that zebrafish might be a simpler system for intravital imaging because a line of zebrafish that was transparent throughout its life had recently been developed (White et al., 2008). These fish allowed intravital imaging of adults without the complication of using the surgically implanted imaging windows required in mice (Alieva et al., 2014). We believed that it was important to use an adult organism because cancer is primarily a disease of adults so we needed an adult microenvironment to properly model metastasis (Siegel et al., 2017). Our first goal was to use intravital imaging in adult zebrafish to study the interactions between tumor cells, innate immune cells, and thrombocytes, the fish equivalent to platelets, during metastasis. There was a wealth of literature showing that these interactions were important for metastasis (Gay and Felding-Habermann, 2011; Joyce and Pollard, 2008; Labelle and Hynes, 2012). However, most studies had been performed on fixed tissue harvested at various time points following injection (Ferjancic et al., 2013; Gil-Bernabé et al., 2012a; Labelle and Hynes, 2012; Labelle et al., 2011; Qian et al., 2011; 2009). These studies could give the broad temporal order of these interactions but could not capture the true dynamic picture.

As described in appendix A, we encountered a number of issues during these studies. The first issue we encountered was that tumor cells did not appear to interact with thrombocytes. This was surprising given the important roles played by platelets during metastasis in mice (Gay and Felding-Habermann, 2011; Gil-Bernabé et al., 2012b; Labelle and Hynes, 2012; Labelle et al., 2011; 2014). One possibility for the lack of interaction was that there were not enough thrombocytes present due to irradiation. However, even in unirradiated fish, there do not appear to be many thrombocytes in circulation. To date the role of coagulation and thrombocytes in metastasis in zebrafish remains untested. It would seem prudent to inhibit thrombocyte function or coagulation and evaluate whether that affects metastasis before further studies of tumor cell-thrombocyte interactions.

We also encountered an issue with the mpx:EGFP line of fish where despite having EGFP-labeled neutrophils as embryos, we could not find labeled neutrophils in the adult. Given that many of the lines of fish with labeled lineages have been made to study cells during embryonic development, care must be taken to confirm that the cell type of interest is still labeled in the adult (Ellett et al., 2011; Lawson and Weinstein, 2002; Lin et al., 2005; Mathias et al., 2006; Renshaw et al., 2006). A related issue is that immune cell types in adult zebrafish are not well characterized. In mice, different subsets of cells such as neutrophils or macrophages can have opposing roles during tumor progression and metastasis (Joyce and Pollard, 2008). It may prove challenging to study immune cell interactions in zebrafish adults until the adult complement of immune cells is better characterized.

Given the issues described above, we instead decided to only characterize the behavior of the tumor cells themselves at the metastatic site in adult zebrafish. We injected the ZMEL1

zebrafish melanoma line, that had been previously developed in the lab, into transparent Casper fish (Heilmann et al., 2015). At the time this work started, retro-orbital (RO) injections were the standard injection method for adult fish (Pugach et al., 2009). While this injection method works well in older fish, it did not work well in the 6-10-week-old fish that were used in our experiments. This led to few metastases forming in the animal following RO injections. We chose to use 6-10 week old fish as they are physically adult fish, yet young enough that there is a minimal wait time to get fish for experiments. To overcome the difficulties with RO injections, we developed a new intravenous injection protocol to inject cells into the common cardinal vein.

Using this new injection method, cells formed many tumors throughout the animal. This result that a zebrafish tumor cell line can form tumors following injection into circulation may help provide an answer to a long standing question in the zebrafish metastasis field. It has long been observed that zebrafish tumors rarely metastasize and it has been questioned if they do in fact metastasize through hematogenous circulation (Stern and Zon, 2003). Our experiments clearly demonstrate that zebrafish tumor cells are capable of forming metastases following intravenous injection. This demonstrates that the ZMEL1 cell line is competent to survive in circulation, extravasate, and grow in multiple organs. Furthermore, other groups have found metastases far removed from primary tumors suggesting hematogenous travel (Heilmann et al., 2015; Tang et al., 2016). While these results highly suggest that zebrafish tumors can metastasize through hematogenous circulation, most zebrafish tumors, including the ZMEL1, have a rather limited metastatic propensity. In order to study metastasis, highly metastatic cell lines are a valuable reagent. One potential use for the intravenous injection method therefore

might be to generate *in vivo* selected lines with higher metastatic potential. Serial selection experiments have already been performed following repeated implantation in the dorsal musculature of a fish. By the 7th, passage in fish, one such line had greatly enhanced metastatic potential (Tang et al., 2016). It would be interesting to compare the gene expression profiles of lines *in vivo* selected for spontaneous and experimental metastasis. This analysis could lead to the identification of new genes involved in metastasis. *In vivo* selected zebrafish lines could be compared to *in vivo* selected human or mouse cell lines to identify aspects of metastasis that are conserved between mammals and fish.

One organ where the ZMEL1 cells formed tumors following intravenous injection was the skin and the sub-dermal muscle. Cells in these locations could be imaged using standard confocal microscopy. We first characterized the early events at the metastatic site: arrest, extravasation, and early growth. One interesting observation from this study was that shortly following extravasation, tumor cells were observed to have large protrusions that often wrapped around blood vessels. These protrusions were then seen to disappear over the next few days. Given the role that protrusions have been shown to play in the early proliferation of tumor cells at the metastatic site, the composition of the protrusions we saw could be of interest (Shibue et al., 2012).

As we injected the ZMEL1 line into flk:dsRed zebrafish, the fish's fluorescent vasculature could be used as landmarks allowing imaging of the same location for up to two weeks. We followed individual tumor cells during this time at the metastatic site as they grew from single disseminated tumor cells into macroscopic metastases. We observed that cells during this time

were very dynamic. We observed a great deal of movement in the first few days and the dynamic extension and retraction of protrusions at 9 days post-injection.

As our zebrafish cell line proved difficult to manipulate, we also attempted to inject human tumor cell lines into these fish. Despite testing multiple methods of immunosuppression as well as the use of genetically immunocompromised fish, almost all human tumor cells were cleared within 48 hours post-injection. Xenotransplantation currently remains a challenge for use of zebrafish in cancer research (White et al., 2013). However, recent progress in creating genetically immunocompromised zebrafish and in other immunosuppression techniques hint that this challenge may be overcome in the near future (Moore et al., 2016; Tang et al., 2014; Zhang et al., 2016).

Our studies of the ZMEL1 cell line were hampered by our inability to manipulate them using retro or lentiviral vectors. Due these difficulties, we switched to performing experiments in embryos, which allowed us to use human cells which we could manipulate. We over-expressed four genes known to promote melanoma metastasis in mice (BMI1, CDCP1, MCAM, and YAP-AA) (Ferretti et al., 2016; Lamar et al., 2012; Liu et al., 2011; Xie et al., 1997). We screened these genes for their ability to promote brain metastasis in zebrafish embryos 4 days post-injection. YAP-AA (YAP S127A,S381A, a mutant form of YAP that is insensitive to the Hippo pathway) promoted brain metastasis in this experiment.

This result highlights that zebrafish embryos can be used to model brain metastasis. Most studies of xenografted tumor cells in the brain of zebrafish embryos have been performed following injection into the hindbrain ventricle (Haldi et al., 2006; Hamilton et al., 2016; Lal et al., 2012; Roh-Johnson et al., 2017; Vittori et al., 2015; Welker et al., 2016). These studies have

primarily investigated brain tumors using the embryonic brain as an orthotopic context although a few have studied melanoma cells in the brain microenvironment. Few studies have assayed brain metastasis in the zebrafish using experimental or spontaneous metastasis experiments (Stoletov et al., 2013). While, hind brain injections can be useful for looking at some behaviors that influence metastasis such as tumor growth or interactions with stromal cells at the metastatic site, they only model some of the events of metastasis. Some important steps of metastasis that are not modeled by hindbrain injections are extravasation and the early survival of tumor cells in a perivascular niche. These steps have been shown to be important for brain metastasis in murine systems (Kienast et al., 2009). Our observation that control cells generated relatively few brain metastases at baseline suggests that the zebrafish embryo might be a system well-suited to study of genes that enhance brain metastasis.

We next sought to determine how YAP-AA was promoting brain metastasis in the zebrafish embryo. We followed individual embryos over time following injection of YAP-over-expressing cells and determined that YAP promoted metastasis within the first 10 hours of injection. Furthermore all of YAP's enhancement of metastasis was occurring during this time. Given the timing of the mammalian cell cycle, this indicated that YAP's known roles in promoting proliferation were probably not the reason for enhanced metastasis in our system (Alberts et al., 2008; Warren et al., 2018). We also quickly determined that YAP was likely not enhancing arrest, extravasation, or survival in circulation.

These results turned out to be fortuitous for our experiments. One of the major difficulties in studying YAP's role in metastasis in mice is that it can be difficult to determine exactly how YAP is promoting metastasis because YAP can regulate so many different

processes. (Janse van Rensburg and Yang, 2016; Warren et al., 2018). The fact that YAP-AA was not observed to enhance extravasation, survival in circulation, or tumor growth, eliminated these processes as complications from our experiments. One strength of zebrafish embryos as compared to mice might be in providing a simpler model system for experiments in which processes can be studied in isolation.

In further experiments, we determined that YAP was specifically enhancing metastasis to the brain. Surprisingly, there was only a very slight (but not statistically significant) effect on metastasis to the tail (the other major location where cells end up following intravenous injection into embryos) nor much of an increase in the total number of cells in circulation (again this increase was not statistically significant). When we performed time-lapse imaging of the brain of embryos for 12 hours, we observed that more YAP-AA cells were arriving through circulation than control cells. To see where these cells were coming from, we performed time-lapse imaging of the whole embryo. We observed that these cells appeared to be arriving from the tail and confirmed that cells could travel from the tail to the brain using the photoconvertible protein Dendra2.

These results illustrate that future studies of metastasis in zebrafish embryos should monitor tumor cells throughout the entire embryo rather than in single locations. Many studies of metastasis in zebrafish have solely focused on the behavior of tumor cells in the tail (He et al., 2012; Sharif et al., 2015; Stoletov et al., 2010; Teng et al., 2013). While most tumor cells do lodge in the tail following injection, accounting for the cells that landed elsewhere proved to be quite instructive in our study of YAP biology. Furthermore, many studies use the numbers of cells in the tail as their only readout on metastasis. If we had only used this readout, we might

have missed YAP-AA's effects completely as YAP had only a minor effect on tail metastasis. Our results demonstrate that tumor cells can behave differently in different regions of the embryo. Therefore, it seems prudent for future researchers to look at how tumor cells behave in different locations in the embryo in future studies.

The next question we sought to address was how YAP-AA was promoting tumor cell escape from the tail. *In vitro* assays showed that YAP-AA enhanced tumor cell homophilic adhesion as well as adhesion to human endothelial cells. In addition, YAP-AA promoted metastasis in a cell autonomous manner when YAP-AA and EV control cells were co-injected into zebrafish embryos. Finally, YAP-AA promoted migration in transwell migration assays. From these observations, we hypothesized that YAP-AA might be promoting escape from the tail by promoting intravascular migration. Intravascular migration has been previously reported to occur in the tail of zebrafish embryos (Stoletov et al., 2010).

With this hypothesis in mind we sought to identify how YAP-AA might be enhancing migration in this system. Consistent with many other studies, YAP's ability to regulate transcription was required to promote metastasis in our system (Lamar et al., 2012; Warren et al., 2018). When we looked at global F- and G-actin levels, YAP-AA over-expression led to greatly increased levels of F-actin, suggesting that YAP was enhancing motility by enhancing actin polymerization. YAP-AA did not affect the activity of cofilin as determined by the levels of phospho-cofilin. These results suggested that YAP-AA's mechanism of promoting motility was different from a previously reported mechanism where YAP promotes motility by enhancing cofilin activity, which decreased the global levels of F-actin (Qiao et al., 2017).

We also used our imaging techniques in zebrafish embryos as part of a collaboration with Michelle Chen, a graduate student in the lab of Roger Kamm in the MIT departments of Biological and Chemical Engineering. In these experiments, we studied the interactions between neutrophils and tumor cells in the context of systemic inflammation. Human tumor cells and LPS-stimulated human neutrophils were co-injected into circulation in zebrafish embryos and imaged. Through these experiments, we confirmed observations made in an *in vitro* microfluidic device that neutrophils associated with arrested clusters of tumor cells migrate but remain near to tumor cell clusters. In contrast, neutrophils not near arrested tumor cells migrated faster and further distances.

These experiments demonstrate that the interactions between human tumor cells and human leukocytes can also be studied in the zebrafish. To date, there have been few studies where human tumor cells and human immune cells are co-injected into embryos (Wang et al., 2015). Of particular interest to our lab have been neutrophils and macrophages. These cell types are in the parenchyma and not in circulation in 2-day-old embryos (Ellett et al., 2011; Mathias et al., 2006; Renshaw et al., 2006; Yoo and Huttenlocher, 2011). However, they have been shown to play important roles in circulation during metastasis in mice (Labelle and Hynes, 2012). Co-injection of human tumor cells with these leukocytes into zebrafish embryos could be a powerful method to study their interactions in real time through intravital imaging.

Future Work

During the time when the work described in this thesis took place, the use of zebrafish to study cancer was becoming increasingly popular. The use of adult zebrafish in particular was a nascent field when this work began and led us to encounter a number of technical limitations. The description of these challenges thus far may discourage future researchers from attempting experiments with adults. However, some of the technical limitations that were present during the work described in this thesis have been since been overcome (Fazio et al., 2017; Zhang et al., 2016) (Moore et al., 2016; Tang et al., 2014). Given these advances, there are a number of potential experiments that the adult zebrafish techniques we developed could be useful for.

The intravenous injection technique we developed has a number of potential uses. One obvious experiment that could be done would be large-scale experimental metastasis assays. Large panels of ZMEL1 cell lines (or another zebrafish line) with candidate genes over-expressed or knocked down could be generated and injected into adult Casper fish. Experimental metastasis assays in mice are limited by the cost of housing large numbers of mice. Given that zebrafish are small and cheap to maintain, large numbers of fish can be used in a single experiment (White et al., 2013). Furthermore, while in mice the end point of such assays is typically 4-6 weeks after injection, only 2 weeks was sufficient to see many macroscopic metastases in zebrafish in our experiments (Gómez-Cuadrado et al., 2017). Additionally, the quantification of metastasis in Casper fish through whole body fluorescence imaging is rapid and simple. In mice, quantification of metastasis is more difficult since it requires luminescent imaging using luciferase or the dissection of each mouse to remove individual organs for analysis (Zinn et al., 2008).

Another variation of this experiment could involve changing the genetic background of the host fish rather than the tumor cells. This experiment would address how genes in stromal cells affect metastasis. In general, most metastasis experiments manipulate genes in tumor cells to see how they influence metastasis. This may be due to the fact that the difficulty and time required to make a knockout mice frequently means it is not practical to make a knockout mouse to study the role of a gene of interest in the stroma. The development of CRISPR reagents for use in zebrafish permits the rapid generation of knockout fish through the injection of these reagents into embryos at the one cell stage (Chang et al., 2013; Hwang et al., 2013a; 2013b; Jao et al., 2013). Furthermore, a recently developed tissue-specific CRISPR vector could be used in cases where global knockouts are lethal or the function of a gene within a specific cell type is of interest (Ablain et al., 2015).

The development of the orthotopic injection of ZMEL1 melanoma cells into the skin by our group and others allows experiments like the ones described above to be performed but for metastasis from a primary tumor rather than experimental metastasis assays (Heilmann et al., 2015). These experiments could screen for genes that influence the early steps of the metastatic cascade in tumor cells or the stroma. Again, the ability to inject and maintain large numbers of zebrafish is a distinct advantage when compared to mice.

In addition to being used for screens, another use for our injection techniques in adult zebrafish could be to understand genes that have already been identified to play a role in metastasis. Currently, intravital imaging in mice remains a specialized technique that is only routinely used in a limited number of labs. The techniques we described in chapter 2 and appendix A could allow more groups to add intravital imaging at the metastatic site or a

primary tumor to their methods toolkit. With the ability to genetically manipulate the ZMEL1 cell line, ZMEL1 cells could be made to express other fluorophores, which would enable the interactions between ZMEL1 cells and other cell types to be imaged (Fazio et al., 2017).

In contrast to the adult zebrafish described above, our work with zebrafish embryos described in chapter 3 and appendix A relied on existing techniques. Our hope is that this work illustrates how zebrafish embryos can be a powerful tool for unravelling the biology of metastasis. Our study of YAP was a modest attempt to better understand this powerful and complicated oncogene. Our observations suggested that YAP might promote metastasis through a new an intriguing mechanism. However, there are a number of questions that have arisen from this work that remain to be addressed.

First, if YAP-AA does enhance intravascular migration, this leads to the question of how common intravascular migration is. If YAP-AA does enhance intravascular migration, it would be the second gene reported to do so after Twist1 (Stoletov et al., 2010). A first experiment would be to assay other known metastasis-promoting genes to see if any of them also promote intravascular migration. Since Twist1 and YAP are both known to promote EMT, one of the first places to start would be to test if over-expression of other EMT-promoting genes causes intravascular migration (Overholtzer et al., 2006),.

Second, another open question about intravascular migration is whether it occurs in mammalian systems. To date, there has not been an intravital imaging study that imaged Twist1 or YAP over-expressing cells to see how they behaved in circulation in mice. The vasculature in the liver may be closest to the location where intravascular migration was observed in our studies in the zebrafish embryo in terms of vessel diameter and blood flow

velocities (Aird, 2007). Intravital imaging of Twist1 or YAP-AA over-expressing cells in the liver of mice following injection could address whether this phenomenon occurs in mice as well or if it is restricted to zebrafish embryos.

If intravascular migration does occur in mice, another potential place to look for it would be in the primary tumor. A potential role of intravascular migration in the primary tumor becomes apparent when one considers a paradox in how tumor cells enter circulation to metastasize. It has been proposed that the majority of intravasation occurs within the primary tumor, rather than at vessels around the invasive margin (Deryugina and Kiosses, 2017). However, vessels within the tumor often have greatly reduced blood flow, which may not allow tumor cells to be swept away into circulation (Padera et al., 2004; Tong et al., 2004). Therefore, cells within the vasculature of primary tumors might migrate within blood vessels to regions of better blood flow to enter circulation. Determining if this process in fact occurs, could be answered using intravital imaging in adult zebrafish by imaging orthotopic primary tumors formed following the intradermal injection of ZMEL1 cells. Alternatively, intravital imaging of primary tumors in the mammary fat pads of mice could also address this question. If intravascular migration is discovered to be an EMT-related phenotype, the interactions between intravascular tumor cells and platelets at the metastatic site would be of particular interest as platelets can induce an EMT in intravascular tumor cells (Labelle et al., 2011).

If intravascular migration does occur in mammals, the next question is whether it influences the dissemination of tumor cells throughout the body. A key experiment would be to see if YAP over-expression changes the distribution of tumor cells throughout the body of a mouse. In such an experiment, tumor cells expressing luciferase would be injected

intravenously into a mouse via tail vein or intrasplenic injections to deliver cells to the lung or liver respectively. Mice would then be imaged with whole-animal bioluminescent imaging shortly after injection to establish a baseline. The mouse would then be imaged for up to 48 hours to compare where tumor cells are over time. While this technique cannot image single cells, it could provide insight into the general distribution of tumor cells throughout an animal.

If YAP over-expression is enhancing dissemination following arrest in the first capillary bed encountered, then one would expect the control cells to remain in the first vascular bed during the course of the experiment. However, YAP-over-expressing cells would be seen to spread beyond the first capillary bed to other organs over time. As discussed in chapter 3, if YAP over-expression can cause tumor cells to spread more widely, this has grave implications for cancer patients.

Finally, another open question from our study is what genes are responsible for YAP's ability to promote migration in A375 and HT-29 cells. Answering this question may prove to be challenging because YAP regulates a large number of genes, and this set of genes can vary considerably between cell lines (Yu et al., 2015). One experiment might be to perform RNA-seq on A375 and HT-29 cells to look for genes that are regulated by YAP in both. Any genes involved in migration which are regulated by YAP in both cell lines would be prime candidates for promoting migration. However, if there is not much overlap in the gene expression patterns, studying the individual cell lines might be required. YAP targets in A375 or HT-29 cell lines with known roles in migration could be knocked down or over-expressed and screened for their effect on migration *in vitro* or in embryos.

Concluding Remarks

This thesis set out to use zebrafish as a tool for the intravital imaging metastasis. We first developed new methods for the intravital imaging of metastasis in adult zebrafish. We demonstrated the utility of these methods by following ZMEL1 cells over two weeks at the metastatic and characterizing their behavior. We believe that these methods will prove useful for other researchers in the field as well.

We also used zebrafish embryos to gain new insight into the biology of the oncogene YAP, a potent enhancer of metastasis. Through intravital imaging in zebrafish embryos, we observed that YAP promoted dissemination by allowing YAP-AA over-expressing tumor cells to escape from the first capillary bed they encountered and re-enter circulation. Once in circulation, YAP-AA cells could spread to other locations in the embryo, such as the brain. We hypothesize that YAP-AA is promoting escape from this first capillary bed by promoting intravascular migration. Escape from the first capillary bed encountered represents a new mechanism for dissemination during metastasis. We also hope that our study of YAP in zebrafish embryos serves to demonstrate how they can be a powerful system to uncover new biology and may inspire other researchers to add zebrafish to their research program.

References:

Ablain, J., Durand, E.M., Yang, S., Zhou, Y., and Zon, L.I. (2015). A CRISPR/Cas9 vector system for tissue-specific gene disruption in zebrafish. Developmental Cell *32*, 756–764.

Aird, W.C. (2007). Phenotypic heterogeneity of the endothelium: II. Representative vascular beds. Circulation Research *100*, 174–190.

Alberts, B., Wilson, J., and Hunt, T. (2008). Molecular biology of the cell (New York: Garland Science).

Alieva, M., Ritsma, L., Giedt, R.J., Weissleder, R., and van Rheenen, J. (2014). Imaging windows for long-term intravital imaging: General overview and technical insights. Intravital *3*, e29917.

Chang, N., Sun, C., Gao, L., Zhu, D., Xu, X., Zhu, X., Xiong, J.-W., and Xi, J.J. (2013). Genome editing with RNA-guided Cas9 nuclease in zebrafish embryos. Cell Res. *23*, 465–472.

Deryugina, E.I., and Kiosses, W.B. (2017). Intratumoral Cancer Cell Intravasation Can Occur Independent of Invasion into the Adjacent Stroma. CellReports *19*, 601–616.

Ellett, F., Pase, L., Hayman, J.W., Andrianopoulos, A., and Lieschke, G.J. (2011). mpeg1 promoter transgenes direct macrophage-lineage expression in zebrafish. Blood *117*, e49–e56.

Fazio, M., Avagyan, S., van Rooijen, E., Mannherz, W., Kaufman, C.K., Lobbardi, R., Langenau, D.M., and Zon, L.I. (2017). Efficient Transduction of Zebrafish Melanoma Cell Lines and Embryos Using Lentiviral Vectors. Zebrafish *14*, 379–382.

Ferjancic, S., Gil-Bernabe, A.M., Hill, S.A., Allen, P.D., Richardson, P., Sparey, T., Savory, E., McGuffog, J., and Muschel, R.J. (2013). VCAM-1 and VAP-1 recruit myeloid cells that promote pulmonary metastasis in mice. Blood.

Ferretti, R., Bhutkar, A., McNamara, M.C., and Lees, J.A. (2016). BMI1 induces an invasive signature in melanoma that promotes metastasis and chemoresistance. Genes & Development *30*, 18–33.

Fidler, I.J. (1970). Metastasis: quantitative analysis of distribution and fate of tumor emboli labeled with 125 I-5-iodo-2'-deoxyuridine. J. Natl. Cancer Inst. *45*, 773–782.

Gay, L.J., and Felding-Habermann, B. (2011). Contribution of platelets to tumour metastasis. 1–12.

Gil-Bernabé, A.M., Ferjancic, S., Tlalka, M., Zhao, L., Allen, P.D., Im, J.H., Watson, K., Hill, S.A., Amirkhosravi, A., Francis, J.L., et al. (2012a). Recruitment of monocytes/macrophages by tissue factor-mediated coagulation is essential for metastatic cell survival and premetastatic niche establishment in mice. Blood *119*, 3164–3175.

Gil-Bernabé, A.M., Ferjancic, S., Tlalka, M., Zhao, L., Allen, P.D., Im, J.H., Watson, K., Hill, S.A., Amirkhosravi, A., Francis, J.L., et al. (2012b). Recruitment of monocytes/macrophages by tissue factor-mediated coagulation is essential for metastatic cell survival and premetastatic niche establishment in mice. Blood *119*, 3164–3175.

Gómez-Cuadrado, L., Tracey, N., Ma, R., Qian, B., and Brunton, V.G. (2017). Mouse models of metastasis: progress and prospects. Disease Models & Mechanisms *10*, 1061–1074.

Haldi, M., Ton, C., Seng, W.L., and McGrath, P. (2006). Human melanoma cells transplanted into zebrafish proliferate, migrate, produce melanin, form masses and stimulate angiogenesis in zebrafish. Angiogenesis *9*, 139–151.

Hamilton, L., Astell, K.R., Velikova, G., and Sieger, D. (2016). A Zebrafish Live Imaging Model Reveals Differential Responses of Microglia Toward Glioblastoma Cells In Vivo. Zebrafish *13*, 523–534.

He, S., Lamers, G.E., Beenakker, J.-W.M., Cui, C., Ghotra, V.P., Danen, E.H., Meijer, A.H., Spaink, H.P., and Snaar-Jagalska, B.E. (2012). Neutrophil-mediated experimental metastasis is enhanced by VEGFR inhibition in a zebrafish xenograft model. J. Pathol. *227*, 431–445.

Heilmann, S., Ratnakumar, K., Langdon, E.M., Kansler, E.R., Kim, I.S., Campbell, N.R., Perry, E.B., McMahon, A.J., Kaufman, C.K., van Rooijen, E., et al. (2015). A Quantitative System for Studying Metastasis Using Transparent Zebrafish. Cancer Res. *75*, 4272–4282.

Hwang, W.Y., Fu, Y., Reyon, D., Maeder, M.L., Kaini, P., Sander, J.D., Joung, J.K., Peterson, R.T., and Yeh, J.-R.J. (2013a). Heritable and precise zebrafish genome editing using a CRISPR-Cas system. PLoS ONE *8*, e68708.

Hwang, W.Y., Fu, Y., Reyon, D., Maeder, M.L., Tsai, S.Q., Sander, J.D., Peterson, R.T., Yeh, J.-R.J., and Joung, J.K. (2013b). Efficient genome editing in zebrafish using a CRISPR-Cas system. Nat. Biotechnol. *31*, 227–229.

Janse van Rensburg, H.J., and Yang, X. (2016). The roles of the Hippo pathway in cancer metastasis. Cell. Signal. *28*, 1761–1772.

Jao, L.-E., Wente, S.R., and Chen, W. (2013). Efficient multiplex biallelic zebrafish genome editing using a CRISPR nuclease system. Proc. Natl. Acad. Sci. U.S.a. *110*, 13904–13909.

Joyce, J.A., and Pollard, J.W. (2008). Microenvironmental regulation of metastasis. Nat Rev Cancer *9*, 239–252.

Kienast, Y., Baumgarten, von, L., Fuhrmann, M., Klinkert, W.E.F., Goldbrunner, R., Herms, J., and Winkler, F. (2009). Real-time imaging reveals the single steps of brain metastasis formation. Nature Medicine *16*, 116–122.

Labelle, M., and Hynes, R.O. (2012). The Initial Hours of Metastasis: The Importance of Cooperative Host-Tumor Cell Interactions during Hematogenous Dissemination. Cancer Discovery *2*, 1091–1099.

Labelle, M., Begum, S., and Hynes, R.O. (2011). Direct Signaling between Platelets and Cancer Cells Induces an Epithelial-Mesenchymal-Like Transition and Promotes Metastasis. Cancer Cell *20*, 576–590.

Labelle, M., Begum, S., and Hynes, R.O. (2014). Platelets guide the formation of early metastatic niches. Proc. Natl. Acad. Sci. U.S.a. *111*, E3053–E3061.

Lal, S., La Du, J., Tanguay, R.L., and Greenwood, J.A. (2012). Calpain 2 is required for the invasion of glioblastoma cells in the zebrafish brain microenvironment. J. Neurosci. Res. *90*, 769–781.

Lamar, J.M., Stern, P., Liu, H., Schindler, J.W., Jiang, Z.-G., and Hynes, R.O. (2012). The Hippo pathway target, YAP, promotes metastasis through its TEAD-interaction domain. Proc. Natl. Acad. Sci. U.S.a. *109*, E2441–E2450.

Lawson, N.D., and Weinstein, B.M. (2002). In vivo imaging of embryonic vascular development using transgenic zebrafish. Developmental Biology *248*, 307–318.

Lin, H.-F., Traver, D., Zhu, H., Dooley, K., Paw, B.H., Zon, L.I., and Handin, R.I. (2005). Analysis of thrombocyte development in CD41-GFP transgenic zebrafish. Blood *106*, 3803–3810.

Liu, H., Ong, S.-E., Badu-Nkansah, K., Schindler, J., White, F.M., and Hynes, R.O. (2011). CUB-domain-containing protein 1 (CDCP1) activates Src to promote melanoma metastasis. Proc. Natl. Acad. Sci. U.S.a. *108*, 1379–1384.

Luzzi, K.J., MacDonald, I.C., Schmidt, E.E., Kerkvliet, N., Morris, V.L., Chambers, A.F., and Groom, A.C. (1998). Multistep Nature of Metastatic Inefficiency. The American Journal of Pathology *153*, 865–873.

Massagué, J., and Obenauf, A.C. (2016). Metastatic colonization by circulating tumour cells. Nature *529*, 298–306.

Mathias, J.R., Perrin, B.J., Liu, T.X., Kanki, J., Look, A.T., and Huttenlocher, A. (2006). Resolution of inflammation by retrograde chemotaxis of neutrophils in transgenic zebrafish. Journal of Leukocyte Biology *80*, 1281–1288.

Moore, J.C., Tang, Q., Yordán, N.T., Moore, F.E., Garcia, E.G., Lobbardi, R., Ramakrishnan, A., Marvin, D.L., Anselmo, A., Sadreyev, R.I., et al. (2016). Single-cell imaging of normal and malignant cell engraftment into optically clear prkdc-null SCID zebrafish. J. Exp. Med. *213*, 2575–2589.

Overholtzer, M., Zhang, J., Smolen, G.A., Muir, B., Li, W., Sgroi, D.C., Deng, C.-X., Brugge, J.S., and Haber, D.A. (2006). Transforming properties of YAP, a candidate oncogene on the chromosome 11q22 amplicon. Proc. Natl. Acad. Sci. U.S.a. *103*, 12405–12410.

Padera, T.P., Stoll, B.R., Tooredman, J.B., Capen, D., di Tomaso, E., and Jain, R.K. (2004). Pathology: cancer cells compress intratumour vessels. Nature *427*, 695–695.

Pugach, E.K., Li, P., White, R., and Zon, L. (2009). Retro-orbital injection in adult zebrafish. J Vis Exp.

Qian, B.-Z., Li, J., Zhang, H., Kitamura, T., Zhang, J., Campion, L.R., Kaiser, E.A., Snyder, L.A., and Pollard, J.W. (2011). CCL2 recruits inflammatory monocytes to facilitate breast-tumour metastasis. Nature *475*, 222–225.

Qian, B., Deng, Y., Im, J.H., Muschel, R.J., Zou, Y., Li, J., Lang, R.A., and Pollard, J.W. (2009). A Distinct Macrophage Population Mediates Metastatic Breast Cancer Cell Extravasation, Establishment and Growth. PLoS ONE *4*, e6562.

Qiao, Y., Chen, J., Lim, Y.B., Finch-Edmondson, M.L., Seshachalam, V.P., Qin, L., Jiang, T., Low, B.C., Singh, H., Lim, C.T., et al. (2017). YAP Regulates Actin Dynamics through ARHGAP29 and Promotes Metastasis. CellReports *19*, 1495–1502.

Renshaw, S.A., Loynes, C.A., Trushell, D.M.I., Elworthy, S., Ingham, P.W., and Whyte, M.K.B. (2006). A transgenic zebrafish model of neutrophilic inflammation. Blood *108*, 3976–3978.

Roh-Johnson, M., Shah, A.N., Stonick, J.A., Poudel, K.R., Kargl, J., Yang, G.H., di Martino, J., Hernandez, R.E., Gast, C.E., Zarour, L.R., et al. (2017). Macrophage-Dependent Cytoplasmic Transfer during Melanoma Invasion In Vivo. Developmental Cell *43*, 549–562.e6.

Sharif, G.M., Schmidt, M.O., Yi, C., Hu, Z., Haddad, B.R., Glasgow, E., Riegel, A.T., and Wellstein, A. (2015). Cell growth density modulates cancer cell vascular invasion via Hippo pathway activity and CXCR2 signaling. 1–11.

Shibue, T., Brooks, M.W., Inan, M.F., Reinhardt, F., and Weinberg, R.A. (2012). The outgrowth of micrometastases is enabled by the formation of filopodium-like protrusions. Cancer Discovery *2*, 706–721.

Siegel, R.L., Miller, K.D., and Jemal, A. (2017). Cancer Statistics, 2017. CA Cancer J Clin *67*, 7–30.

Stern, H.M., and Zon, L.I. (2003). Cancer genetics and drug discovery in the zebrafish. Nat Rev Cancer *3*, 533–539.

Stoletov, K., Kato, H., Zardouzian, E., Kelber, J., Yang, J., Shattil, S., and Klemke, R. (2010). Visualizing extravasation dynamics of metastatic tumor cells. Journal of Cell Science *123*, 2332–2341.

Stoletov, K., Strnadel, J., Zardouzian, E., Momiyama, M., Park, F.D., Kelber, J.A., Pizzo, D.P., Hoffman, R., VandenBerg, S.R., and Klemke, R.L. (2013). Role of connexins in metastatic breast cancer and melanoma brain colonization. Journal of Cell Science *126*, 904–913.

Tang, Q., Abdelfattah, N.S., Blackburn, J.S., Moore, J.C., Martinez, S.A., Moore, F.E., Lobbardi, R., Tenente, I.M., Ignatius, M.S., Berman, J.N., et al. (2014). Optimized cell transplantation using adult rag2 mutant zebrafish. Nat Meth *11*, 821–824.

Tang, Q., Moore, J.C., Ignatius, M.S., Tenente, I.E.S.M., Hayes, M.N., Garcia, E.G., n, N.T.Y.A., Bourque, C., He, S., Blackburn, J.S., et al. (2016). Imaging tumour cell heterogeneity following cell transplantation into optically clear immune- deficient zebrafish. Nature Communications *7*, 1–10.

Teng, Y., Xie, X., Walker, S., White, D.T., Mumm, J.S., and Cowell, J.K. (2013). Evaluating human cancer cell metastasis in zebrafish. BMC Cancer *13*, 1–1.

Tong, R.T., Boucher, Y., Kozin, S.V., Winkler, F., Hicklin, D.J., and Jain, R.K. (2004). Vascular normalization by vascular endothelial growth factor receptor 2 blockade induces a pressure gradient across the vasculature and improves drug penetration in tumors. Cancer Res. *64*, 3731–3736.

Vittori, M., Motaln, H., and Turnšek, T.L. (2015). The study of glioma by xenotransplantation in zebrafish early life stages. J. Histochem. Cytochem. *63*, 749–761.

Wang, J., Cao, Z., Zhang, X.-M., Nakamura, M., Sun, M., Hartman, J., Harris, R.A., Sun, Y., and Cao, Y. (2015). Novel mechanism of macrophage-mediated metastasis revealed in a zebrafish model of tumor development. Cancer Research *75*, 306–315.

Warren, J., Xiao, Y., and Lamar, J. (2018). YAP/TAZ Activation as a Target for Treating Metastatic Cancer. Cancers *10*, 115–137.

Welker, A.M., Jaros, B.D., Puduvalli, V.K., Imitola, J., Kaur, B., and Beattie, C.E. (2016). Standardized orthotopic xenografts in zebrafish reveal glioma cell-line-specific characteristics and tumor cell heterogeneity. Disease Models & Mechanisms *9*, 199–210.

White, R.M., Sessa, A., Burke, C., Bowman, T., LeBlanc, J., Ceol, C., Bourque, C., Dovey, M., Goessling, W., Burns, C.E., et al. (2008). Transparent Adult Zebrafish as a Tool for In Vivo Transplantation Analysis. Cell Stem Cell *2*, 183–189.

White, R., Rose, K., and Zon, L. (2013). Zebrafish cancer: the state of the art and the path forward. Nature Reviews Drug Discovery *13*, 624–636.

Xie, S., Luca, M., Huang, S., Gutman, M., Reich, R., Johnson, J.P., and Bar-Eli, M. (1997). Expression of MCAM/MUC18 by human melanoma cells leads to increased tumor growth and metastasis. Cancer Res. *57*, 2295–2303.

Yoo, S.K., and Huttenlocher, A. (2011). Spatiotemporal photolabeling of neutrophil trafficking during inflammation in live zebrafish. Journal of Leukocyte Biology *89*, 661–667.

Yu, F.-X., Zhao, B., and Guan, K.-L. (2015). Hippo Pathway in Organ Size Control, Tissue Homeostasis, and Cancer. Cell *163*, 811–828.

Zhang, B., Shimada, Y., Hirota, T., Ariyoshi, M., Kuroyanagi, J., Nishimura, Y., and Tanaka, T. (2016). Novel immunologic tolerance of human cancer cell xenotransplants in zebrafish. Transl Res *170*, 89–98.e3.

Zinn, K.R., Chaudhuri, T.R., Szafran, A.A., O'Quinn, D., Weaver, C., Dugger, K., Lamar, D., Kesterson, R.A., Wang, X., and Frank, S.J. (2008). Noninvasive bioluminescence imaging in small animals. Ilar J *49*, 103–115.

Appendix A

Imaging Tumor Cell Interactions with Innate Immune Cells in Zebrafish

The contents of this appendix were written by David Benjamin with editing by Jess Hebert and Richard Hynes. The experiments described in this chapter were performed by David Benjamin with the exception of the ones described in Figures 5 and 6, which were performed by Michelle Chen, and those described in figure 7, which were a collaboration between David Benjamin and Michelle Chen. Figures 5-7 in this appendix are adapted from the manuscript:

Michelle B. Chen, Cynthia Hajal, David C. Benjamin, Cathy Yu, Hesham Azizgolshani, Richard O. Hynes, Roger, D. Kamm. **Inflamed neutrophils sequestered at entrapped tumor cells via chemotactic confinement promotes tumor cell extravasation**. *PNAS* Submitted

Attempts to Image Tumor Cell Leukocyte Interactions in Adult Zebrafish

When the adult zebrafish work described in this thesis began, the original idea was to use adult zebrafish as a tool for imaging the interactions between tumor cells, platelets, neutrophils, and macrophages. As described in chapter 1, platelets, neutrophils, and macrophages have been shown to play important roles at the metastatic site. At the time, it was known that these cells were recruited to tumor cells at the metastatic site in a defined order. Platelets are the first cell to interact with tumor cells, being seen in association with tumor cells immediately upon tumor cell arrest (Im et al., 2004; Labelle et al., 2011; 2014). Neutrophils are the next cell type to arrive (Labelle et al., 2014). Neutrophils cooperate with platelets and endothelial cells to recruit monocytes/macrophages, which are the last of these cell types to arrive (Ferjancic et al., 2013; Gil-Bernabé et al., 2012; Laubli et al., 2009; Qian et al., 2011; 2009).

Most studies of these interactions had been done in fixed tissues that were harvested from mice sacrificed at sequential time points post-injection. While this approach yielded a wealth of information on the temporal order of interactions, they were unable to follow individual tumor cells over time. This led to a number of questions that remained unanswered. As platelets were the first cell type to be seen in conjunction with arrested tumor cells, an open question was when platelets and tumor cells first interacted. Did this happen when tumor cells intravasated, while tumor cells were traveling in circulation, or upon arrest? What fraction of arrested tumor cells are associated with platelets? How long do platelets remain in contact with tumor cells? Do neutrophils show a preference for cells in contact with platelets? Are platelets and neutrophils still around when monocytes/macrophages are recruited? Finally, what

happens to tumor cells that are not observed to have a specific interaction? Do they fail to metastasize?

The combination of the availability of lines with fluorescently-labeled thrombocytes (the fish equivalent of platelets), neutrophils, and macrophages, along with the ease of imaging, made zebrafish seem to be an ideal system in which to answer these questions. In the end, these studies encountered numerous technical challenges that led us to set aside imaging tumor cell-leukocyte interactions in the adult fish. It is my hope that a description of this adult fish work will aid future researchers who may wish to attempt these experiments in adult zebrafish. I will also describe some results that we did not have time to follow that might be of interest. Finally, we did study the interactions between tumor cells and neutrophils during the course of this thesis work, but in embryos rather than adults. This work was a collaboration with Michelle Chen from Roger Kamm's lab in the departments of Biological and Mechanical Engineering.

To study tumor cell-leukocyte interactions, lines of zebrafish were acquired that had fluorescently-labeled thrombocytes (CD41:EGFP, CD41:mCherry), neutrophils (mpx:EGFP), macrophages (MPEG1:EGFP,MPEG1:mCherry), total leukocytes (CD45:dsRed), and endothelial cells (Fli1:EGFP, Flk1:dsRed). These fish were crossed into the Casper background and to each other in order to allow intravital imaging of tumor cell interactions with multiple cell populations of interest.

It quickly became apparent that imaging leukocyte interactions in adult zebrafish would be more challenging than originally anticipated. First, the maximum depth of imaging achieved in the adult zebrafish was 200um using two-photon imaging (See Chapter 2). This depth

allowed the imaging of the skin and muscle directly underneath but not any internal organs. Second, the lineage-labeled fish that were acquired had been generated to study the behavior of leukocytes in embryos (Ellett et al., 2011; Lawson and Weinstein, 2002; Lin et al., 2005; Mathias et al., 2006; Renshaw et al., 2006). They had not been monitored for expression of the lineage markers in adults. It was discovered that, while the mpx:EGFP embryos have many fluorescent neutrophils as previously reported (Mathias et al., 2006; Renshaw et al., 2006; Yoo and Huttenlocher, 2011), adults only had fluorescent signal from the gut, an organ that was outside this 200um range (Fig 1A). We did not observe any circulating GFP+ cells (Fig 1A). This result meant that our original plan to image tumor cell-neutrophil interactions would not be feasible. The CD45:dsRed fish (which labels all leukocytes) also turned out to be less useful than originally thought. DsRed expression in the adults of this line was extremely low, making imaging almost impossible to see any leukocytes in these fish (data not shown). The MPEG1:EGFP, MPEG1:mCherry, CD41:EGFP, and CD41:EGFPmCherry fish did all have labeled cells in adults (Fig 1B and C).

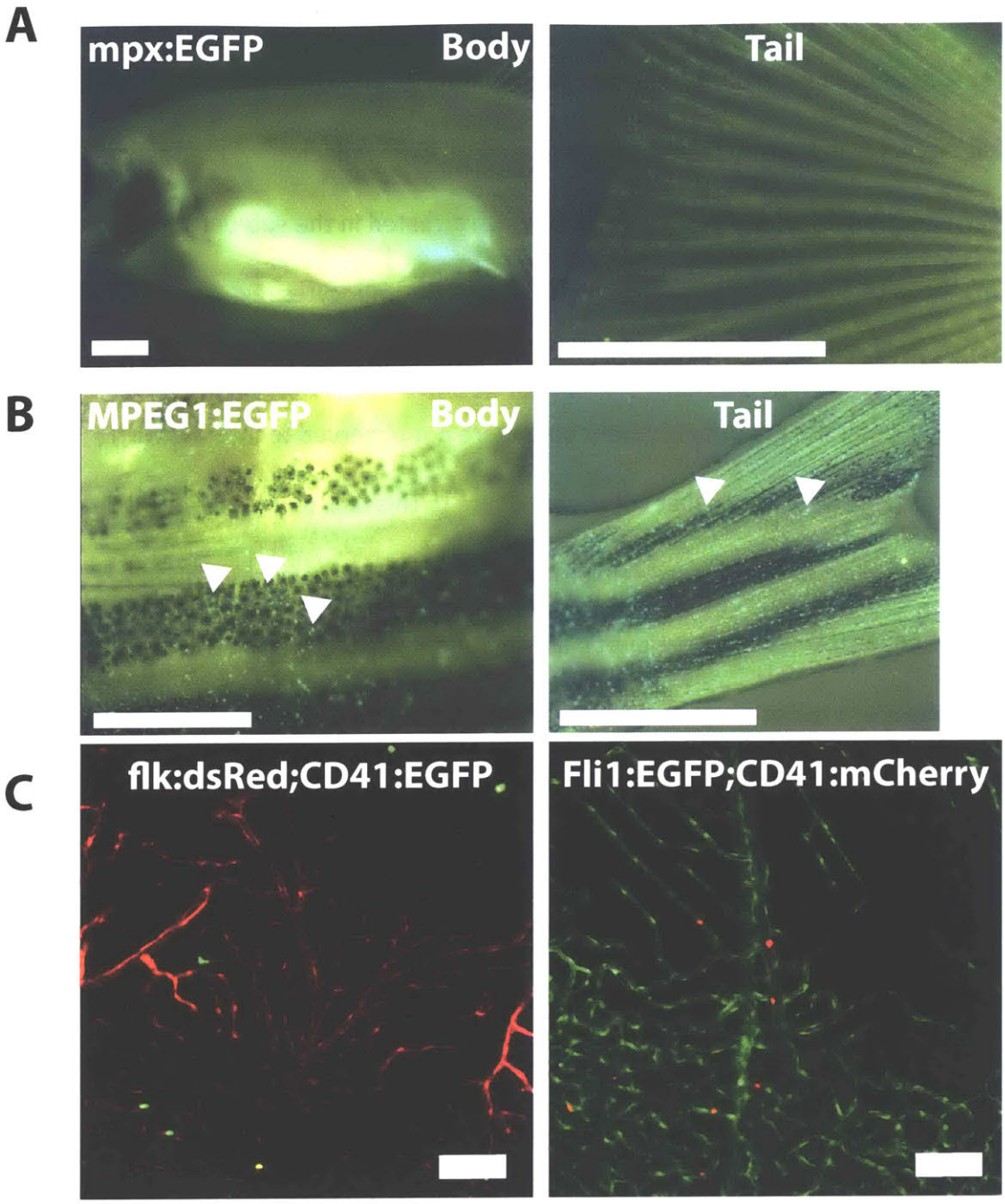

Figure 1. Example images of fluorescently-labeled cell lineages in adult Casper fish. (**A**) Images of mpx:EGFP;casper fish. Scale bar is 1mm. (**B**) Images of MPEG1:EGFP fish. Scale bars are 500μm (left) and 1mm (right). (**C**) (left) Confocal image of a flk:dsRed;CD41:EGFP;casper fish (right) Confocal image of a Fli1:GFP;CD41:mCherry zebrafish. Scale bar is 100μm.

We performed some initial experiments to try to image the interactions between the zebrafish ZMEL1 cell line and thrombocytes in the CD41:EGFP fish. Tumor cells were labeled with Cell Tracker Deep Red (a far red dye) and intravenously injected into flk:dsRed;CD41:EGFP;casper fish. Tumor cells which arrested in the sub-dermal musculature were imaged in real time to look for interactions with thrombocytes (Fig 2A). Interactions were defined as a cases where a thrombocyte was arrested within one cell radius of a tumor cell. Using these criteria, the majority of tumor cells were not observed to interact with thrombocytes (Fig 2B). A factor that could contribute to this lack of interactions is that, at the time of these experiments, we were using irradiation to immunosuppress fish for transplantation, as this was before genetically immunocompromised zebrafish were available. When the effect of irradiation on thrombocytes was determined by counting thrombocytes in confocal imaging movies, it was observed that fish had approximately half the number of thrombocytes as prior to irradiation (Fig 2C). We did not quantify the numbers of other immune cell types, but other studies of cell numbers following irradiation suggest that myeloid and lymphoid cells follow similar kinetics to those we observed for thrombocytes (Traver et al., 2004). The development of immunocompromised zebrafish since these experiments were performed would get around this problem (Moore et al., 2016; Tang et al., 2014).

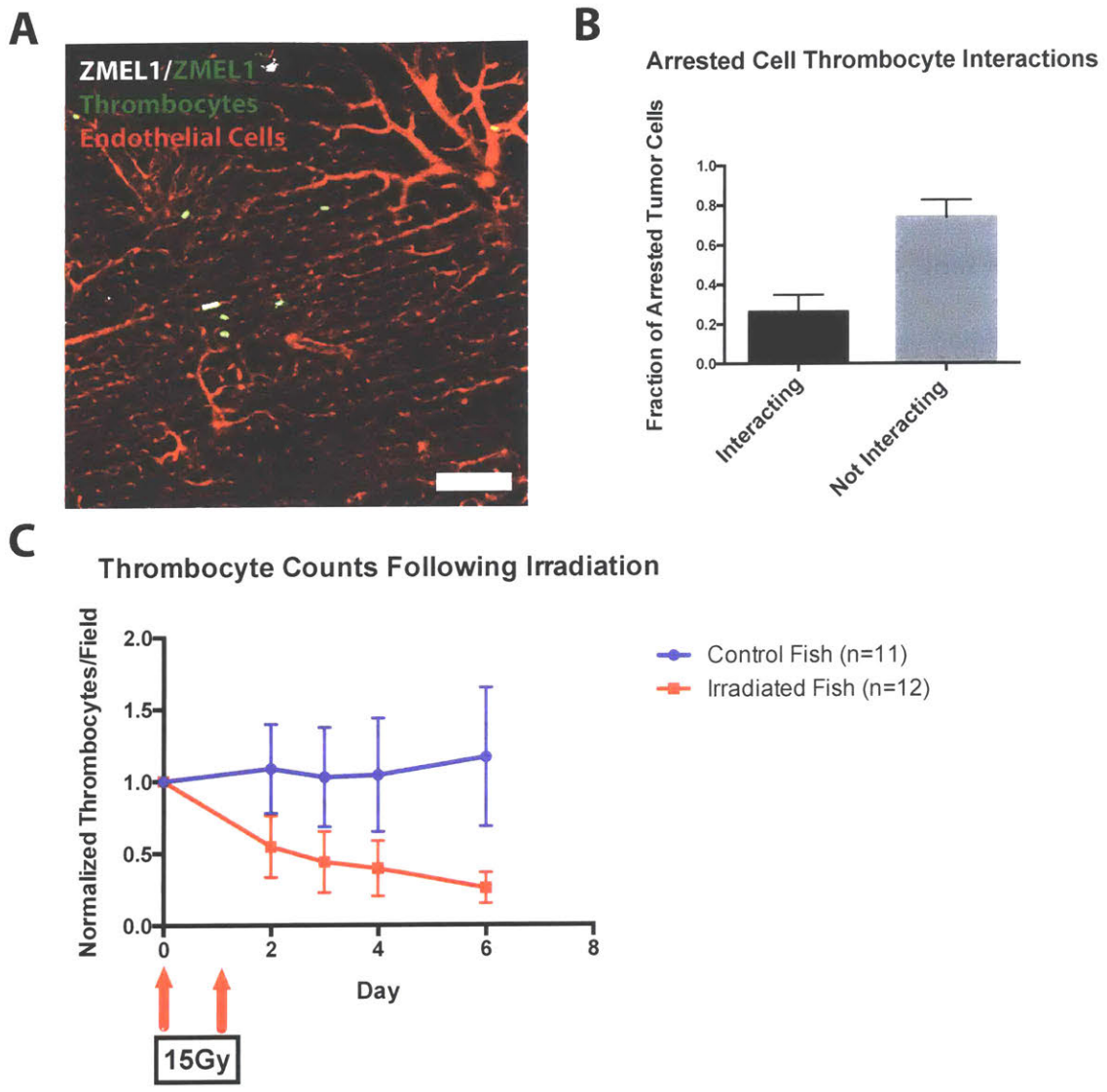

Figure 2. ZMEL1 cells do not interact with thrombocytes in circulation. (**A**) Still frame from a movie of cell tracker far-red-labeled ZMEL1 injected into a flk:dsRed;CD41:EGFP embryo which was used to quantify ZMEL1-thrombocyte interactions. Scale bar is 100μm. (**B**) Quantification of arrested tumor cell interactions with ZMEL1 cells (**C**) Thrombocyte counts over time following irradiation with 15Gy at day 0 and day 1. Thrombocyte counts were normalized to the number at day 0. n=11 fish per condition across two independent experiments. Gy, Gray.

Finally, as we could not get human cells to grow in adult zebrafish, we were limited to zebrafish cell lines (our attempts to grow human cells in adult zebrafish are described in detail in Chapter 2). We did most of our work with the ZMEL1 cell line, which was derived from a $P53^{-/-}$; MITFA:$BRAF^{V600E}$ melanoma model (Heilmann et al., 2015; Patton et al., 2005). This cell line already expresses GFP, which precluded it from being used to image tumor cell-leukocyte interactions over time. In order to do time-lapse imaging, fluorescently-labeled leukocytes and fluorescently-labeled vasculature are required. The fluorescently-labeled vasculature is required for use as a landmark to return to the same location over time (See chapter 2 for details on using the vasculature as landmarks). As all of the fluorescently-labeled zebrafish were either red or green, this did not provide us with enough colors to image all three cell types simultaneously.

We attempted to make cell lines from other tumor types as well as non-fluorescent zebrafish melanomas. However, we were not able to generate other cell lines. We also thought about using CRISPR technology to knock out GFP in the ZMEL1 cell line. However, we did not have much success getting retroviral or lentiviral expression systems to work in the ZMEL1 cell line, so we could not express CRISPR reagents in these cells. We also could not deliver another fluorescent label, such as a far-red fluorescent protein that would allow us to distinguish tumor cells from leukocytes *in vivo*.

During this time, we also attempted to make ZMEL1 cells over-expressing human genes known to promote metastasis in melanoma in mice including CDCP1, RhoC, and YAP using a lentiviral expression system (Clark et al., 2000; Lamar et al., 2012; Liu et al., 2011). The thought was that if these genes also promoted ZMEL1 metastasis in adult fish, intravital imaging in

adults could offer new insights into how these genes promoted metastasis. However, we only managed to make a ZMEL1 cell line cell line over-expressing human RhoC (Fig 3A). We tested whether the ZMEL1-RhoC line was more metastatic than an empty vector control line following intravenous injection. Two weeks after injection, fish were sacrificed and imaged. It was observed that RhoC did not promote metastasis in this system (Fig 3B and C). Even if RhoC had promoted metastasis, it would have been challenging to continue to work with the ZMEL1 line as further manipulations would have been necessary. It has recently been reported that another lentiviral transduction system has been used successfully to transduce the ZMEL1 cell line, suggesting that future studies may have more success in this endeavor (Fazio et al., 2017).

During this time, we also developed intradermal injections. These injections are orthotopic for the ZMEL1 melanoma cell line and allow spontaneous metastasis assays. Using a glass capillary needle, we were able to inject $2x10^3$ cells intradermally. These cells grew into tumors within the dermis over time (Fig 3D and E). However, given the difficulties outlined above in working with the ZMEL1 cell line, we switched to using zebrafish embryos.

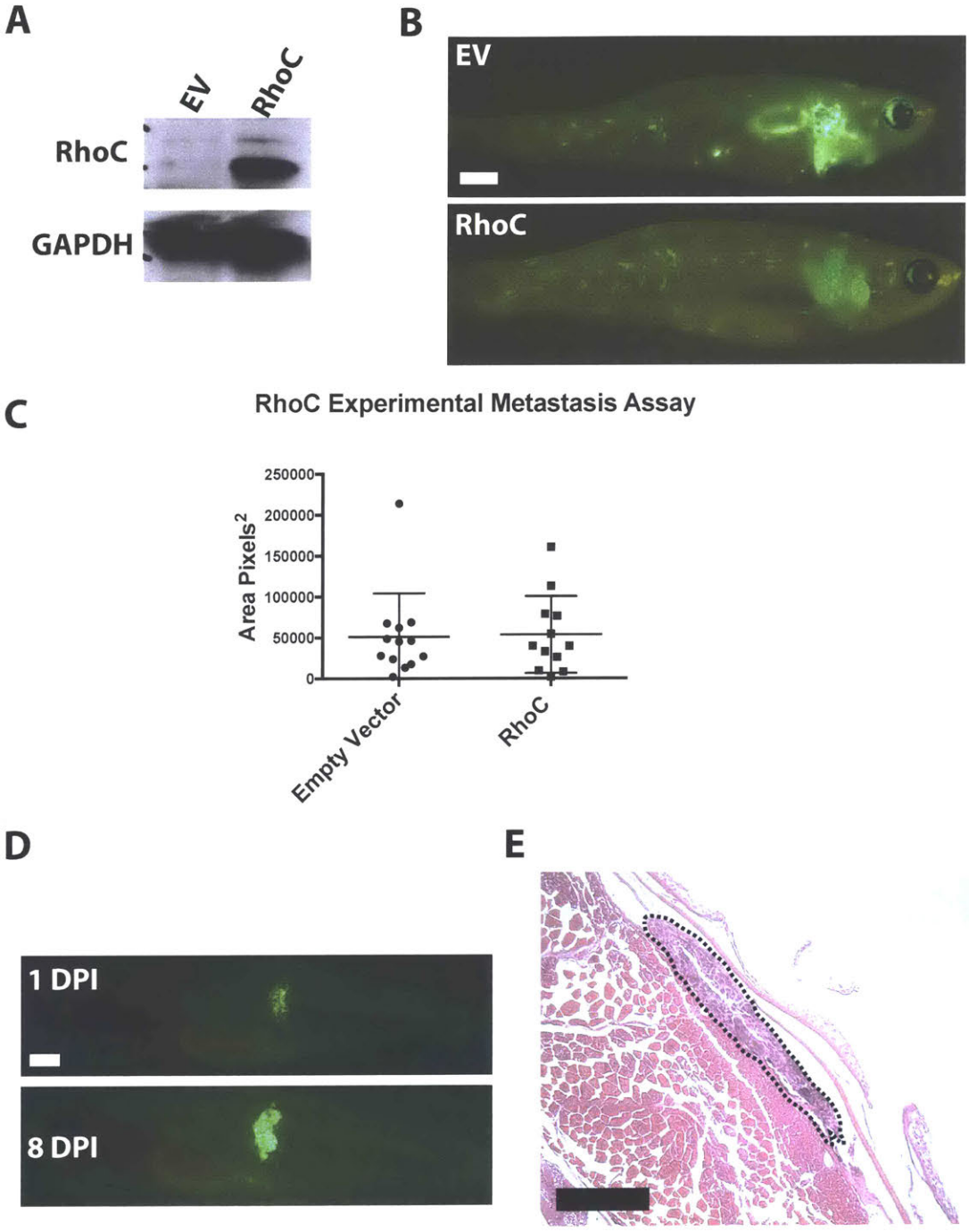

Figure 3. RhoC over-expression does not enhance ZMEL1 metastasis following intravenous injection. (**A**) Western blot of ZMEL1 cells showing over-expression of human RhoC. (**B**) Representative images of Casper zebrafish two weeks post-injection with control of RhoC over-expressing ZMEL1 cells. Scale bar is 1mm. (**C**) Quantification of metastasis 2 weeks post-intravenous injection of control of RhoC over-expressing ZMEL1 cells. n= 12 fish per condition. Statistics were calculated using a two-tailed student's t-test. (**D**) A Casper fish over 8 days following intradermal injection with ZMEL1 cells. (**E**) Histology showing tumor cells growing in the dermis of a fish following intradermal injection. Scale bar is 100μm.

Paired Cell Line Experiments in Zebrafish Embryos

Using zebrafish embryos allowed us to use human and mouse cell lines which are amenable to infection with standard lentiviral and retroviral vectors. There are also many sets of paired cell lines that differ in their metastatic potential, which were derived through *in vivo* selection for metastatic ability (Clark et al., 2000; Kang et al., 2003; Minn et al., 2005). A paper published a few years earlier suggested that the co-injection of cell lines with differing metastatic potential into zebrafish could be a fruitful avenue of research (Chapman et al., 2014). In this study, it was observed that, when poorly and highly invasive cells were co-injected into zebrafish embryos, the poorly metastatic cells were induced to invade along with the highly metastatic cells. Furthermore, the mode of invasion by the highly metastatic cells switched from one independent of MMP activity to one dependent on MMP activity. This study suggested that interactions between heterogeneous sub-populations can play an important role in metastasis. It is well known that tumors are highly heterogeneous and contain clones with unique sets of mutations and metastatic abilities (Marusyk et al., 2012). However, how the interactions of subpopulations of cells with different metastatic ability *in vivo* influences metastasis remains unclear.

To try and address this question, we co-injected cell lines *in vivo*-selected for metastatic ability into the perivitelline space of 2-day-old embryos. The embryos were then imaged 1 and 4 days post-injection to see if any behaviors emerged in heterogeneous tumors that were absent in homogeneous tumors. We observed that MA2 cells and their parental A375 line arranged themselves in a reproducible pattern in the resulting primary tumors. By 4 days post-injection (DPI), the MA2 cells were always found along the periphery while the A375 cells were

in the core of the tumor (Fig 4A). The cells were evenly mixed on day 1 post-injection, indicating that this arrangement was not just due to random chance but was an active process (Fig 4A). When the co-localization of the two signals was calculated, the decrease of Pearson's R value between 1 and 4DPI was highly significant, indicating that this was a reproducible phenomenon (Fig 4B). As a control, differentially labeled A375 cells were co-injected into the pericardial space. These two populations remained evenly mixed over 4 days (Fig 4C) indicating that the arrangement of the MA2 and A375 cells in mixed tumors was not an artifact of injection.

These initial observations were not followed up, so their significance remains unknown. A key experiment would be to perform orthotopic co-injection of A375 and MA2 cells in the skin of immunocompromised mice. The pericardial space of a zebrafish embryo is an artificial injection location so it is possible that this phenotype is an artifact of this experimental system. If these cells arrange themselves in a similar fashion in a more relevant system, it might suggest that this phenotype would be worthy of further study.

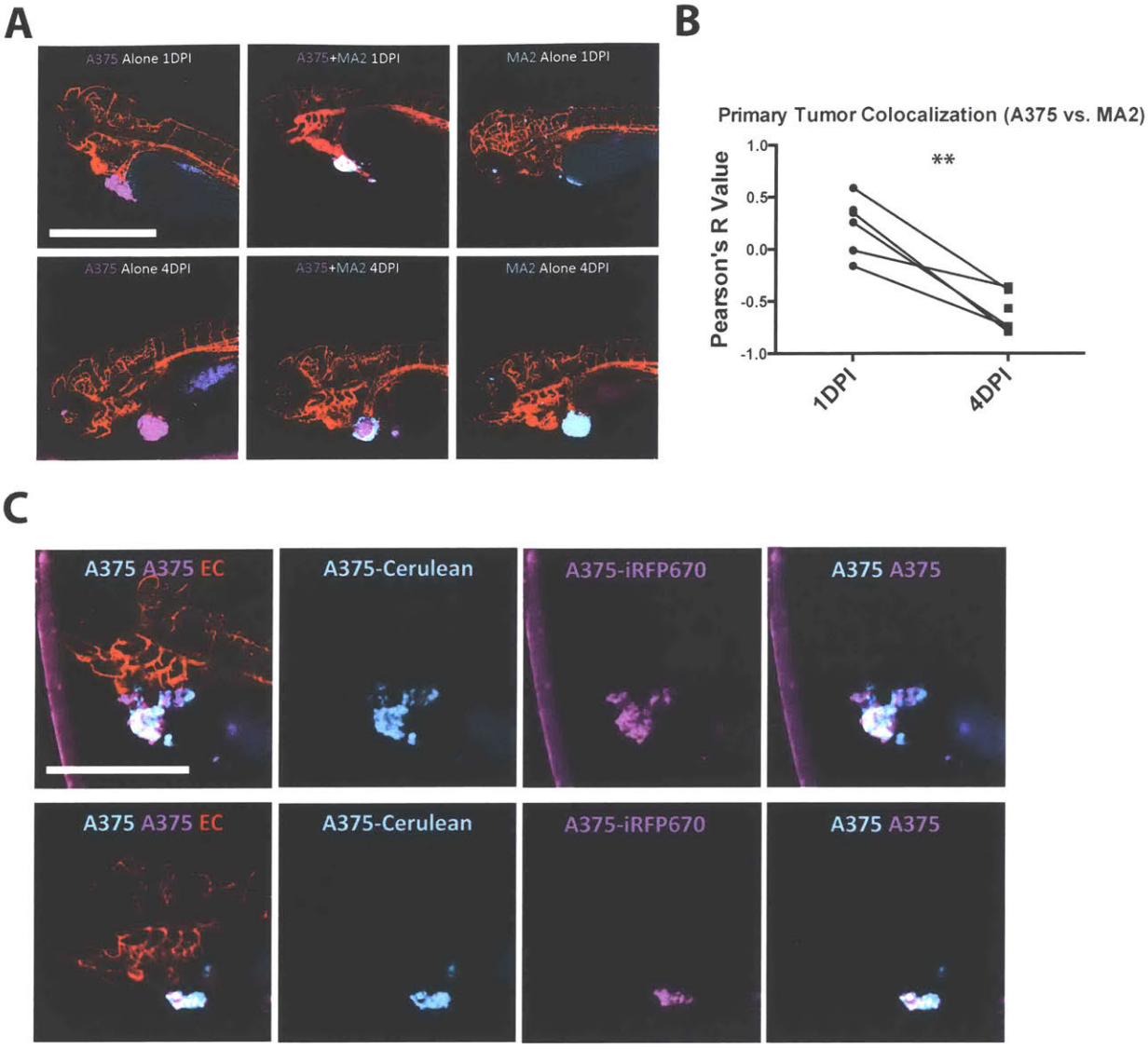

Figure 4. A375 and MA2 cells occupy discrete positions in heterogeneous tumors. (**A**) Images of flk:dsRed embryos injected with A375 alone, MA2 alone, or A375 + MA2 cells. Embryos were imaged 1 and 4 days post-injection (DPI). A375 cells express iRFP670 (magenta) while MA2 cells express cerulean (cyan). Endothelial cells express dsRed. Scale bar is 500μm. (**B**) The colocalization of heterogeneous tumors was calculated over time by calculating the Pearson's R value between the cyan and magenta channels. p=0.0054 using a two-tailed student's t-test. n=8 embryos. (**C**) Images of two flk:dsRed embryos injected with A375 cells labeled with either cerulean (cyan) or iRFP670 (magenta). Scale bar is 500μm.

Studies of Tumor Cell Neutrophil Interactions in Embryos

In the end, we did study the interactions of tumor cells with neutrophils, but in embryos rather than adults. These experiments were performed in collaboration with Michelle Chen, a graduate student in Roger Kamm's lab in the departments of Biological and Mechanical Engineering at MIT. The project we collaborated on was studying the interactions between tumor cells and neutrophils in circulation in the context of systemic inflammation.

Currently, most primary tumors are treated using surgical resection. However, a recurrent issue for patients following surgery is infection. In recent years, it has been observed that systemic infection promotes the development of distant metastases (Auguste et al., 2007; Lin et al., 2011; Noh et al., 2013). Given the key role that neutrophils (PMNs) play in responding to infection, there has been a great deal of interest in studying how neutrophils activated by systemic infection can promote metastasis.

The Kamm lab had previously generated a microfluidic device in which human umbilical vein endothelial cells (HUVECs) form microvascular networks in a fibrin gel (Chen et al., 2013) . Tumor cells can be perfused into this network to study arrest, extravasation, and the interactions between tumor cells (TCs) and leukocytes (Chen et al., 2016; Spiegel et al., 2016). Recently, a new version of this device was developed with 8 microvascular networks in parallel (Fig 5A). Continuous flow can be established using an integrated reservoir that applies a pressure difference across the network (Fig 5B). PMNs were stimulated with LPS for 30 minutes and co-injected into these networks. Following injection, PMNs were seen to cluster with arrested and extravasating tumor cells (Fig 5C). Stimulation with LPS markedly increased the aggregation index of the PMNs and tumor cells. Blocking adhesive molecules such as CD11b and

ICAM-1 lowered the aggregation index, indicating that these clusters formed through active adhesive interactions rather than through passive trapping. Furthermore, beads of the same size as TCs also had a low aggregation index (Fig 5D).

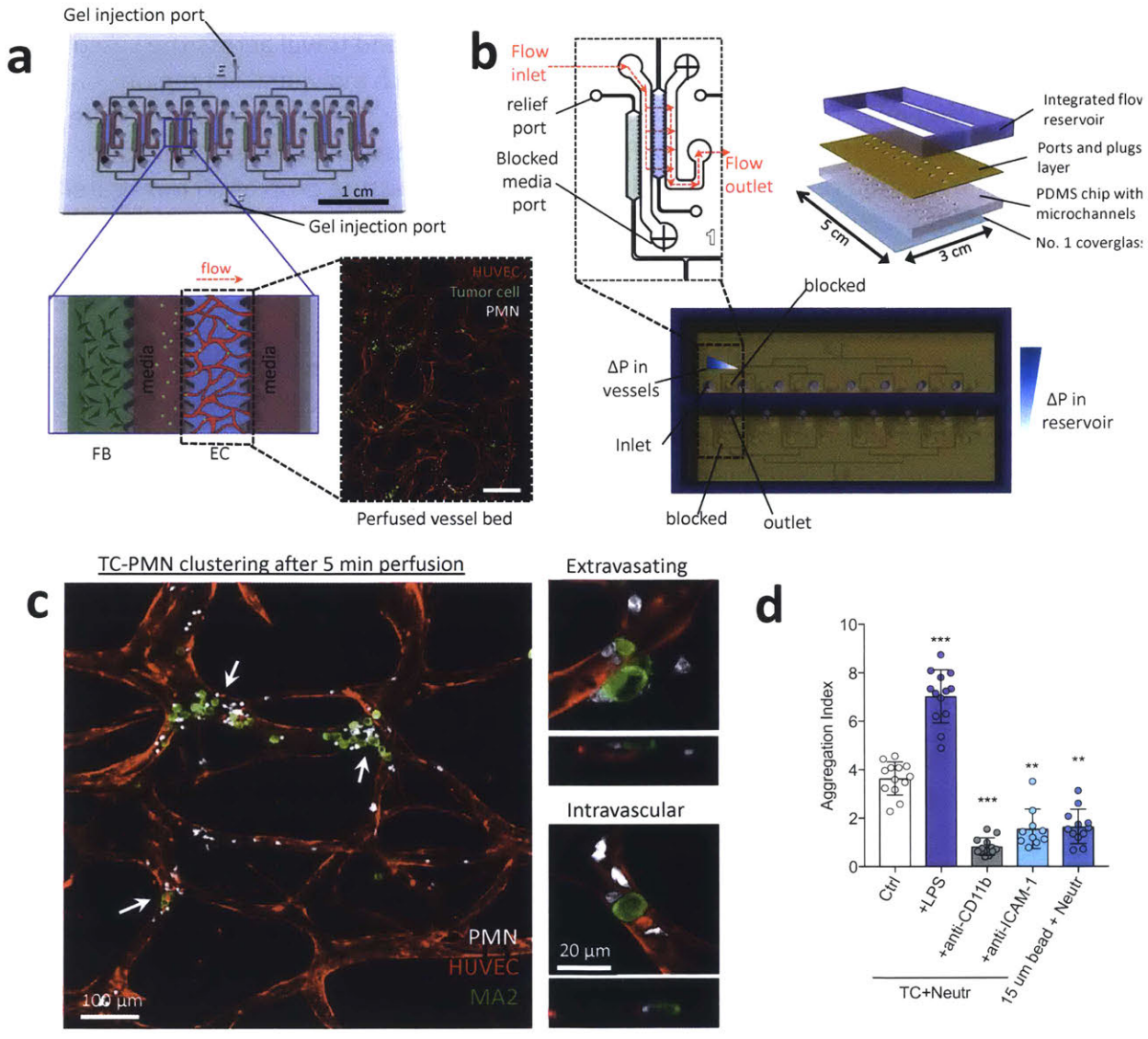

Figure 5. Multiplexed microfluidic chip allows higher throughput and robust formation of microvascular beds and quantification of TC-PMN intravascular aggregate formation and arrest. (A) Each chip houses 8 independent hydrogel regions for the formation of microvessel beds. 8 gel regions are connected by branching channels on each side to facilitate parallel injection of HUVEC or FB suspensions. Gels are prevented from bursting via the use of relief ports downstream of the hydrogel region. After 4 days of culture, perfusable vascular beds form in the HUVEC chambers with the help of paracrine signaling from supporting fibroblasts (green region). TCs/PMNs are introduced into the flow inlets and travel across the vascular bed by a short-term (~ 1 min) pressure drop application across each individual gel region. Fluorescence inset depicts a confocal projection of one perfused vascular network. Scale bar in fluorescent image is 200 microns. **(B)** To induce continuous media flow over ~6 hrs after cell perfusion, an integrated reservoir sustaining a hydrostatic pressure drop of ~5 mm water is secured on top of the PDMS chip. The medium in the reservoir is connected to the flow inlets and outlets on the PDMS chip via an acrylic layer that simultaneously allows access and blocks specific reservoirs at required positions. **(C)** Representative images of arrested TC-PMN clusters in microvessels. White arrows depict TC-PMN clusters (for definition of "clusters", see Methods). Higher magnification examples of extravasating and non-extravasated MA2 cells from within TC-PMN clusters. **(D)** Quantification of degree of tumor cell-PMN aggregate formation during intravascular arrest. Aggregation Index is defined as the fraction of TCs clustered with neutrophils multiplied by the average number of neutrophils per cluster (10-13 devices per condition). *$p<0.05$, **$p<0.01$, ***$p<0.001$, and error bars indicate SD.

A benefit of this *in vitro* system is that it allows multiplexed time-lapse imaging. It was observed that PMNs were highly migratory along the surface of the endothelium, and some actively extravasated in this system (Movie 1). Furthermore, the PMNs associated with clusters were observed to have markedly different behavior from free neutrophils (Movies 2 and 3). Cluster-associated PMNs were defined as being within 150μm of a tumor cell (Fig 6A). Cluster-associated PMNs were observed to migrate at a lower speed and have much lower displacements when compared with free PMNs (Fig 6B). When the migration tracks of free vs. cluster-associated PMNs were plotted, the cluster-associated PMNs exhibited a striking restriction to the region around tumor cell clusters (Fig 6C). Consistent with previous reports, co-injection of PMNs along with tumor cells enhanced tumor cell extravasation in the microfluidic device. Furthermore, LPS-stimulated PMNs were better at enhancing extravasation than unstimulated neutrophils (Fig 6D).

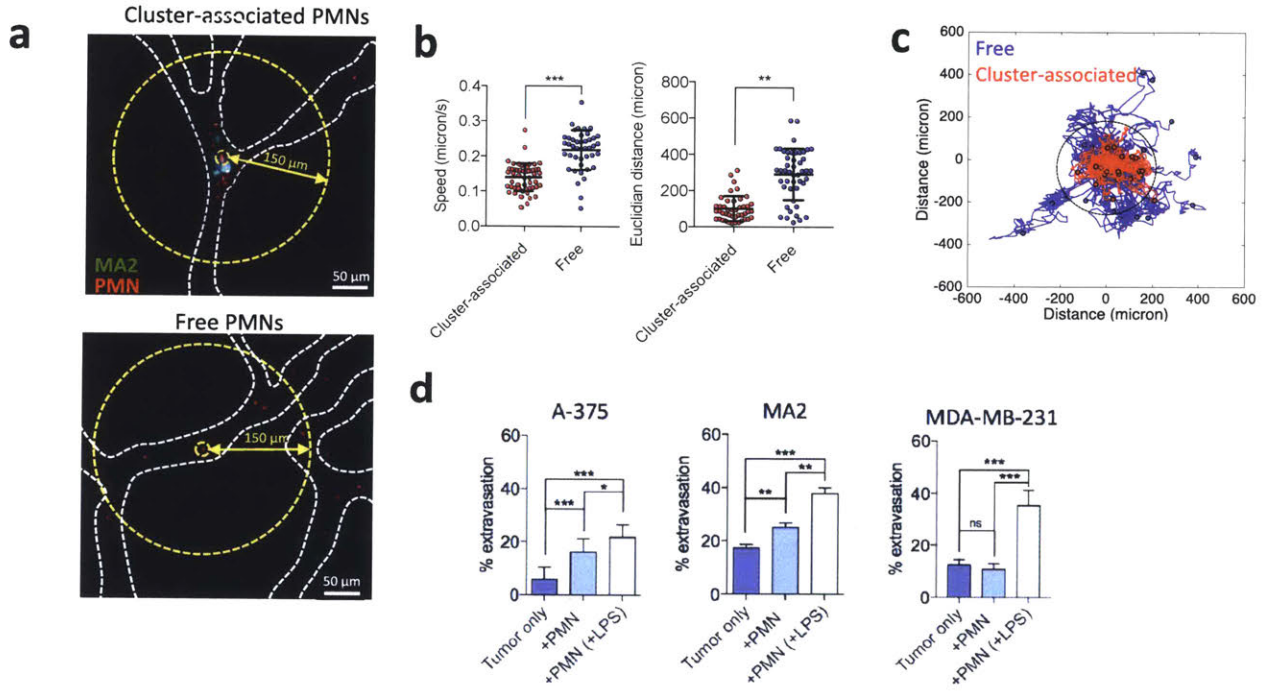

Figure 6. Cluster-associated PMNs exhibit migratory confinement behavior (A) Examples of cluster-associated PMNs and free PMNs arrested intraluminally (for criteria to define cluster-associated vs free, see Methods). To be considered either associated or free PMNs they must be > 150 µm from any other TC-PMN cluster. **(B)** Migration speed and end-to-end distance from original position of cluster-associated vs. free PMNs (43-53 PMNs per condition over 5 devices). **(C)** Representative migration tracks of free (blue) and cluster- associated (red) PMNs over 90 min (40 s time step). Dotted circle delineates the 150 m radius. **(D)** Percentage of extravasated cells at 6 hrs for A375, A-375-MA2 and MDA-MB-231 when co-perfused with quiescent PMNs or LPS activated PMNs at a 1:5 ratio.

These results were intriguing, but their relevance to the situation *in vivo* was unclear. It was decided that intravital imaging of tumor cells and neutrophils at the metastatic site over time was necessary to determine if the confinement of neutrophil migration near tumor cell clusters occurred *in vivo*. The ease of time-lapse imaging in zebrafish embryos combined with their ability to accept human xenotransplants made them an ideal system in which to perform these experiments. Further supporting the use of this system, a previous study that co-injected human macrophages and tumor cells into 2-day-old zebrafish embryos suggested that injected human myeloid cells could function in zebrafish embryos and interact with tumor cells to promote metastasis (Wang et al., 2015).

Human PMNs were stimulated with LPS and co-injected with either A375 or MA2 tumor cells into 2-day-old flk:dsRed zebrafish embryos. Following injection, clusters of tumor cells and PMNs were observed in the tail of the embryo (Fig 7A). Time-lapse imaging indicated that, in agreement with the *in vitro* device results, PMNs near clusters showed confined motility relative to free neutrophils (Fig 7B and Movies 4 and 5). Furthermore, co-injection of neutrophils also enhanced extravasation of tumor cells in the zebrafish embryo.

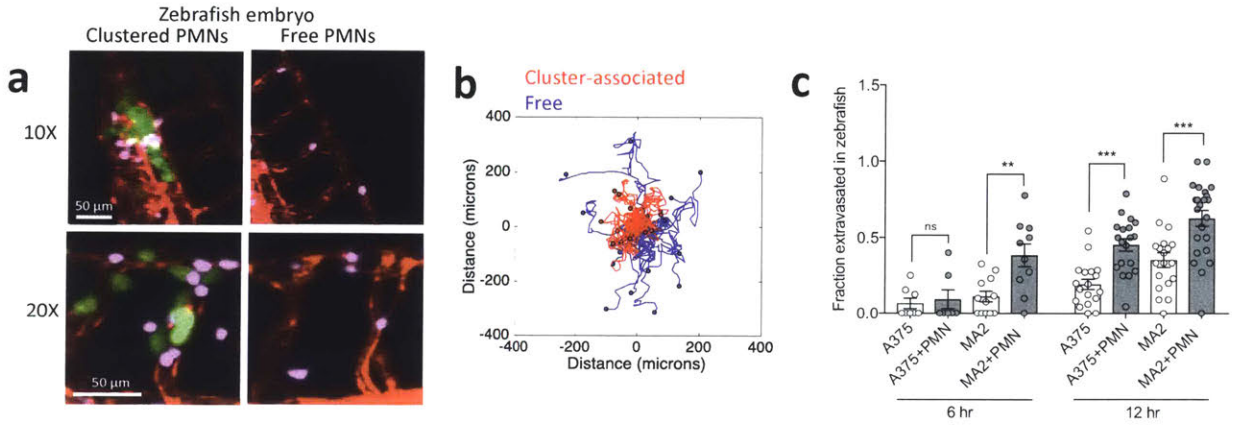

Figure 7. Inflamed PMNs are also sequestered at T-PMN clusters and enhance extravasation rates of A375 and MA2 *in vivo*. **(A)** Examples of intravascular cluster-associated and free PMNs (pink) when co-injected with MA2 cells (green) in flk:dsRed (red) zebrafish embryos (at different magnifications). **(B)** Migration tracks of cluster-associated or free PMNs in the ISV, DLAV, or DA vessels of zebrafish embryos. **(C)** Extravasation rates of A375 and MA2 cells with or without co-perfusion with inflamed PMNs at 6 and 24 hrs (n=7-12 embryos for A375 conditions, n=18-23 embryos for MA2 conditions. Error bars indicate SEM, *p<0.05, **p<0.01, ***p<0.001).

These results indicated that data from the *in vitro* microfluidic system were also true in an *in vivo* system. This work underscores a theme in this thesis that the events at the metastatic site are dynamic and can only be fully appreciated through time-lapse imaging. This study showed that neutrophils remain migratory when arrested with tumor cells in the vasculature. However, compared to free neutrophils, they move more slowly and remain in the vicinity of arrested tumor cells. These neutrophils near tumor cells then promote metastasis through enhancing tumor cell extravasation. Work described in Michelle's manuscript went on to identify some of the key factors involved in the confined motility by neutrophils. These factors could potentially be therapeutic targets that could be used to prevent metastasis in patients with post-surgical infection.

Movies

Movie 1. Confocal slice movie of stimulated neutrophils (white) migrating in a lumen within the on-chip microvascular bed (red). Images are taken every 12s.
URL: https://youtu.be/vs-o__jUtn4
Alternative URL: https://www.davidcbenjamin.com/movie-1

Movie 2. Inflamed PMNs at a TC-PMN cluster exhibiting dispersion migratory behavior (red = PMNs, cyan = MA2). Images taken every 35s.
URL: https://youtu.be/WjGZp2TDUmQ
Alternative URL: https://www.davidcbenjamin.com/movie-2

Movie 3. Inflamed PMNs at a TC-PMN cluster exhibiting confined migratory behavior (red = PMNs, green = MA2). Images taken every 35s.
URL: https://youtu.be/TR-favGRlPs
Alternative URL: https://www.davidcbenjamin.com/movie-3

Movie 4. Free neutrophils (magenta) migrating along the endothelium (red) in a 2-day-old flk:dsRed zebrafish embryo. Image taken every 30s.
URL: https://youtu.be/W6b_DNjT5DU
Alternative URL: https://www.davidcbenjamin.com/movie-4

Movie 5. Neutrophils (magenta) migrating in association with tumor cells (green) arrested in the tail vasculature (red) in a 2-day-old flk:dsRed zebrafish embryo. Image taken every 30s.
URL: https://youtu.be/cAgK8l3maA4
Alternative URL: https://www.davidcbenjamin.com/movie-5

References:

Auguste, P., Fallavollita, L., Wang, N., Burnier, J., Bikfalvi, A., and Brodt, P. (2007). The host inflammatory response promotes liver metastasis by increasing tumor cell arrest and extravasation. The American Journal of Pathology *170*, 1781–1792.

Chapman, A., del Ama, L.F., Ferguson, J., Kamarashev, J., Wellbrock, C., and Hurlstone, A. (2014). Heterogeneous Tumor Subpopulations Cooperate to Drive Invasion. CellReports *8*, 688–695.

Chen, M.B., Lamar, J.M., Li, R., Hynes, R.O., and Kamm, R.D. (2016). Elucidation of the Roles of Tumor Integrin β1 in the Extravasation Stage of the Metastasis Cascade. Cancer Research *76*, 2513–2524.

Chen, M.B., Whisler, J.A., Jeon, J.S., and Kamm, R.D. (2013). Mechanisms of tumor cell extravasation in an in vitro microvascular network platform. Integr Biol (Camb) *5*, 1262–1271.

Clark, E.A., Golub, T.R., Lander, E.S., and Hynes, R.O. (2000). Genomic analysis of metastasis reveals an essential role for RhoC. Nature *406*, 532–535.

Ellett, F., Pase, L., Hayman, J.W., Andrianopoulos, A., and Lieschke, G.J. (2011). mpeg1 promoter transgenes direct macrophage-lineage expression in zebrafish. Blood *117*, e49–e56.

Fazio, M., Avagyan, S., van Rooijen, E., Mannherz, W., Kaufman, C.K., Lobbardi, R., Langenau, D.M., and Zon, L.I. (2017). Efficient Transduction of Zebrafish Melanoma Cell Lines and Embryos Using Lentiviral Vectors. Zebrafish *14*, 379–382.

Ferjancic, S., Gil-Bernabe, A.M., Hill, S.A., Allen, P.D., Richardson, P., Sparey, T., Savory, E., McGuffog, J., and Muschel, R.J. (2013). VCAM-1 and VAP-1 recruit myeloid cells that promote pulmonary metastasis in mice. Blood.

Gil-Bernabé, A.M., Ferjancic, S., Tlalka, M., Zhao, L., Allen, P.D., Im, J.H., Watson, K., Hill, S.A., Amirkhosravi, A., Francis, J.L., et al. (2012). Recruitment of monocytes/macrophages by tissue factor-mediated coagulation is essential for metastatic cell survival and premetastatic niche establishment in mice. Blood *119*, 3164–3175.

Heilmann, S., Ratnakumar, K., Langdon, E.M., Kansler, E.R., Kim, I.S., Campbell, N.R., Perry, E.B., McMahon, A.J., Kaufman, C.K., van Rooijen, E., et al. (2015). A Quantitative System for Studying Metastasis Using Transparent Zebrafish. Cancer Res. *75*, 4272–4282.

Im, J.H., Fu, W., Wang, H., Bhatia, S.K., Hammer, D.A., Kowalska, M.A., and Muschel, R.J. (2004). Coagulation facilitates tumor cell spreading in the pulmonary vasculature during early metastatic colony formation. Cancer Res. *64*, 8613–8619.

Kang, Y., Siegel, P.M., Shu, W., Drobnjak, M., Kakonen, S.M., Cordon-Cardo, C., Guise, T.A., and Massagué, J. (2003). A multigenic program mediating breast cancer metastasis to bone. Ccell *3*, 537–549.

Labelle, M., Begum, S., and Hynes, R.O. (2011). Direct Signaling between Platelets and Cancer Cells Induces an Epithelial-Mesenchymal-Like Transition and Promotes Metastasis. Cancer Cell *20*, 576–590.

Labelle, M., Begum, S., and Hynes, R.O. (2014). Platelets guide the formation of early metastatic niches. Proc. Natl. Acad. Sci. U.S.a. *111*, E3053–E3061.

Lamar, J.M., Stern, P., Liu, H., Schindler, J.W., Jiang, Z.-G., and Hynes, R.O. (2012). The Hippo pathway target, YAP, promotes metastasis through its TEAD-interaction domain. Proc. Natl. Acad. Sci. U.S.a. *109*, E2441–E2450.

Laubli, H., Spanaus, K.S., and Borsig, L. (2009). Selectin-mediated activation of endothelial cells induces expression of CCL5 and promotes metastasis through recruitment of monocytes. Blood *114*, 4583–4591.

Lawson, N.D., and Weinstein, B.M. (2002). In Vivo Imaging of Embryonic Vascular Development Using Transgenic Zebrafish. Developmental Biology *248*, 307–318.

Lin, H.-F., Traver, D., Zhu, H., Dooley, K., Paw, B.H., Zon, L.I., and Handin, R.I. (2005). Analysis of thrombocyte development in CD41-GFP transgenic zebrafish. Blood *106*, 3803–3810.

Lin, J.-K., Yueh, T.-C., Chang, S.-C., Lin, C.-C., Lan, Y.-T., Wang, H.-S., Yang, S.-H., Jiang, J.-K., Chen, W.-S., and Lin, T.-C. (2011). The influence of fecal diversion and anastomotic leakage on survival after resection of rectal cancer. J. Gastrointest. Surg. *15*, 2251–2261.

Liu, H., Ong, S.-E., Badu-Nkansah, K., Schindler, J., White, F.M., and Hynes, R.O. (2011). CUB-domain-containing protein 1 (CDCP1) activates Src to promote melanoma metastasis. Proc. Natl. Acad. Sci. U.S.a. *108*, 1379–1384.

Marusyk, A., Almendro, V., and Polyak, K. (2012). Intra-tumour heterogeneity: a looking glass for cancer? Nat Rev Cancer *12*, 323–334.

Mathias, J.R., Perrin, B.J., Liu, T.X., Kanki, J., Look, A.T., and Huttenlocher, A. (2006). Resolution of inflammation by retrograde chemotaxis of neutrophils in transgenic zebrafish. Journal of Leukocyte Biology *80*, 1281–1288.

Minn, A.J., Gupta, G.P., Siegel, P.M., Bos, P.D., Shu, W., Giri, D.D., Viale, A., Olshen, A.B., Gerald, W.L., and Massagué, J. (2005). Genes that mediate breast cancer metastasis to lung. Nature *436*, 518–524.

Moore, J.C., Tang, Q., Yordán, N.T., Moore, F.E., Garcia, E.G., Lobbardi, R., Ramakrishnan, A., Marvin, D.L., Anselmo, A., Sadreyev, R.I., et al. (2016). Single-cell imaging of normal and

malignant cell engraftment into optically clear prkdc-null SCID zebrafish. J. Exp. Med. *213*, 2575–2589.

Noh, H., Eomm, M., and Han, A. (2013). Usefulness of pretreatment neutrophil to lymphocyte ratio in predicting disease-specific survival in breast cancer patients. J Breast Cancer *16*, 55–59.

Patton, E.E., Widlund, H.R., Kutok, J.L., Kopani, K.R., Amatruda, J.F., Murphey, R.D., Berghmans, S., Mayhall, E.A., Traver, D., Fletcher, C.D.M., et al. (2005). BRAF Mutations Are Sufficient to Promote Nevi Formation and Cooperate with p53 in the Genesis of Melanoma. Current Biology *15*, 249–254.

Qian, B.-Z., Li, J., Zhang, H., Kitamura, T., Zhang, J., Campion, L.R., Kaiser, E.A., Snyder, L.A., and Pollard, J.W. (2011). CCL2 recruits inflammatory monocytes to facilitate breast-tumour metastasis. Nature *475*, 222–225.

Qian, B., Deng, Y., Im, J.H., Muschel, R.J., Zou, Y., Li, J., Lang, R.A., and Pollard, J.W. (2009). A Distinct Macrophage Population Mediates Metastatic Breast Cancer Cell Extravasation, Establishment and Growth. PLoS ONE *4*, e6562.

Renshaw, S.A., Loynes, C.A., Trushell, D.M.I., Elworthy, S., Ingham, P.W., and Whyte, M.K.B. (2006). A transgenic zebrafish model of neutrophilic inflammation. Blood *108*, 3976–3978.

Spiegel, A., Brooks, M.W., Houshyar, S., Reinhardt, F., Ardolino, M., Fessler, E., Chen, M.B., Krall, J.A., DeCock, J., Zervantonakis, I.K., et al. (2016). Neutrophils Suppress Intraluminal NK Cell-Mediated Tumor Cell Clearance and Enhance Extravasation of Disseminated Carcinoma Cells. Cancer Discovery *6*, 630–649.

Tang, Q., Abdelfattah, N.S., Blackburn, J.S., Moore, J.C., Martinez, S.A., Moore, F.E., Lobbardi, R., Tenente, I.M., Ignatius, M.S., Berman, J.N., et al. (2014). Optimized cell transplantation using adult rag2 mutant zebrafish. Nat Meth *11*, 821–824.

Traver, D., Winzeler, A., Stern, H.M., Mayhall, E.A., Langenau, D.M., Kutok, J.L., Look, A.T., and Zon, L.I. (2004). Effects of lethal irradiation in zebrafish and rescue by hematopoietic cell transplantation. Blood *104*, 1298–1305.

Wang, J., Cao, Z., Zhang, X.-M., Nakamura, M., Sun, M., Hartman, J., Harris, R.A., Sun, Y., and Cao, Y. (2015). Novel mechanism of macrophage-mediated metastasis revealed in a zebrafish model of tumor development. Cancer Research *75*, 306–315.

Yoo, S.K., and Huttenlocher, A. (2011). Spatiotemporal photolabeling of neutrophil trafficking during inflammation in live zebrafish. Journal of Leukocyte Biology *89*, 661–667.

Appendix B.

Materials and Methods

The contents of this chapter were written by David Benjamin. The methods corresponding to chapter 2 is a reproduction work originally published in BMC Cancer with minor alterations. The original paper can be located using the following reference:

David C. Benjamin and Richard O. Hynes. (2017). **Intravital imaging of metastasis in adult Zebrafish**. BMC Cancer *17*, 660-672

Some of the methods corresponding to Appendix A were written by David Benjamin and Michelle Chen and are modified from the following manuscript

Michelle B. Chen, Cynthia Hajal, David C. Benjamin, Cathy Yu, Hesham Azizgolshani, Richard O. Hynes, Roger, D. Kamm. **Inflamed neutrophils sequestered at entrapped tumor cells via chemotactic confinement promotes tumor cell extravasation**. *PNAS* Submitted

Chapter 2 Methods:
Zebrafish Husbandry

Zebrafish were housed in a room maintained at 28°C with a 14-hour light, 10-hour dark cycle. Fish not in experiments were housed in a re-circulating water system and fed brine shrimp three times a day. During experiments, fish injected with zebrafish tumor cells were housed individually in plastic cups containing approximately 400mL of aquarium makeup water (AMW) and were fed brine shrimp once per day. Zebrafish injected with human tumor cells were maintained in glass bottles in 100mL of AMW in a 34°C water bath and fed brine shrimp once per day. Prior to experimentation, zebrafish were acclimated to the increased temperature by raising the water temperature by 1°C per day.

The *casper* (*roy*$^{-/-}$;*nacre*$^{-/-}$) line was a kind gift from Dr. Leonard Zon (Boston Children's Hospital). The *flk:dsRed2* line was originally developed in the laboratory of Dr. Kenneth Poss (Duke) and was a kind gift from Dr. Mehmet Yanik (MIT). It was crossed into the *casper* background. The *fli1:egfp* line was acquired from ZIRC (Eugene Oregon) and was crossed into the *casper* background. The *rag2*$^{450fs/+}$ and *prkdc*$^{D3612fs/+}$;*casper* lines were kind gifts from Dr. David Langenau (MGH). The *rag2*^{450fs} line was crossed into the *casper* background. The *rag2*$^{450fs/+}$;*casper* and *prkdc*$^{D3612fs/+}$;*casper* lines were maintained as heterozygotes. Heterozygotes were crossed, and homozygotes, which were used in experiments, were identified using previously described genotyping protocols (Moore et al., 2016; Tang et al., 2014)1. Young adult zebrafish used for experiments were between 6 and 10 weeks old and were housed at a density of 15 fish per 3L tank. Fish that were noticeably smaller than the majority of the fish in a tank were not injected. Prior to injection with ZMEL1 zebrafish melanoma cells (Heilmann et al., 2015), immunocompetent Casper fish were irradiated with

two doses of 15 Gray (Gy), one and two days prior to injection, using a GC 40E gamma irradiator (Theratronics).

Prior to injection with human tumor cells, zebrafish were either irradiated with 15Gy or 20Gy at one and two days before injection, or treated with 15μg/mL dexamethasone starting 2 days before injection. Embryos were maintained at 34C for the course of experiments involving human cells. Embryos were dechorionated by adding 12uL of 30mg/mL pronase (Sigma) to a 10cm dish containing 80 embryos 16 hours prior to injections.

Histology

Zebrafish were euthanized by soaking in 0.1% tricaine on ice for 20 minutes. Fish were then fixed for 24 hours in Bouin's fixative (Sigma). Following fixation, fish were soaked in water for 3 hours and decalcified by soaking in Richard Allan decalcifying solution (ThermoFisher) for 16 hours. Fish were then rinsed with water, dehydrated in ethanol, embedded in paraffin, and cut into 5μm thick sections. Sections were stained with hematoxylin and eosin (H&E) using a ThermoShandon Varistain Gemini (ThermoFisher) staining machine according to manufacturer's instructions.

Cell Culture

The ZMEL1 zebrafish melanoma cell line(Heilmann et al., 2015) was maintained in DMEM high-glucose medium (ThermoFisher) supplemented with 10% fetal bovine serum (FBS, Sigma), L-glutamine (2mM, ThermoFisher), and primocin (0.1mg/mL, Invivogen) as were the human breast cancer line, LM2 (A kind gift from Dr. Joan Massagué (Memorial Sloan Kettering Cancer Center)), and the human melanoma cell line, MA2 (previously described (Xu et al., 2008) ATCC CRL-3223) . MDA-MB-435 human melanoma cells (ATCC HTB-129) were cultured in L15

medium (Thermofisher) supplemented with 10% FBS, L-glutamine (2mM, ThermoFisher), primocin (0.1mg/mL, Invivogen), bovine insulin (0.01mg/mL, Sigma), and glutathione (0.01mg/mL, Sigma). ZMEL1 cells were grown at 32C with 5% CO_2. LM2 and MA2 cells were grown at 37C with 5% supplemental CO_2. MDA-MB-435 cells were grown at 37C without supplemental CO_2.

Intravenous, Retro-Orbital, and Embryo Injections

Cells for injection were harvested from a confluent 10cm plate by trypsinization for 5 minutes with 2mL of 0.25% trypsin in versene. Trypsin was quenched using 4mL of serum-containing medium. Cells were washed twice with sterile phosphate-buffered saline (PBS) and were re-suspended at $5x10^5$ cells/uL in sterile PBS (intravenous), $1x10^4$ cells/uL in sterile PBS (retro-orbital), or $4x10^6$ cells in 100uL sterile PBS (embryos).

For retro-orbital injections, a removable needle syringe (Hamilton) with a 26-gauge 15mm length needle with point style 4 and a 30-degree angle (Hamilton) was used. 1µL of cell suspension was injected retro-orbitally into each fish as previously described (Pugach et al., 2009). The needle was rinsed with 70% ethanol and PBS between each injection.

For intravenous and embryo injections, glass capillary tubes (Borosilicate, 1mm outer diameter, 0.58mm inner diameter, Warner Instruments) were siliconized using Sigmacote reagent (Sigma). Briefly, both ends of the tubes were dipped in Sigmacote until the reagent filled the entire tube. Sigmacote was removed from tubes by dipping tubes onto a Kimwipe (Kimtech) and allowing reagent to flow out. Tubes were then submerged in distilled, deionized

water to remove HCl by-products. The water was removed and the capillaries were allowed to dry for 24 hours.

Siliconized glass capillary needles were pulled on a P-87 micropipette puller (Sutter Instrument) set to heat=800, pull=150, vel =150, time=200 and pressure=600. Pulled needles were then used on a picospritzer II (General Valve) microinjector set to dispense 30ms pulses at 25PSI. The dispensed volume was measured using an ocular micrometer (Nikon) by dispensing 0.5% phenol red solution into mineral oil. The needle tip was progressively broken until it dispensed 20nL drops for intravenous injections or 2nL for embryo injections. Once filled, the needle was used to inject into the common cardinal vein of 8 adult fish before being refilled. The needle was only changed if it broke during the course of injections. Multiple fish were anesthetized and injected in rapid succession to minimize the time for cells in suspension to settle in the needle.

Prior to intravenous injections, young adult zebrafish were anesthetized in 0.017% tricaine (Sigma) in AMW buffered to pH 7.4 with sodium bicarbonate. Fish were allowed to remain in anesthetic-containing water until unresponsive to touch. Once anesthetized, fish were transferred to a dry 10cm dish cover for injection. Following injection, fish were transferred to AMW without anesthetic to recover.

Embryos were anesthetized in 0.017% tricaine in AMW buffered to pH 7.4. Once all swimming ceased, 30 embryos were placed into a 10cm dish half-filled with 2% agarose and the water was removed. 4nL of cells in PBS were injected into the Duct of Cuvier where it enters the heart as previously described (Stoletov et al., 2010). Embryos were then washed off with fresh AMW, and housed in 24 well plates (one fish per well) for the duration of the experiment.

Confocal Intravital Imaging

Anesthesia was induced by placing a single fish in 50ppm eugenol (Pulpdent Corp) in AMW. Once opercular movements slowed, the fish was placed in one well of a 6-well glass bottom dish (Mattek, uncoated 1.5 glass thickness) such that the posterior was in the center of the glass and the head rested on the plastic surrounding it. The posterior of the fish was then immobilized by adding 2% low-melt agarose dropwise. A small amount of 15ppm eugenol in AMW was added dropwise to the gills to allow respiration while the agarose solidified. Once the agarose solidified, the well was filled with 15ppm eugenol in AMW. Fish were monitored every minute for opercular movements. If they ceased, fresh AMW without eugenol was added until they resumed. If the fish began to wake up, 50ppm eugenol in AMW was added for 2 minutes to re-induce anesthesia and was then replaced with 15ppm eugenol for maintenance of anesthesia. Fish were imaged on a Nikon-A1R inverted confocal microscope. Images for quantification were acquired using the resonant scanner. Representative images were acquired with the galvanometer scanner. Overview fields to identify vascular landmarks and quantify cell numbers were taken using a 10x objective to image a Z-stack containing 17 steps with a 6.8µm step size. Extravasation and cell morphology was observed using a water immersion 40X long-working-distance objective to obtain a Z-stack of 49 steps with a 0.3µm step size.

Representative images were processed in ImageJ (NIH) following acquisition. Briefly, images were first de-speckled and contrast-adjusted. Images were then stacked using the Z-projection function with the maximum-intensity algorithm. Contrast was further adjusted using the shadows and highlights function in Photoshop (Adobe).

Imaging on a Dissecting Microscope

Prior to imaging, zebrafish were anesthetized in 0.017% tricaine in AMW buffered to pH7.4 with sodium bicarbonate. Zebrafish were then placed on a dry 10cm dish top cover. The area around the fish was dried, leaving a small meniscus of water covering the fish to allow for respiration. Fish were briefly imaged using a Leica M165 FC dissecting microscope.

Embryo Imaging

Each well of a 96 well glass-bottom plate (MatTek) was filled with 60uL of 2% agarose. A 3D-printed pin tool was placed into the wells to generate molds for holding the embryos in a lateral position as previously described (Wittbrodt et al., 2014). Embryos were anesthetized during imaging in 0.017% tricaine in AMW buffered to pH 7.4. Embryos were imaged on a Nikon A1R inverted confocal microscope. Embryos were imaged with a 10X objective to collect Z-stacks with 14 steps and a 7.4um step size.

Chapter 3 Methods:

Tumor Cell Burden Calculations:

Tumor cell burden was defined as the percent area of an organ (brain or tail) occupied by tumor cell nuclei (from the H2B-EGFP signal). To calculate tumor cell burden, images were first blinded and Z-projections were generated using the maximum intensity algorithm in ImageJ. The organ of interest was then manually outlined using the vasculature as a guide and its area calculated using ImageJ. The image was manually thresholded on the green channel to minimize quantification of autofluorescence. The area of green signal within the organ was then calculated with the ImageJ analyze particles function with size set to 0-infinity and circularity set to 0.00-1.00.

Raw tumor cell burden in figure 3 was calculated as the total area of tumor cell nuclei in μm^2 in a given organ. The normalized tumor cell burden in figure 3 was the raw tumor cell burden at each time point normalized to the raw tumor cell burden at the 10HPI time point for each embryo. The unconverted tumor cell burden in figure 5 was calculated by taking the raw tumor cell burden based on the far red channel (iRFP670 signal). The converted tumor cell burden in figure 5 was calculated by taking the raw tumor cell burden based on the red channel (converted Dendra2 signal).

Statistical Analysis:

Statistical analysis was performed using Graphpad Prism (Graphpad Software).

Zebrafish Husbandry:

Zebrafish were housed in a re-circulating water system in a room maintained at 28C. The fish were kept on a 14-hour light – 10-hour dark cycle. The *casper* (*roy*$^{-/-}$;*nacre*$^{-/-}$) line was a kind gift from Dr. Leonard Zon (Boston Children's Hospital). The *flk:dsRed2* line was originally developed in the laboratory of Dr. Kenneth Poss (Duke) and was a kind gift from Dr. Mehmet Yanik (MIT). The *fli1:EGFP* line was obtained from the Zebrafish International Resource Center (Eugene Oregon). The *flk:dsRed2* and *fli1:EGFP* lines were crossed into the casper background. Following injection with tumor cells, embryos were maintained at 34C for the course of experiments. Following injection, embryos were housed in 6 well plates with 30 embryos per well for experiments with a single time point. For time course experiments, single embryos were housed in wells in 48 well plates between imaging. Plates were kept in a water bath to maintain them at 34C.

Cell Culture:

The A375, HT-29, and 293-FS cell lines were cultured in DMEM high glucose medium supplemented with 10% fetal bovine serum (FBS, Sigma), L-glutamine (2mM, ThermoFisher), and primocin (0.1mg/mL, Invivogen). HUVECS were grown in EGM medium (Lonza) supplemented with the EGM-2 BulletKit (Lonza). All cell lines were sorted for fluorescent protein expression on an FACSAria cell sorter (BD) to ensure that the entire population was fluorescent.

Vectors and Lentiviral Transduction:

The YAP wildtype, YAP-AA, and YAP-AA with various mutations were a kind gift from Dr. John Lamar. They were all cloned into the pHAGE lentiviral expression system. The pHAGE backbone was a kind gift from Dr. Tyler Jacks. iRFP670, and Cerulean were acquired from addgene. Dendra2 was a kind gift from Dr. Frank Gertler. All fluorescent proteins were cloned into pHAGE.

1 day prior to transfection, 293FS cells were split 1:6 into 1 well of a 6 well plate. The following day 9.6uL of XtremeGene 9 DNA transfection reagent (Sigma) was added to 100uL of OptiMEM serum-free media (Gibco), vortexed and let incubate for 5 mins at room temperature. 400ng of psPAX2 vector, 400ng of VSVG vector, and 400ng of the pHAGE construct were then added to the tube. The tube was vortexed and let sit for 20 minutes at room temperature before being added to the 293FS cells. The media was supplemented with 10mM sodium butyrate to enhance viral titers. The following day, the media was replaced with fresh media. 48 hours post-transfection, the media was filtered through a 0.45μm syringe filter (Pall Corporation) and added to the cells to be infected. Polybrene (EMD Millipore) was added to the viral supernatant a concentration of 8μg/mL to enhance infection efficiency. The following day the viral media was removed and cells were selected with 2.5μg/mL puromycin (Gibco), 600μg/mL hygromycin B (Invitrogen), or 5μg/mL blasticidin (Invivogen).

Embryo Injections and Imaging:

Embryo injections were performed as previously described (Benjamin and Hynes, 2017). Embryos were imaged on an A1R inverted confocal microscope (Nikon) using the resonant

scanner. For time point imaging, Z stacks were acquired with a 7.4μm step size using a 10X objective. For time-lapse imaging, Z stacks were acquired with 7.4μm step size using a 10X objective with an additional 1.5X zoom lens for a total magnification of 15X. Whole embryos were imaged using a 4X objective to acquire Z stacks with a 15μm step size. For time-lapse imaging, Z stacks were acquired every 2-3 minutes for 12 hours following injection.

Embryos were mounted for imaging at single time points using a 3D printed pin tool as previously described (Benjamin and Hynes, 2017; Wittbrodt et al., 2014). For time lapse imaging, 24 well glass bottom plates (Mattek) were coated with 2% agarose. Once the agarose solidified, a square indentation was carved into the agarose using a flat head screw driver. Individual embryos were added to each indentation, and oriented to lay on their side. Most of the water was then removed and molten 0.8% agarose containing 0.02% Tricaine and buffered to pH7.0 with sodium bicarbonate was gently added to each well to immobilize the embryo. Once the agarose solidified, 1mL of aquarium makeup water with 0.02% tricaine buffered to pH7.0 with sodium bicarbonate was added to the well. Embryos were maintained at 34C for the duration of time lapse imaging through the use of a heated enclosure.

Cell Tracking:

Tail movies were Z-projected in ImageJ using the maximum intensity projection algorithm. 7 Hour periods where the fish did not drift were identified (167 frames) for each movie as drift in the fish could interfere with analysis. Particles were tracked using the green channel (H2B-EGFP) with the FIJI plugin Trackmate V3.6.0 during these time periods. Blobs were identified using the LoG detector with the following settings: Threshold=2000, Radius=7, and sub-pixelation enabled. Spots were not thresholded. Tracks were generated using the Simple

LAP tracker algorithm with the following settings: linking max distance=50, gap-closing max distance=50, gap-closing max frame gap=1. Only tracks that lasted longer than 2 frames were included for analysis to filter out cells that were not arrested in the tail.

Endothelial Adhesion Assay:

96 well plates were coated with 0.02mg/mL human Fibronectin in PBS for 1 hour at 37C. The PBS was removed and $5x10^4$ HUVECS in 200uL of EBM (Lonza) (supplemented with the EGM-2 bulletkit (Lonza)) were added to each well. Cells were allowed to form a confluent monolayer over 48 hours. Once the monolayer was formed, media was aspirated and $1.2x10^5$ A375 cells in 380uL of pre-warmed EBM (supplemented with the EGM-2 bulletkit) was added to each well. Cells were allowed to settle and adhered to the endothelium for 30 minutes at 37C. Media was added to each well until it the media was slightly above the rim of the well. The plate was sealed using a plastic cover taking care to avoid air bubbles. Wells with air bubbles were not analyzed. Pre-spin images were taken using an inverted fluorescent microscope (Zeiss). The plate was inverted and spun for 10 minutes at 300g at room temperature in an Allegra 6R centrifuge (Beckman). While keeping the plate inverted, each well was imaged on an upright fluorescent microscope (Zeiss).

Cell Clustering Assay:

The cell clustering assay was performed as previously described with some modifications (Patel et al., 2006). Cells were suspended at $2x10^5$ cells/mL in HBSS (Gibco) containing 1% FBS, 5mM $CaCl_2$, and 5mM $MgCl_2$. Cells were strained through a 0.25μm strainer to ensure a single cell suspension. 500uL of cells in HBSS were added to each well of a 24 well low adhesion plate. The plate was agitated at 70rpm at 37C and 5% CO_2 in an incubator for 2

hours. The plate was left on the bench top for 10 minutes following agitation to allow the clusters to settle. The plate was then gently agitated to spread the clusters evenly around the well and let sit for 10 more minutes prior to imaging on an inverted fluorescent microscope (Zeiss) using a 5x objective.

Transwell Migration Assays:

Cells were grown in serum-free media for one day prior to the assay. Transwell plates with a polycarbonate membrane at 8μm pore size (Costar 3422) were used. On the day of the assay, cells were trypsinized and re-suspended at $5x10^5$ cells/mL in serum-free media. 600uL of 10% serum-containing media was added to the lower portion of the transwell. 200uL of cells ($1x10^5$) cells were added to the top of the transwell. The next day, 3, 5x fields were taken of each well in the green channel (H2B-EGFP) on an inverted fluorescent microscope (Zeiss) using a 5X objective to get the baseline number of cells. Each well was then washed 1x with PBS and the top of the membrane was scraped with a cotton swab to remove cells that did not migrate. Each well was then washed 3x with PBS and then 5 5x fields were imaged. Images were thresholded and cell numbers were counted automatically using the ImageJ analyze particles function. The fraction of cells transmigrated was the average number of cells after scraping divided by the average number of cells before scraping.

F- and G-Actin Purification

F- and G-actin were purified using the G-Actin/F-Actin kit (Cytoskeleton Inc) with some modifications to the protocol. Cells were trypsinized and 5x10^6 cells were aliquoted into 1.5mL Eppendorf tubes. Cells were then lysed in 500uL of LAS2 buffer, homogenized by pipetting up and down with a P200 pipette, and incubated at 37C for 10 minutes while rotating.

Cellular debris was pelleted by centrifugation at 2000rpm in a benchtop centrifuge. 100uL of cell lysate was used for each condition and 10uL was used for the 10% input control. All samples were aliquoted into ultracentrifuge tubes (Beckman). As a positive control, 1uL of the F-actin enhancing solution (Phalloidin) was added to one 100uL aliquot. As a negative control, Latrunculin A (Cayman Chemicals) was added to one 100uL aliquot. All samples were then incubated for 10 minutes at 37C while rotating. Samples were then spun at 45,000rpm (90,000g) (Beckman TLA45 rotor) for 2 hours at 37C. Samples were further processed according to the kit instructions.

Western Blotting:

Cells were lysed in Cell Lysis Buffer (Cell Signal Technologies) containing cOmplete protease inhibitor (Sigma) and Phos-stop phosphatase inhibitor (Sigma). 20-30ug of protein was boiled in 2X laemmli buffer (Biorad) with 5% (v/v) 2-mercapto-ethanol (Sigma) and run on 4-20% Tris-Glycine gradient gels (Invitrogen). Proteins were transferred to nitrocellulose membranes (GE) using a Transblot Turbo semi-dry transfer system (Biorad) and blotted using the indicated antibodies. The antibodies used in this study were α-BMI1 (Cell Signal 5856S), α-CDCP1 (Cell Signal 4115S), α-FLAG (Sigma F1804), α-GAPDH (Millipore MAB374), α-MCAM (Cell Signal 13475S), α-TAZ (Cell Signal 4883S), α-YAP (Cell Signal 14074S), α-YAP/TAZ (Cell Signal 8418S).

Appendix A Methods:

Zebrafish Husbandry

Adult zebrafish were housed as previously described (Benjamin and Hynes, 2017). Prior to injection with ZMEL1 zebrafish melanoma cells (Heilmann et al., 2015), immunocompetent *casper* fish were irradiated with two doses of 15 Gray (Gy), one and two days prior to injection, using a GC 40E gamma irradiator (Theratronics).

Adult Zebrafish Imaging

Adult zebrafish intravital confocal imaging and imaging using a dissecting microscope were performed as previously described (Benjamin and Hynes, 2017).

Adult Zebrafish Intradermal Injections

Glass capillary tubes (Borosilicate, 1mm outer diameter, 0.58mm inner diameter, Warner Instruments) were siliconized using Sigmacote reagent (Sigma). Siliconized tubes were pulled on to generate needles using a P-87 micropipette puller (Sutter Instrument) with the following settings: heat=800, pull=150, vel =150, time=200 and pressure=600. The tip of the needle was broken such that it dispended 4nL drops using a PLI-90A Pico-Liter Injector (Warner Instruments) set to an injection pressure of 2.0 PSI and an injection time of 0.10 seconds. Cells were trypsinized, washed twice in PBS and re-suspended at 5x10^5 cells/μL in PBS. A 6-10 week old Casper fish was anesthetized in 0.05% tricaine until it was unresponsive to touch. The fish was then placed on a 10cm Petri dish cover with the head to the left and the ventral site closest to the researcher and placed under a dissecting microscope. The capillary needle was then

gently brought down until it touched the skin of the fish using a micromanipulator. The needle was then gently pushed forwards until it slid underneath the scales of the fish. 4nL of PBS/cells (2,000 cells) were then injected into the dermis. The needle was then gently removed and the fish returned to normal aquarium water to recover.

Embryo Pericardial Injections

The injection needle and cells were prepared as described above except the cells were re-suspended at 4x10^6 cells in 100μL of PBS. Using a micromanipulator, the needle was inserted into the pericardial space taking care not to disrupt the heart. 4nL (160 cells) were injected into the pericardial space.

Zebrafish Embryo Extravasation assay

The *casper* (*roy*$^{-/-}$;*nacre*$^{-/-}$) line was a kind gift from Dr. Leonard Zon (Children's Hospital). The *flk:dsRed2* line (originally developed by Dr. Kenneth Poss (Duke)) was a kind gift from Dr. Mehmet Yanik (MIT). The *flk:dsRed2* line was then crossed into the *casper* background. Embryos were 48 hours old when injected. One day before injection, embryos were dechorionated by adding 12 uL of 30 mg/mL pronase (Sigma) to each 10 cm plate containing embryos and incubating overnight.

Prior to injections, embryos were anesthetized in 0.02% tricaine (Sigma) buffered to pH 7.4 in aquarium make up water (AMW). Anesthetized embryos were then transferred to a 10 cm dish half-filled with 2% agarose and excess water was removed. Embryos were injected with

4 nL of $4x10^4$ tumor cells per L in PBS or $4x10^4$ tumor cells and $2x10^5$ human LPS-pre-stimulated PMNs per L in PBS. Tumor cells and neutrophils were mixed together immediately prior to injections. The cells were injected into the Duct of Cuvier just before it enters the heart. Embryos were maintained at 34C following injection.

Injections were performed with borosilicate glass capillary needles (Warner Instruments) that were siliconized using sigmacote reagent (Sigma). Needles were pulled using a P-87 micropipette puller (Sutter Instrument) with the following settings: heat=800, pull=150, vel =150, time=200 and pressure=600. The tip of the needle was broken such that it dispended 2 nL drops using a PLI-90A Pico-Liter Injector (Warner Instruments) set to an injection pressure of 2.0 PSI and an injection time of 0.10 seconds.

For time-lapse imaging, embryos were placed in a single well of a 6 well, glass-bottomed plate (MatTek) containing a thin layer of 2% agarose. They were then covered in 0.8% agarose containing 0.01% tricaine buffered to pH 7.4. Once the agarose solidified, the well was filled with AMW containing 0.01% tricaine buffered to pH 7.4.

For time point imaging, each well of a 96 well glass-bottom plate (MatTek) was filled with 60 L of 2% agarose. A previously described pin tool (Wittbrodt et al., 2014) was inserted into the wells for 20 min to generate agarose molds to orient embryos laterally for imaging. At the given time points, embryos were anesthetized in 0.01% tricaine in AMW buffered to pH 7.4 and added to each well.

Embryos were imaged on an A1R inverted confocal microscope (Nikon) using the resonant scanner with a 10x objective and 1.5x zoom. For time-lapse imaging, Z- stacks of 50 m with a 7.6 m step size were acquired every 14 seconds for 3 hrs. Fish were imaged within 6 hrs of injection. For time point imaging, a single 100 μm Z- stack with a 7.6 μm step size was acquired for each fish.

For all other experimental methods from our collaboration with the Kamm lab see:

Michelle B. Chen, Cathy Yu, David C. Benjamin, Hesham Azizgolshani, Richard O. Hynes, Roger, D. Kamm. **Inflamed neutrophils sequestered at entrapped tumor cells via chemotactic confinement promotes tumor cell extravasation**. *PNAS* Submitted

References:

Benjamin, D.C., and Hynes, R.O. (2017). Intravital imaging of metastasis in adult Zebrafish. BMC Cancer *17*, 660.

Heilmann, S., Ratnakumar, K., Langdon, E.M., Kansler, E.R., Kim, I.S., Campbell, N.R., Perry, E.B., McMahon, A.J., Kaufman, C.K., van Rooijen, E., et al. (2015). A Quantitative System for Studying Metastasis Using Transparent Zebrafish. Cancer Res. *75*, 4272–4282.

Moore, J.C., Tang, Q., Yordán, N.T., Moore, F.E., Garcia, E.G., Lobbardi, R., Ramakrishnan, A., Marvin, D.L., Anselmo, A., Sadreyev, R.I., et al. (2016). Single-cell imaging of normal and malignant cell engraftment into optically clear prkdc-null SCID zebrafish. J. Exp. Med. *213*, 2575–2589.

Patel, S.D., Ciatto, C., Chen, C.P., Bahna, F., Rajebhosale, M., Arkus, N., Schieren, I., Jessell, T.M., Honig, B., Price, S.R., et al. (2006). Type II cadherin ectodomain structures: implications for classical cadherin specificity. Cell *124*, 1255–1268.

Pugach, E.K., Li, P., White, R., and Zon, L. (2009). Retro-orbital injection in adult zebrafish. J Vis Exp.

Stoletov, K., Kato, H., Zardouzian, E., Kelber, J., Yang, J., Shattil, S., and Klemke, R. (2010). Visualizing extravasation dynamics of metastatic tumor cells. Journal of Cell Science *123*, 2332–2341.

Tang, Q., Abdelfattah, N.S., Blackburn, J.S., Moore, J.C., Martinez, S.A., Moore, F.E., Lobbardi, R., Tenente, I.M., Ignatius, M.S., Berman, J.N., et al. (2014). Optimized cell transplantation using adult rag2 mutant zebrafish. Nat Meth *11*, 821–824.

Wittbrodt, J.N., Liebel, U., and Gehrig, J. (2014). Generation of orientation tools for automated zebrafish screening assays using desktop 3D printing. BMC Biotechnol *14*, 36–36.

Xu, L., Shen, S.S., Hoshida, Y., Subramanian, A., Ross, K., Brunet, J.-P., Wagner, S.N., Ramaswamy, S., Mesirov, J.P., and Hynes, R.O. (2008). Gene expression changes in an animal melanoma model correlate with aggressiveness of human melanoma metastases. Molecular Cancer Research *6*, 760–769.